STUDIA UNIVERSITATIS
BABEŞ-BOLYAI

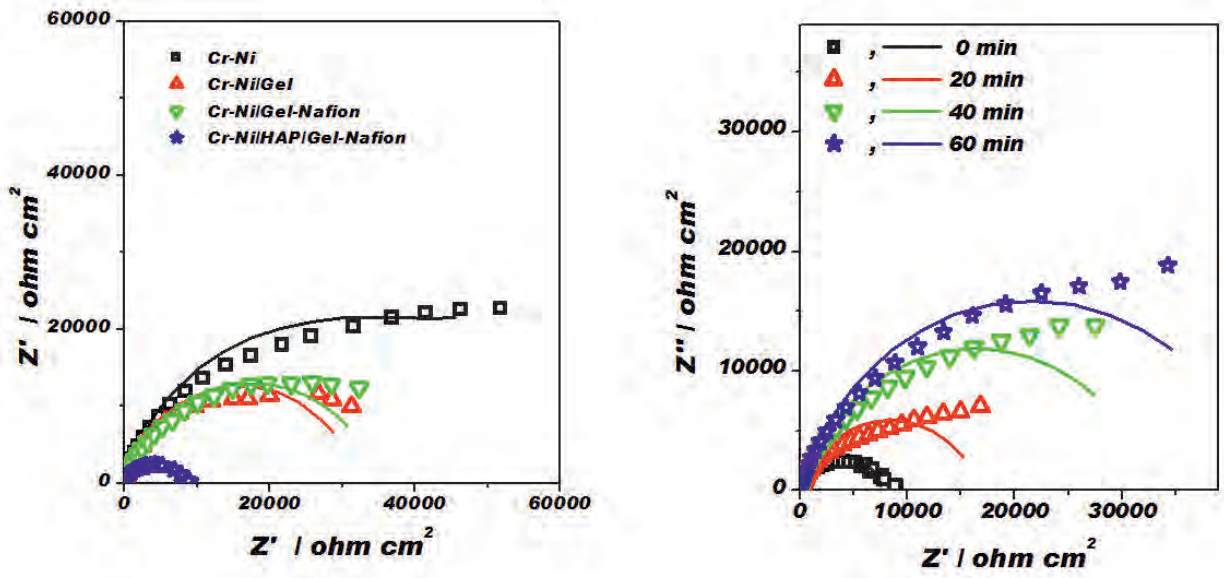


# CHEMIA

1/2019

# STUDIA
# UNIVERSITATIS BABEŞ-BOLYAI

## CHEMIA

**1/2019**

http://chem.ubbcluj.ro/~studiachemia/; studiachemia@chem.ubbcluj.ro
http://www.studia.ubbcluj.ro/serii/chemia/index_en.html

**YEAR** **Volume 64 (LXIV) 2019**
**MONTH** **MARCH**
**ISSUE** **1**

# S T U D I A
# UNIVERSITATIS BABEŞ–BOLYAI
# CHEMIA

## 1

**ISSUE DOI:10.24193/subbchem.2019.1**

**STUDIA UBB EDITORIAL OFFICE:** B.P. Hasdeu no. 51, 400371 Cluj-Napoca, Romania, Phone + 40 264 405352

### CUPRINS – CONTENT – SOMMAIRE – INHALT

MASOUD GIAHI, DEEPAK PATHANIA, SHILPI AGARWAL, GOMAA A. M. ALI, KWOK FENG CHONG, VINOD KUMAR GUPTA, Preparation of Mg-Doped $TiO_2$ Nanoparticles for Photocatalytic Degradation of Some Organic Pollutants ..... 7

VLADIMIR D. DIMITRIJEVIĆ, MAJA N. STANKOVIĆ, DRAGAN M. ĐORĐEVIĆ, IVAN M. KRSTIĆ, MILICA G. NIKOLIĆ, ALEKSANDAR LJ. BOJIĆ, NENAD S. KRSTIĆ, The Preliminary Adsorption Investigation of *Urtica Dioica* L. Biomass Material as a Potential Biosorbent for Heavy Metal Ions ..... 19

GIANINA ELENA DAMIAN, VALER MICLE, IOANA MONICA SUR, Lead and Copper Removal from Multi-Metal Contaminated Soils Through Soil Washing Technique Using Humic Substances as Washing Agents: The Influence of the Washing Solution pH ..... 41

MUSTAFA KEMAL SANGUN, CEMAL TURAN, BEYZA ERSOY ALTUN, Examination of Macro and Micro Elements in *Psetta Maksima* and *Solea Vulgaris* from the Black and North Eastern Mediterranean Seas ..... 53

IRINA SMICAL, ADRIANA MUNTEAN, VALER MICLE, ZOLTÁN TÖRÖK, Study Regarding the Presence of Some Heavy Metals (Chromium, Copper, Manganese and Zinc) in the Green Waste Compost..... 63

THOMAS DIPPONG, CRISTINA MIHALI, ALEXANDRA AVRAM, FIRUTA GOGA, Influence of Total Chloride, Arsenic and Aluminum Contents on Microorganisms of Open Wells..... 79

ANDRA TĂMAŞ, SORINA BORAN, The Rheological Behavior of the Mixtures of Castor Oil with Adipic Esters..... 93

DHAFIR TAMWEEN AJEEL AL-HEETIMI, ZAINAB ABBAS AL-DULAIMY, ASAL AHMED AL-JAWARY, OMAR SABEEH AL-KHAZRAJY, Excess and Deviations Properties for the Binary Solvent Mixtures of Tetrahydrofurfuryl Alcohol with Some Aromatic Hydrocarbons at 298.15k..... 103

MARIUS-ADRIAN BREHAR, MELINDA VÁRHELYI, VASILE-MIRCEA CRISTEA, DANIEL CRÎSTIU, ȘERBAN-PAUL AGACHI, Influent Temperature Effects on the Activated Sludge Process at a Municipal Wasteater Treatment Plant..... 113

IOANA CARMEN FORT, GRAZIELLA L. TURDEAN, REKA BARABAS, DANIELA POPA, ANA ISPAS, MARIANA CONSTANTINIUC, Study of the Hydrogen Peroxide Based Whitening Gel on the Corrosion of Dental Metallic Alloys ..... 125

DAN-ALEXANDRU TĂTARU, DAN-MIRCEA OLINIC, MARIA OLINIC, ANDRADA-ELENA URDA-CÎMPEAN, REMUS ORĂSAN, CĂLIN HOMORODEAN, High-Dose Statin Prior to Primary Percutaneous Coronary Intervention Reduces Oxidative Stress Burden in Patients with Acute ST-Elevation Myocardial Infarction ..... 135

ANGELA COZMA, ADRIANA FODOR, OLGA HILDA ORĂȘAN, RAMONA SUHAROSCHI, CRINA MUREȘAN, ROMANA VULTURAR, DOREL SAMPELEAN, VASILE NEGREAN, DANA POP, ADELA SITAR-TĂUT, A Comparison between Insulin Resistance Scores Parameters in Identifying Patients with Metabolic Syndrome..... 147

ADRIAN MIHAI VARVARA, CRISTINA GASPARIK, BOGDAN CULIC, COSMINA IOANA BONDOR, ELENA BIANCA VARVARA, GABRIEL FURTOS, MARIOARA MOLDOVAN, DIANA DUDEA, Radiopacity Analysis of Some Chairside Computer-Aided Design-Computer-Aided Manufacturing Milling Materials..... 161

FLAVIA POP, DANIEL NĂSUI, ZORICA VOȘGAN, CRISTINA MIHALI, CLAUDIA BUTEAN, Chemical Stabilization of Fats Rich in Long Chain Polyunsaturated Fatty Acids by Antioxidants Addition ..... 173

MUHAMMAD YASEEN, NOUMAN RASOOL, ZAHID FAROOQ, SHAHBAZ NAZIR, SHUMAILA CHOHAN, A Pilot Study for the use of Coumarin-480 to Enhance the Fingermarks ..... 185

MIUȚA FILIP, DOINA PRODAN, MARIOARA MOLDOVAN, MIHAELA VLASSA, Determination of Nitrate and Nitrite Content in *Zonar* Milk Serum and Derived Dairy Drinks Using Ion-Pair Reversed-Phase High Performance Liquid Chromatography..... 197

GABRIEL ARMENCEA, CRISTIAN BERCE, MILICA TODEA, ADRIANA VULPOI, DAN LEORDEAN, SIMION BRAN, CRISTIAN DINU, MADALINA LAZAR, ONDINE LUCACIU, LIANA CRISAN, IOAN BARBUR, BOGDAN CRISAN, FLORIN ONISOR, SERGIU VACARAS, GRIGORE BACIUT, MIHAELA BACIUT, Innovative Chemical Coating Protocol for Titanium Alloy Implants ..... 207

AURA RUSU, PAULA ANTONOAEA, ADRIANA CIURBA, MAGDALENA BÎRSAN, GABRIEL HANCU, NICOLETA TODORAN, Development of a Rapid Capillary Zone Electrophoresis Method to Quantify Levofloxacin and Meloxicam from Transdermal Therapeutic Systems ..... 219

Studia Universitatis Babes-Bolyai Chemia has been selected for coverage in Thomson Reuters products and custom information services. Beginning with V. 53 (1) 2008, this publication is indexed and abstracted in the following:

- Science Citation Index Expanded (also known as SciSearch®)
- Chemistry Citation Index®
- Journal Citation Reports/Science Edition

STUDIA UBB CHEMIA, LXIV, 1, 2019 (p. 7-18)
(RECOMMENDED CITATION)
DOI:10.24193/subbchem.2019.1.01

# PREPARATION OF Mg-DOPED $TiO_2$ NANOPARTICLES FOR PHOTOCATALYTIC DEGRADATION OF SOME ORGANIC POLLUTANTS

**MASOUD GIAHI[a*], DEEPAK PATHANIA[b], SHILPI AGARWAL[c], GOMAA A. M. ALI[d,e], KWOK FENG CHONG[e], VINOD KUMAR GUPTA[c*]**

**ABSTRACT.** In this study, the sol-gel method was used to prepare Mg-doped $TiO_2$ nanoparticles from titanium tetraisopropoxide and magnesium sulfate as the dopant precursors. Mg-doped $TiO_2$ shows the formation of anatase phase with polyhedral and spherical particles with an average size of 25-30 nm. X-ray diffraction, X-ray photoelectron spectroscopy, transmission electron microscopy and photoluminescence were used to characterize the prepared material. The photocatalytic degradation performance of rhodamine B, nonylphenol ethoxylates, pseudoephedrine hydrochloride, and nicotine on Mg-doped $TiO_2$ was studied under UV irradiation. The photocatalytic degradation shows that 98.92, 98.00, 98.00 and 97.95% of rhodamine B, nonylphenol ethoxylates, pseudoephedrine hydrochloride, and nicotine was decomposed by Mg-doped $TiO_2$, respectively.

***Keywords:*** *Mg-doped $TiO_2$; Organic pollutants; Photocatalytic degradation; Photoluminescence; Sol-gel*

[a] *Islamic Azad University, Department of Chemistry, South Tehran Branch, Tehran, Iran*
[b] *Central University of Jammu, Department of Environmental Sciences, Samba, Jammu and Kashmir-181143, India*
[c] *Center of Excellence for Advanced Materials Research, Faculty of Science, King Abdulaziz University, Jeddah 21589, Saudi Arabia*
[d] *Al-Azhar University, Faculty of Science, Chemistry Department, Assiut, 71524, Egypt*
[e] *Universiti Malaysia Pahang, Faculty of Industrial Sciences & Technology, Gambang, 26300 Kuantan, Malaysia*
* *Corresponding authors: m_giahi@azad.ac.ir and vinodfcy@gmail.com*

## INTRODUCTION

Nowadays, heterogeneous photocatalytic degradation using $TiO_2$ becomes potentially cost-effective and environmentally sustainable treatment technique [1-3]. $TiO_2$ is a promising candidate photocatalyst due to its high photocatalytic activity, good chemical and biological stability, high energy efficiency, relatively low-cost and nontoxicity [4]. Due to its photoactivity and photocatalytic ability to degrade contaminants, nanocrystalline $TiO_2$ is attractive and widely used as a photocatalyst [5-8].

$TiO_2$ powders in the presence of UV or visible light is used to decompose many organic materials in aqueous solutions [9-11]. Water pollutions in the forms of organic and inorganic substances become a critical environmental problem, where, clean water is one of the strategic issues for human life. Water could be contaminated *via* natural or artificial foreign materials from various sources such as industrial effluents, agricultural runoff and chemical spills [12-19]. These effluents include nonbiodegradable, toxic organic materials [20-22]. Recent studies indicate that during manufacturing and processing operations, a substantial amount toxic organic materials enter into the environment [23, 24].

In this work, we synthesized Mg-doped $TiO_2$ nanophotocatalyst by sol-gel method and then we applied it for photochemical degradation of some environmental pollutants in aqueous solution in the presence of UV light. The results showed this nanophotocatalyst has a good degradation efficiency for the studied environmental pollutants.

## RESULTS AND DISCUSSION

### *X-ray diffraction*

The diffractograms of pure and Mg-doped $TiO_2$ nanoparticles (0.75 and 1.5 at.%) are shown in Figure 1. It is obvious from the patterns, the anatase phase is the main phase in all samples [25]. However, a weak diffraction peak along (1 1 0) indicating the rutile phase is observed for pure titania showing the formation of a mixed phase structure for this sample. Mg atoms are easily inserted into the crystal lattice of $TiO_2$ due to small the ionic radius of $Mg^{2+}$ (0.57 Å) compared to than $Ti^{4+}$ (0.68 Å) ion [26]. Pure phase was observed with no individual peaks of Mg in the pattern. Moreover, Scherrer's formula was used to calculate the particles size (PS) of Mg-doped $TiO_2$ [27-29]:

$$PS = \frac{0.89\lambda}{\beta \cos\theta} \quad (1)$$

where $\lambda$ is the wavelength of the used Cu-$K_\alpha$ radiation ($\lambda$ = 1.54056 Å), $\beta$ is the full width at half maximum *and θ the scattering angle.*

The calculated grain sizes of pure, 0.75 and 1.5 at.% Mg-doped $TiO_2$ nanoparticles are 24, 22 and 21 nm, respectively. This proves that the crystallite size was decreased with increasing in Mg doping content. The decrement of crystallite size with Mg can be assigned to the smaller ionic radius of Mg compared to Ti.

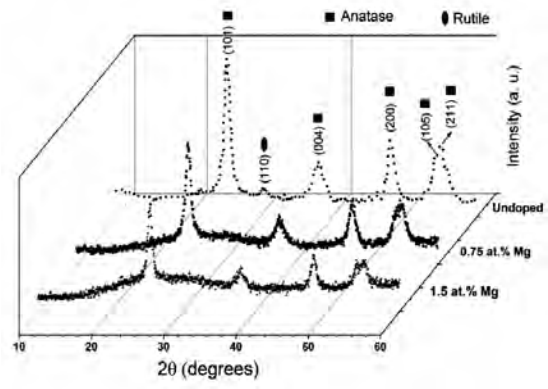


**Figure 1.** X-ray patterns of pure and Mg-doped $TiO_2$ nanoparticles.

### *Transmission electron microscopy analysis*

Figure 2 shows the TEM images of the prepared nanoparticles for morphological study. Polyhedral and spherical particles with a particles size of the range 25-30 nm are clearly observed. The particles size obtained from TEM data is in a good agreement with that obtained by XRD calculations. The size of pure $TiO_2$ is bigger than Mg-doped $TiO_2$ in both methods. This average grain size is related to different growth orientations [30].

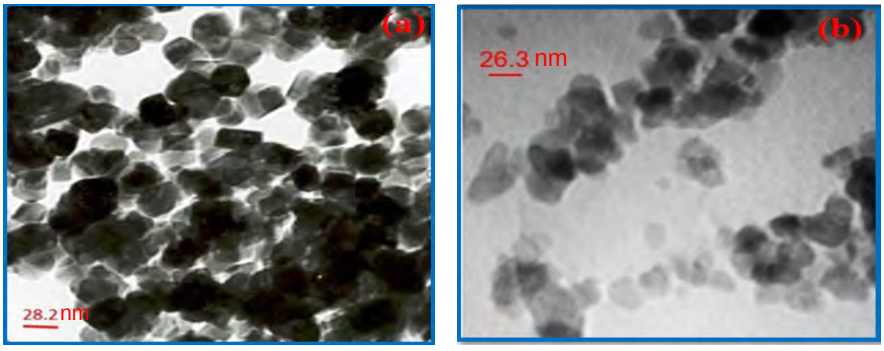


**Figure 2.** Typical TEM micrographs for undoped (a) and 1. 5 at.% Mg-doped $TiO_2$ (b) nanoparticles.

### *X-ray photoelectron spectroscopy*

To investigate the chemical composition of Mg-doped $TiO_2$, XPS analysis was performed and displayed in Figure 3. The peaks with binding energies at 458.63 eV and 464.01 eV are ascribed to Ti $2p_{3/2}$ and Ti $2p_{1/2}$. These values are in good agreement with those reported for $TiO_2$ [31]. The peak at 51.23 eV is related to Mg 2p, which is typical of $Mg^{2+}$ that bonds with an oxygen atom. The inset of Figure 3 gives the atomic percentage of the elements involved in the compound. The presence of a high amount of carbon is expected for the synthesis methods performed in ambient air.

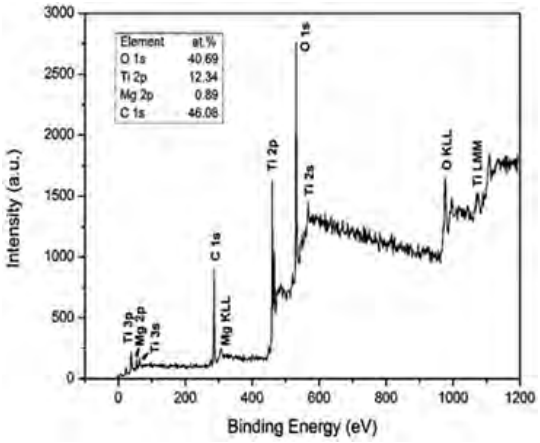


**Figure 3.** XPS survey spectrum for 1.5 at.% Mg-doped $TiO_2$ nanoparticles, the inset shows the atomic ratio of the elements.

### *Photoluminescence spectra*

The charge carrier trapping, mobility and transfer to the surface of photocatalysts could be studied using PL spectra. PL spectrum of $TiO_2$ anatase phase shows broadband as it is an indirect bandgap semiconductor related to radiative recombination of charge carriers. The related PL spectra of the prepared nanoparticles are displayed in Figure 4. The spectra were obtained with an excitation wavelength of 310 nm. The valence band (VB) electrons receive sufficient energy to transfer to the conduction band (CB) when it is irradiated with light of a longer or equal wavelength to its bandgap. These electrons then go back from CB to VB with emission of energy as PL radiation [32]. As it is evident from Figure 4, a strong peak occurs around 356 nm that can be ascribed to the mentioned band–to–band transition. Other PL processes that can take place, include the transfer of excited electrons from CB to other

intermediate bands, *via* non–radiative process, and from the intermediate bands to VB by radiative transition causing PL signals [33]. The inset of Figure 4 depicts the deconvoluted spectrum for pure $TiO_2$ nanoparticles. The recombination of electrons–holes in surface defects/surface oxygen vacancies could be seen as a small emission below 356 nm occurs at 341 nm [34]. Meanwhile, the shoulder peak at 370 nm can be attributed to an emission of intermediate band transition of titania. Besides, it is obvious that the peak intensity becomes stronger with the increase of the doping amount of Mg, pointing that a higher amount of Mg brings a higher recombination rate, which may result in an excessive formation of Mg doping from the recombination centre.

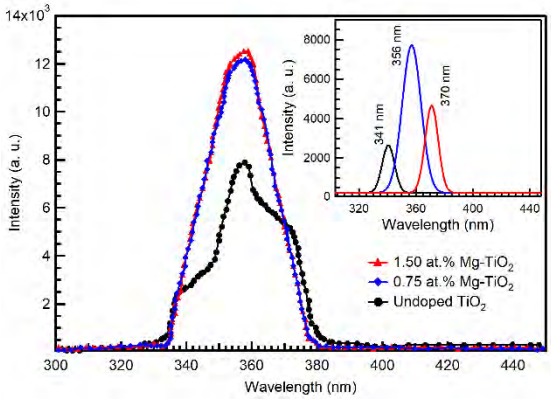


**Figure 4.** Photoluminescence spectra for pure and 1.5 at.% Mg-doped $TiO_2$ nanoparticles.

### *Degradation optimum conditions*

To obtain the degradation optimum conditions of rhodamine B, nonylphenol ethoxylates, pseudoephedrine hydrochloride and nicotine, their reactions in the presence of pure $TiO_2$ and Mg-doped $TiO_2$ were studied. The photocatalytic degradation (D) was calculated as follows [35]:

$$D(\%) = \frac{(A_o - A_t)}{A_o} x100 \quad (2)$$

where $A_o$ is the initial absorbance of environmental pollutants and $A_t$ is the absorbance of environmental pollutants after t minutes.

Employing different concentrations of Mg-doped $TiO_2$ varying from 0.04 to 0.44 g $L^{-1}$, the effect of initial concentration of the pollutants varying from 10 to 50 mg $L^{-1}$ and the initial concentration of oxidant such as potassium peroxodisulfate and hydrogen peroxide varying from 1 to 7 mM in pH range of 2.0- 12.0 in the presence of UV light [36-40].

The results, are presented in Figure 5 (rhodamine B), Figure 6 (nonylphenol ethoxylates), Figure 7 (pseudoephedrine hydrochloride) and Figure 8 (nicotine), which indicate that photodegradation efficiency unequivocally increases with increasing irradiation time. In addition, Mg-doped $TiO_2$ shows high degradation ratios than pure $TiO_2$ for all organic materials under study. Where the degradation ratio was found to be 98.92, 98.00, 98.00 and 97.95% for rhodamine B, nonylphenol ethoxylates, pseudoephedrine hydrochloride, and nicotine, respectively, in the case of Mg-doped $TiO_2$. While, for pure $TiO_2$, it was found to be 90.22, 95.00, 91.00 and 91.01% for rhodamine B, nonylphenol ethoxylates, pseudoephedrine hydrochloride, and nicotine, respectively. The optimum conditions for degradation are presented in Figure 9 and listed in Table 1.

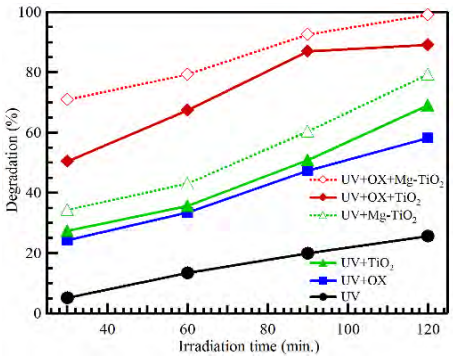


**Figure 5.** Degradation of rhodamine B in aqueous solutions: conditions are, rhodamine B concentration =10 mg $L^{-1}$, pure $TiO_2$ = 0.28 g $L^{-1}$, Mg-doped $TiO_2$ = 0.20 g $L^{-1}$, OX ($K_2S_20_8$) = 3 mM, pH = 10, V = 25 mL.

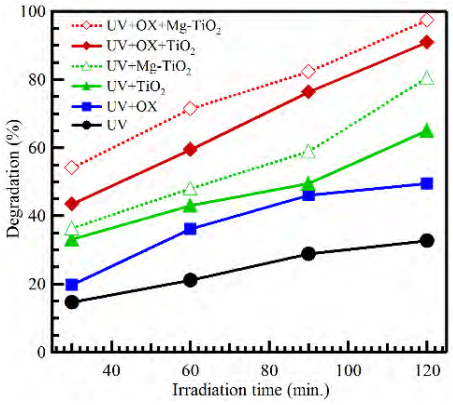


**Figure 6.** Degradation of nonylphenol ethoxylates in aqueous solutions: conditions are: nonylphenol ethoxylates 6 mol concentration = 20 mg $L^{-1}$, pure $TiO_2$=0.28 $gL^{-1}$, Mg-doped $TiO_2$ = 0.28 g $L^{-1}$, OX ($H_2O_2$) = 1 mM, pH = 6, V = 25 mL.

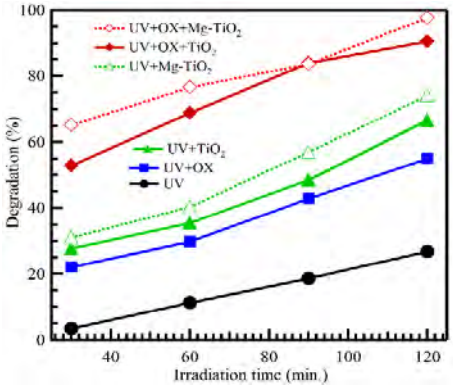


**Figure 7.** Degradation of pseudoephedrine hydrochloride in aqueous solutions: conditions are, pseudoephedrine hydrochloride concentration = 10 mg $L^{-1}$, pure $TiO_2$ = 0.28 g $L^{-1}$, Mg-doped $TiO_2$ = 0.28 g $L^{-1}$, OX ($H_2O_2$) = 5 mM, pH = 6, V = 25 mL.

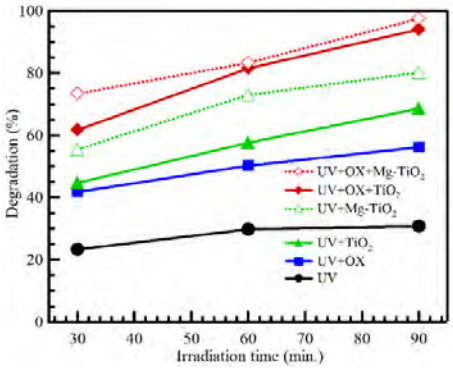


**Figure 8.** Degradation of nicotine in aqueous solutions: conditions are, nicotine concentration = 20 mg $L^{-1}$, pure $TiO_2$ = 0.28 g $L^{-1}$, Mg-doped $TiO_2$ = 0.20 g $L^{-1}$, OX ($K_2S_2O_8$) = 3 mM, pH = 7, V = 25 mL.

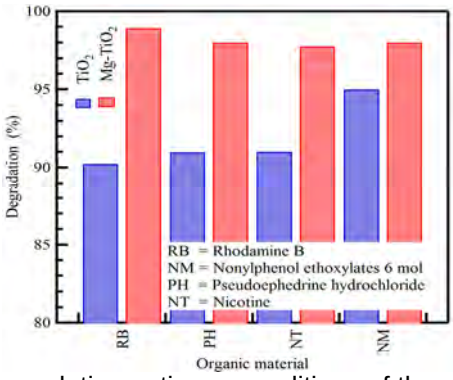


**Figure 9.** The degradation optimum conditions of the organic pollutants using pure $TiO_2$ and Mg-doped $TiO_2$.

**Table 1.** The degradation optimum conditions of some environmental pollutants using pure $TiO_2$ and Mg-doped $TiO_2$.

| Photocatalyst | Pollutant | Optimum conditions | | | | | Degradation (%) |
|---|---|---|---|---|---|---|---|
| | | Conc. of photocatalyst (ppm) | Conc. of pollutant (ppm) | Oxidant (mM) | Irradiation time (min) | pH | |
| Pure $TiO_2$ | Rhodamine B | 280 | 10 | 3 ($K_2S_2O_8$) | 90 | 10 | 90.22 |
| Mg-doped $TiO_2$ | | 200 | 10 | 3 ($K_2S_2O_8$) | 60 | 10 | 98.92 |
| Pure $TiO_2$ | Nonylphenol ethoxylates | 280 | 20 | 1 ($H_2O_2$) | 90 | 6 | 95.00 |
| Mg-doped $TiO_2$ | | 280 | 20 | 1 ($H_2O_2$) | 90 | 6 | 98.00 |
| Pure $TiO_2$ | Pseudoephedrine hydrochloride | 280 | 10 | 5 ($H_2O_2$) | 120 | 6 | 91.00 |
| Mg-doped $TiO_2$ | | 280 | 10 | 5 ($H_2O_2$) | 120 | 6 | 98.00 |
| Pure $TiO_2$ | Nicotine | 280 | 20 | 3 ($K_2S_2O_8$) | 90 | 7 | 91.01 |
| Mg-doped $TiO_2$ | | 200 | 20 | 1 ($K_2S_2O_8$) | 90 | 7 | 97.95 |

*Degradation mechanism*

The photocatalytic degradation of organic material pollutants takes place *via* photoexcitation of the semiconductor and then the formation of an electron-hole pair on the surface of photocatalyst (Eq. 3). The direct oxidation of organic material (OM) to reactive intermediates (Eq. 4) is due to the high oxidative potential of the holes ($h_{VB}^+$) in photocatalyst. Hydroxyl radicals ($\mathrm{OH}^\bullet$) are formed either by the reaction of the hole with $OH^-$ (Eq. 5) or by water decomposition (Eq. 6). These strong radicals are non-selective oxidants which lead to partial or complete mineralization of several OM [41-46].

$$\mathrm{Mg-doped\ TiO_2} + \mathrm{h\nu} \rightarrow \mathrm{Mg-doped\ TiO_2}\ (e_{CB}^- + h_{VB}^+) \quad (3)$$

$$h_{VB}^+ + \mathrm{OM} \rightarrow \mathrm{OM}^{\bullet+} \rightarrow \mathrm{oxidation\ of\ OM} \quad (4)$$

$$h_{VB}^+ + \mathrm{OH}^- \rightarrow \mathrm{OH}^\bullet \quad (5)$$

$$h_{VB}^+ + H_2\mathrm{O} \rightarrow \mathrm{H}^+ + \mathrm{OH}^\bullet \quad (6)$$

Molecular oxygen could be reduced to superoxide anion (Eq. 7) by the action of the conduction band electron ($e_{CB}^-$) on the catalyst surface. In the presence of organic materials, this radical forms organic peroxides (Eq. 8) or hydrogen peroxide (Eq. 9) [47].

$$e_{CB}^- + O_2 \rightarrow O_2^{\bullet-} \quad (7)$$

$$O_2^{\bullet-} + \mathrm{OM} \rightarrow OM - OO^\bullet \quad (8)$$

$$O_2^{\bullet-} + \mathrm{H_2O}^\bullet + H^+ \rightarrow \mathrm{H_2O_2} + O_2 \quad (9)$$

The construction of hydroxyl radicals is due to the conduction band electrons. These radicals have been showed as the primary cause of organic material mineralization [48-50] (Eq. 10).

$$OH^{\bullet} + OM \rightarrow \text{degradation of OM} \quad (10)$$

## CONCLUSIONS

In this work, Mg-doped $TiO_2$ nanoparticles was prepared by the sol-gel method. This photocatalyst was examined by XRD, TEM, XPS and PL analyses. Mg-doped $TiO_2$ shows polyhedral and spherical particles with an average size of 25-30 nm. The photocatalyst was applied for the degradation of rhodamine B, nonylphenol ethoxylates, pseudoephedrine hydrochloride and nicotine as pollutants. Mg-doped $TiO_2$ shows a superb degradation of these pollutants between 98-99%.

## EXPERIMENTAL PROCEDURE

### *Materials*

Titanium tetraisopropoxide, magnesium sulfate, ethanol, nitric acid, hydrochloric acid, nonylphenol ethoxylates, rhodamine B and nicotine were obtained from Merck. The pseudoephedrine hydrochloride was laboratory prepared and purified.

### *Preparation of pure and Mg-doped $TiO_2$ nanoparticles*

Initially, solutions A and B were prepared as follows: Solution A, 13.3 mL of absolute ethanol, 2.0 mL of deionized water and magnesium sulfate (0.75 and 1.50 wt.%) were mixed. Solution B, 7.0 mL of titanium tetraisopropoxide and 13.3 mL of absolute ethanol were mixed under stirring for 5 min. Then 1 mL of $HNO_3$ was added to the prepared mixture drowsily under stirring for 10 min. Then solution A was slowly added to solution B with vigorous stirring until the transparent sol was obtained. The gel was prepared by aging the solution for 48 h at room temperature. The derived gel was dried at 100 °C and then calcined at 400 °C for 4 h. The doping concentrations are expressed as a weight percentage of titanium atoms. Pure $TiO_2$ is also prepared with the same procedure without adding magnesium sulfate.

### *Characterizations*

The crystalline structure and phase purity were investigated using X-ray diffraction (XRD) by a BRUKER D8 ADVANCE X-ray diffractometer. The morphologies and elemental analyses were determined by transmission electron microscopy (TEM) and X-ray photoelectron spectroscopy (XPS), respectively. The charge carrier trapping, mobility and transfer to the surface of the photocatalysts were studied using photoluminescence (PL) spectroscopy.

### *Photocatalytic reactor and degradation procedure*

Photodegradation experiments were performed with a thermostatic cylindrical Pyrex reactor with a 50 mL capacity reactor system under the irradiation of a UV lamp. A mercury lamp (36 W) was used as UV light source. Around 25 mL of the four environmental pollutant solutions (rhodamine B, nonylphenol ethoxylates, pseudoephedrine hydrochloride and nicotine) with a primary concentration of 20 mg $L^{-1}$ was placed into the Pyrex reactor. A known amount of Mg-doped $TiO_2$ photocatalyst (5 and 7 mg, equivalent to 200 and 280 ppm, respectively) was added to the pollutant solution and oxidant (Table 1). Diluted HCl and NaOH solutions were used to adjust the pH. The mixture was then irradiated with the UV lamp up to 120 min. Magnetically stirring (60 rpm) was used throughout the experiment. At regular time intervals, 1 mL was withdrawn then diluted to 5 mL, centrifuged and the absorbance was measured. The quantitative estimation of the environmental pollutants was carried out using a UV-Vis spectrophotometer (Model Jenway 6405) at their $\lambda_{max}$.

## ACKNOWLEDGMENT

Financial support by Lahijan Branch, Islamic Azad University Grant No. 17.20.5.3515 is gratefully acknowledged.

## REFERENCES

1. W. Baran, E. Adamek, A. Sobczak, A. Makowski, *Applied Catalysis B: Environmental*, **2009**, *90*, 516.
2. T.A. Devi, N. Ananthi, T.P. Amaladhas, *Journal of Nanostructure in Chemistry*, **2015**, *6*, 75.
3. Y.-X. Zhang, Y. Jia, *Materials Science and Engineering*: B, **2018**, *228*, 123.
4. O. Moradi, K. Zare, M. Monajjemi, M. Yari, H. Aghaie, *Fullerenes, Nanotubes and Carbon Nanostructures*, **2010**, *18*, 285.
5. A. Abbasi, J.J. Sardroodi, *Journal of Nanostructure in Chemistry*, **2017**, *7*, 345.

6. V.R. Posa, V. Annavaram, A.R. Somala, *Bulletin of Materials Science*, **2016**, *39*, 759.
7. É. Karácsonyi, L. Baia, A. Dombi, V. Danciu, K. Mogyorósi, L. Pop, G. Kovács, V. Coşoveanu, A. Vulpoi, S. Simon, *Catalysis today*, **2013**, *208*, 19.
8. Z. Pap, É. Karácsonyi, L. Baia, L.C. Pop, V. Danciu, K. Hernádi, K. Mogyorósi, A. Dombi, *Physica Status Solidi* (b), **2012**, *249*, 2592.
9. F. Abbaszadeh, O. Moradi, M. Norouzi, O. Sabzevari, *Journal of Industrial and Engineering Chemistry*, **2014**, *20*, 2895.
10. N.S. Begum, H.M. Farveez Ahmed, *Bulletin of Materials Science,* **2008**, *31*, 43.
11. G. Zhao, J. Zou, C. Li, J. Yu, X. Jiang, Y. Zheng, W. Hu, F. Jiao, *Journal of Materials Science: Materials in Electronics,* **2018**, *29*, 7002.
12. M.S. Derakhshan, O. Moradi, *Journal of Industrial and Engineering Chemistry, **2014**, 20, 3186.*
13. S.M.S. Arabi, R.S. Lalehloo, M.R.T.B. Olyai, G.A.M. Ali, H. Sadegh, *Physica E: Low-dimensional Systems and Nanostructures*, **2019**, *106*, 150.
14. H. Sadegh, G.A.M. Ali, A.S.H. Makhlouf, K.F. Chong, N.S. Alharbi, S. Agarwal, V.K. Gupta, *Journal of Molecular Liquids,* **2018**, *258*, 345.
15. S.P. Lee, G.A.M. Ali, H. Algarni, K.F. Chong, *Journal of Molecular Liquids,* **2018**, *277*, 175.
16. H. Sadegh, G.A.M. Ali, V.K. Gupta, A.S.H. Makhlouf, R. Shahryari-ghoshekandi, M.N. Nadagouda, M. Sillanpää, E. Megiel, *Journal of Nanostructure in Chemistry*, **2017**, *7*, 1.
17. O.A. Habeeb, K. Ramesh,G.A.M. Ali, R.M. Yunus, *Desalination and Water Treatment*, **2017**, *84*, 205.
18. H. Sadegh, G.A.M. Ali, Z. Abbasi, M. N. Nadagouda, *Studia Universitatis Babes-Bolyai Chemia*, **2017**, *62*, 233.
19. S. Agarwal, H. Sadegh, M. Majid, A.S.H. Makhlouf, G.A.M. Ali, A.O.H. Memar, R. Shahryari-ghoshekandi, I. Tyagi, V.K. Gupta, *Journal of Molecular Liquids*, **2016**, *218*, 191.
20. H.H. Abdel Ghafar, G.A.M. Ali, O.A. Fouad, S.A. Makhlouf, *Desalination and Water Treatment*, **2015**, *53*, 2980.
21. V.K. Gupta, S. Agarwal, H. Sadegh, G.A.M. Ali, A.K. Bharti, A.S. Hamdy, *Journal of Molecular Liquids*, **2017**, *237*, 466.
22. K. Byrappa, A.K. Subramani, S. Ananda, K.M.L. Rai, R. Dinesh, M. Yoshimura, *Bulletin of Materials Science,* **2006**, *29*, 433.
23. S. Samadi, M. Yousefi, F. Khalilian, A. Tabatabaee, *Journal of Nanostructure in Chemistry*, **2014**, *5*, 7.
24. S. Agarwal, H. Sadegh, M. Monajjemi, A.S. Hamdy, G.A.M. Ali, A.O.H. Memar, R. Shahryari-ghoshekandi, I. Tyagi, V.K. Gupta, *Journal of Molecular Liquids*, **2016**, *218*, 191.
25. H.-S. Kil, Y.-J. Jung, J.-I. Moon, J.-H. Song, D.-Y. Lim, S.-B. Cho, *Journal of Nanoscience and Nanotechnology*, **2015**, *15*, 6193.
26. H.S. Wahab, A.A. Hussain, *Journal of Nanostructure in Chemistry*, **2016**, *6*, 261.
27. A. Patterson, *Physical Review*, **1939**, *56*, 978.

28. O.A. Fouad, G.A.M. Ali, M.A.I. El-Erian, S.A. Makhlouf, *Nano,* **2012**, *7*, 1250038.
29. O.A. Fouad, S.A. Makhlouf, G.A.M. Ali, A.Y. El-Sayed, *Materials Chemistry and Physics*, **2011**, *128*, 70.
30. N. Rohani, F.F. Bamoharram, A. Marjani, M.M. Heravi, *Journal of Nanostructure in Chemistry*, **2017**, *7*, 171.
31. B.S. Surendra, M. Veerabhdraswamy, K.S. Anantharaju, H.P. Nagaswarupa, S.C. Prashantha, *Journal of Nanostructure in Chemistry*, **2018**, *8*, 45.
32. M. Mohamed Jaffer Sadiq, A. Samson Nesaraj, *Journal of Nanostructure in Chemistry*, **2014**, *5*, 45.
33. O. Moradi, M. Aghaie, K. Zare, M. Monajjemi, H. Aghaie, *Journal of Hazardous Materials*, **2009**, *170*, 673.
34. B. Shariatzadeh, O. Moradi, *Polymer Composites,* **2014**, *35*, 2050.
35. R. Zeynolabedin, K. Mahanpoor, *Journal of Nanostructure in Chemistry*, **2017**, *7*, 67.
36. D. Robati, B. Mirza, R. Ghazisaeidi, M. Rajabi, O. Moradi, I. Tyagi, S. Agarwal, V.K. Gupta, *Journal of Molecular Liquids*, **2016**, *216*, 830.
37. S. Agarwal, I. Tyagi, V.K. Gupta, F. Golbaz, A.N. Golikand, O. Moradi, *Journal of Molecular Liquids*, **2016**, *218*, 494.
38. M. Noei, M. Ebrahimikia, N. Molaei, M. Ahadi, A.A. Salan, O. Moradi, *Russian Journal of Physical Chemistry A*, **2016**, *90*, 2221.
39. B. Enayatpour, M. Rajabi, M. Yari, S.M. Reza Mirkhan, F. Najafi, O. Moradi, A.K. Bharti, S. Agarwal, V.K. Gupta, *Journal of Molecular Liquids*, **2017**, *231*, 566.
40. M. Rajabi, K. Mahanpoor, O. Moradi, *RSC Advances,* **2017**, *7*, 47083.
41. H. Mahmoodian, O. Moradi, B. Shariatzadeha, T.A. Salehf, I. Tyagi, A. Maity, M. Asif, V.K. Gupta, *Journal of Molecular Liquids,* **2015**, *202*, 189.
42. F. Najafi, O. Moradi, M. Rajabi, M. Asif, I. Tyagi, S. Agarwal, V.K. Gupta, *Journal of Molecular Liquids*, **2015**, *208*, 106.
43. M. Yari, M. Rajabi, O. Moradi, A. Yari, M. Asif, S. Agarwal, V.K. Gupta, *Journal of Molecular Liquids*, **2015**, *209*, 50.
44. M. Giahi, N. Badalpoor, S. Habibi, H. Taghavi, *Bulletin of the Korean Chemical Society*, **2013**, *34*, 2176.
45. M. Giahi, S. Saadat Niavol, H. Taghavi, M. Meskinfam, *Russian Journal of Physical Chemistry A*, **2015**, *89*, 2432.
46. L.-C. Pop, I. Tantis, P. Lianos, *International journal of hydrogen energy*, **2015**, *40*, 8304.
47. J. Wang, G. Liu, Y. Liu, C. Zhou, Y. Wu, *CLEAN–Soil, Air, Water*, **2017**,
48. D. Robati, B. Mirza, M. Rajabi, O. Moradi, I. Tyagi, S. Agarwal, V.K. Gupta, *Chemical Engineering Journal,* **2016**, *284*, 687.
49. M. Rajabi, B. Mirza, K. Mahanpoor, M. Mirjalili, F. Najafi, O. Moradi, H. Sadegh, R. Shahryari-ghoshekandi, M. Asif, I. Tyagi, S. Agarwal, V.K. Gupta, *Journal of Industrial and Engineering Chemistry*, **2016**, *34*, 130.
50. D. Robati, M. Rajabi, O. Moradi, F. Najafi, I. Tyagi, S. Agarwal, V.K. Gupta, *Journal of Molecular Liquids*, **2016**, *214*, 259.

STUDIA UBB CHEMIA, LXIV, 1, 2019 (p. 19-39)
(RECOMMENDED CITATION)
DOI:10.24193/subbchem.2019.1.02

# THE PRELIMINARY ADSORPTION INVESTIGATION OF *URTICA DIOICA* L. BIOMASS MATERIAL AS A POTENTIAL BIOSORBENT FOR HEAVY METAL IONS

**VLADIMIR D. DIMITRIJEVIĆ[a], MAJA N. STANKOVIĆ[a], DRAGAN M. ĐORĐEVIĆ[a*], IVAN M. KRSTIĆ[b], MILICA G. NIKOLIĆ[a], ALEKSANDAR L.J. BOJIĆ[a] AND NENAD S. KRSTIĆ[a]**

**ABSTRACT.** The removal of Cu(II) ions from aqueous solutions by adsorption onto nettle after incomplete incineration (IIN) has been studied in batch mode. The experimental isotherm results have been fitted using Langmuir, Freundlich, Temkin and Dubinin-Radushkevich equations. A comparison of kinetic models applied to the adsorption of Cu(II) ions on the adsorbent was evaluated for the pseudo-first order, the pseudo-second order and Elovich kinetic models. The pseudo-second order kinetic model was found to correlate the experimental data well. To evaluate competitive adsorption the batch experiments were carried out among the Cu(II), Pb(II) and Cd(II). The affinity order for the ternary system was Pb(II) > Cu(II) > Cd(II). FTIR and SEM analysis indicated that IIN could be used as an efficient biosorbent whose chemical structure and morphology is not altered during adsorption process.

***Keywords:*** *biosorption, heavy metals, kinetic study, thermodynamic study, Urtica dioica L.*

## INTRODUCTION

Heavy metal pollution has become one of the biggest problems in the context of environmental pollution due to their solubility, mobility and ability to accumulate in the soil. Wastes with high content of metals directly or indirectly discharged into the environment which causes its pollution. [1]

[a] *University of Niš, Faculty of Sciences and Mathematics, Department of Chemistry, 18000 Niš, Republic of Serbia*
[b] *University of Niš, Faculty of Occupational Safety, 18000 Niš, Republic of Serbia*
** Corresponding author: dragance73@yahoo.com*

Chemical vapor deposition and electrochemical treatment are not effective for highly diluted solutions and produce a large amount of sludge. On other side, ion exchanges, as well as technology based on purification by membrane, belong to expensive technology.

All rigorous standards of allowable concentrations of contaminants and environmental protection have caused the quest for better and cheaper methods of purification of polluted water. For this purpose, develop various kinds of substances capable to adsorb pollutants. As a particularly significant adsorbent must be mentioned activated charcoal. Activated carbon can be produced starting from different precursors such as peat, wood, stone fruits, etc. [2-6]

The maximum allowed concentration of copper for drinking water which is regulated by the United States Environmental Protection Agency in 2010 is 1.3 mg $dm^{-3}$. [1]

Lead belongs to the group of the highly toxic elements, with a cumulative-toxic effect. Prolonged exposure to low-level toxicity (< 240 μg $dm^{-3}$) can lead to various psychological disorders and learning disabilities among children.

Cadmium is one of the most dangerous poisons of the working and living environment. Once it enters the body, cadmium is transported into the blood by red blood cells and a highly molecular blood protein – albumin. The maximum allowed concentration for drinking water which is regulated by the United States Environmental Protection Agency in 2010 is 5×10-3 mg $dm^{-3}$. [1]

Heavy metal adsorption onto some biomass, such as nettle, grapevine, marigold, linden, geranium, chestnut and maple naturally dried [7], Salvinia [8], Ludwigia stolonifera [9], Urtica dioica and Sedum spectabile [10], nettle [11,12], Neem leaves [13].

Nettle is traditionally used as a medicinal plant. In modern phytotherapy are known different preparations based on nettles. Medicinal raw materials are leaves and above-ground part.[14] In the literature, is also known that this plant is used for phytoremediation. In several studies authors used a nettle ash as a low cost adsorbent for the removal heavy M(II) metals from aqueous solution. [11,12,15-17]

The aim of this study was to show that the product of incomplete combustion obtained from a disused plant material nettle can be used as a potentially inexpensive and readily available biosorbent for the removal of heavy metals from aqueous solutions. A model system for studying the biosorption was a solution of M(II) metal ions (Cu, Pb and Cd) concentration in the range of maximum concentration that could occur in polluted waters from the surrounding city of Nis due to industrial processes. The effect of various experimental parameters such as contact time, initial Cu(II) concentration,

biosorbent dosage and metal ions competition has been investigated. The equilibrium data were fitted to Langmuir, Freundlich, Temkin, and Dubinin–Radushkevich isotherm models, while the kinetics data were correlated according to various kinetics models (pseudo-first order, pseudo-second-order and Elovich model).

## RESULTS AND DISCUSSION

### *FTIR characterization of nettle biosorbent*

FTIR spectra of raw nettle, after incomplete combustion, such as complete combustion and after adsorption treatment are given in Figure 1.

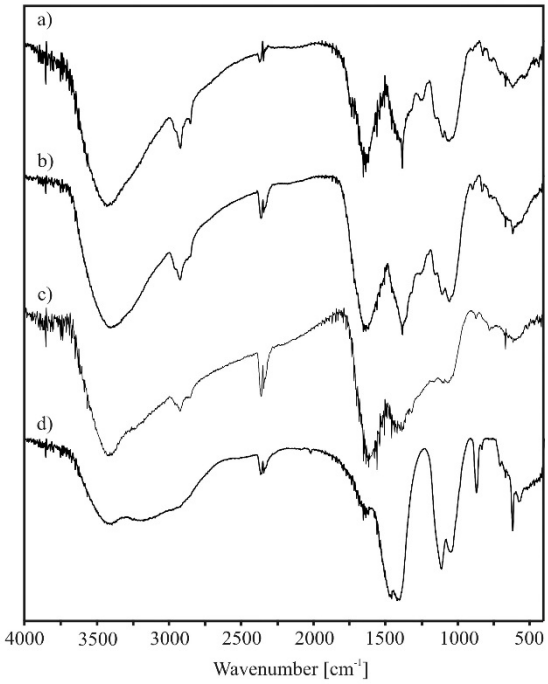


**Figure 1.** FTIR spectra of: a) raw nettle, b) after incomplete incineration nettle, c) after Cu(II) adsorption treatment and d) after complete incineration

The spectrum of raw nettle shows characteristic adsorption bands for a plant material (Fig. 1a). A broad band between 3200 and 3600 $cm^{-1}$ attributed to the hydroxyl groups in phenol and aliphatic structures, bands centered around 2920 $cm^{-1}$, predominantly arising from CH stretching in $–CH_3$ or

–$CH_2$– groups, a band at 1640 $cm^{-1}$ indicates the fingerprint region of CO, C–O and O–H groups. The band at 1383 $cm^{-1}$ corresponding to C-O stretching. The region between 1250 and 1000 $cm^{-1}$ is the fingerprint region, OH, and C-H bending vibration and C-O stretching vibration absorption bands. The intense band at 1061 $cm^{-1}$ can be assigned to the C-O of alcohols and carboxylic acids. Bands in the region from 700 to 400 $cm^{-1}$ are attributed to halogen compounds. [18-23] In the FTIR spectrum of incomplete burning/ incineration nettle shown in Fig. 1b there is no significance changes compared to spectrum of raw plant material, which indicates that it is made incomplete incineration of plant, and all organic functional groups are put on hold. After completed incineration in oven (500-600 °C) all organic matter (functional group) were removed from nettle, which are confirm with presentation of inorganic biomineral bands in FTIR spectra: 3400-3100 $cm^{-1}$ Si-OH vibrations; 1636 $cm^{-1}$ calcium oxalate; 1456 and 1419 $cm^{-1}$ asymmetric calcite stretching; 1112 and 1052 $cm^{-1}$ biogenic silica; 870 $cm^{-1}$ out of plane deformation calcite; 618 $cm^{-1}$, halogenides (Fig. 1d). [24]

The FTIR spectra for the copper loaded biosorbent (Fig. 1c) showed wavenumbers and intensity of some peaks that were shifted or substantially lower than those before biosorption. A band assigned to O–H stretching vibrations showed a decrease in intensity and shift from 3420 to 3428 $cm^{-1}$ probably indicating copper ions interacted with hydroxyl groups. A shifting of band from 1640 $cm^{-1}$ to 1623 $cm^{-1}$ indicates involvement of CO, C–O and O–H groups in copper(II) binding. The band corresponding of C-O stretching was shifted to 1450 $cm^{-1}$, and the bands from region of 1250 and 1000 $cm^{-1}$ showed a decrease in intensity (practically disappear in the spectrum), which also suggests the involvement of C–O and -OH group in binding copper(II) ions. [21,23]

### *SEM-EDX characterization of nettle biosorbent*

The morphological characteristics of biosorbent surfaces were examined by scanning electron microscopy (Fig. 2). It can be observed that material is of fibrous and stripes structure which is characteristic for cellulosic material. After incomplete incineration nettle structure became uneven rugged and porous. These structure characteristics allow better diffusion of solution and probably increase possibility for investigated metal ions to penetrate into the biosorbent and their adsorption onto numerous active sites of biosorbent. There are no differences in the biosorbent structure before and after copper adsorption, and the presence of adsorbed metal ion with SEM cannot be verified due to scale of this micrographs and the dimension of copper ion.

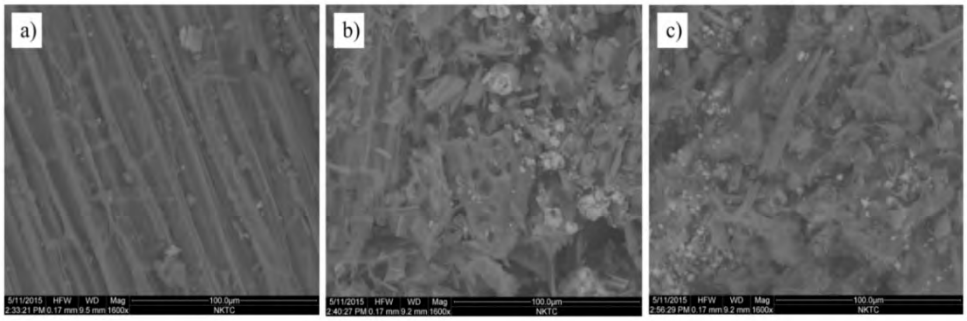


**Figure 2.** SEM micrographs of: a) raw nettle, b) after incomplete incineration nettle and c) after Cu(II) adsorption treatment

EDX analysis of a raw nettle, after incomplete incineration nettle (hereafter IIN) and after biosorption of Cu(II) ions was shown in Figure B. This analysis provides information about elemental content of investigation biomaterial. The presence of C (wt% ca. 60), O (wt% ca. 23) and K (wt% ca. 14) as major elements and other minor elements (P, S, Cl, Mg, and Ca) indicate the chemical composition characteristic for plant material (Fig. 3a). Increase peak intensity (pi) from 1030 to 1740 and weight percent from 60% to 68% for C; and decrease the same parameters for O (pi: from 330 to 240; and wt: from 23 wt% to 14%) compared to untreated nettle indicate incomplete burning treatment of biomaterial (Fig 3b). The presence of peak of copper (Fig 3c) indicate the adsorption of the metal ion to the surface of the nettle biosorbent.

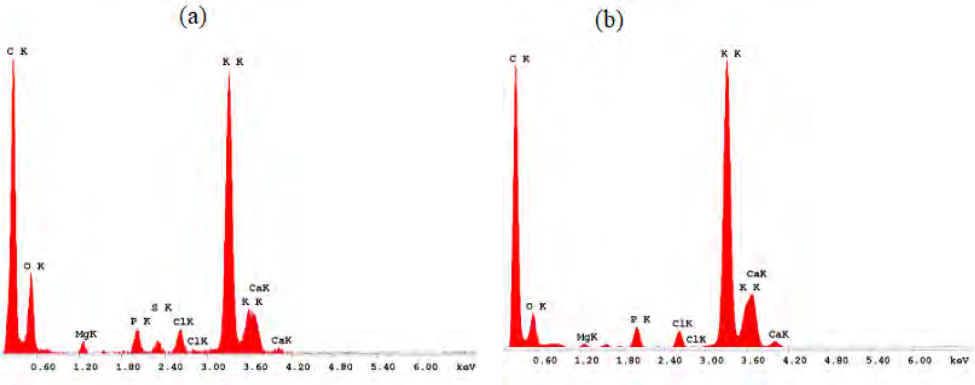


**Figure 3.** EDX spectra of: a) raw nettle, b) after incomplete incineration of nettle

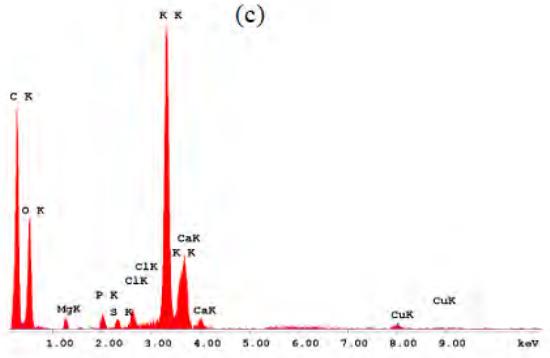


**Figure 3.** EDX spectra of c) after Cu(II) adsorption treatment

### *Effect of biosorbent type on adsorption process*

The effect of contact time on the residual concentration of Cu(II) ions in aqueous solution with raw nettle and nettle after incomplete incineration is shown at Fig. 4.

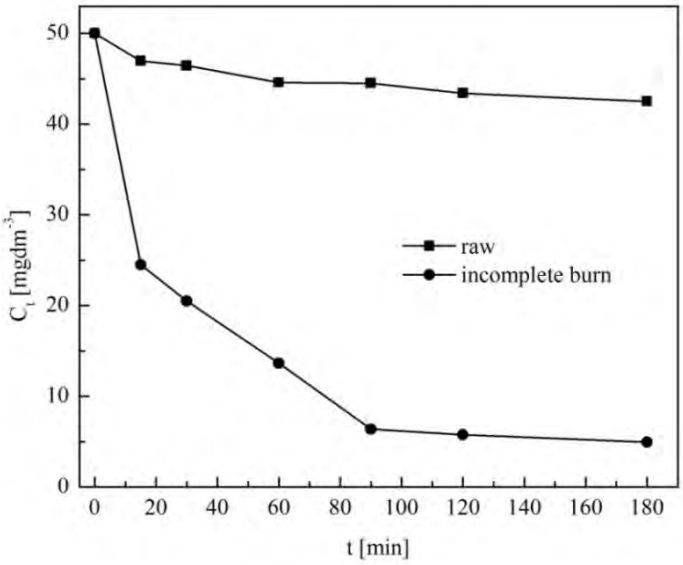


**Figure 4.** Effect of contact time on removal Cu(II) by raw nettle and nettle after incomplete incineration (initial Cu(II) concentration 50 mg dm$^{-3}$, temp. 20±0.5 °C, pH 5.0±0.1, biosorbent dose 4.0 g dm$^{-3}$)

Experiments were performed with model wastewaters containing Cu(II) ions at an initial concentration of 50.0 mg $dm^{-3}$, a biosorbent dose of 4.0 g $dm^{-3}$, at 20±0.5°C and pH 5.0. These results indicate that raw nettle is not efficient biosorbent, but after incomplete incineration it became a very efficient biosorbent for removal Cu(II) ions from wastewater. The concentration of copper declined sharply with contact time in the first 10 min, then decreased slightly to 90 min, and after that reached equilibrium. The initial fast phase occurs due to a high availability of the number of active binding sites (functional groups) on the biosorbent surface, and it is typically controlled by the diffusion process from the solution to the surface. A further increase in contact time did not show a significant decrease of Cu(II) concentration, which occurs due to diffusion of the copper ions into the inner part of the biomass. [21]

### *Effect of initial Cu(II) concentration*

The influence of initial Cu(II) concentration on pollutant removal from aqueous solution by INN (4.0 g $dm^{-3}$) was studied in the concentrations range from 10.0 to 200.0 mg $dm^{-3}$ at 20±0.5 °C and pH 5.0±0.1. The effect of initial Cu(II) concentration on removal efficiency is shown in Fig. 5.

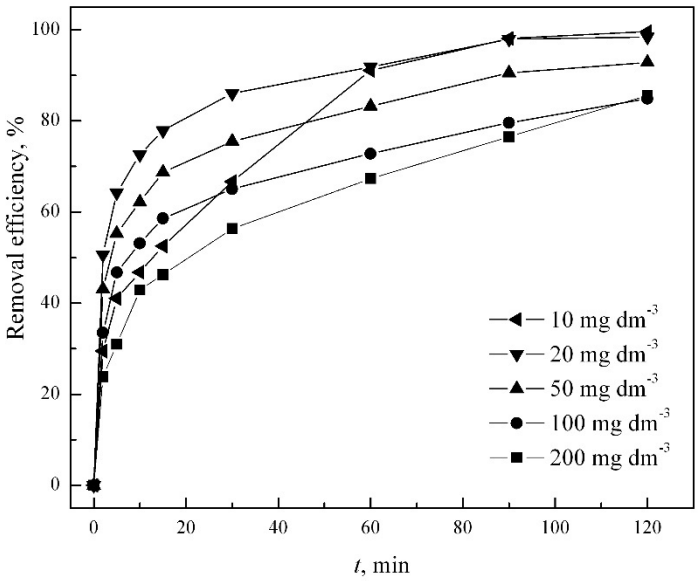


**Figure 5.** Effects of initial Cu(II) concentration on removal Cu(II) by IIN (initial Cu(II) concentration 10.0-200.0 mg $dm^{-3}$, temp. 20±0.5 °C, pH 5.0±0.1, biosorbent dose 4.0 g $dm^{-3}$)

The initial copper concentration is a driving force to overcome mass transfer resistance for metal ion transport between the solution and the surface of the adsorbent. The amount of Cu(II) uptake increased by increasing the initial Cu(II) concentration (Table 1), but adsorption percentages decrease with increase in the Cu(II) concentration. At low concentrations of copper(II) ions, greater availability of the exchangeable sites on the surface area interact with all adsorbate ions present in the solution more rapid reaching the almost 100% adsorption. On the other side saturation of the available active sites on the surface functional groups prevent further copper ion uptake with increase of Cu(II) concentration. [11]

### *Effect of biosorbent dosage*

Batch experiments were performed at different biosorbent dosage ranging from 1.0 to 8.0 g $dm^{-3}$ in contact with model waste waters containing Cu(II) ions at an initial concentration of 50.0 mg $dm^{-3}$ at 20±0.5 °C and pH 5.0±0.1. The influence of biosorbent dosage on removal efficiency is shown in Fig. 6.

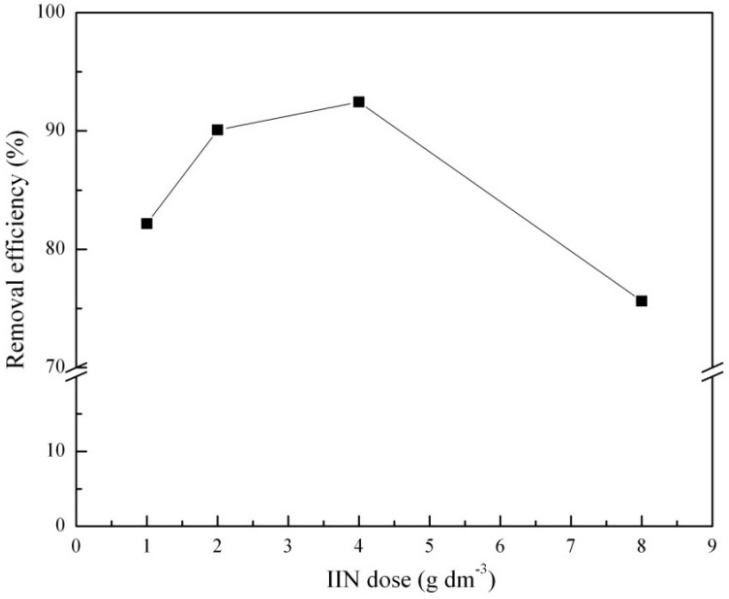


**Figure 6.** Effect of biosorbent dosage in a removal of Cu(II) ions (initial Cu(II) concentration 50.0 mg $dm^{-3}$, temp. 20±0.5 °C, pH 5.0±0.1)

The biosorbent dosage determines the capacity of a biosorbent for a given initial concentration. The biosorption efficiency for Cu(II) ions as a function of biosorbent dosage was investigated. The efficiency of biosorption sharply increases with the biosorbent loading up to 4.0 g $dm^{-3}$. This result can be explained by the fact that the biosorption sites remain unsaturated during the biosorption because the number of sites available for biosorption increases by increasing the biosorbent dosage. [21] However, the copper uptake decreased when the biosorbent concentration exceeded 4.0 g $dm^{-3}$. For the optimum biosorbent dosage 4.0 g $dm^{-3}$ was taken. This dosage showed the highest removal efficiency as shown in Figure 6.

***Sorption kinetics***

Kinetics studies provide information on the rate of the sorption metal uptake which is very important for biosorption process design. [25]

*Pseudo-first-order model*

The pseudo-first order rate equation is represented in logarithmic form as: [26]

$$\ln(q_e - q_t) = \ln q_e - kt \quad (1)$$

where $q_e$ is the mass of metal ions adsorbed at equilibrium (mg $g^{-1}$), $q_t$ is the mass of metal adsorbed at time $t$ (mg $g^{-1}$), and k is the pseudo-first order reaction rate equilibrium constant ($min^{-1}$).

A straight line of $\ln(q_e - q_t)$ vs $t$ indicates that the pseudo-first order kinetics model should be applied. However, in a true pseudo-first order process, $\ln q_e$ should be equal to the intercept and $k$ equal to the slope of plot of $\ln(q_e - q_t)$ against $t$, respectively.

*Pseudo-second-order model*

The pseudo-second-order equation based on equilibrium adsorption can be expressed in linearized form as [27]

$$\frac{t}{q_t} = \frac{1}{k_2 q_e^2} + \frac{1}{q_e} t \quad (2)$$

where $k_2$ is the pseudo-second order reaction rate equilibrium constant (g $mg^{-1}$ $min^{-1}$). For the applicability of the pseudo-second-order kinetics model a plot of $t/q_t$ against $t$ should give a linear relationship.

**Table 1.** Pseudo-first, pseudo-second-order and Elovich model parameters for biosorption of Cu(II) ions using IIN

| | **Concentration Cu(II), mg dm$^{-3}$** | | | | |
|---|---|---|---|---|---|
| | **10.0** | **20.0** | **50.0** | **100.0** | **200.0** |
| $q_e^{exp}$ | 2.49 | 4.92 | 11.60 | 21.22 | 42.81 |
| *Pseudo-first model* | | | | | |
| $k_1$ | 0.0359 | 0.0485 | 0.0338 | 0.0256 | 0.0312 |
| $q_e$ | 2.11 | 2.80 | 6.64 | 12.52 | 15.53 |
| $R^2$ | 0.9941 | 0.9644 | 0.9665 | 0.9560 | 0.5907 |
| *Pseudo-second model* | | | | | |
| $k_2$ | 0.0296 | 0.0527 | 0.0161 | 0.0070 | 0.0075 |
| $q_e$ | 2.76 | 5.04 | 11.91 | 21.65 | 43.40 |
| $R^2$ | 0.9950 | 0.9995 | 0.9987 | 0.9974 | 0.9990 |
| *Elovich model* | | | | | |
| β | 2.1277 | 1.7146 | 0.6629 | 0.3353 | 0.1547 |
| α | 0.7681 | 27.1794 | 27.5691 | 26.088 | 25.749 |
| $R^2$ | 0.9783 | 0.9957 | 0.9987 | 0.9970 | 0.9449 |

The values of $q_{e,exp}$ and the $q_{e,cal}$ from the pseudo-second-order kinetic model were very close to one another. The calculated coefficients of determination for pseudo-second-order kinetics ($R^2$) were closer to 1 than coefficient for the pseudo-first-order kinetics. Overall conclusion is that the pseudo second-order mechanism is predominant and that the adsorption process of the copper(II) ions is most likely to be controlled by the chemisorption process. [11,12]

*Elovich model*

The Elovich model describes many of reaction mechanisms including bulk and surface diffusion and the activation and deactivation of catalytic surfaces: [28]

$$q_t = \frac{1}{\beta}(\ln\alpha\beta) + \frac{1}{\beta}\ln t \qquad (3)$$

where α is the initial adsorption rate (mg g$^{-1}$ min$^{-1}$), and β is the desorption constant (g mg$^{-1}$). If the Elovich equation is applicable with a slope of (1/β) and an intercept of (1/β)ln(αβ), plot of $q_t$ versus ln$t$ should give a linear relationship.

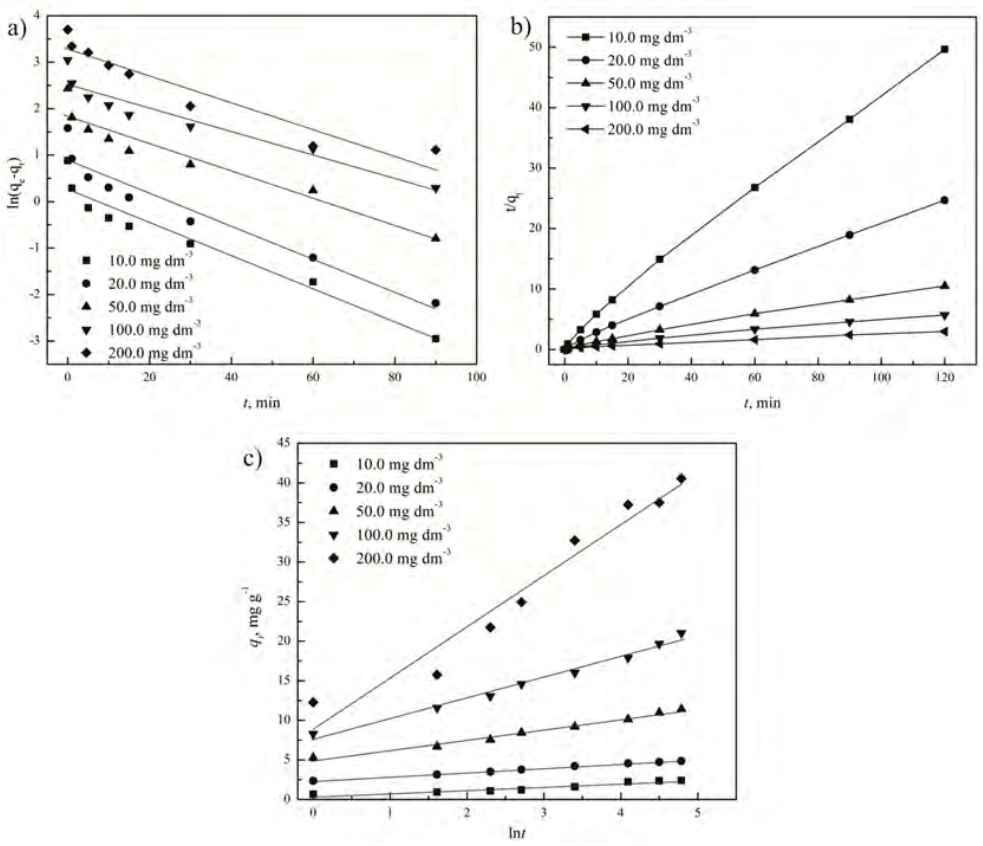


**Figure 7.** Kinetic models a) pseudo-first, b) pseudo-second, c) Elovich

Fig. 7c depicts a plot of the Elovich equation for the investigated data. In this case, a linear relationship between Cu(II) biosorbed, $q_t$ and *lnt* was not obtain for overall concentration range. However, good correlation with the Elovich model was observed for initial copper(II) concentrations of 20.0 mg $dm^{-3}$, 50.0 mg $dm^{-3}$ and 100.0 mg $dm^{-3}$ with determination coefficients of 0.9957, 0.9987 and 0.9970, respectively. Table 1 lists the kinetic constants obtained from the Elovich equation. It can be observed that with increasing the initial copper(II) concentration from 10.0 to 200.0 mg $dm^{-3}$ the value of β decreased from 2.1277 to 0.1547. Nevertheless, the determination coefficients obtained from Elovich equation are lower than those calculated from the pseudo-second-order equation.

### *Adsorption isotherms*

Adsorption isotherm is a graphical representation that maps the distribution of adsorbable solute between the liquid and solid phases at various equilibrium concentrations. [29] The adsorption isotherm data have been got by varying the initial metal concentration while the other parameters are kept constant. Besides to the Langmuir and Freundlich isotherm models, which are commonly used in describing adsorption, the experimental data were fitted to the Temkin and Dubinin-Radushkevich isoterm models.

*Langmuir isotherm model*

This isotherm model describes quantitatively the formation of a monolayer adsorbate on the outer surface of the adsorbent, and after that no further adsorption takes place. Thus, the Langmuir represents the equilibrium distribution of metal ions between the solid and liquid phases. [30] The Langmuir model assumes that the uptake of metal ions occurs on a homogeneous surface by monolayer adsorption without any interaction between adsorbed ions. [31] Based upon these assumptions, Langmuir represented the following equation:

$$q_e = \frac{q_{max} K_L C_e}{1 + K_L C_e} \tag{4}$$

The Langmuir parameters can be determined from a linearized form, by plotting $C_e/q_e$ vs. $C_e$:

$$\frac{C_e}{q_e} = \frac{1}{K_L q_{max}} + \frac{1}{q_{max}} C_e \tag{5}$$

where $C_e$ is the equilibrium concentration of adsorbate (mg $dm^{-3}$), $q_{max}$ is the Langmuir equilibrium constant related to maximum monolayer coverage capacity (mg $g^{-1}$), and $K_L$ is the Langmuir constant which is related to the enthalpy of adsorption ($dm^{-3}$ $mg^{-1}$).

The values of $q_{max}$ and $K_L$ were calculated from the slope and intercept of the Langmuir plot of $C_e/q_e$ vs. $C_e$. [31] This is the most often used isotherm applied for explaining the adsorption equilibrium. However, the Langmuir isotherm offers no insights into the mechanism aspects of biosorption. [32]

*Freundlich isotherm model*

This is commonly used to describe the adsorption characteristics for the heterogeneous surface. It is represented by the equation: [33]

$$q_e = K_F C_e^{\frac{1}{n}} \quad (6)$$

where $K_F$ is Freundlich isotherm constant (mg $g^{-1}$), and n is adsorption intensity.

This model assumes that the uptake of metal ions occurs by multilayer adsorption where the stronger binding sites are occupied first and the binding strength decreases with increasing degree of site occupation. [34,35] This reason it is more indicative for the physical mechanism of adsorption.

Freundlich empirical adsorption isotherm equation can be expressed in the logarithmic, linear form as:

$$\log q_e = \log K_F + \frac{1}{n} \log C_e \quad (7)$$

The constant $K_F$ is an approximate indicator of adsorption capacity, while 1/n is a function of the strength of adsorption in the adsorption process. [36] If n = 1 then the partition between the two phases are independent of the concentration. If value of 1/n is below one it indicates a normal adsorption. On the other side, 1/n being above one indicates cooperative adsorption. [37] 1/n is a heterogeneity parameter, the smaller 1/n, the greater heterogeneity should be expected. This expression reduces to a linear adsorption isotherm when 1/n = 1. If n lies between 1 and 10, this indicates a favorable sorption process. [38]

*Temkin isotherm model*

This isotherm contains a factor that explicitly taking into the account of adsorbent–adsorbate interactions. By ignoring the extremely low and large value of concentrations, the model assumes that heat of adsorption (function of temperature) of all molecules in the layer would decrease linearly rather than logarithmic with coverage. [30,31,34] This equation implies that the adsorption is characterized by a uniform distribution of binding energies, up to some maximum binding energy. [39] The model is given by the following equation: [30,31]

$$q_e = \frac{RT}{b_T} \ln(A_T C_e) \quad (8)$$

$$q_e = \frac{RT}{b_T} \ln A_T + \frac{RT}{b_T} \ln C_e \quad (9)$$

where $A_T$ is Temkin isotherm equilibrium binding constant ($dm^3\ g^{-1}$) which corresponds to the maximum binding energy, $b_T$ is Temkin isotherm constant related to heat of sorption ($J\ mol^{-1}$), R is universal gas constant ($8.314\ J\ mol^{-1}K^{-1}$), and T is absolute temperature (K).

*Dubinin–Radushkevich isotherm model*

The Dubinin-Radushkevish isotherm was chosen to estimate the characteristics porosity of the biomass and the apparent energy of adsorption. [40] Dubinin–Radushkevich isotherm is generally applied to express the adsorption mechanism with a Gaussian energy distribution onto a heterogeneous surface. [41,42] The model has often successfully fitted high solute activities and the intermediate range of concentrations data well. The model is represented by the equation below:

$$q_e=(q_s)\exp(-K_{ad}\varepsilon^2) \tag{10}$$

$$\varepsilon=\left[RT\ln\left(1+\frac{1}{C_e}\right)\right] \tag{11}$$

where $q_s$ is theoretical isotherm saturation capacity ($mg\ g^{-1}$), $K_{ad}$ is Dubinin - Radushkevich isotherm constant ($mol^2\ kJ^{-2}$), and ε is Dubinin–Radushkevich isotherm constant.

Dubinin–Radushkevich isotherm equation can be expressed in the logarithmic, linear form as:

$$\ln q_e=\ln q_s-K_{ad}\varepsilon^2 \tag{12}$$

Table 2 shows the isotherm parameters for Langmuir, Freundlich, Temkin and Dubinin-Radushkevich isotherms. The fitting of the data to the Langmuir, Freundlich, Temkin and Dubinin-Radushkevich isotherms shows that the biosorption of Cu(II) ions by IIN follows Freundlich model better than the others based on the coefficients of determination ($R^2$). This phenomenon suggests that multilayer sorption takes place on the surface of biomass. KF and n were calculated from the slope of the Freundlich plot and were found to be 5.2588 L mg-1 and 1.8468, respectively. The value of KF and n shows high adsorption capacity i.e. easy separation of heavy metal ions from wastewater. The fact that the magnitude of n (which is related to the distribution of bonded ions on the sorbent surface) is greater than 1 represents that adsorption of Cu(II) is favorable. [11,12,23]

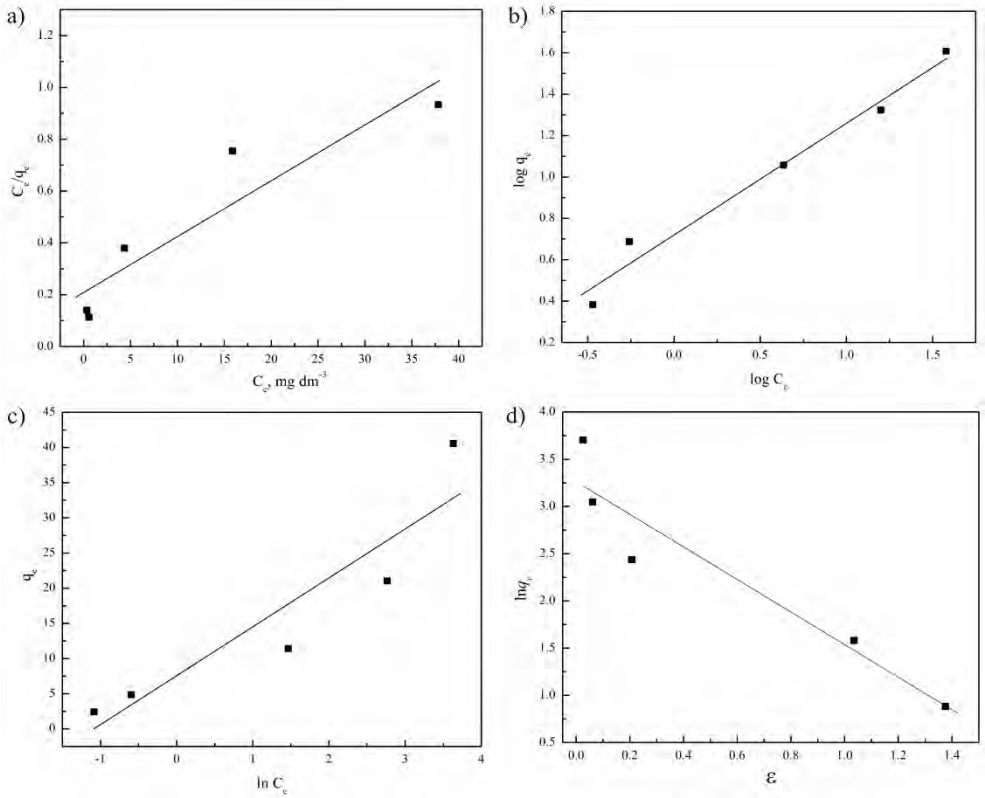


**Figure 8.** The isotherm model plots for adsorption Cu(II) ions onto IIN:
a) Langmuir, b) Freundlich, c) Temkin, and d) Dubinin-Radushkevich

**Table 2.** Langmuir, Freundlich, Temkin and Dubinin-Radushkevich parameters for the adsorption isotherms of Cu(II) by IIN

| **Isotherms** | **Constants** | | |
|---|---|---|---|
| *Langmuir* | $q_{max}$ (mg g$^{-1}$) | $K_L$ (L mg$^{-1}$) | $R^2$ |
| $C_e/q_e=1/K_Lq_{max} + C_e/q_{max}$ | 46.47 | 0.1023 | 0.8193 |
| *Freundlich* | n | $K_F$ (L mg$^{-1}$) | |
| $\log q_e = \log K_F + (1/n)\log C_e$ | 1.8468 | 5.2588 | 0.9698 |
| *Temkin* | $b_T$ (kJ mol$^{-1}$) | $A_T$ (L mg$^{-1}$) | |
| $q_e = (RT/b_T)\ln A_T + (RT/b_T)\ln C_e$ | 352.64 | 2.9208 | 0.8041 |
| *Dubinin-Radushkevich* | $q_s$ | $K_{ad}$ (mol$^2$ kJ$^{-2}$) | |
| $\ln q_e=\ln q_s-K_{ad}\varepsilon^2$ | 26.08 | $2.86\times10^{-7}$ | 0.8741 |

### Adsorption behaviour in ternary solutions

Wastewaters usually contain more than one metal ion and the examination of multiple metal interactions simultaneously is very important for precise interpretation of adsorption data. [43] The competitive adsorption among the Cu(II), Pb(II) and Cd(II) (1:1:1) in the ternary systems were conducted in batch systems with initial total concentration of 50.0 mg $dm^{-3}$ and the biosorption was performed in the same conditions as it is described for a single ion solution. The single metal ion removal efficiency of IIN was 92.0%, 86.8%, and 99.9% for Cu(II), Cd(II) and Pb(II), respectively. The efficiency of metal removal of IIN were found to be 77.4%, 66.6% and 93.0% for Cu(II)–Cd(II)–Pb(II) system (Fig. 9). Therefore, adsorption order in ternary system was found to be Pb(II) > Cu(II) > Cd(II), which is in agreement with previous studies. [44-47] These results indicated the highest decline of 20% in removal efficiency for Cd(II) followed by 15% for Cu(II) and 6% for Pb(II) in comparison to single metal system. It has been already concluded that the metal with the highest uptake capacity in the single metal system showed greater effect of inhibition on the biosorption of other metal ions in the multi-metal system, and when the lead ions exist in aqueous solution, the uptake of copper and cadmium decreased significantly. [48]

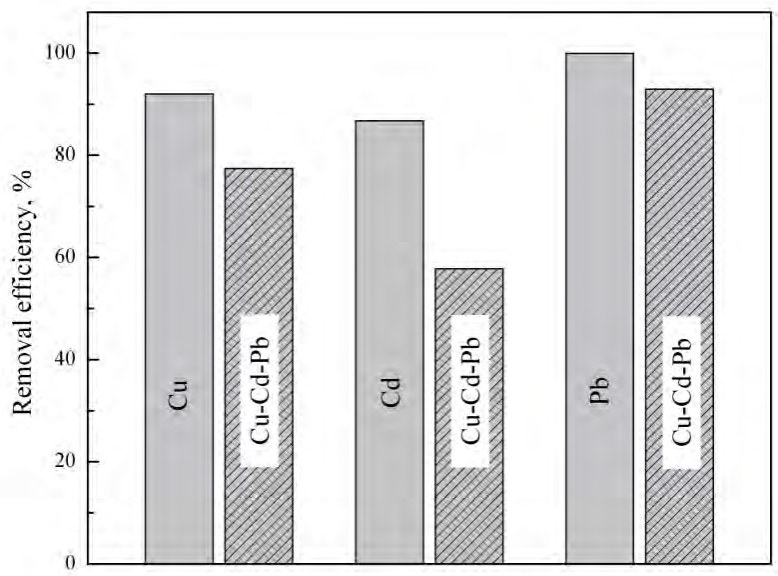


**Figure 9.** Removal efficiency of IIN for Cu(II), Cd(II) and Pb(II) ions for the sorption from the single-metal system and ternary-metals system

## CONCLUSIONS

The present study indicated that the nettle after incomplete incineration (IIN) is an effective adsorbent for the removal of Cu(II) from aqueous solutions. SEM results indicate that surface of raw material has fibrous structure. IIN structure became unequally rugged and porous which presents a suitable morphological profile to bind Cu(II) ions. The effect of contact time on the residual concentration of Cu(II) ions in aqueous solution with raw nettle and IIN indicated that raw nettle is not efficient biosorbent, but after incomplete incineration it became very efficient. Batch experiments with different initial Cu(II) concentrations showed that copper uptake was increased by increasing the initial Cu(II) concentration, but, in the same time, removal efficiency decreases. The optimum biosorbent dosage was determined to be 4.0 g $dm^{-3}$. The sorption kinetics followed the pseudo-second order model. The batch adsorption data was successfully correlated with Freundlich isotherm model ($R^2$ = 0.9698). The competitive adsorption of Cu(II), Pb(II) and Cd(II) (1:1:1) in the ternary systems indicated that in all cases, there was an inhibitory effect of one metal on binding others and that the adsorption order was Pb(II) > Cu(II) > Cd(II).

Nettle is very cheap material and the created sludge could be easily eliminated so nettle can be used as a potentially good biosorbent for the removal of heavy metals from wastewaters.

## EXPERIMENTAL SECTION

### *Reagents and Chemicals*

All chemicals ($CuSO_4 \times 5H_2O$, $Pb(NO_3)_2$, $Cd(NO_3)_2$, Merck) were of analytical grade and used without further purification. Deionized water (<5 µS $cm^{-1}$) was used to prepare all aqueous solutions. Standard stock solutions of metal ions of 1000 mg $dm^{-3}$ were used to prepare appropriate concentrations for the sorption studies. The pH of the solutions was adjusted pH-metrically to the required value with nitric acid or sodium hydroxide (0.1/0.01 M), without buffering. The pH of solutions was determined by a SensION3 (HACH, USA) pH meter.

### *Preparation of biosorbent*

Biosorbent was obtained by incomplete incineration of dried nettle in covered porcelain pot. Nettle of the same levels of vegetation were collected from localities in vicinity of city of Niš (Serbia) and air dried prior to testing.

***FTIR Characterization of biosorbent***

The functional groups available on the surface of nettle before and after preparation, as well as adsorption of Cu(II) ions were detected by KBr technique using FTIR spectroscopy (Bomem Hartman & Braun MB-100 spectrometer). The spectra were recorded at room temperature in a range from 4000 to 400 $cm^{-1}$. The KBr pellets were prepared from 1.5 mg of finely powdered biosorbent dispersed in 150 mg of anhydrous KBr. The obtained FTIR spectra were analyzed using ACD/Labs 10 software.

***SEM-EDX Characterization of biosorbent***

A Scanning Electron Microscope (FEI Quanta 200 microscope) was used to examine the surface morphology of the biosorbent. An energy dispersive X-ray spectrometer with the scanning electronic microscope (SEM-EDX) was used to determine the chemical composition of the biomass before and after metal uptake.

***The batch adsorption experiments***

The adsorption experiments were conducted in 250 $cm^3$ Erlenmeyer flasks, containing 125 $cm^3$ different concentrations (from 10.0 to 400.0 mg dm-3) of the model solution containing Cu(II) ions during 120 min. Aliquots of solutions were withdrawn at preset time intervals, the biomaterial was removed by filtration through a 0.45 μm membrane filter and the filtrates were analyzed for metal ions. All experiments were conducted at ambient temperature (20.0±0.5°C), at initial pH 5.0±0.1 and carried out in triplicates. The experiments were performed using magnetic stirrer on 200 rpm.

Competitive biosorption of Cu(II), Pb(II) and Cd(II) was investigated in ternary system, in 250 cm3 Erlenmeyer flasks containing metals in mass ratio 1:1:1 with total concentration of 50 mg $dm^{-3}$ to avoid increasing of the ionic strength compared to single metal experiment. The experiment was performed during 120 min period.

The concentrations of residual M(II) ions in the solution before and after adsorption were determined by using an atomic absorption spectrophotometer (AASAnalyst 300, Perkin–Elmer, USA) at standard wavelengths for investigated metals.

The adsorption capacity of the biosorbent, $q_e$ (mg $g^{-1}$), at equilibrium was calculated as:

$$q_e = \frac{(C_0 - C_e)V}{m} \tag{13}$$

where qe is the amount of M(II) ion adsorbed per unit weight of the adsorbent, V is the volume of solution, $C_0$ is the initial concentration of metal ion (mg $dm^{-3}$), $C_e$ is the equilibrium metal ion concentration (mg $dm^{-3}$), and m is the mass of the adsorbent (g).

The metal removal efficiency, RE (%), of the adsorbent was estimated according to the following equation:

$$RE = \frac{C_0 - C_e}{C_0} \times 100\% \quad (14)$$

where $C_0$ and $C_e$ are the initial and equilibrium concentrations (mg $dm^{-3}$) of M(II) ions in solution, respectively.

## ACKNOWLEDGMENTS

This work was supported by the Ministry of Education, Science and Technological Development of the Republic of Serbia under Grant TR34008.

## REFERENCES

1. R.S. Nikolić, J.M. Jovanović, G.M. Kocić, N.S. Krstić, Glutathione and Lipoic Acid Benefit Effects on Liver, Kidney, Brain and Pancreatic Tissue from Cd-, Pb- and Cu- Provoked Lipid Peroxidation Monitoring via MDA Content among Wistar Rats. In J. Campbell (ed) "Malondialdehyde (MDA): Structure, Biochemistry and Role in Disease" Nova Science Publishers, Inc.: Hauppauge NY 11788-3619, **2015**, pp. 55-83.
2. N. Das, R. Vimala, P. Karthika, *Indian journal of Biotechnology*, **2008**, *7(2)*, 159.
3. B. Volesky, in "*Biotechnology and Bioengineering Symposium*", **1986**, pp. 121-6 (John Wiley & Sons: New York).
4. B. Volesky, "*Biosorption of heavy metals*", CRC press, Boca Raton, Florida, **1990**.
5. J.L. Wang, "*Immobilization techniques for biocatalysts and water pollution control*", Science Press, Beijing, **2002**.
6. P. Nowicki, M. Skrzypczak, R. Pietrzak, *Chemical Engineering Journal*, **2010**, *162(2)*, 723.
7. C. Biriescu, V. Chiriac, H. Popovici, D. Vlascici, *Annals of West University of Timisoara*, **2012**, *21(1)*, 7.
8. B. Dhir, R. Kumar, *International Journal of Environmental Research*, **2010**, *4(3)*, 427.
9. H. Elifantz, E. Tel-Or*, Water, air, and soil pollution*, **2002**, *141(1-4)*, 207.
10. M. Grubor, *Archives of Biological Sciences*, **2008**, *60(2)*, 239.

11. Z. Mousavy, S. Seyedi, *Journal of the Chilean Chemical Society*, **2010**, *55(3)*, 307.
12. H.Z. Mousavi, S, Seyedi, *International Journal of Environmental Science & Technology*, **2011**, *8(1)*, 195.
13. I. Oboh, E. Aluyor, T. Audu, *Leonardo Journal of Sciences*, **2009**, *14*, 58.
14. D. Kregiel, E. Pawlikowska, H. Antolak. *Molecules*, **2018**, *23(7)*, 1664.
15. C. Malone, D. Koeppe, R.J. Miller, *Plant Physiology*, **1974**, *53(3)*, 388.
16. A.S. Moffat, *Science*, **1995**, *269(5222)*, 302.
17. J. Shaw, "*Heavy metal tolerance in plants: evolutionary aspects"*, CRC press, Boca Raton, Florida, **1989**.
18. C.D. Lingegowda, J.K. Kumar, A.D. Prasad, M. Zarei, S. Gopal, *Romanian Journal of Biophysics*, **2012**, *22(3-4)*, 137.
19. M.N. Stanković, N.S. Krstić, I.J. Slipper, J.Z. Mitrović, M.D. Radović, D.V. Bojić, A. Lj. Bojić, *Australian Journal of Chemistry*, **2013**, *66(2)*, 227.
20. M.A. Maobe, R.M. Nyarango, *World Applied Sciences Journal*, **2013**, *21(8)*, 1128.
21. N.M. Salem, A.M. Farhan, A.M. Awwad, *American Journal of Environmental Engineering*, **2012**, *2(5)*, 123.
22. M.K. Baseri, S. Baker, *Romanian Journal of Biophysics*, **2011**, *21*, 277.
23. Y. Mariswamy, W.E. Gnanaraj, J.M. Antonisamy, *Asian Journal of Pharmaceutical and Clinical Research*, **2012**, *5(2)*, 4.
24. E.J. Baran, C.H. Rolleri, *Brazilian Journal of Botany*, **2010**, *33(3)*, 519.
25. Z. Kariuki, J. Kiptoo, D. Onyancha, *South African Journal of Chemical Engineering*, **2017**, *23*, 62.
26. K.D. Kowanga, E. Gatebe, G.O. Mauti, E.M. Mauti, *The Journal of Phyto Pharmacology*, **2016**, *5(2)*, 71.
27. J.-P. Simonin, *Journal Chemical Engineering*, **2016**, *300*, 254.
28. K. Steve, T. Erika, M. Reynold, T. Paul, "*Activated carbon: A unit operations and processes of activated carbon".* Environmental engineering, 2nd ed. PWS Publishing Co. **1998**.
29. C. Ng, J.N. Losso, W.E. Marshall, R.M. Rao, *Bioresource technology*, **2002**, *85(2)*, 131.
30. M. Barbera, G. Gurnari, "*Wastewater Treatment and Reuse in the Food Industry"*, Springer, **2017**.
31. N. Velinov, S. Najdanović, M. Radović, J. Mitrović, M. Kostić, D. Bojić, A. Bojić, *Cellulose Chemistry and Technology*, **2019**, *53(1-2)*, 175.
32. Y. Liu, Y-J. Liu, *Separation and Purification Technology*, **2008**, *61(3)*, 229.
33. N.D. Hutson, R.T. Yang, *Adsorption*, **1997**, *3(3)*, 189.

34. N. Ayawei, A.T. Ekubo, D. Wankasi, E.D. Dikio, *Oriental Journal of Chemistry*, **2015**, *31(3)*, 38.
35. Y. Khambhaty, K. Mody, S. Basha, B. Jha, *Chemical Engineering Journal*, **2009**, *145(3)*, 489.
36. E. Voudrias, K. Fytianos, E. Bozani, *Global Nest International Journal*, **2002**, *4*, 75.
37. S.V. Mohan, J. Karthikeyan, *Environmental Pollution*, **1997**, *97(1)*, 183.
38. S. Goldberg, Equations and Models Describing Adsorption Processes. In M.A. Tabatabai, D.L. Sparks (eds) "Chemical Processes in Soils" SSSA Book Series 8, Soil Science Society of America: Madison, WI, **2005**, pp. 489-517.
39. Y. Kim, C. Kim, I. Choi, S. Rengaraj, J. Yi, *Environmental science & technology*, **2004**, *38(3)*, 924.
40. M.J. Horsfall, A.I. Spiff, A. Abia, *Bulletin of the Korean Chemical Society*, **2004**, *25(7)*, 969.
41. A. Günay, E. Arslankaya, I. Tosun, *Journal of Hazardous Materials*, **2007**, *146(1)*, 362.
42. A. Dąbrowski, *Advances in colloid and interface science*, **2001**, *93(1)*, 135.
43. A. Hammaini, F. Gonzalez, A. Ballester, M. Blázquez, J. Munoz, *Minerals Engineering*, **2003**, *16(8)*, 723.
44. D.-L.D. Mitić, "Removal of heavy metals from water using biosorbent based on Lagenaria vulgaris", PhD, **2012**, University of Niš, Serbia, Niš, Serbia.
45. W-B. Lu, W-C. Kao, J-J. Shi, J-S. Chang, *Journal of hazardous materials*, **2008**, *153(1)*, 372.
46. S.K. Papageorgiou, F. Katsaros, E. Kouvelos, N. Kanellopoulos. *Journal of Hazardous Materials*, **2009**, *162(2)*, 1347.
47. Y.-R. Cao, Z. Liu, G-l. X-b. Jing, H Xu, *Chemical Engineering Journal*, **2010**, *164(1)*, 183.
48. C. Mahamadi, T. Nharingo Cheng, *Bioresource Technology*, **2010**, *101(3)*, 859.

STUDIA UBB CHEMIA, LXIV, 1, 2019 (p. 41-52)
(RECOMMENDED CITATION)
DOI:10.24193/subbchem.2019.1.03

# LEAD AND COPPER REMOVAL FROM MULTI-METAL CONTAMINATED SOILS THROUGH SOIL WASHING TECHNIQUE USING HUMIC SUBSTANCES AS WASHING AGENTS: THE INFLUENCE OF THE WASHING SOLUTION pH

**GIANINA ELENA DAMIAN[a*], VALER MICLE[a], IOANA MONICA SUR[a]**

**ABSTRACT.** The effect of three humic washing solution pH values (3.0, 7.0 and 9.6-its natural pH) on the removal efficiency of Pb and Cu from multi-metal contaminated soil collected nearby "Larga de Sus" mine from Zlatna (Alba County, Romania) was investigated, at laboratory scale, by an ex-situ soil washing technique. In this study, a commercial soluble humic sample extracted from German Leonardite was used as washing agent to remove Pb and Cu from polluted soil. Soil washing experiments were conducted in a stirrer with orbital-rotation oscillation at a liquid/solid ratio (L/S ratio; mL:g) of 8:1, concentration of humic washing solution of 2% and various stirring times (4, 6, 12, 24 and 40 hours). The removal efficiency of Cu and Pb increased with increasing pH from 3.0 to 9.6. In investigated experimental conditions, the best removal efficiencies (60.3% in case of Cu and 48.08% in case of Pb) were obtained at alkaline pH values of humic washing solution.

***Keywords:*** *humic substances, soil washing, heavy metals, washing solution pH*

## INTRODUCTION

Soil contamination with lead and copper is a worldwide concern associated with anthropogenic activity, especially with mining and metallurgical activity [1]. Up to now, there are a variety of decontamination methodologies for soil remediation. Soil washing, that generally uses chemical solutions to

[a] *Technical University of Cluj-Napoca, Faculty of Materials and Environmental Engineering, Department of Environmental Engineering and Sustainable Development Entrepreneurship, 103-105 Muncii Ave, Cluj Napoca, Romania*
** Corresponding author: gianina_ln@yahoo.com*

extract heavy metals from soil, represents a valid, efficient, rapid, relatively inexpensive and very promising method for removing heavy metals from multi-metal contaminated soils, as reported by many researchers [2-6]. However, soil washing is a promising strategy if the applied extracting agent minimally changes the original solid matrix, original characteristics and does not leave toxic residues in the treated soil [7]. For these reasons, humic substances that are natural organic compounds ubiquitous in the environment [8] may have the potential of becoming extracting agents in soil washing technology because are environmentally benign, can support soil structure and improve soil physical, chemical and biological properties [9]. They have a strong propensity to form stable complexes with heavy metals cations in the pH range encountered in the soil environment [10]. Humic carboxylic -COOH and phenolic -OH groups from their structure besides alcoholic and amin functional groups are mainly involved in the formation of metal-humic complexes [11].

However, the ability of humic substances to complex with cations is strongly pH dependent. Humic substances change their structure depending on pH and the type of metals present. Humic substances are made up of hundreds of different molecules of many different sizes with many ways to orient themselves by twisting, bending, compressing, and expanding. They are held together loosely by weak forces in a colloidal state. Slight changes in pH will actually cause the humic polymers to fracture, breaking up the original molecules. The fractured molecules are then free to associate with numerous other free radicals, metals or impurities. High pH makes humic substances open up their long-chain polymers, whereas low pH makes them close (aggregation of the humic molecules) [12]. Increasing the $H^+$ concentration (decreasing pH) causes the protonation of the humic carboxylic -COOH groups, which eventually leads to precipitation - this usually begins at pH ~ 3-2 and reaches completion at pH ~ 2-1 [13]. The aggregation reduces the exposure of functional groups [12]. Deprotonating of these functional groups occurs at increasing pH and these behave as negatively charged moieties, attracting the positively charged heavy metal ions and protons (binding heavy metals) [14]. It is known that humic substances have a higher affinity for $Pb^{2+}$ and $Cu^{2+}$ that react with carboxylic and phenolic groups. The higher pH of the solution, the higher is the adsorption ability of the ions [15].

Therefore, investigating extractability of Cu and Pb from contaminated soil using humic substances solution as a function of washing solution pH is of great interest in terms of environmental impact of these metals and due to the ability of humic substances to change their structure for bounding Cu and Pb and others heavy metals as a function of pH.

Inspite of the fact that many researchers studied the potential of humic substances to extract heavy metals from contaminated soil through soil washing, investigating various factors affecting the process [3-5, 9, 10, 16], not much attention has been given to investigating the ability of humic substances to extract Cu and Pb from soil as a function of pH and on the effect of humic solution pH on the Cu and Pb removal efficiency [6, 17, 18].

Consequently, the aim of the present research was to investigate the influence of the humic washing solution pH on the Cu and Pb removal from soil collected nearby “Larga de Sus” mine from Zlatna (Alba County, Romania) using commercial humic substances extracted from Leonardite as washing agent for contaminated soil and to extend the knowledge regarding the ability of humic substances to extract Cu and Pb from soils at various humic solution pH values.

## RESULTS AND DISCUSSION

*Soil characterization*. The initial values of heavy metals concentration in the soil sample collected nearby “Larga de Sus” mine are significant and were compared with normal values and threshold limits established by Romanian legislation [19]. As it can be seen in Figure 1, the concentration of Cu and Pb exceeds more than 2 and 6 times the intervention threshold limit, respectively.

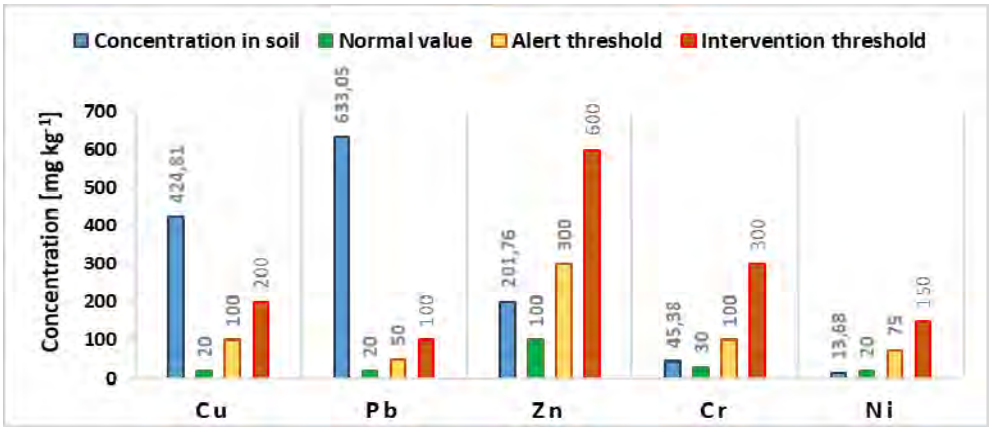


**Figure 1.** Heavy metals concentration of soil collected nearby “Larga de Sus” mine

On the contrary, the concentration of Zn and Cr in soil sample used in washing experiments exceeds only the normal value of Zn and Cr stipulated by the same legislation, while Ni concentration doesn't exceed any limit established by Romanian legislation in case of Ni.

According to the measured pH value, soil collected nearby "Larga de Sus" mine was classified as slightly acidic (pH: 5.86).

*Washing experiment results*. The influence of the humic washing solution pH on the Cu and Pb removal efficiency from soil collected nearby "Larga de Sus" mine in comparison with blank samples (samples without humic substances) at various pH values, along stirring time is illustrated in Figure 2.

Along investigated stirring time, Cu removal efficiency from soil collected nearby "Larga de Sus" mine increase as the pH of the humic washing solution increase (Figure 2a). Highest Cu removal efficiency (60.3 %) was observed in case of using humic washing solution at an alkaline pH (9.6-its natural pH), while the lowest Cu removal efficiency, ranging from 1.1% to 18.7%, was recorded in acidic conditions (pH of humic washing solution: 3.0). Instead, in the absence of humic substances in the washing solution, when pH was increased, Cu removal efficiency from soil collected nearby "Larga de Sus" mine decreased (Figure 2a). In the absence of humic substances in the washing solution, when pH was increased from acidic to alkaline values, Cu removal efficiency decreased from values range between 38.3% and 43.2% to values range between 4.1% and 9.5%, along investigated stirring time. This fact was expected as it is well known that using distilled water with strong acids as washing solution for heavy metal contaminated soil favors the extraction of heavy metals from soil. Similar percentages (40%-61%) were obtained by Moutsatsou et al. (2006) when studied the extractability of heavy metals from multi-metal contaminated soil using 1M HCl as washing agent.

In the presence of humic substances in the washing solution, at pH 7.0 the Cu removal efficiency range from 10.4% to 27.4% along investigated stirring time, while in the absence of humic substances in the washing solution, Cu removal efficiency range from 22.7% to 26.5% along investigated stirring time.

The results indicated in Figure 2a also show that Cu removal efficiency was improved with more than 2 to 9 times when washing solution contained humic substances besides distilled water (pH 9.6) unlike when measurements were made on samples in absence of humic substances.

But, in acidic conditions, Cu removal efficiency decreased by 2 to 38 times when washing solution contained humic substances besides distilled water and HCl than when the humic substances were missing from washing

solution. The same fact was observed after 4, 12, 24 and 40 hours at pH 7. Thus, the ability of humic substances to remove Cu from soil is inhibited in acidic conditions (in the presence of HCl). Others authors [17] have also reported similar findings for removal of Cu from soil by humic substances and suggested that the decreasing of Cu removal efficiency with decreasing the humic washing solution pH may be attributed to the fact that a low pH values (pH 2-3), humic substances molecules become more compact, its functional groups (mainly humic carboxylic -COOH groups) involved in the formation of metal-humic complexes protonate and thus the ability of humic substances to attract the positively charged heavy metal ions is decreased [12-14]. Whereas, improved Cu removal efficiency at higher pH is due to the increased formation of Cu-humate complexes and because there is no strong competition from $H^+$ for COOH binding sites [17].

In the case of Pb (Figure 2b), at shorter stirring times (up to 6 hours), increasing humic washing solution pH to 9.6 does not led to an important increase in Pb removal efficiency. Instead, Pb removal efficiency even decreased with increasing pH of the humic washing solution. More accurate, Pb removal efficiency was 11.9%, 11.02% and 0.29% in the case of the pH of the humic washing solution of 3.0, 7.0 and 9.6, respectively. The same fact was observed in absence of humic substances along all investigated stirring time: as pH was increased, Pb removal efficiency decreased from values range between 14.6% and 37.9% to values range between 0.7% and 4.1%.

But, at 6 hours of stirring, increasing humic washing pH from 3.0 to 9.6 led to an increase in Pb removal efficiency from 23.9% to 48.08%. After 6 hours of stirring, the values of Pb removal efficiency obtained in case of humic washing solution at pH 3.0, 7.0 and 9.6 (23.9%, 27.2% and 48.08%) are higher than the value obtained on samples in absence of humic substances (17.1%, 11.7% and 1.54%). The improved Pb removal efficiency observed in the presence of humic substances at high pH values is because there is no strong competition from $H^+$ for COOH binding sites of the humic substances [17] and could be attributed to the fact that humic substances open up their long-chain polymers, the humic carboxylic -COOH groups deprotonate and behave as negatively charged moieties, attracting the positively charged Pb ions [12-14] increasing the formation of Pb-humate complexes.

After this stirring time, in the presence of humic substances in the washing solution, Pb removal efficiency does not follow the same trend. Thus, after 12 hours of stirring, Pb removal efficiency was highest at pH 3.0 (35.4%) and at pH 9.6 (34.1%) than at pH 7.0 (15.7%). After 12 hours of stirring, at all investigated pH values, the Pb removal efficiency is higher in the presence of humic substances than in the absence of humic substances in washing solution (Figure 2b).

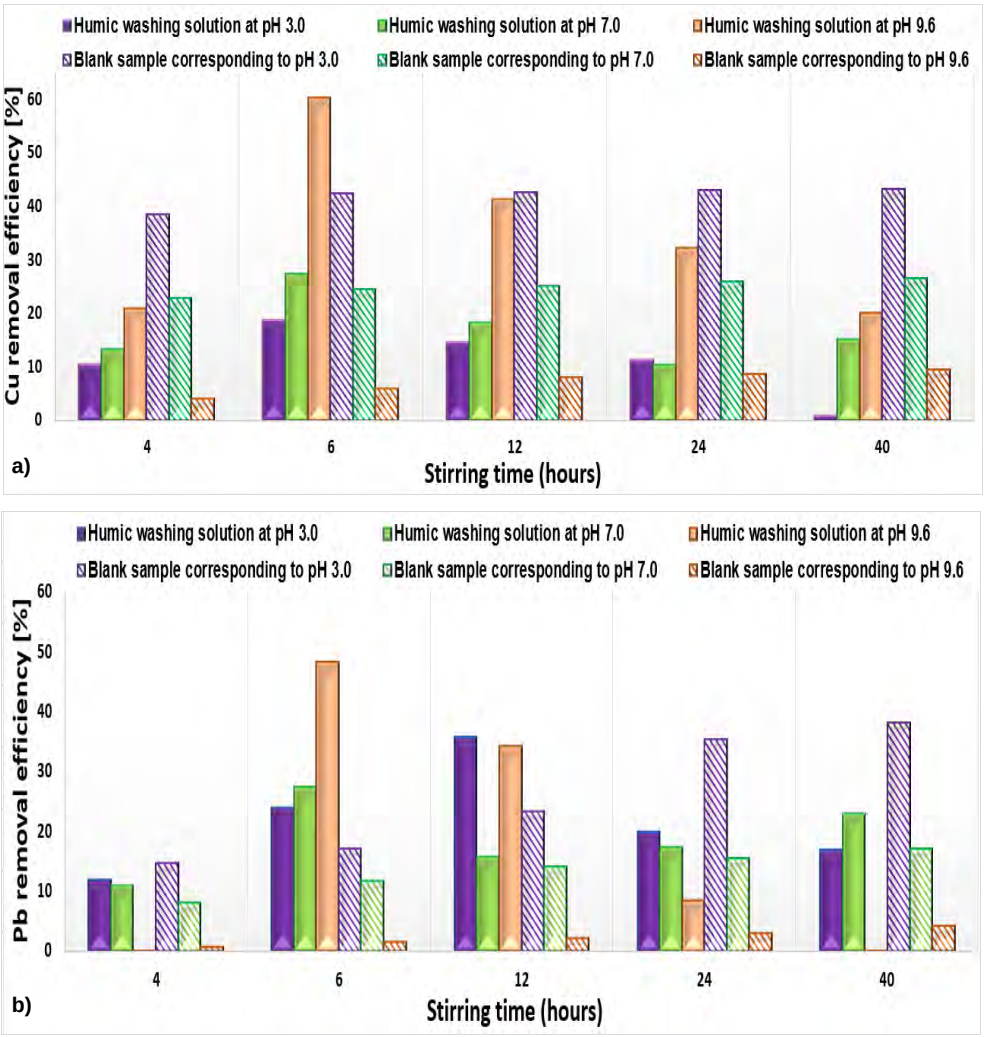


**Figure 2.** The effect of the washing solution pH on Cu (a) and Pb (b) removal efficiency from soil during investigated stirring time

After 24 hours of stirring, the Pb removal efficiency is higher in the presence of humic substances in washing solution than in the absence of humic substances in washing solution except for acidic conditions when the absence of humic substances in washing solution gave better results. In the presence of humic substances in the washing solution, Pb removal efficiency

slightly increased with decreasing pH of the humic washing solution and after the investigated stirring time (40 hours), Pb removal efficiency was highest at pH 7.0 (22.8%) than at pH 3.0 and 9.6. Similar results were obtained by Kulikowska et al. (2015) that noted that Pb removal using humic substances from sewage sludge compost was highest at pH 7.0 than at alkaline and acidic pH or having the same value on both acidic and alkaline conditions. Others authors reported that Pb removal efficiency with citric acid decreased with increasing pH (over pH = 4.0) [20]. Also, Pb solubility reached a maximum at pH 7.1 and then decreased presenting insignificant alteration up to pH = 8.9 when Pb mobilization under 0.1M EDTA was studied [2].

The observed variation of Pb removal efficiency with pH along stirring time, in the presence of humic substances in the washing solution, indicates that the optimal pH for leaching Pb from soil collected from “Larga de Sus” mine using humic washing solution depends also on stirring time. Thus, at shorter stirring times (up to 6 hours) and at longer stirring times (over 24 hours) acidic or neutral pH is more indicated for humic washing solution than alkaline pH in order to obtain highest Pb removal efficiencies, whereas between 6-12 hours of stirring alkaline pH would give better removal efficiencies than neutral and acidic pH. Besides stirring time available and chosen for soil remediation, choosing the optimal pH of the humic washing solution for leaching Pb from soil collected from “Larga de Sus” mine should also depend on the optimal pH of the humic washing solution for leaching Cu and others heavy metals present in the soil sample.

Thus, after 6 hours of stirring, an alkaline pH (9.6) of the investigated humic washing solution would give the highest removal efficiency for both Cu and Pb (60.3% and 48.08%), whereas if only shorter stirring time is available for soil remediation (up to 4 hours), a neutral pH of the investigated humic washing solution will be best to effectively remove both Cu and Pb than acidic or alkaline pH. But to generalize this statement, should also consider the influence of the humic washing solution pH on leaching others heavy metals or others pollutants present in the soil sample in order to achieve an effective and whole soil remediation.

The variation of Cu and Pb concentration from soil collected nearby “Larga de Sus” mine as a function of humic washing solution pH, along stirring time is illustrated in Figure 3.

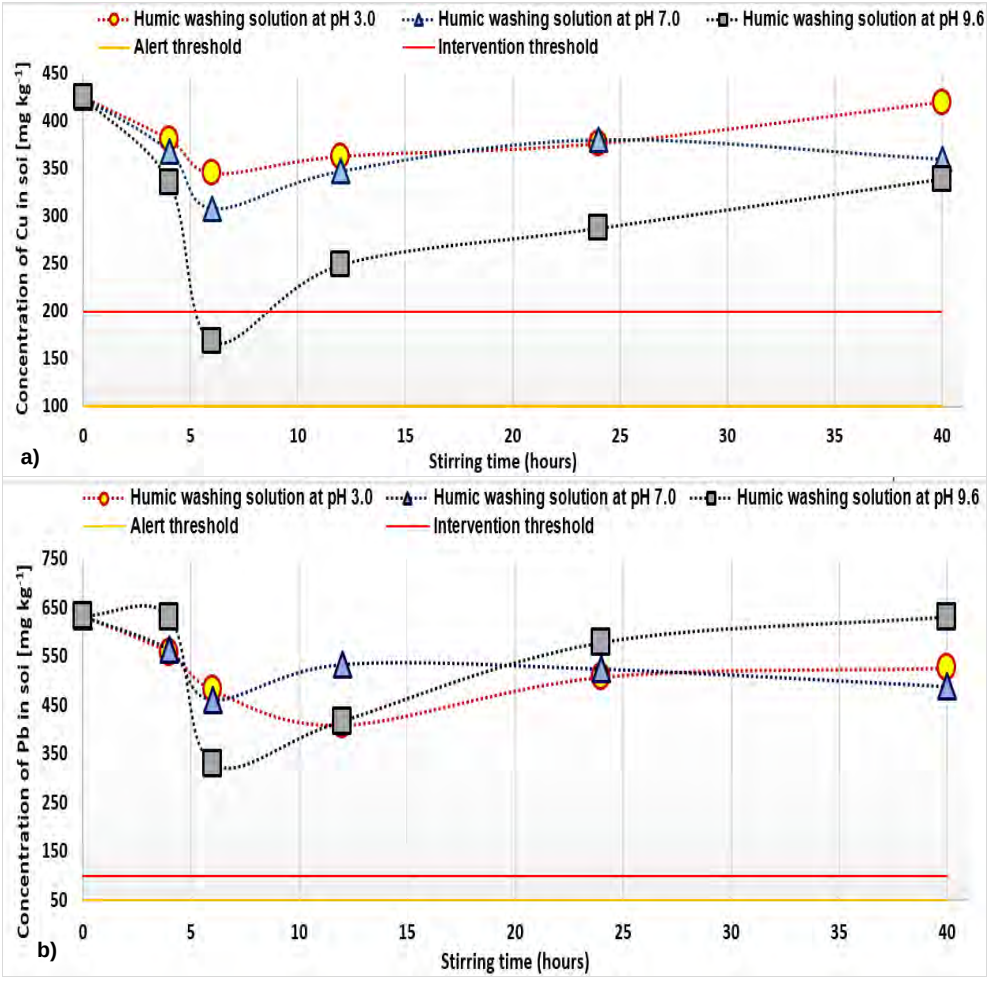


**Figure 3.** The variation of Cu (a) and Pb (b) concentration in soil during investigated stirring time as a function of humic washing solution pH

In investigated experimental conditions, after 6 hours of stirring, the concentration of Cu from soil decreased with more than 30 mgkg$^{-1}$ below the intervention threshold limit (200 mgkg$^{-1}$) established by Romanian legislation [19] when pH of the humic washing solution was 9.6 (Figure 3a). The concentration of Pb from soil decreased to almost half of its initial value, after 6 hours of stirring, in case of humic washing solution with pH 9.6 (Figure 3b), but didn't decrease under the alert limits established by the same legislation.

Along all investigated stirring time, when pH of the humic washing solution was decreased to neutral and acidic pH values, the limits established by the Romanian Legislation were reached neither in the case of Cu nor in the case of Pb.

Thus, the removal of Cu and Pb from the soil collected from "Larga de Sus" mine in the presence of humic substances in washing solution is favored by high pH values of the washing solution. In the absence of humic substances in the washing solution, the removal of Cu and Pb from studied soil is favored by low pH values of the washing solution.

## CONCLUSIONS

The present study has evidenced that Cu and Pb removal from soil collected nearby "Larga de Sus" mine from Zlatna (Alba County, Romania) using commercial humic substances extracted from Leonardite as washing agent is highly dependent on humic washing solution pH and on stirring time.

In the presence of humic substances in the washing solution, the Cu removal efficiency increase with increasing the pH of the humic washing solution. The highest Cu removal efficiency (60.3 %) was observed after 6 hours of stirring, in case of using humic washing solution at an alkaline pH (9.6-its natural pH), while only 10.4-27.4% and 1.1-18.7% of Cu was leached at pH 7.0 and 3.0, respectively. In the absence of humic substances in the washing solution, the highest Cu removal efficiency (43.2%) was obtained in acidic conditions.

In case of Pb, in the presence of humic substances in the washing solution, the results indicated that optimal pH for leaching Pb from soil collected from "Larga de Sus" mine depend more on stirring time, acidic or neutral pH being more indicated than alkaline pH up to 6 hours and over 24 hours of stirring. After 6 hours of stirring, an alkaline pH (9.6) of the investigated humic washing solution gave the highest removal efficiency for both Cu and Pb (48.08%). The values obtained after 6 hours of stirring are significantly higher in the presence of humic substances in washing solution (pH 9.6-natural pH) than in the absence of humic substances in the washing solution (pH 3.0), for both Cu and Pb.

## EXPERIMENTAL SECTION

*Study area and sampling*. The contaminated soil sample used in soil washing experiments was collected from 10-90 cm depth from a pasture located at about 800 meters downstream the "Larga de Sus" mine (Figure 4).

The study area falls within the Zlatna mining perimeter located in South Apuseni Mountains (Alba County, Romania), where the extraction of gold-silver and polymetallic ores of Cu, Zn, and Pb date from the Dacian-Roman period [21].

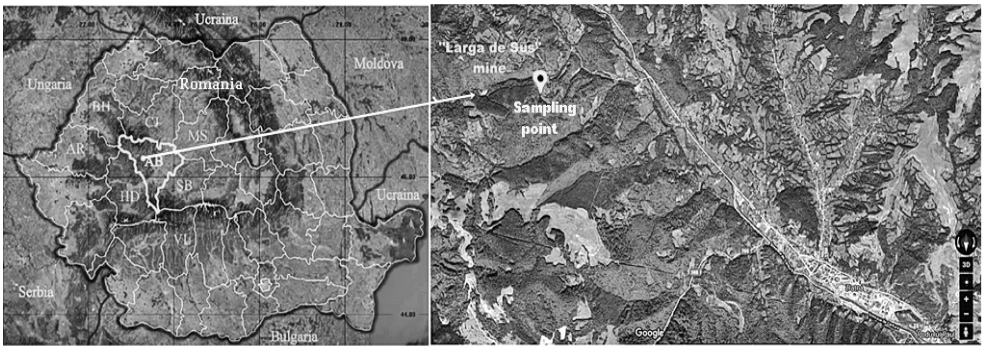


**Figure 4.** Location of the "Larga de Sus" mine and sampling point

Heavy metals concentration of the collected soil sample was determined through Atomic Absorption Spectrometry (AAS) using a SHIMADZU AA-6800 spectrometer.

Prior to the AAS analysis, the soil sample was dried at 95°C, crumbled and milled to pass through a 250 µm sieve. Then, 3g of the processed sample was placed with 1ml distilled water, 21 ml of concentrated HCl (Hydrochloric Acid) and 7 ml of concentrated $HNO_3$ (Nitric Acid) in a 100 ml glass flask and left for mineralization for 2 hours (glass flask was heated on a sand bath).

The mineralised sample was then filtered into a 100 ml volumetric flask, filled to the mark with distilled water and analysed for heavy metal concentration.

Reference solutions for spectrometer calibration were also prepared using analytical grade chemicals and distilled water.

Soil pH was measured in a suspension of soil and distilled water at a L/S ratio (mL:g) of 2.5:1 using a Hanna HI 3512 pH-meter.

*Humic substance*. The heavy metals concentration of the humic sample was determined by AAS. For the AAS analysis, humic sample, dissolved in distilled water in which was added hydrogen peroxide ($H_2O_2$) at a humic substances solution:$H_2O_2$ ratio of 5:1, was mineralized for 1 hour on a sand bath. After cooling, mineralized sample was filtered through 0.45 µm pore size filter into a 50 ml glass flask and analysed for heavy metals concentration using a SHIMADZU AA-6800 spectrometer.

pH of the humic sample was measured using a Hanna HI 3512 pH-meter in a suspension of humic substance and distilled water at a L/S ratio of 20:1 ($mLg^{-1}$). The results obtained are summarised in Table 1.

**Table 1.** Characteristics of humic sample used for soil washing experiment

| Parameter | Unit | Value | Parameter | Unit | Value |
|---|---|---|---|---|---|
| Water content | % | 17.7[a] | pH | - | 9.60[b] |
| Loss of ignition of dry substance as humic acids | % | 70.7[a] | Cu | mg $L^{-1}$ | 0,6785[b] |
| | | | Pb | mg $L^{-1}$ | < IDL*[b] |
| Calcium (Ca) | mgkg$^{-1}$ | 10300[a] | Ni | mg $L^{-1}$ | 0,1433[b] |
| Potassium (K) | mgkg$^{-1}$ | 99300[a] | Cr | mg $L^{-1}$ | < IDL*[b] |
| Magnesium (Mg) | mgkg$^{-1}$ | 1230[a] | Zn | mg $L^{-1}$ | < IDL*[b] |

[a] provided and determined by Humintech GmbH (supplier) through accredited laboratories
[b] determined
*IDL: Instrument detection limit

*Soil washing experiment*. The soil washing experiment using washing solution with humic substances and washing solution without humic substances (blank washing solution) was conducted at a L/S ratio of 8:1 (mLg$^{-1}$) in a 100 ml batch reactor with continuous orbital rotation-oscillation stirring at 100 oscillations/minute. Polluted soil was stirred with blank washing solution and 2% humic washing solution having different pH values (3.0, 7.0 and 9.6) for different time intervals (4, 6, 12, 24 and 40 hours) then samples were collected and filtered through 0.45 µm pore size filter. The natural pH of the humic washing solution (9.6) was decreased to neutral and acidic values using concentrated HCl (35-38%), pH being measured using a Hanna HI 3512 pH-meter. The pH of the blank washing solution was decreased with the same volume of concentrated HCl used to decrease the pH of the humic washing solution.

The concentration of Cu and Pb from treated soil samples was determined by AAS. For the AAS analysis, treated soil samples were subjected to the same processing steps as explained above.

Removal efficiency of metal ions by soil washing was calculated using the following equation [14]:

$$\textit{Removal efficiency (\%)} = [(C_0 - C_F) / C_0] * 100$$

where, $C_0$ is initial metals concentration (mgkg$^{-1}$) of soil, and $C_F$ is the final concentration of metals (mgkg$^{-1}$) in soil, after soil washing treatment.

All the experiments and analyses were performed in duplicate at 25°C and the average values were reported. All chemicals were of analytical grade or ultra-pure.

## ACKNOWLEDGMENTS

The authors thank sales team from S.C. SEMPLANT ROMHOL S.R.L Company (Bucharest, Romania) and HUMINTECH GmbH Company (Grevenbroich, Germany), for supplying the soluble humic sample extracted from German Leonardite (commercially found as Powhumus WSG-85).

## REFERENCES


1. I.M. Sur, V. Micle, T. Gabor, *Studia UBB Chemia*, **2016**, *LXI (3)*, 355.
2. A. Moutsatsou, M. Gregou, D. Matsas, V. Protonotarios, *Chemosphere*, **2006**, *63*, 1632.
3. M. Soleimani, M.A. Hajabbasi, M. Afyuni, S. Akbar, *Journal of Environmental Quality Abstract*, **2010**, *39*, 855.
4. O.K. Borggaard, H.C.B. Hansen, P.E. Holm, J.K. Jensen, S.B. Rasmussen, N. Sabiene, L. Steponkaite, B.W. Strobel, *Soil and Sediment Contamination: An International Journal*, **2009**, *18*, 369.
5. O.K. Borggaard, P.E. Holm, J.K. Jensen, M. Soleimani, B.W. Strobel*, Acta Agriculturae Scandinavica, Section B - Soil and Plant Science*, **2011**, *61,* 577.
6. T. Yang, M.E. Hodson, *Science of the Total Environment*, **2019**, *647*, 290.
7. M. Race, R. Marotta, M. Fabbricino, F. Pirozzi, R. Andreozzi, L. Cortese, P. Giudicianni, *Journal of Environmental Chemical Engineering*, **2016**, *4*, 2878.
8. I.V. Perminova, K. Hatfield, "Use of Humic Substances to Remediate Polluted Environments: From Theory to Practice", *Springer*, Netherlands, **2005**.
9. F. Meng, G. Yuan, J. Wei, D. Bi, Y.S. Ok, H. Wang, *Chemosphere*, **2017**, *181*, 461.
10. F. Meng, G. Yuan, J. Wei, D. Bi, Y.S. Ok, H. Wang, *Environmental Science and Pollution Research*, **2017**, *24(29)*, 23006.
11. L. Boruvka, O. Drabek, *Plant Soil and Environment,* **2004**, *50(8),* 339.
12. L. Mayhew, *Acres USA-A voice for eco-agriculture*, **2004**, *34*, 8.
13. R. Wandruszka, *Geochemical Transactions*, **2000**, *2*, 6.
14. M. Bahemmat, M. Farahbakhsh, M. Kianirad, *Journal of Hazardous Materials*, **2016**, *312*, 307.
15. M. Ubner, "Interaction of Humic Substances with metal cations", *Tallinn University of Technology, TUT Press, Tallinn, Estonia*, **2004**.
16. M.A. Shaker, H.M. albishri, *Chemosphere*, **2014**, *111*, 587.
17. D. Kulikowska, Z. M. Gusiatin, K. Bułkowska, B. Klik, *Journal of Hazardous Materials*, **2015**, *300*, 882.
18. D. Kulikowska, Z. M. Gusiatin, K. Bułkowska, K. Kierklo, *Chemosphere*, **2015**, *136*, 42.
19. Order No. 756 of November 3, 1997 for the Approval of the Regulation on Environmental Pollution Assessment. Eminent: Ministry of Waters, Forests and Environmental Protection. (Published in: Official Gazette No 303 bis of 6 November 1997).
20. M. Niinae, K. Nishigaki, K. Aoki, *Materials Transactions*, **2008**, *49***,** 2377.
21. A.A. Keri, S. Avram, T. Rusu, *ProEnvironment ProMediu*, **2010**, *3*, 318.

STUDIA UBB CHEMIA, LXIV, 1, 2019 (p. 53-61)
(RECOMMENDED CITATION)
DOI:10.24193/subbchem.2019.1.04

# EXAMINATION OF MACRO AND MICRO ELEMENTS IN *PSETTA MAKSIMA* AND *SOLEA VULGARIS* FROM THE BLACK AND NORTH EASTERN MEDITERRANEAN SEAS

**MUSTAFA KEMAL SANGUN[a]*, CEMAL TURAN[b], BEYZA ERSOY ALTUN[b]**

**ABSTRACT.** The objective of this study was to determine the levels of essential (Ca, K, Na, Mg, Co, Cu, Cr, Fe, Mn) and non-essential (Al, As, Ba, Cd, Ni, Pb, Sr, Li, B) elements in the muscle, liver and skin of *P. maxima* and *S. vulgaris.* Analysis of variance was performed to determine significant differences among tissues. There were no significant differences in the metal concentrations among the tissues of both species with the exception of Fe and Li. The levels of essential metals such as Na, K, Ca and Mg were higher than 10 mg/kg; Fe and Cu were lower than 10 mg/kg. The results showed that the *P. maksima* and S*. vulgaris* are a good dietary source of essential nutrients. However, the concentrations of some non-essential metals in tissues of *P. maksima* and *S. vulgaris* exceeded the acceptable values for human consumption.

***Keywords:*** *Psetta maksima, Solea vulgaris, elements, minerals, heavy metals.*

## INTRODUCTION

Due to the increased interest in defining the biological roles of nutrients and their function in the ethology of chronic diseases, knowledge of dietary nutrient intake is needed to optimize human health [1].

[a] Hatay *Mustafa Kemal University, Faculty of Arts and Sciences, Department of Chemistry, 31060 Antakya, Hatay, Turkey*
[b] *Iskenderun Technical University, Faculty of Marine Science and Technology, 31200 Iskenderun, Hatay, Turkey*
**Corresponding author ksangun@gmail.com*

Fish flesh is an important source of minerals. The contents of K, Na, Mg and Ca are up to 10 mg/kg, whereas those of Fe and Cu are less than 10 mg/kg [2-4]. Many elements, which are present in seafood, are essential for human life at low concentrations and, however, they can be toxic at high concentrations. Therefore, many consumers regard any presence of these elements in fish as a hazard to health [5].

For the normal metabolism of fish, the essential metals must be taken up from waters, food or sediment. However, similar to the route of essential metals, non-essential ones are also taken by fish and accumulate in their tissues. Ecological need, sex, size and molt of marine animals were also found to affect metal accumulation in their tissues [6].

Many studies have been conducted on the elements in tissues of fish species in different parts of the world [7-14]. A few studies were done for metals in tissues of the *S. vulgaris* in literature, but it was not reported in Turkey. Moreover, there is no data for the *P. maxima* in literature.

The objective of this study was to determine the levels of both the various essential (Ca, K, Na, Mg, Co, Cu, Cr, Fe, Mn) and non-essential (Al, As, Ba, Cd, Ni, Pb, Sr, Li, B) elements in the muscle, liver and skin of two commercially valuable fish species *P. maxima* from the Black Sea and *S. vulgaris* from Iskenderun Bay, North Eastern Mediterranean Sea.

## RESULTS AND DISCUSSION

The concentrations of the macro-microelements analysed in the muscle, liver and skin of *P. maksima* and *S. vulgaris* with means ± standard deviation are given in Table 1 and Table 2.

Analysis of variance was performed to determined significant differences among tissues. Results from this analysis showed that there were no significant differences between the metal concentrations in the tissues of both species with the exception of Fe and Li.

The content (mg/kg) of muscle was 2931.27±234.48 mg Na, 443.03±112.25 mg K, 414.73±132.82 mg Ca, 1744.38±309.36 mg Mg. The levels of macro elements Na, K, Ca and Mg in a given muscle were always higher in *P. maksima* than in *S. vulgaris*. In *P. maksima*, the concentrations of Na, K, Ca, Mg were highest in muscle. However, the highest concentrations in tissues of *S. vulgaris* were found in the liver and skin.

The Ca and K values in muscle of fish samples are lower and the Na, Mg values are higher than that reported in *M. potassou, M. merluccius, S. vulgaris* from Mediterranean (Spain) and similar results reported from Baltic Herring [15-16].

**Table 1**. Levels (mg metal/kg, wt) of metals in the muscle, liver and skin of *P. maksima.*

| Element | Muscle | Liver | Skin |
|---|---|---|---|
| Na | 2931.27±234.48* | 2716.87±589.09 | 2787.44±249.51 |
| K | 443.03±112.25 | 132.93±42.79 | 318.20±160.12 |
| Ca | 414.73±132.82 | 283.25±50.01 | 289.73±50.01 |
| Mg | 1744.38±309.36 | 1191.78±104.03 | 1729.56±361.22 |
| Fe | 3.26±1.58[a] | 64.67±31.53[b] | 4.48±1.82[a] |
| Cu | 15.49±8.12 | 3.85±1.51 | 12.79±6.38 |
| Mn | 0.83±0.15 | 10.50±4.89 | 6.82±0.50 |
| Ba | 3.05±1.09 | 5.92±0.43 | 3.96±1.25 |
| Li | 4.35±1.71[a] | 8.59±2.32[b] | 8.59±0.55[b] |
| Ni | 7.08±1.35 | 27.83±4.58 | 8.28±5.66 |
| As | 2.42±0.36[b] | 4.78±1.29 | 2.16±0.13 |
| Al | 3.68±0.29[a] | 2.58±0.68 | 3.56±2.06 |
| B | ND | ND | ND |
| Cd | 0.13±0.09[b] | 0.15±0.10 | 0.14±0.09 |
| Co | 0.71±0.06 [a] | 0.35±0.11 | 0.37±0.05 |
| Cr | 0.61±0.05[a] | 0.32±0.16 | 0.78±0.31 |
| Pb | 1.11±0.05[a] | 0.54±0.33 | 2.24±1.70 |
| Sr | 0.31±0.14 | 0.53±0.14 | 1.28±0.86 |

ND: Not determined [below the limits of detection].

*Standard deviation is given with ±, n=3 within the column values with different letters are significantly different ($P<0.05$), values without letters are not significantly different ($P>0.05$).

The Na, K, Ca, and Mg concentrations in liver of *P. maksima* and *S. vulgaris* were 2716.87-3147.34 mg/kg, 132.93-394.98 mg/kg, 283.25-382.82 mg/kg, 1191.78-2030.87 mg/kg, respectively. The Na, Ca, Mg values in muscle and liver of fish samples are higher than those obtained by Ersoy in ten fish species from different region of North Eastern Mediterranean Sea (Turkey) [17]. The K value was found lower than reported [17].

The Na, K, Ca, and Mg levels in skin of *P. maksima* and *S. vulgaris* ranged between 2787.44-3074.19 mg/kg, 318.20-714.49 mg/kg, 289.73-284.20 mg/kg, 1729.56-1160.62 mg/kg, respectively. Although skin is a consumed part of the fish, it has not been investigated in previous studies.

Fe concentrations in muscle, liver and skin ranged between 3.26-64.67 mg/kg for *P. maksima* and ranged 3.42-112.90 mg/kg for *S. vulgaris*. The Fe concentrations in liver of two fish species-as opposed to the skin

and muscle increased significantly ($P<0.05$). The organs, such as the liver, gonads, kidney and gills are metabolically active tissues and accumulate metals of higher levels [18-19].

**Table 2.** Levels (mg metal/kg, wt) of metals in the muscle, liver and skin of *S. vulgaris.*

| Element | Muscle | Liver | Skin |
|---|---|---|---|
| Na | 2064.85±365.02* | 3147.34±332.06 | 3074.19±1087.69 |
| K | 330.78±62.60 | 394.98±342.45 | 714.49±10.03 |
| Ca | 232.41±16.39 | 382.82±193.62 | 284.20±117.08 |
| Mg | 1726.19±155.42 | 2030.87±1500.60 | 1160.62±107.23 |
| Fe | 3.42±0.45[a] | 112.90±45.60[b] | 32.06±08.95[a] |
| Cu | 11.90±4.62 | 58.17±48.20 | 4.54±1.63 |
| Mn | 8.04±3.92 | 9.01±6.41 | 1.72±0.40 |
| Ba | 4.35±1.44 | 2.09±1.38 | 8.29±6.40 |
| Li | 9.41±3.52 | 24.50±21.91 | 4.18±1.45 |
| Ni | 16.13±9.71 | 12.13±7.61 | 6.84±0.86 |
| As | 12.07±0.19[b] | 2.98±1.18 | 1.57±0.48 |
| Al | 3.06±1.17 | 2.47±0.72 | 4.49±2.63 |
| B | ND | ND | ND |
| Cd | 0.39±0.04[b] | 0.20±0.14 | 0.17±0.01[a] |
| Co | 0.34±0.05[b] | 0.20± 0.19 | 0.44±0.05 |
| Cr | 0.02±0.01[b] | 0.37±0.06[a] | 13.33±0.21 [a] |
| Pb | 0.71±0.60 | 1.41± 1.20 | 1.65±0.16 |
| Sr | 1.00±0.14 | 1.39±0.56 | 4.24±2.90 |

ND: Not determined [below the limits of detection].

*Standard deviation is given in parenthesize, n=3 within the column values with different letters are significantly different ($P<0.05$), values without letters are not significantly different ($P>0.05$).

The Fe level in muscle of fish samples was similar to those reported by numerous studies in fish species from different areas [13, 20-22]. The Fe values in liver are similar to reported by Ersoy and Yilmaz in different fish species [13, 17].

The Fe levels (4.48-32.06 mg/kg) in skin of both species are lower than that reported by Yilmaz in *M. cephalus* and *T. mediterraneus* from Iskenderun Bay [23].

The Mn values in tissues of fish samples ranged from 0.83 to10.50 mg/kg for *P. maksima* and ranged from 1.72 to 9.01 mg/kg for *S. vulgaris*. The Mn levels in muscle of *P. maksima* and *S. vulgaris* was similar to those reported by numerous studies in fish species from different areas [9,17,20,21]. The Mn values in liver were higher than that reported by Ersoy [17]. There is no data concerning Mn level in skin of fish.

The Cu concentrations in muscle, liver and skin ranged from 3.85 to 15.49 mg/kg for *P. maksima* and ranged from 4.54 to 58.17 mg/kg for *S. vulgaris*. The Cu results in muscle of *S. vulgaris* reported by other researcher were much lower than our values [8,9,15]. However, the values in liver of this species are similar to our values determined in liver. On the other hand, the values in muscle of *P. maksima* and *S. vulgaris* are similar to those reported [24]. The Cu level in skin of fish samples is similar to those obtained by Yilmaz [13, 23].

According to the regulations which made by commission of European Union and Turkey, permissible limit for Cu in muscle of fish is 20 mg/kg wet weight [25]. The Cu levels in muscle of both species were not exceed given consumption levels. The Pb values in muscle, liver and skin of fish samples were 0.71-1.11 mg/kg, 0.54-1.41 mg/kg, 1.65-2.24 mg/kg, respectively. The Pb concentrations in muscle of two fish species are similar to those reported by Yilmaz [23]. However, some researcher reported that the Pb concentrations in muscle and liver of different fish species from other areas were much lower than in Pb values determined in our study [20,26]. The Pb values in skin of fish samples were lower than obtained by Yilmaz [23].

The Cd concentrations in muscle, liver and skin ranged between 0.13, 0.15 and 0.14 mg/kg for *P. maksima* and between 0.39, 0.20 and 0.17 mg/kg for *S. vulgaris*, respectively. The results of Cd levels in muscle and liver of *S. vulgaris* are similar to those reported for the *S. vulgaris* from other areas [8-9]. The Cd results in muscle of *P. maksima* and *S. vulgaris* in agreement with those reported in numerous studies [6,21,28]. There is no data concerning the Cd values in skin of fish. The Cd value in muscle of *P. maksima* and *S. vulgaris* exceed acceptable value for Cd in muscle of fish is 0.1 mg/kg wet weight for human consumption designated by the regulations [25]. From the fish health point of view, the Cd value in muscle of fish samples may also be considered as an important warning signal.

As concentrations in muscle, liver and skin for *P. maksima* were 2.42, 4.78 and 2.16 mg/kg, respectively. These values for *S. vulgaris* were 12.07, 2.98 and 1.57 mg/kg, respectively. The As values in muscle and liver of *S. vulgaris* were much higher in the same species [9,21]. Mormede & Davies found lower levels of As in different fish from the Rockall Trough [26]. The As

levels in muscle of fish is 1 mg/kg wet weight due to the regulations in Turkey [25]. The As value in muscle of fish samples exceed acceptable values. Especially, The As values in muscle of *S. vulgaris* were significantly high.

The Cr and Ni concentrations in muscle for fish species obtained were 0.02-0.61 mg/kg and 7.08-16.13 mg/kg, respectively. The Cr values muscle of fish samples are similar to those obtained by numerous studies in fish from different areas [7,9,20]. However, some researchers found much higher levels of Cr in muscle of North Eastern Mediterranean fish [6,29].

The Cr and Ni concentrations in liver of fish samples were found 0.32-0.37, 12.13-27.83 mg/kg, respectively. The Cr contents in liver of *P. maksima* and *S. vulgaris* was lower than reported in Mediterranean Fish [6,29]. However, lower values of Cr found in *S. vulgaris* from other areas [9]. Ni concentrations in muscle and liver for *S. vulgaris* and *P. maksima* were higher than reported [6,29]. The Cr and Ni values in skin of *P maksima* were 0.78 mg/kg and 8.28 mg/kg. However, the values of *S. vulgaris* in skin were 13.33 mg/kg Cr and 6.84 mg/kg Ni. The Cr values in skin of fish samples are similar for *M. cephalus* and *T. mediterraneus* [23]. Whereas the Ni content is skin was higher than reported by the same researcher [23].

The Co concentrations in muscle, liver and skin of *P. maksima* were 0.71, 0.35 and 0.37 mg/kg, respectively. This values for *S. vulgaris* were 0.34, 0.20, 0.44 mg/kg, respectively. The results of Co in muscle of *P. maksima* and *S. vulgaris* are similar to those reported for fish from Black Sea Coast in Turkey [20]. These results in muscle were lower than reported [28]. The concentrations in liver and skin of fish have not been studied in previous works.

The Al concentration in muscle of *S. vulgaris* and *P. maksima* was 3.06 and 3.68 mg/kg, respectively. The Al concentrations in liver and skin of fish ranged from 2.7 to 4.48 mg/kg. There is no data concerning the Al values in tissues.

The Ba, Li, Sr and B were also obtained in different tissues of *P. maksima* and *S. vulgaris*. The Ba concentrations in tissues of both species ranged from 2.09 to 8.29 mg/kg. The Li concentration in tissues of fish samples ranged between 4.18-24.50 mg/kg. The Li values in muscle of *P.maksima* reduced significantly ($P<0.05$) according to liver and skin of the same species. The Sr concentrations in muscle, liver and skin of two fish species were between 0.31-1, 0.53-1.39, 1.28-4.24 mg/kg, respectively. The B concentrations in muscle, liver and skin of fish samples were not detectable (below limits of detection). Unfortunately, there are no data concerning the Ba, Li, Sr and B concentrations in muscle, liver and skin of the marine fish.

## CONCLUSIONS

The elements in tissues of *P. maksima* have not been investigated in previous studies. Data concerning mineral content of *S. vulgaris* was not reported in Turkey. Hence, the present study might be accepted as representative data for *P. maksima* and *S. vulgaris* that the species are studied firstly at this region.

The obtained results provided evidence that the studied *P. maksima* and S*. vulgaris* are a good dietary source of essential macro-micronutrients and the levels of some metals were even higher than acceptable values for human consumption.

These results can also be used to test the chemical quality of the marine food, in order to evaluate the possible risk associated with their consumption by human.

Further studies are needed to determine these minerals might have on the health of the consumer.

## EXPERIMENTAL SECTION

### Materials and Methods

#### *Samples Preparation*

The *P. maksima* samples were obtained from Şile in the Black Sea Coast and *S. vulgaris* samples were obtained from Iskenderun Bay in North eastern Mediterranean Sea.

Periodically taken fishes samples were kept in cold iced boxes and transported into Mustafa Kemal University, Science, Research and Application Center (MKUFAM), Tayfur Sökmen Campus, Antakya, as soon as probable under standard conditions. MKUFAM Lab was completed digestion and elements analyses.

#### *Digestion Procedures*

For analyses, approximately 0.5 g sample was digested with 10 mL high purity nitric acid (Merck) in CEM® Mars5 (Version 045012) microwave. The conditions of the digestion are 10 min. for ramp time, 10 min hold time at 210°C and 200 Psi. After digestion the samples filtered through Whatman®quantitative (No: 42, 110mm*) filter papers. Laboratory grade hydrochloric acid is added into the initial digested and the sample is refluxed. This digested samples are filtered and the filter paper and residues are rinsed with hot hydrochloric acid and then hot reagent water. Filter paper and residue are returned to the digestion flask, refluxed with extra hydrochloric

and then filtered again. The digested portion is then diluted to a final volume of 20 ml [30]. A blank digest was carried out in the same way. All metals were determined against aqueous standards.

At least three replicates for each sample was prepared in order to increase sensitivity in readings.

### *Analytic Procedures*

Determination of all metal concentrations was carried out by inductively coupled plasma atomic emission spectrometry (ICP-AES) (Varian model-Liberty Series II). For the calibration of the ICP-AES a High Purity® Multi Standards was used. The following emission lines were used; As 189.041, Ca 393.366, Cd 228.802, Co 228.616, Cr 367.716, Cu 324.754, Fe 259.940, K 766.490, Mg 279.553, Mn 257.610, Na 588.995, Ni 221.647, Pb 220.353, Al 396.152, Ba 455.403, Sr 407.771, Li 670.784, B 249.773. Metal concentrations were calculated mg/kg wet weight.

### *Statistical Analysis*

Analysis of variance was used to evaluate the analysis data, and significant differences among means were determined by One-way analysis of variance (ANOVA) and Duncan's Multiple Range Test (P=0.05) (SPSS 12 for windows).

## REFERENCES

1. W. Sawaya, F. Al-Awadi, N. Eid, B. Dashti, Food composition, Kuwaiti composite dishes (1st ed.). Kuwait: Kuwait Institute for Scientific Research **1998**.
2. U. Kietzman, K. Priebe, D. Rakow, K. Reichstein, Ictiologia general. In inspeccion veterinaria de pescados (editorial acribia) Zaragoza, Spain, **1974**, p. 21.
3. A.A. Paul, D.A.T. Southgate, The composition of foods. Amsterdam: Elsevier Science Ltd. **1978**.
4. M.P. Navarro, *Review Agroquim Tecnology Alimentarius*, **1991**, *31*, 330.
5. J. Oehlenschlager, Identifying heavy metals in fish. In H.A. Bremmer, Safety and quality issues in fish processing Woodhead Publishing Limited and CRC Press LLC. **2002**, p. 95.
6. M. Canli, G. Atli, *Environmental Pollution*, **2003**, *121*, 129.
7. K. Chandrashekar, Y.G. Deosthale, *Journal of Food Composition and Analysis*, **1993**, *6(2*), 195.
8. A. Hamza-Chaffai, M. Roméo, A. El Abed, *Bulletin Environmental Contamination and Toxicology*, **1996**, *56*, 766.

9. J. Usero, C. Izquierdo, J. Morillo, I. Gracia, *Environment International*, **2003**, *29*, 949.
10. X. Wang, T. Sato, B. Xing, S. Tao, *Science of the Total Environment*, **2005**, *350*, 28.
11. P. Herman, S. Harangi, M. Fehér, I. Fábián, E. Baranyai, *Studia Univ. Babes-Bolyai Chem*., **2017**, *62(2)*, 213.
12. M. Turkmen, Y. Tepe, A. Türkmen, M.K. Sangun, A. Ateş, E. Genç, *Bull. Environ. Contam. Toxicol.* **2013**, *90*, 702.
13. A.B. Yılmaz, M.K. Sangun, D. Yağlıoglu, C. Turan, *Food Chem.* **2010**,*123*, 410.
14. D. Ayas, A. Kosker, G. Agilkaya, M. Bakan, D Yaglioglu, *Natural and Engineering Sciences*, **2018**, *3(3*), 248.
15. I. Martínez-Valverde, M.J. Periago, M. Santaella, G. Ros, *Food Chemistry*, **2000**, *71,* 503.
16. R. Tahvonen,T. Aro, J. Nurmi, H. Kallio, *Journal of Food Composition and Analysis*, **2000**, *13,* 893.
17. B. Ersoy, Nutrient composition and heavy metal contents of the fish consumed during the hunting season in the northeast Mediterranean (Adana-Karataş) region. Cukurova University, PhD Thesis. Adana, **2006**, p142.
18. P. Allen, *Toxicology and Environmental Chemistry*, **1994**, *44*, 101.
19. P. Allen, *Archives of Environmental Contamination and Toxicology*, **1995**, *29*, 8.
20. S. Topcuoglu, C. Kirbasoglu, N. Gungor, *Environment International*, **2002**, *27*, 521.
21. M. Tuzen, *Food Chemistry*, **2003**, *80*, 119.
22. M. Eken, F. Turan, F. Aydın, S. Karan, *Natural and Engineering Sciences*, **2018**, *3(2),* 169.
23. A.B. Yilmaz, *Environmental Research*, **2003**, *92*, 277.
24. F. Kargin, *Water Air Soil and Pollution*, **1996**, *90*, 557.
25. European Community, Rule N.466, European Official Gazette, 16th Marc **2001**.
26. S. Mormede, I. M. Davies, Continental Shelf Research, **2001**, *21*, 899.
27. Council of Europe, Resolution AP (96) 4 on maximum and guideline levels and on source directed measures aimed at reducing the contamination of food by lead, cadmium and mercury. Adopted by the Committee of Ministers on 2 October **1996**.
28. C. Tamira, S.Q.H. Shane, R.F. Ambrose, *Marine Pollution Bulletin*, **2001**, *42(3),* 224.
29. M. Kalay, O. Ay, M. Canli, 1999 *Bulletin Environmental Contamination and Toxicology*, **2001**, *63*, 673.
30. M.K. Sangun, H.G. Ozdilek, *Asian Journal of Chemistry*, **2007**, *19(1)*, 621.

STUDIA UBB CHEMIA, LXIV, 1, 2019 (p. 63-78)
(RECOMMENDED CITATION)
DOI:10.24193/subbchem.2019.1.05

# STUDY REGARDING THE PRESENCE OF SOME HEAVY METALS (CHROMIUM, COPPER, MANGANESE AND ZINC) IN THE GREEN WASTE COMPOST

**IRINA SMICAL[a*], ADRIANA MUNTEAN[b], VALER MICLE[c], ZOLTÁN TÖRÖK[d]**

**ABSTRACT.** The composting is one of the most effective recycling method of green waste. The presence of some heavy metals, such as chromium, copper, manganese and zinc may influence the compost quality. The bioavailable and unavailable metal forms for plants determined by sequential analysis showed similarities in relation to the percentages of extracted forms. The lowest percentages were recorded for the bioavailable metal forms for plants uptake. Thus, the succession F6>F5>F4>F3>(F1+F2) is characteristic for chromium, the succession F5>F6>F4>F3>(F1+F2) is characteristic for copper and zinc and the succession F5>F4>F6>F3>(F1+F2) is characteristic to the zinc and manganese. Thus, by adding some organic additives, like manure, the micronutrients and heavy metals regime is influenced.

***Keywords:*** *green waste, compost, manure, heavy metal*

[a] *North University Centre of Baia Mare, Technical University of Cluj-Napoca Engineering of Mineral Resources, Materials and Environment Department, Victor Babes str., no. 62A, 430083, Baia Mare, Romania*
[b] *Maramureș Water Management System, Someș-Tisa Basinal Water Administration, no. 2, Hortensiei Street, 430294, Baia Mare, Romania*
[c] *Technical University of Cluj-Napoca, Faculty of Materials and Environmental Engineering, Department: Environment Engineering and Entrepreneurship of Sustainable Development, 103-105 Muncii Blvd., 400641 Cluj– Napoca, Romania*
[d] *Faculty of Environmental Science and Engineering, Babeș-Bolyai University of Cluj-Napoca, 30 Fântânele Street, Cluj County, Romania*
**Corresponding author: irina.smical@yahoo.com*

## INTRODUCTION

The bio-waste composting is an efficient method of organic waste conversion into something valuable with positive consequences for the economy and environment. The compost represents a good product for soil, enhancing its quality due to the high nutritive elements content, especially nitrogen and carbon, but also as sorbent for heavy metals in aqueous environment [1].

Even the toxicity of some metals is reduced during composting, the final product may have heavy metals which could be transferred to soil and groundwater [2-4]. From soil, heavy metals may enter the human body through the food chain and could cause ilnesses due to metals toxicity [5]. The manure addition to the compost in order to increase its quality may enhance the heavy metals content by its own metals content [6]. The metals transfer depends to the plant uptake which is directly correlated with metals mobility and bioavailability [7]. A major role in the transferring process plays the chemical forms of the metals and their binding in the soil structure which is strongly influenced by the organic matter content [8-9].

Singh and Kalamdhad [10] showed that during water hyacinth composting process the concentration of some metals, such as $Cr_{total}$, $Cu^{2+}$, $Mn^{2+}$ and $Zn^{2+}$ was increased.

The data presented in this paper complete the study “Influence of Some Natural Organic Additives on the Quality of Vegetal Compost” [11].

## RESULTS AND DISCUSSION

The results of analysis of the final compost samples (18$^{th}$ June 2014) [11], were compared with the values provided by the good practices codes regarding the composting issued by the National Institute of Research-Development for Pedology, Agrochemistry and Environmental Protection – NIRDPAEP-IRPA, Bucharest [12], as it is showed in Table 1.

**Table 1.** The compost conductivity

| Analyzed parameter | Bulk A | Bulk B | Bulk C | NIRDPAEP-IRPA [12] | |
|---|---|---|---|---|---|
| | | | | Minimum | Maximum |
| Conductivity, µS/cm | 2312±24 | 2380±27 | 1786±18 | < 5000 | |

Results are mean±standard deviation of 10 replicates per each group.

The final values of the conductivity are much below the maximum limit, the lowest value being for bulk C (Table 1) – without organic additives, most probably because of the slowly micro-biological activity in this bulk.

### Physical compost features

The compost colour was dark brown to black and its texture and smell was similar to that of wet soil. The particles size was less than 2 cm and they were homogenous distributed. However, the bulk C content was slightly rougher than the other two bulks, which might be explained by the less decomposing of the organic matter.

Statistical analysis performed using simple correlation by calculating the Pearson coefficient showed negative or statistically insignificant correlations for the confidence level of 5% between different forms of the metals [13] (Table 2).

**Table 2.** Significant statistical correlation of the different metal forms

| The form of the metal | Total | F1 | F2 | F3 |
|---|---|---|---|---|
| **F1** | $Cr_A$; $Cr_C$; $Zn_A$; $Zn_C$ | - | - | - |
| **F2** | $Mn_A$; $Mn_B$ | $Cr_A$; $Cr_B$; $Cr_C$ | - | - |
| **F3** | - | - | - | - |
| **F4** | - | $Cu_C$; $Mn_B$; | $Cu_C$ | - |
| **F5** | $Cr_A$; $Cr_C$ | $Cr_A$; $Cr_C$ | $Cr_A$; $Cr_C$ | - |

Note: $X_y$ – X- chemical symbol of the metal; y –bulk symbol

All analyzed metals in compost showed a decrease of their concentration during composting with the exception of copper, which showed a high value in bulk C (with no additives). This may be explained thought the fact that the oxidations conditions were not met and that this element did not leach despite of the high moisture in the compost. For all metals, the sequential analysis revealed that no more than 1% of the total extractible metal content might be available for plants uptake (F1+F2).

Significant quantities of metals were found in the fractions most resistant to extraction, unavailable for plants uptake (F3, F4 and F5). About 30 - 40% of the metals were in the residual state (F6), considered as constitutive form of the matrix. The percentage of the metal fractions in the total extracted amount allowed the interpretation of the evolution of each metallic element (Figure 1-16).

### The total chromium evolution

The total chromium showed the extreme values of the chromium concentration of 59.2 mg $kg^{-1}$ on 24$^{th}$ July 2013, reaching the maximal compost decomposition phase, towards to 90.6 mg $kg^{-1}$ at the beginning of the compost process on 29$^{th}$ April 2013 (Figure 1). The initial total chromium concentrations ranged from 81.6 mg $kg^{-1}$ (in bulk C) to 90.6 mg $kg^{-1}$ (in bulk A) much below the limit of 3000 mg $kg^{-1}$ provided by NIRDPAEP-IRPA [12].

The bulks A and B (with organic additives) showed a decrease of the total chromium concentration up to the decomposition phase (24$^{th}$ July 2013) thereafter the values began to increase but however to the values lower by 1.08 times in bulk B and by 1.25 times in bulk A towards to the initial ones. In bulk C the evolution of the total chromium decreased by 1.15 time towards the initial values (Figure 1).

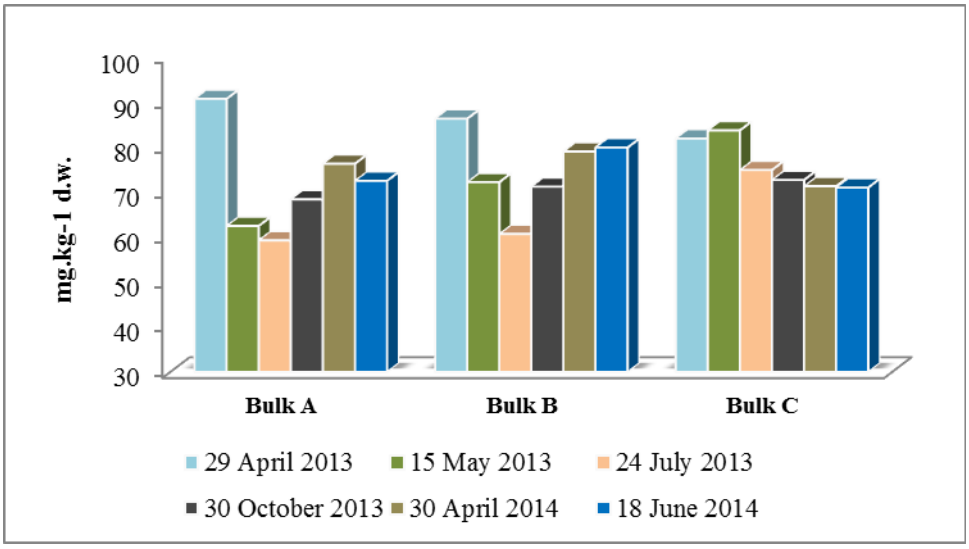


**Figure 1.** The total chromium in compost

In bulks A and B for chromium, the forms F3 (organically bound "mobilisable") and F4 (organically complexed or carbonates „mobilisable") are below 15% of the total extracted, while in bulk C these forms showed values over 15% (Figure 2, 3, 4). It is noticeable that in all bulks, the form F5 (sulfides „mobilisable") has negatively evolved during composting likely to soluble forms F1 and F2 of the metal (Figure 2, 3, 4).

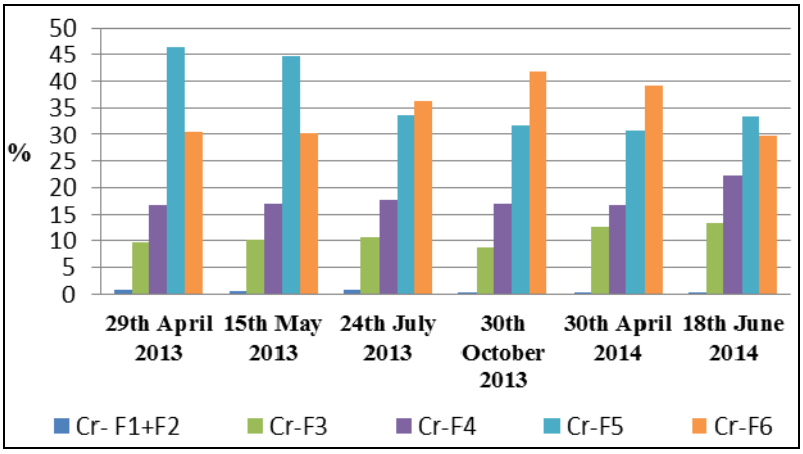


**Figure 2.** The chromium concentration in bulk A

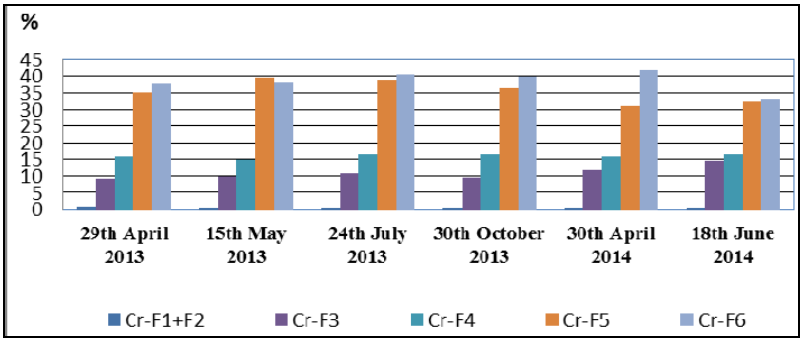


**Figure 3.** The chromium concentration in bulk B

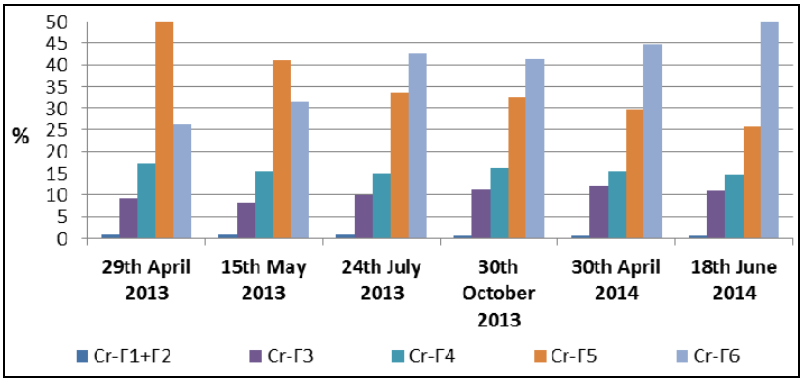


**Figure 4.** The chromium concentration in bulk C

### The copper evolution

The total form of copper concentrations were below the value of 8400 mg $kg^{-1}$ provided by the Romanian regulations [12]. In the bulk A, the total form of copper concentration was lower by 1.57% than the initial one, while in bulks B and C the values increased by 1.72% and 2.13%, respectively. This might be due to the cattle manure addition in bulk A which positively influenced the copper evolution (Figure 5).

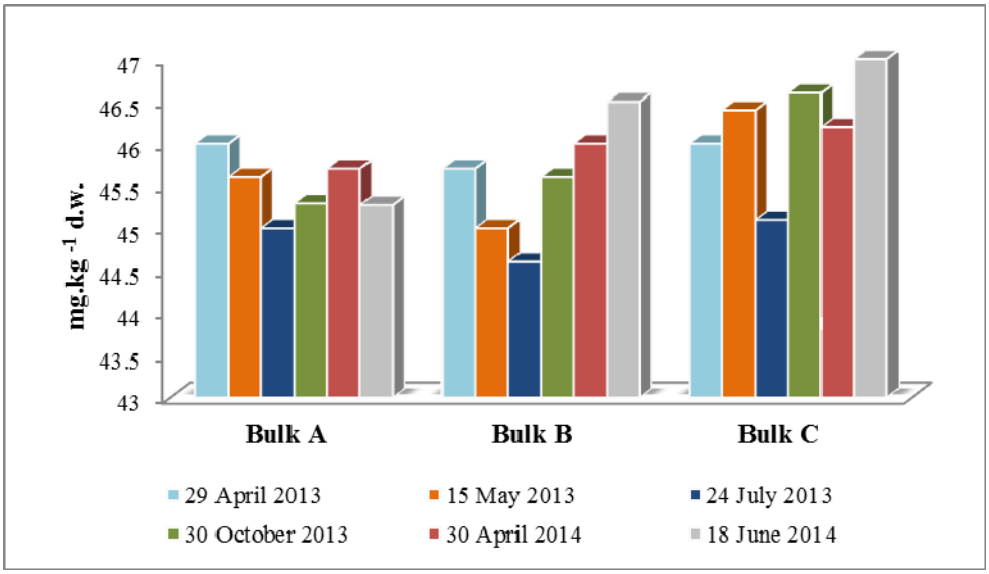


**Figure 5.** The total form of copper in compost

The sequential analysis revealed the lowest values of the bioavailable copper forms for plants in bulk A (1.01%) and the highest values (1.23%) in bulk C in the thermophile phase of composting. Similar with other research results [14, 15], the highest copper concentrations are contained by forms F5 and F6 (sulfides „mobilisable") and residual, respectively (Figure 6, 7, 8). The correlation coefficients were identified only for bulk C for forms F4, F1 and F2 (Table 2 4).

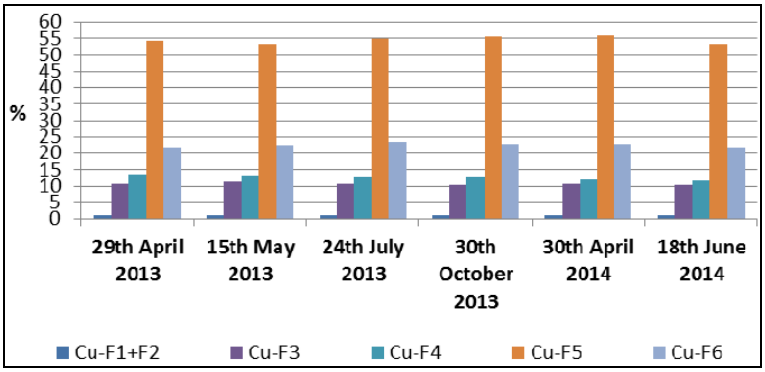


**Figure 6.** The copper concentration in bulk A

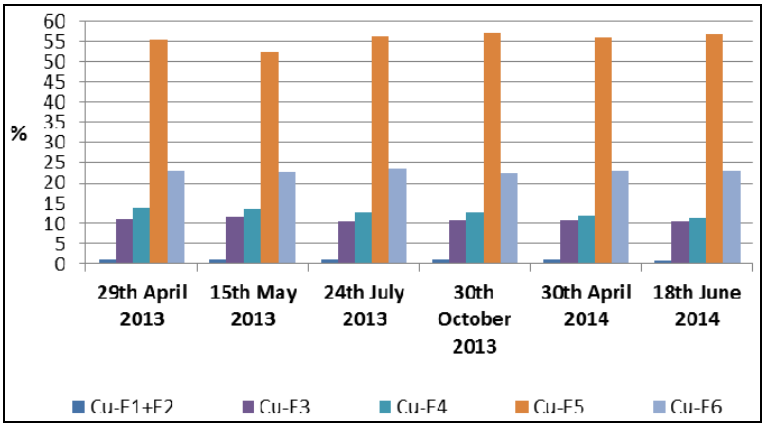


**Figure 7.** The copper concentration in bulk B

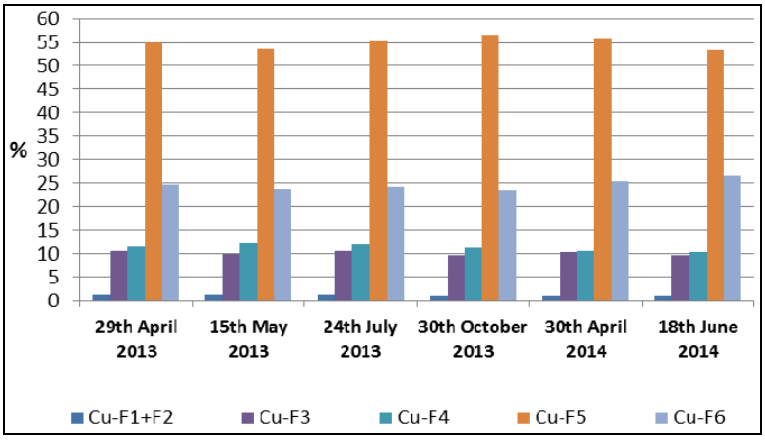


**Figure 8.** The copper concentration in bulk C

### The zinc evolution

The zinc concentration value determined for each compost bulk did not exceed the maximum value concentration of 7500 mg $kg^{-1}$ provided by the Romanian in force regulations [12] (Figure 9). In each bulk the final total zinc value decreased by 1.49 times (bulk A), 1.48 times (bulk B) and 1.36 times (bulk C) towards to the initial value (Figure 10, 11, 12). Similar results revealed by other papers showed the same negative trend for zinc in composting process [14, 15].

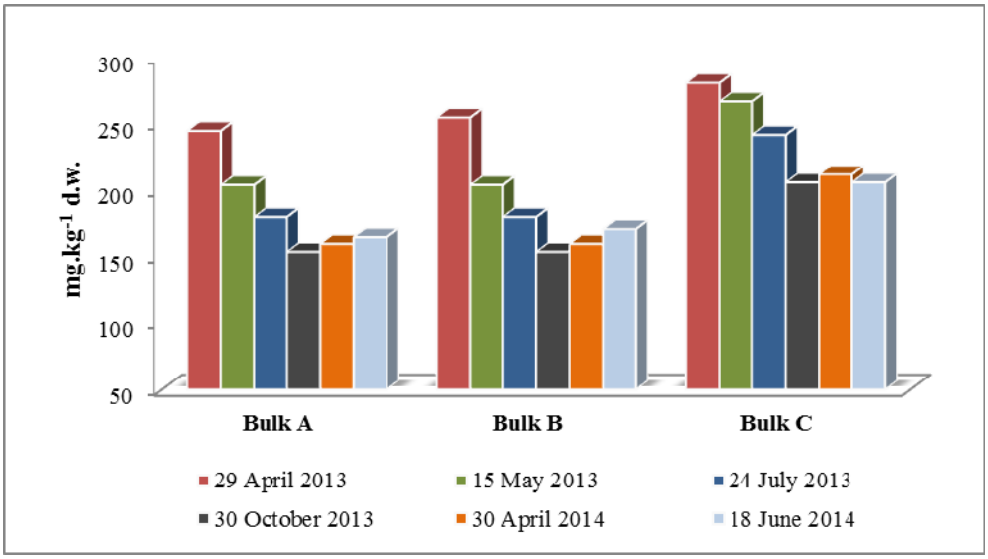


**Figure 9.** The total form of zinc in compost

The highest bioavailable percent for the zinc form for plants (F1+F2) was identified in bulk A (1.46%) at the beginning of the composting. This might be explained by the presence of organic additives in the bulks A and B. Referring to the correlation coefficients for zinc, distinct significantly values have been identified among the exchangeable „mobile" form (F1) and total form, in bulk A and C (Figure 10,11,12). It was possible that the cattle manure to stimulate the zinc leaching in close correlation with the pH evolution.

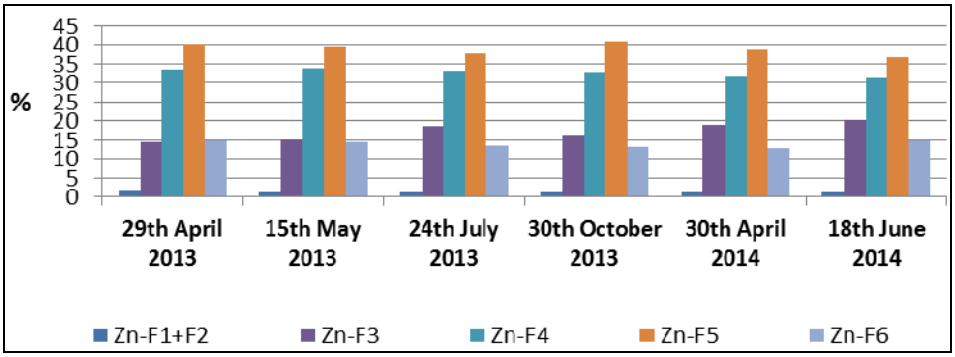


**Figure 10.** The zinc concentration in bulk A

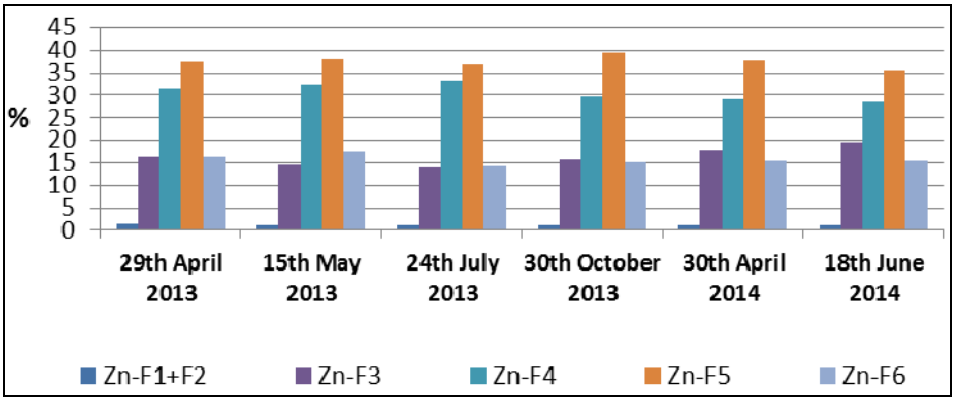


**Figure 11.** The zinc concentration in bulk B

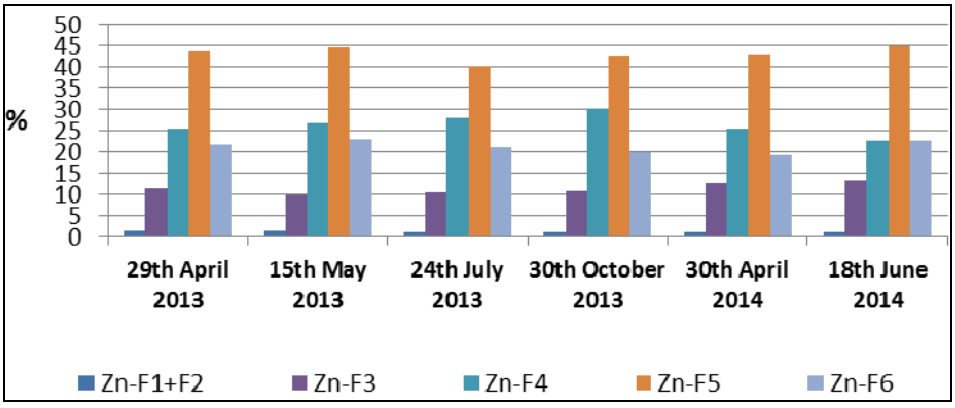


**Figure 12.** The zinc concentration in bulk C

### The manganese evolution

The total form of manganese showed a negative evolution in bulks A and B and almost constant one in bulk C (Figure 13). The highest decrease was noticed in bulk B (1.25 times). The total form of manganese ranged from 62.5 mg $kg^{-1}$ in bulk B at the final composting and 79 mg $kg^{-1}$ in bulk C at the beginning of the composting process (Figure 14, 15, 16). The manganese values are not provided by the Romanian in force regulations [12].

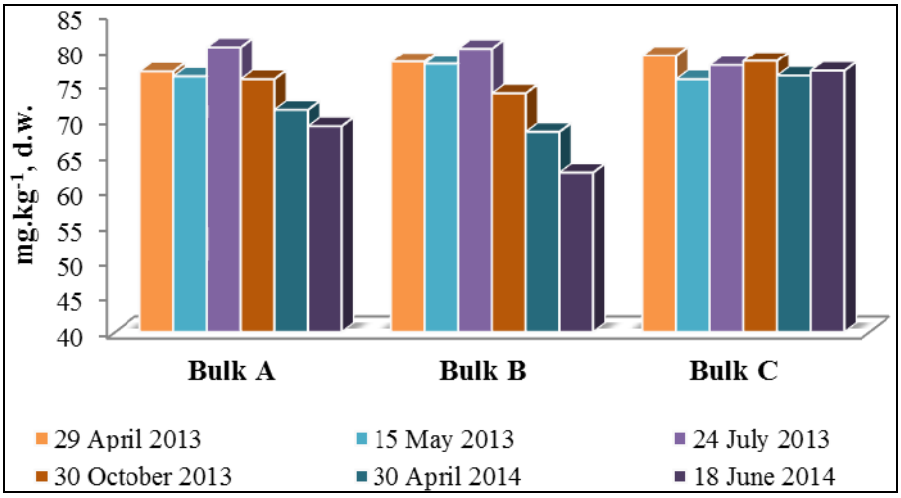


**Figure 13.** The total form of manganese in compost

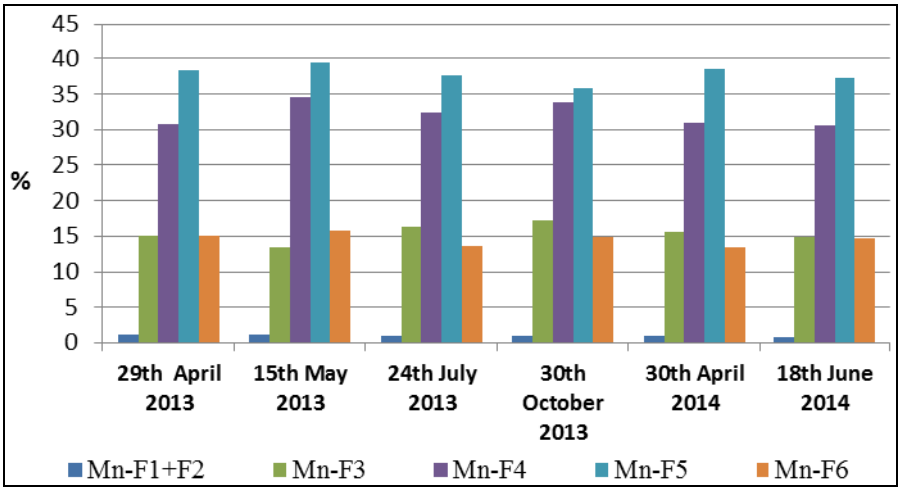


**Figure 14.** The manganese concentration in bulk A

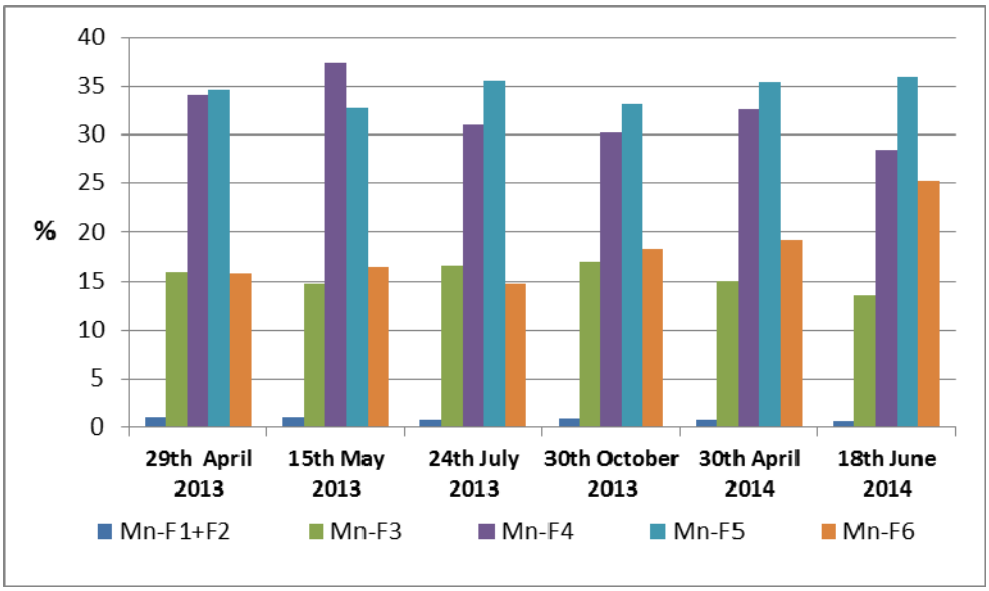


**Figure 15.** The manganese concentration in bulk B

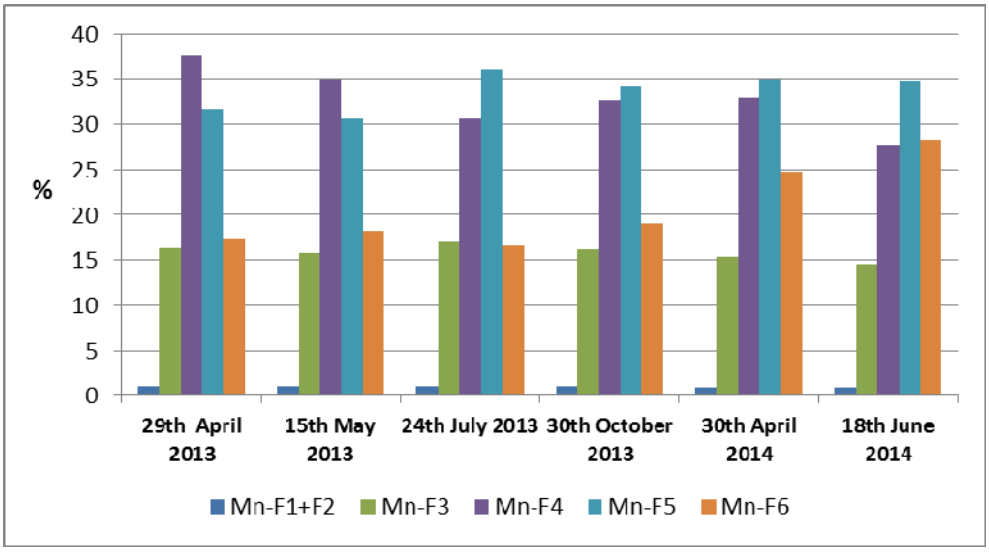


**Figure 16.** The manganese concentration in bulk C

At the final composting, the percentage of bioavailable magnesium for plants uptake (F1+F2) increased as follows: bulk B < bulk C < bulk A. It was obvious that the organic additive used in bulk B influenced the manganese leaching. The highest percentages of manganese were noticed for forms F4 and F5, namely the „mobilisable" forms in the sulfide and carbonates, or organically complexed forms where the additives probably did not allow the manganese releasing from this forms. The similar trend of manganese for forms F1 and F2 was revealed by other researches [14, 16]. The correlation coefficients of the manganese and humic substances were statistically insignificant but there were significant correlations among various metal forms (Table 2).

## CONCLUSIONS

The total form of the analyzed metallic elements did not exceed the maximum limits, neither at the beginning nor at the end of composting.

The bioavailable and unavailable metal forms for plants determined by sequential analysis showed similarities in relation to the percentages of extracted forms.

The lowest percentages were for the bioavailable metal forms for uptake of the plants. Thus, the succession F6 >F5>F4>F3>(F1+F2) was characteristic for chromium, the succession F5>F6>F4>F3>(F1+F2) for copper and zinc and the succession F5>F4>F6>F3>(F1+F2) for manganese.

In accordance with the experiment results it can be concluded that the manure additives positively influenced the composting.

## EXPERIMENTAL SECTION

### The preparation of the bulks and sampling the compost for physico-chemical analysis

The three bulks of bio-waste consisted in a mixture of wood chips, fresh grass, dry leaves, hay. In addition to this, about 8% cattle manure was added to the bulk A and about 11% of poultry manure to the bulk B. The bulk C had no manure.

The bulks preparation method, the compost sampling and the physico-chemical properties of the compost (table 3) are presented in detail in the paper "Influence of Some Natural Organic Additives on the Quality of Vegetal Compost" [11].

To establish the proportions of materials subjected to the composting process the data from the literature on the C:N ratio were used for each type of material according to table 3.

**Table 3.** The C:N ratio of the materials included in composting process [17]

| Ingredient of compost | Ratio C:N |
|---|---|
| Wood chips | 400:1 |
| Poultry manure | 12:1 |
| Dry leaves | 35:1 |
| Fresh grass | 20:1 |
| Cattle manure | 16:1 |
| Hay | 25:1 |

By Davidescu and Davidescu [18] the nutrients content in the cattle and poultry manure (total N, $P_2O_5$, $K_2O$) are showed in table 4.

**Table 4.** The nutrients content in the cattle manure and the poultry manure [18]

| Nutrient | Cattle manure | Poultry manure |
|---|---|---|
| | (%, dry weight) | |
| Total N | 0.7 - 2 | 3 - 5 |
| $P_2O_5$ | 0.3 - 1.2<br>(0.13-0.52 in P) | 2 - 3<br>(0.08 - 1.3 in P) |
| $K_2O$ | 0.8 - 0.9<br>(0.6 - 0.7 in K) | 1.1 - 2.5<br>(0.9 – 2 in K) |

At the end of the 15 months (29th April 2013 - 21st July 2014) of composting, samples from every bulk were taken and analyzed in the laboratory [11].

### Sampling and preliminary preparation of compost to determine the characteristics

The Protocol used in this research provided that the samples of each pile must be taken after removing a layer of 5-10 cm. The representative sample was obtained by application of the quarter method [19] on the sample resulted from the mix of 6 samples of about 1 kg each other, sampled from each pile.

The study protocol provided that the samples of each pile were taken after removing a layer of 5-10 cm and the representative sample that arrived in the laboratory was obtained after applying the quarter method [19] on the sample obtained by homogenizing 6 samples of approx. 1 kg, taken from each pile. For the physico-chemical analysis, the samples were prepared according to ”Methods Book for the Analysis of Compost” [19].

To determine the conductivity the samples were ground to size <10 mm and analyzed in fresh state.

**Chemical analysis**

To make the chemical analyses of the compost a representative sample was taken from each bulk (A, B, C) of the homogenized compost at various time of decomposing process.

Thus, the conductivity was potentiometric determined, using a ratio of 10:1 of double-distilled water suspension and compost. It was measured with a laboratory conductometer, Orion 3 Star type, manufactured by Thermo Scientific. The quantification limit of the method is 3 μS $cm^{-1}$.

The total form of the trace metalic elements (Cr, Cu, Zn, Mn) was determined from the acidic digestions of the sample. The digestion was made according to the *„Digestion Application Note DG-EN-04 for Milestone microwave oven"* [20]. In this regard, 0.25 g of the each compost sample was mineralized with 7 ml of HNO3 65%, 1 ml of HCl 37%, 1.5 ml of HF 40%, 45 minutes at 240°C. After dissolution, volumetric solution was directly analyzed by flame atomic absorption (Mn and Zn) and graphite furnance (Cu, Cr), using the Perkin Elmer spectrophotometer, type Aanalyst 700. The bioavailable and unavailable metals for plants were determined according to the method of Sposito [21]. This procedure is also used in various researches regarding the metals state [22, 14]. The extractable metals were analyzed using a ratio of 1:4 of compost and different extractant solutions by flame atomic absorption (Mn and Zn) and graphite furnance (Cr si Cu, table 5). Each result was obtained as an average of three individual readings of the analyzed sample. It was validated with the relative standard deviation using the equipment software - WinChemLab. The used calibration curves were validated using the quality coefficient (R2), being acceepted only values ≥0.990.

The content of each metal in the soil matrix was established after achieving the extraction in accordance with the protocol of the sequential extraction, provided by table 5.

**Table 5.** Experimental conditions used to determine extractable metals, in accordance with the method of Sposito [11, 14, 21, 22]

| Heavy metals | Extractant solution | Duration of shaking |
|---|---|---|
| F1 - Exchangeable - „mobile" | $KNO_3$ 0.5 M | 16 hours |
| F2 - Soluble -„mobile" | $H_2O$ | 2 hours, for three times |
| F3 - Organically bound - „mobilisable" | NaOH 0.5 M | 16 hours |
| F4 - Organically complexed or carbonates - „mobilisable" | EDTA 0.5 M | 6 hours |
| F5 - Sulfides - „mobilisable" | HNO3 4 M | 6 hours at 80°C |

The ashed residue obtaining from the last step of the sequential extraction was subjected to the digestion procedure using a mixture of HNO3, 65% with HCl 37% (volume ratio 1:1). It was put in Teflon tubes which was inserted in a microwave oven (Milestone type), for 30 minute at 220 °C [11, 23]. This metal form is called ”Residual fraction - F6” [22, 23].

## REFERENCES


1. J. Martinho, B. Campos, I. Brás, E. Silva, *Environment Protection Engineering*, **2015**, 41, 2, 57.
2. G. Chen, G. Zeng, C. Du, D. Huang, L. Tang, G. Wang Land Shen, *Journal of Hazardous Materials,* **2010**, 181**,** 211.
3. J. Singh, A. S. Kalamdhad, *International Research Journal of Environment Sciences,* **2013***,* 2, 4, 59.
4. P. Castaldi, L. Santona, P. Melis, *Fresenius Environmental Bulletin*, **2006**, 15, 9b, 1133.
5. K.G. Scheckel, R.L. Chaney, N.T. Basta, J.A. Ryan, *Advances in Agronomy Elsevier*, **2009**, 104, 52.
6. M. Vukobratović, Z. Vukobratović, Z. Lončarić, D. Kerovac, *Acta Horticulturae 1034: International Symposium on Growing Media and Soilless Cultivation,* **2014**, 75, 591.
7. I. Smical, V. Hotea, V. Oros, J. Juhasz, E. Pop, *Environmental Engineering and Management Journal*, **2008**, 7, 5, 609.
8. A.K. Gupta, S. Sinha, *Bioresource Technology*, **2007**, 98**,** 1788.
9. F. Ingelmo, M.J. Molina, M. Desamparados Soriano, A. Gallardo, L. Lapeña, *Journal of Environmental Management,* **2012***,* 95, 104.
10. J. Singh, A.S. Kalamdhad, *Ecological Engineering*, **2013**, 52, 59.
11. I. Smical, A. Muntean, V. Micle, *Environmental Engineering and Management Journal*, 2016, 15, 5, 1041.
12. National Institute of Research-Development for Pedology, Agrochemistry and Environmental Protection – IRPA, Bucharest, Romania (NIRDPAEP-IRPA) 2014 *Codes of good practices. Composting (http://www.icpa.ro/Coduri/Compostarea.pdf), 6.*
13. M. Ardelean, *Academic Press Cluj Napoca,* **2008.**
14. M. Ahmed, A. Idris, S.R.S. Omar, *Journal of Engineering Science and Technology*, **2007**, **2** 81-94.
15. B. Manohara, S.L. Belagali, *International Journal of Innovative Research in Science, Engineering and Technology*, **2014**, 3, 2, 9664.
16. Z. Y. Hseu, *Bioresource Technology,* **2004**, 95, 53.
17. C. Bachert, W. Bidlingmaier, S. Wattanachira, Handbook on composting in uncovered piles (rows), *European Compost Network ECN/ORBIT,* **2008.**

18. D. Davidescu, V. Davidescu, *Romanian Academy Publishing House Bucharest*, **1992**, 133.
19. Federal Compost Quality Assurance Organisation (FCQAO) and Bundesgütegemeinschaft Kompost e.V. (BGK), Federal Compost Quality Assurance Organisation (FCQAO) and Bundesgütegemeinschaft Kompost e.V. (BGK), **2003**, 6.
20. Digestion Application Note DG-EN-04, Fly Ash, Milestone Microwave Laboratory System, 1.
21. G. Sposito, L.J. Lund, A.C. Chang, *Soil Science Society of America Journal*, **1982**, 46, 260.
22. H.E. Qingsong, Y. Ren, I. Mohamed, M. Ali, W. Hassan, F. Zeng, *Soil & Water Res*., **2013**, 8, 71.
23. Digestion Application Note DG-EN-08 – in accordance with USEPA Method 3051 1998 Microwave assisted acid digestion of sediments, sludge, soils, and oils, *Washington, DC: U.S. Environmental Protection Agency Office of Wastewater Management, 1.*

STUDIA UBB CHEMIA, LXIV, 1, 2019 (p. 79-92)
(RECOMMENDED CITATION)
DOI:10.24193/subbchem.2019.1.06

# INFLUENCE OF TOTAL CHLORIDE, ARSENIC AND ALUMINUM CONTENTS ON MICROORGANISMS OF OPEN WELLS

**THOMAS DIPPONG[a], CRISTINA MIHALI[a], ALEXANDRA AVRAM[b], FIRUTA GOGA[b,*]**

**ABSTRACT.** The paper presents the level and spatial distribution of total chloride, arsenic and aluminum contents, and that of microbiological parameters (coliform bacteria, *E. coli* bacteria, intestinal enterococci) from water wells situated in the Seini area, both on the surface and in depth, using the geostatistical module of ArcGIS. The relations between the levels of microorganisms and the concentrations of chemical parameters (total chlorides, As and Al) were established using Table Curve program for generating 3D mathematical models.

***Keywords:*** *total chloride, arsenic, aluminum, microorganism, drinking water*

## INTRODUCTION

Groundwater represents the world's most exploited raw material and supplies around 31.5 % of the global population with drinking and domestic water [1]. Clean water is a quintessential resource that impacts human quality of life across the globe. With 97.5% of water sources being in the form of salty oceans and 2.15% in that of ice caps and glaciers, the remaining 0.65% is of great importance [2]. With the industrial and agricultural expansion, due primarily to a rapid increase in population, fresh, clean water has become a commodity at present.

[a] *Technical University of Cluj-Napoca, North University Center at Baia Mare, Faculty of Science, 76 Victoriei Street, 430122, Baia Mare, Romania*
[b] *Babeş-Bolyai University, Faculty of Chemistry and Chemical Engineering, 11 Arany Janos str., RO-400028, Cluj-Napoca, Romania*
** Corresponding author: firutagoga@yahoo.com*

Among all contaminants, microorganisms are one of the primary causes of waterborne medical conditions, even if present in low concentrations [2]. However, as it is not economically feasible to test all water sources for every single type of bacteria, the presence of enteric organisms of fecal origin is monitored. Common indicators here come in the form of total coliform bacteria and intestinal enterococci [3]. Microorganisms are relevant markers for the proper health and functioning of the groundwater ecosystem. Thus, by performing microbial analyses such as biomass, activity and diversity of microorganisms, possible organic matter enrichments in groundwater ecosystems could be detected [4].

The spatial distribution characteristics of groundwater presents powerful zonation. This is predominantly caused by the differences in the structures of water storages from mountain to field areas with various scales, water yield properties, and, aquifer permeability [5]. The chemical composition of groundwater and its evolution depend on the mineralogy of the aquifer, overlapping land uses, geochemical processes, the recharge source, as well as the inputs from anthropogenic sources [6]. In terms of its dynamics, groundwater can be classified by the vertical direction (by its depth) into an upper, intense alternation zone, a middle, slow alternation zone, and a bottom, extremely slow alternation zone. In terms of geochemistry and action of microorganisms, aquifers can be classified as high and low-iron content zones [5].

This study is complementary to a previous one about the quality of groundwater in Seini town that focused on heavy metal concentrations [7]. The present study extended the data on the groundwater quality in Seini by the analysis on the microbiological upload of well water samples and spatial distribution of bacterial level in the area [7]. The microbiological data and the chemical parameters, $Cl^-$, As and Al for groundwater samples was analyzed aiming to find an appropriate mathematical model using a computer program of regression analysis.

## RESULTS AND DISCUSSION

### Analysis of the 3D distribution of elements and the microbiological parameters in depth and on the surface of the well water

Figure 1 shows the distribution of concentrations of chloride (mg/L), arsenic (µg/L) and aluminum (µg/L) on the surface and in depth. The mean concentration of total $Cl^-$ was 31.83±17.99 in the range of 11.3-63.8. The levels of Cl- are lower than the maximum admissible concentration of 250 mg/L according to drinking water regulations of Romanian Legislation (Law 311/2004).

Inorganic chloride species from water sterilization and the production of fertilizers, along with organic species derived from the production of pesticides and bleaching of fabric have a strong influence on the $Cl^-$ concentration of plants in the vicinity [6]. Total chlorides content in groundwater derives from natural sources such as weathering of rocks, minerals and soils or anthropogenic sources as spreading of deicers on the roads, wastewater infiltrations, runoff from waste dumps and agriculture practice by irrigation, uses of fertilizers or pesticides [8,9]. The presence of chloride increases the corrosivity of water by enhancing electrical conductivity. In metal pipes, chloride reacts with metal ions to form soluble salts, thus, increasing levels of metals in drinking-water [8].

Aluminum is not a heavy metal, it is an element naturally found in the earth's crust in a proportion of 8% and is thus difficult to avoid. The presence of aluminum in natural or anthropogenic water is due to melting and metal foundries, bitumen sand exploits, oil refining, coal extraction and use or construction [10,11]. In regards to its speciation in potable water, literature reports that the total aluminum concentration is the sum of all colloidal, suspended and monomeric forms [12]. The level of aluminum in water can significantly vary depending on physicochemical and mineralogical factors, generally ranging from 1 to 50 µg/L but rising up to 500–1000 mg/L in more acidic water sources or those rich in organic matter. The highest concentrations of Al were found in the middle and eastern part of the investigated area where the Eutricambisol and Gleisols soils are predominant and the pH was more acidic than in the western part of the town, as was previously reported [7]. The major chemical species of Al that can be present in groundwater are hydroxo-aluminum components and those containing silicon, aluminum species with $Na^+$ and $K^+$ ions, aluminum free ions, aluminum components with F- ions and aluminum species with $SO_4^{2-}$ ions, but aluminum hydroxide complexes and silicon hydroxide complexes are more widespread [13].

Arsenic in water, at natural pH, is found only in inorganic form at valences III and V. Arsenic can enter the food chain through eating contaminated vegetables and meat, and, drinking water. Generally, for humans, trivalent arsenic compounds are 60 times more toxic than pentavalent ones, leading the WHO to regulate its maximum concentration in drinking water at 10 µg/L [9]. The mean As in groundwater was 0.0132±0.00016 µg/L with a low variability indicating the lack of As pollution sources in the area. Following Figure 1 there is an increase in water surface values in densely populated areas. Arsenic content may be due to soil clay content and anthropogenic activities (such as the use of arsenic pesticides and the burning of fossil fuels) [14].

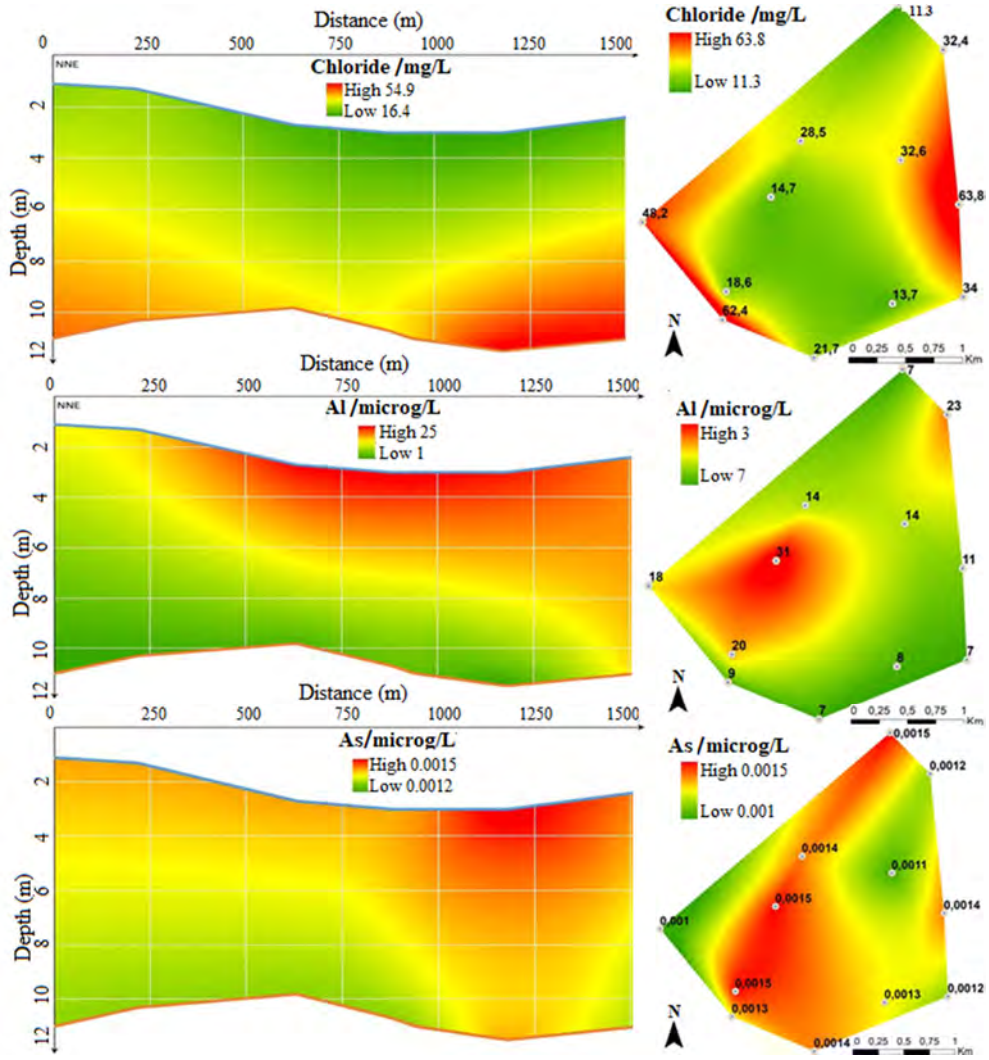


**Figure 1.** Distribution of total chlorides, aluminum and arsenic contents in depth and on the surface

Figure 2 shows the distribution of microbiological parameters (coliform bacteria, E. coli bacteria, and intestinal enterococci) on the surface and in depth of water at the sampling points. The study is very interesting in the conditions in which fountains are open, there being high chances of contamination

with microorganisms. Coliform bacteria in deep water should be lacking if the water sources are not contaminated. It often happens that water contaminated with coliforms reaches boreholes, springs, when it rains during periods of thawing or cracks of the earth. Contaminated water with coliform bacteria should be boiled for at least one minute before it is consumed. Such bacteria are present in the pig and cow farm areas, but also in the area where a well was affected by the floods.

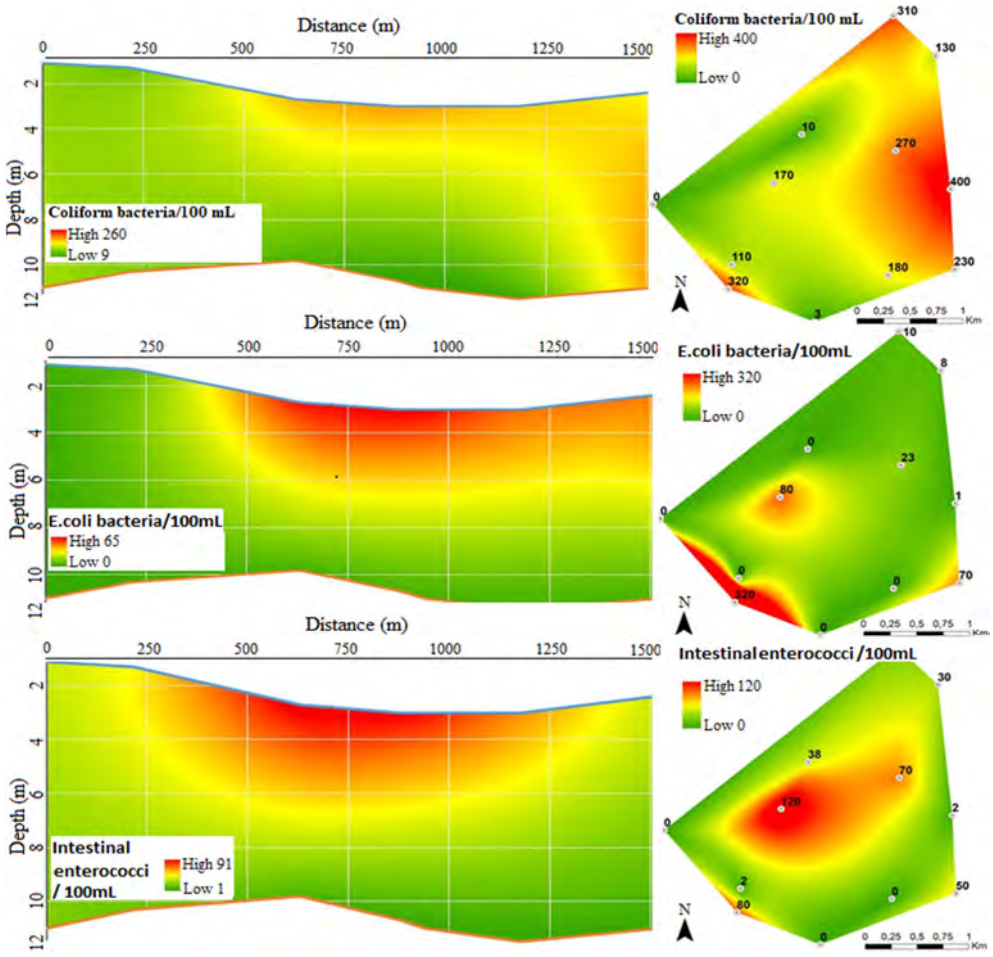


**Figure 2.** Distribution of coliform bacteria, E. coli bacteria and intestinal enterococci in depth and on the surface

Intestinal enterococci are found in surface areas, especially in places where animals are grown and where anthropogenic activities are advanced, or in low areas, as a result of floods that can affect the septic fosses of citizens. According to Figure 2, intestinal enterococci are found on the surface, respectively in the central area of the town, where the population density is higher.

Escherichia coli bacteria, known as E. coli bacteria, is a specific coliform bacterium of fecal origin that lives in the human intestines and intestines of warm blooded animals, also present in their waste. Each country has established its own indicators, among the limits of which the water is considered to meet the conditions necessary for it to be consumed. E. coli bacteria is usually found in the surface layers of the soil, in the areas where animals are grown, and after the manure infiltrates the soil, and then the drinking water affecting large part of the citizens of the town.

Figures 1 and 2 shows the statistical processing of the data presented in the surface distribution maps. The depth of groundwater influences the probability of E. coli bacteria presence. With the increase in well depth, a decrease in the likelihood of contamination by E. coli bacteria was observed [15]. Groundwater microbial quality may be affected by a large environmental and source-specific risk factors such as well design, location and maintenance, septic system location and maintenance, hydrogeological characteristics, and also climatic events like flooding and snowmelt [1,15].

Figure 3 shows the concentration of microorganisms present in all groundwater samples, in the form of E. coli bacteria, Intestinal enterococci and Coliform bacteria. All samples were contaminated, except for samples P7 and P12. A possible explanation is the lack of the systematic water disinfection by chlorination in the open dug and drilled wells. A free residual chlorine concentration below the maximum value of 0.2 mg/L is recommended for prevention of bacterial growth/regrowth [16]. This is common for open dug/ drilled wells found in more rural areas. The mean sequence count of viable microorganisms increased in the following order: P7<P12<P3<P8<P2<P9< P6<<P10<P1 <P4<P5<P11.

E. coli bacteria was found present in P1, P2, P4, P5, P6, P10, and P11 samples in the range of 1 with a maximum of 320 CFU/100mL. Found in samples P1, P2, P3, P4, P5, P6, P8, P9, P10, and P11, Generic Coliform bacteria registered values of 3 CFU/100mL.

On the other hand, the highest value for Intestinal enterococci was registered for samples P1, P2, P3, P4, P5, P6, P8, P10 and P11 at a 2 CFU/100 mL and a total range of 120. Fecal Enterococci have been reported to be much more resistant when in natural environments than their Coliform bacteria counterparts, their presence indicating a strong fecal matter contamination of water [17]. The highest total microorganism contamination was

registered for sample P11. As per most legislation, including WHO guidelines [18] drinking water should be free from any coliform bacteria, E. coli bacteria and intestinal enterococci.

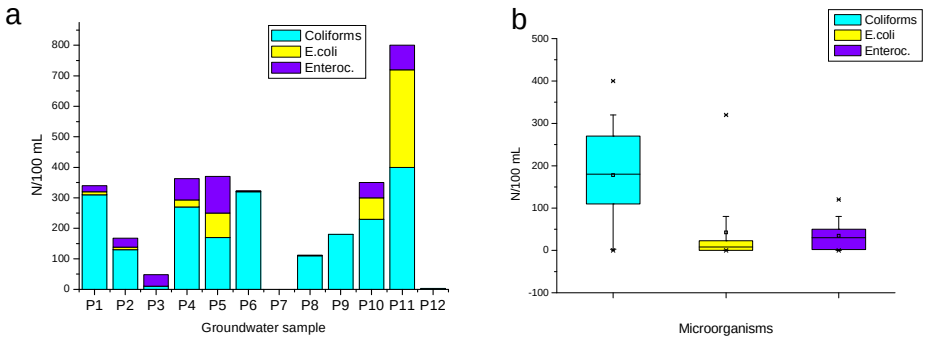


**Figure 3.** Microorganisms in the groundwater samples a) Microorganisms species in P1-P12 groundwater samples; b) Boxplot representation of groundwater contamination

### Cluster analysis

Figure 4 shows the cluster analysis of microorganisms in groundwater samples (a) and the similarities between the indicators of microbiological contamination and the $Cl^-$, Al and As concentrations (b).

The cluster analysis of groundwater samples showed 2 clusters: $C_1$ formed by the majority of the samples with a relatively small bacterial load and $C_2$ where the levels of all the investigated microorganisms are high. $C_1$ is formed by 2 groups: $C_{1a}$ where the total microorganism load was around 350 /100 mL that comprise more wells located in the central part of the town densely populated and $C_{1b}$ with a lower contamination (<100 microorganisms/100 mL). Cluster analysis of variables: microbiological load of groundwater samples depicted in Figure 4 showed high similarity between E. coli bacteria and intestinal enterococci that are very close linked in the dendrogram at double distance to coliforms and to total chlorides content. Total chlorides confer groundwater with improved dissolution properties for both organic and inorganic compounds and also for the nutrients needed for bacteria growth. Al and As formed a distinct cluster at higher distance.

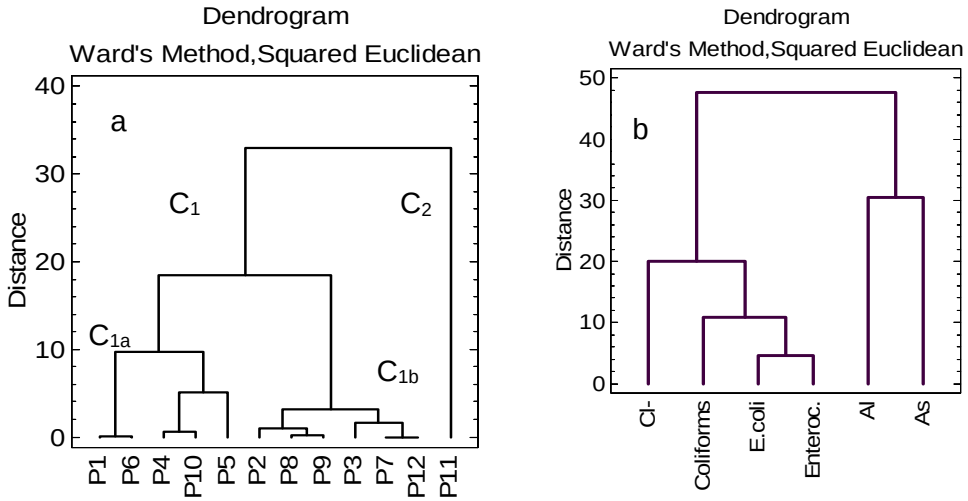


**Figure 4.** Cluster analysis of groundwater samples from Seini: a) Clusters of groundwater samples based on their microbiological characteristics (Coliform bacteria, E. coli bacteria and intestinal enterococci); b) Cluster analysis of similarities between microbiological characteristics and the studied chemical parameters ($Cl^-$, As and Al concentrations)

**Elaboration of 3D mathematical models**

The mathematical models presented in Figure 4 represent the description of the chemical and microbiological properties of the underground water in Seini town. The three elements (chlorine as chloride anions, aluminum, arsenic) give irrelative mathematical models, obtaining low correlation coefficients ($R^2$ much lower than 0.80). However, better mathematical models are obtained in the case of correlations among microbiological characteristics ($R^2 = 0.772$), and in the case of correlation of the microbiological parameters with one element (chlorine, arsenic and aluminum) with correlation when coefficients $R^2 = 0.95$-$0.99$ are obtained.

The 3D mathematical model follows the dependence of the Intestinal enterococci bacteria on coliform bacteria and E. coli bacteria is given by nonlinear equation (1), with $R^2 = 0.772$ and $F = 5.927$.

$$z = 17.96 + 0.026(lnx)^2 + 17.87lny - 0.027y \quad (1)$$

Equation (1) shows the relation between the intestinal enterococci level and that of E.coli bacteria and coliform bacteria. The equation (1) is composed of positive terms as logarithm and a negative term (-0.027y). The positive terms show the simultaneous development of more bacteria species in favorable conditions while the negative term could be related to the microbial competition. It is known that within bacteria communities there is a constant competition with their neighbors for space and resources [19,20].

If the coliform bacteria levels are correlated with the concentration of total chloride and the level of E. coli bacteria, the nonlinear equation (2) is obtained, with $R^2 = 0.865$ and F = 7.705.

$$z = 325.70 - 10.72x + 11.57lny + 0.17dx^2 \quad (2)$$

The influence of aluminum on microbiological parameters leads to a significant increase in the correlation coefficient ($R^2 = 0.900$ and F = 15.67). Thus a 3D mathematical model was obtained showing the dependence of the concentration of E. coli to that of the intestinal enterococci and the concentration of aluminum given by the nonlinear equation (3).

$$\ln z = -27.55 + 30903398x^3 + 0.37y \quad (3)$$

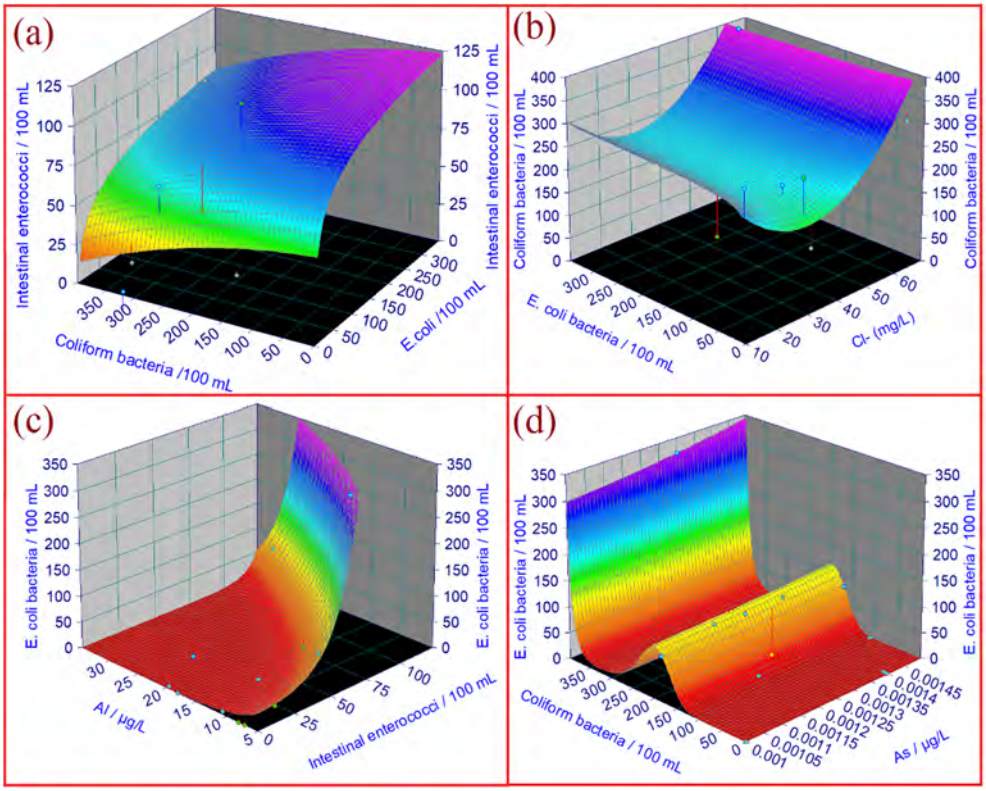


**Figure 5**. The mathematical models 3D between the microbiological parameters and concentration of total chlorides, Al or As in the samples of groundwater: a) the Intestinal enteroccoci (z) = f (E. coli bacteria (x), Coliform bacteria (y)); b) Coliform bacteria (z)= f($Cl^-$(x), E. coli bacteria (y)); c) E. coli bacteria (z)=f (Intestinal enterococci (x), (Al (y)); (d) E. coli bacteria (z)= f(As(x), Coliform bacteria(y))

Similar correlation coefficients are obtained as a result of arsenic use, obtaining a 3D model with the correlation coefficient $R^2$ = 0.985 and F = 302, due to the dependence between E. coli bacteria, arsenic concentrations and coliform bacteria level according to equation (4).

$$z = 4.72 + 0.00051x^2 - 0.24y \quad (4)$$

## CONCLUSIONS

Aluminum, arsenic, E. coli bacteria and intestinal enterococci are distributed in higher concentrations at the surface and in the center of the town, where the population density is higher, while chlorine is distributed at higher concentrations in the deep and at the outskirts of Seini. The distribution maps of the analyzed microorganisms (Coliform bacteria, E. coli bacteria, Intestinal Enterococci) are easy to use and interpret and can be helpful as practical tool for land use and protection zones. Correlations between arsenic, aluminum, and total chlorides contents are very poor (with correlation coefficients below 0.8), without any relevant mathematical model, while correlations between microbiological parameters give a 3D mathematical model with a correlation coefficient of 0.802.

## EXPERIMENTAL SECTION

The town of Seini is located at 26 km west of Baia Mare, 42 km east of Satu Mare and 24 km southeast of Negreşti Oas, is crossed by the Seinel stream that runs in the north-south direction flowing into the River Someș.

The sampling was performed on 12 open wells of 8-14 m depth and 20 cm diameter, located in the Seini area and shown in Figure 6. The sampling was carried out according to SR: ISO 5667-3 / 2013 in polyethylene bottles and the average of obtained values was processed in this paper. The aquifer complex, from which the water specimens were harvested, located in the area of Seini (P1-P6, P9, P10), overlaps in particular with the Seini area's glacis area, which is in contact with the sub-mountain area, cantonated in the quaternary deposits, and is usually intercepted at the contact between the quaternary deposits and the pannonian ones, consisting of clay marl. The location of the samples P7, P8, P11, P12 corresponds to the Somes River terraces. The variation of the waterbath level is closely related to the flow of the Somes River. The position of the P1 sample corresponds to the area of development of the regisols of the Protisoil class [19] formed on unconsolidated colluvial deposits. The soil profile is poorly differentiated and

are porous. The positions of samples P2 and P6, P9, P10 overlap with the Eutricambosoil soil type development area in the Cambisoil class and have water retention capacity and ensure good drainage [19]. Samples P3 and P4 are included in the field surface on which the Gleiosoil type of the Hidrisoils class develops, formed with an excess of groundwater which favor a decrease in aeration and an increase in soil density [19]. Sample P5, is located in a Luvosoil gleic soil type development area of the Luvisoil class, are characterized by the presence of eloquent horizons that are strongly leached by clay and organic colloids in association with the illuvial horizons in which these components are deposited. Appropriate samples of P7, P8, P11 and P12 have the wide development of typical luvosoil are acidic soils [19]. Gleiosoil and Luvisoil types were formed on alluvial / proluvial deposits represented by sands and pebbles from the Pannonic Basin. It is possible that the aquifers are accomodated in these quaternary formations which permits good infiltration and accumulation of waters that form important aquatic states [21].


**Figure 6.** Distribution of sampling points in Seini town

The Al concentrations of samples were measured with the Specord 50 Analytik Jena UV-VIZ spectrophotometer according to the standardized method for low Al concentration (SR ISO 10566 – 2/2001). Al forms a blue color complex with Pyrocatechol Violet reagent at pH 6. The absorbance of this complex was measured at 580 nm in cuvettes of 50 mm. A preliminary step of the analysis was the water sample filtration using a filter membrane

with the pores dimension of 0.45 µm. Then the sample was acidified with $HNO_3$ until a pH in the range of 1.2 - 1.5. To 25 mL of water sample were added the following reagents: 1 mL mixt reagent to eliminate the effect of interfering substances (25 g $MgSO_4 \cdot 7H_2O$, 5 g ascorbic acid, 0.25 g of 1,10-phenanthroline monohydrate dissolved in distilled water and dilute to 100 mL in a calibrated flask), 1 mL of Pyrocatechol Violet solution (0.050g dissolved in distillated water and dilute to 100 mL in a calibrated flask) and finally a buffer solution of hexamethylenetetramine (210 g in 200 mL of distilled water). Then, the sample was left for 15 minutes until the complex formation was accomplished. The absorbance of the complex was measured against a blank reagent. A calibration curve was established using Al solution in concentrations of 2-100 µg/L prepared by appropriate dilution of the standard solution containing 1000 mg Al/L.

Chloride concentration was measured by precipitation titration with silver nitrate according to ISO 9297-2001. A water sample of 50-100 mL adjusted to pH 8.3 with NaOH 0.1 N was titrated with silver nitrate solution in the presence of potassium chromate as indicator, the color of the sample turning from a yellowish-green to a reddish-brown color.

As was determined by graphite furnace atomic absorption spectrometry (GFAAS) following a standardized protocol (SR EN ISO 15586-2004) using a Perkin Elmer AAnalyst 800 spectrophotometer equipped with a graphite furnace. The quality control and quality assurance of the analysis data was realized by using standard procedures, calibration with standard solutions, analysis of blank reagent and analysis of each sample in triplicate. The results were expressed as mean values. Blanks and control samples were measured in parallel. All the reagents used were of analytical degree (PA). The preparation of standard solutions of As was realized using standard solutions of 1,000 ppm, with certified quality and ultrapure water.

The studied microbiological parameters were: Escherichia coli (according to STAS 3001-91), Intestinal enterococci (STAS 3001-91), and coliform bacteria (ISO 4831/2009 European standard).

The samples were collected in presterilized plastic bottles of 100 mL. The preparation step for all the analyzed microbiological parameters was the same. A water sample of 100 mL was filtered through a membrane filter with a porosity of 0.45 µm, using a weak vacuum pump. For intestinal enterococci, after filtration, the membrane was placed using sterile tweezers, on a Slanetz-Bartley medium with the grill upward, in the incubator at 36 ± 2 ˚C for 24 ± 4h. After incubation, the specific colonies of red-brown or pink color were numbered. The result of the analysis was expressed in colony forming units / 100 mL of sample. The analysis of coliforms bacteria and E. coli bacteria was performed by filtering 100 mL of water sample through a 0.45 µm membrane

filter that was placed with a sterile tweezers on agar chromogenic medium in the incubator at 36 ± 2 ˚C for 21-24 hours. After incubation, the filter membranes were examined. The pink-red color spots were numbered indicating the coliform bacteria, and the blue-violet spots indicated the E. coli bacteria. The results of the analysis were expressed in colony forming units /100 mL of sample.

Spatial distribution maps were created using natural neighbor interpolation employing a GIS system and the delimitation of areas with high and low water quality in wells based on indicator values. To draw maps, the values of the indicators were interpolated using the ArcGIS software.

Cluster analysis has been used to group the groundwater sampling points (wells) by their similarity considering their load with the three species of microorganisms. Clusters were generated by Ward's methods based on Squared Euclidean distance in the multidimensional space of data with Statgraphic program.

The mathematical model has been used to describe a system or process that employs mathematical symbols and functions to optimize the design of experiments and better understand the obtained experimental results. The proposed 3D mathematical models are non-linear regression functions with the highest correlation coefficients for a group of 3 parameters generated by the Table Curve program.

## REFERENCES

1. L. Andrade, J. Dwyer, E. O'Neil, P. Hynds, *Environmental Pollution*, **2018**, *236*, 540.
2. D. Li, S. Liu, "Water Quality Monitoring and Management – Basis, Technology and Case Studies", Academic Press, **2019**, chapter 10.
3. M.V. Yates, Drinking Water Microbiology, "Reference Module in Biomedical Sciences", Elsevier, **2018**.
4. J. Voisin, B. Cournoyer, F. Mermillod-Blondin, *Ecological Indicators*, **2016**, *71*, 577.
5. X.Y. Jing, H. Yang, Y. Cao, W. Wang, *Journal of Hydrology*, **2014**, *513*, 30.
6. B. Niu, H. Wang, H.A. Loáiciga, S. Hong, W. Shao, *Science of the Total Environment*, **2017**, *578,* 542.
7. T. Dippong, C. Mihali, M.-A. Hoaghia, E. Cical, A. Cosma, *Ecotoxicology and Environmental Safety*, **2019**, *168*, 88.
8. M.K. Samantara, R.K. Padhi, M. Sowmya, P. Kumaran, K.K. Satpathy, *Groundwater for Sustainable Development*, **2017**, *5*, 49.

9. M. Kumar, A. Puri, *Indian Journal of Occupational and Environmental Medicine*, **2012**, *16*, 40.
10. R. Sadler, B. Maetam, B. Edokpolo, D. Connell, J. Yu, D. Stewart, M.J. Park M, D. Gray, B. Laksono, *Environmental Pollution*, **2016**, *216*, 738.
11. A.H. Panhwar, T. Gul Kazi, Naeemullah, H.I. Afridi, F. Shah, M. B. Arain, S. A. Arain, *Environmental Toxicology and Pharmacology*, **2016**, *43*, 242.
12. M.I.S. Verissimo, M.T.S.R. Gomes, *Analytica Chimica Acta*, **2008**, *617*, 162.
13. C. Marin, A. Tudorache, L. Vlădescu, REV. CHIM. (Bucharest), **2010**, *61*, 431.
14. G. Devic, D. Djordjevic, S. Sakan, *Science of the Total Environment*, **2014**, *468–469*, 933.
15. J. O'Dwyer, P.D. Hynds, K.A. Byrne, M.P. Ryan, C.C. Adley, E*nvironmental Pollution*, **2018**, *237*, 329.
16. A. Farenhorst, R. Li, M. Jahan, H.M. Tun, R. Mi, I. Amarakoon, A. Kumar, E. Khafipour, *Science of the Total Environment*, **2017**, *575*, 813.
16. A. Llopis-Gonzales, A.L. Sanchez, P. Marti Requena, M. Morales Suarez-Varela, *International Journal of Environmental Research and Public Health*, **2014**, *11*, 5527.
17. World Health Organization, Guidelines for Drinking-water Quality – First Addendum to Third Edition, Volume 1 Recommendations, Third Edition.
18. N. Florea, I. Munteanu, “Sistemul Român de taxonomie a solurilor (SRTS)”, **2003**, Editura ESTFALIA București, chapters 2-4.
19. M.E. Hibbing, C.Fuqua, M.R. Parsek, S. B. Peterson, *Nature Reviews Microbiology*, **2010**, *8*, 15.
20. Harta hidrogeologică a României, Scara 1:1000000, Elaborată de Comitetul de stat al Geologiei. Institutul geologic.

STUDIA UBB CHEMIA, LXIV, 1, 2019 (p. 93-102)
(RECOMMENDED CITATION)
DOI:10.24193/subbchem.2019.1.07

# THE RHEOLOGICAL BEHAVIOR OF THE MIXTURES OF CASTOR OIL WITH ADIPIC ESTERS

**ANDRA TĂMAŞ[a], SORINA BORAN[a]***

**ABSTRACT.** The paper presents the rheological behavior study of the mixtures of castor oil with two types of adipic esters. The influence of adipic esters' structure and concentration was determined, as well as that of temperature, on the rheological behavior, by setting the dependence between the shear stress $\tau$ and the shear rate $\dot{\gamma}$. The analysis of the dependence between $\tau$ and $\dot{\gamma}$ demonstrates that the studied solutions present Newtonian behavior. The evolution of samples' viscosity with temperature was characterized by Arrhenius type equations, being established the values of viscous flow activation energy, $E_a$. It was also realized a characterization of annulus fluids flow under the effect of rotational motion, calculating the values of dimensionless criterion Taylor-Reynolds ($Ta_{Re}$).

***Keywords:*** *adipic ester, flow activation energy, Newtonian behavior, Taylor-Reynolds number*

## INTRODUCTION

The complex aliphatic-aromatic esters have the characteristics of lubricants with high performing physico-chemical, rheological and tribo-technical properties. Vegetable oils, on the other hand, have the characteristics of biodegradable lubricants with no negative impact on the enviroment but which, however, are not as competitive as the synthetic ester based oils.

Currently, we aim to obtain lubricating products that do not influence the environment but which have superior lubricating properties. With the proper formulation of the base oil and the proper use of additive packs,

[a] *Politehnica University Timisoara, Faculty of Industrial Chemistry and Environmental Engineering, 6 V. Pârvan Bd., RO-300223, Timisoara, Romania*
**Corresponding author E-mail: sorina.boran@upt.ro*

biodegradable lubricants may be better than conventional lubricants [1]. For this purpose, mixtures of castor oil with two types of adipic esters were prepared in various proportions, and was studied the rheological behavior, as well as the characterization of flow through ring-shaped spaces [2-4].

The adipic esters with complex structure [5-7], with superior lubricating properties, have been synthesized from an aliphatic-aromatic alcohol in conjunction with various aliphatic alcohols of variable length.

The use of mixtures with castor oil is a studied choice, there being a series of studies demonstrating that castor oil is a compound that can bring significant improvements to the properties of the studied final products [8-11].

## RESULTS AND DISCUSSION

The main physico-chemical properties for C1(isodecyl and 2-(*p*-nonyl-fenoxy) ethyl adipate) and C2(isotridecyl and 2-(*p*-nonyl-fenoxy) ethyl adipate) are presented in Table 1. For castor oil and its mixtures with adipic esters, several properties are selectively presented in Table 2. In addition, the kinematic viscosities of the mixtures at two temperature values, as well as the viscosity index, were determined [12].

**Table 1.** The properties of adipic esters at 20°C

| Ester | Formula | $M$/g mol$^{-1}$ | $\rho$/kg m$^{-3}$ | $n_D$ | Saponification index, mg KOH g$^{-1}$ | |
|---|---|---|---|---|---|---|
| | | | | | theoretical | analytical |
| C1 | $C_{33}H_{56}O_5$ | 532 | 971.5 | 1.4830 | 316.38 | 315.74 |
| C2 | $C_{36}H_{62}O_5$ | 574 | 959.6 | 1.4824 | 293.23 | 293.12 |

**Table 2.** Properties of castor oil (CO) and its mixtures with adipic esters at 20°C

| Composition, wt.% | Property | | |
|---|---|---|---|
| | $\rho$ / kg m$^{-3}$ | $n_D$ | Iodine value, g $I_2$ / 100 g |
| **C1/CO** | | | |
| 0/100 | 960.1 | 1.4781 | 86.00 |
| 25/75 | 964.2 | 1.4789 | 39.41 |
| 50/50 | 965.5 | 1.4811 | 22.67 |
| 75/25 | 968.7 | 1.4815 | 15.12 |
| **C2/CO** | | | |
| 25/75 | 956.0 | 1.4794 | 50.06 |
| 50/50 | 959.8 | 1.4808 | 41.22 |
| 75/25 | 959.6 | 1.4821 | 20.16 |

The influence of the ester type in mixtures with castor oil on their rheological behavior has been studied for different ester concentrations, at 3 temperature values. The dependence $\tau = f(\dot{\gamma})$ for the mixtures with 25 wt.% adipic esters is shown in Figure 1 and the obtained rheological equations are shown in Table 3.

It is noted that increasing the number of carbon atoms of the aliphatic alcohol used in the esterification leads to a slightly increase of the mixtures viscosity, but not modify their Newtonian behavior. Also, the increase in temperature leads to the decrease of the viscosity of the mixtures without altering their rheological behavior.

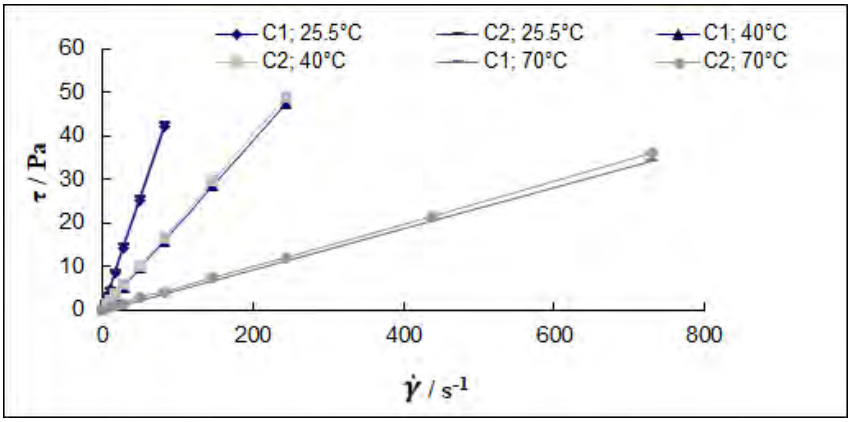


**Figure 1.** Shear stress *vs.* shear rate for the mixtures with 25 wt.% adipic esters

**Table 3.** Rheological equations of the mixtures with 25 wt.% adipic esters

| Temperature, °C | Eq. $\tau = \eta \cdot \dot{\gamma}$ | | Viscosity decreasing*, % |
|---|---|---|---|
| | C1 + CO | C2 + CO | |
| 25.5 | $\tau = 0.5184 \cdot \dot{\gamma}$ | $\tau = 0.5265 \cdot \dot{\gamma}$ | 1.56 |
| 40 | $\tau = 0.1941 \cdot \dot{\gamma}$ | $\tau = 0.1993 \cdot \dot{\gamma}$ | 2.68 |
| 70 | $\tau = 0.0464 \cdot \dot{\gamma}$ | $\tau = 0.0471 \cdot \dot{\gamma}$ | 1.51 |

*Sample with C1 compared with sample with C2

In addition, the influence of the esters' concentration in the mixtures with castor oil was studied. Thus, for the mixtures C2/CO at 25.5°C, the dependence $\tau = f(\dot{\gamma})$ is shown in Figure 2.

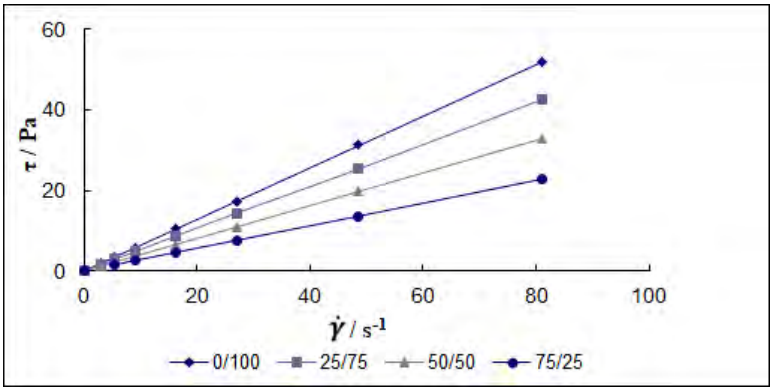


**Figure 2.** Shear stress *vs.* shear rate for the mixtures C2/CO at 25.5°C

From the slope of the obtained straight lines, it was observed that the mixtures containing adipic ester C2 have less viscosity compared to the viscosity of castor oil, the decrease being more pronounced with the increase of the ester content and with the increase of temperature. The mixtures C1/CO presents similar behavior, too. The obtained viscosity values are presented in Table 4.

**Table 4.** Dynamic viscosities of the samples

| wt.% C1 | η / mPa.s | | Viscosity decreasing*% | wt. % C2 | η / mPa.s | | Viscosity decreasing*% |
|---|---|---|---|---|---|---|---|
| | 25.5°C | 70°C | | | 25.5°C | 70°C | |
| 0 | 643.7 | 66.8 | - | 0 | 643.7 | 66.8 | - |
| 25 | 518.4 | 46.4 | 19.5/30.5 | 25 | 526.5 | 47.1 | 18.2/29.5 |
| 50 | 392.3 | 29.0 | 39.1/56.6 | 50 | 404.5 | 30.4 | 37.2/54.5 |
| 75 | 271.1 | 15.6 | 57.9/76.6 | 75 | 281.5 | 16.5 | 56.3/75.3 |

* compared to castor oil, at 25.5°C and 70°C, respectively

The exponential decrease of the mixtures' viscosity with temperature is described by an Arrhenius-type equation:

$$\eta = A \cdot \exp\left(\frac{E_a}{R \cdot T}\right) \quad (1)$$

where $E_a$ is the activation energy of the viscous flow, J mol$^{-1}$, $R$ the universal gas constant, J mol$^{-1}$ K$^{-1}$, $T$ absolute temperature and $A$ is a material constant, Pa s.

Through the measurements at different temperatures, it was possible to establish the dependence $\ln\eta = f(1/T)$ and to calculate the $E_a$ values. Particular expressions of equation (1) for adipic esters/castor oil mixtures are presented in Table 5.

**Table 5.** Arrhenius-type equations for the analyzed mixtures

| **Ester content, wt.%** | **Eq.** $\eta = A\times10^{9}\cdot\exp(E_a/R\cdot T)$ | $E_a$ **/ kJ mol$^{-1}$** |
|---|---|---|
| 0 | $\eta = 17.1\cdot\exp(5207/T)$ | 43.3 |
| 25 (C1) | $\eta = 5.6\cdot\exp(5463/T)$ | 45.4 |
| 25 (C2) | $\eta = 5.0\cdot\exp(5499/T)$ | 45.7 |
| 50 (C1) | $\eta = 1.0\cdot\exp(5872/T)$ | 48.8 |
| 50 (C2) | $\eta = 1.2\cdot\exp(5836/T)$ | 48.5 |
| 75 (C1) | $\eta = 0.13\cdot\exp(6354/T)$ | 52.8 |
| 75 (C2) | $\eta = 0.14\cdot\exp(6342/T)$ | 52.7 |

It is found that at the same concentration of the ester, the values of the flow activation energy are very close and increase with increasing the ester content.

Since lubrication is usually used in rotating systems (bearings, gears etc), the dynamic characteristics (speed, dynamic pressure, shear stress) will be expressed in terms of Taylor-Reynolds number ($Ta_{Re}$) specific to this type of motion. This criterion is also used to characterize fluids flow in ring-shaped spaces (the space bounded by the two coaxial cylinders) under the effect of a controlled rotational motion (the revolution of the inner cylinder).

The values of $Ta_{Re}$ number were calculated using relation (2), taking into account the radii of the inner and outer cylinder ($r_i$ and $r_o$), the inner cylinder revolution number, $n$, and the fluid properties (viscosity $\eta$ and density $\rho$) [4,13]:

$$Ta_{\mathrm{Re}} = \frac{2\cdot\pi\cdot n\cdot r_i\cdot(r_o - r_i)\cdot\rho}{\eta} \qquad (2)$$

Increasing the hydrodynamic regime leads to a pronounced decrease of the ratio between shear stress $\tau$ (experimentally determined) and dynamic

pressure $P_{dyn}$. This ratio is a direct measure of the increase in centrifugal or inertial forces, in correlation with the viscous friction force, depending on the $Ta_{Re}$ number. By analogy with fluids flow through straight pipes, the dynamic pressure of the fluid in motion in ring-shaped spaces is calculated by:

$$P_{dyn} = \frac{\rho \cdot w_{\max}^2}{2} \tag{3}$$

$$w_{\max} = \pi \cdot d_i \cdot n \tag{4}$$

where $w_{max}$ is the speed of the fluid laminar layer placed next to the moving wall (inner cylinder) and $d_i$ is the inner diameter of the ring-shaped space.

For the analyzed samples, at a constant temperature (40°C), the dependence $\tau / P_{din} = f(Ta_{\mathrm{Re}})$ is shown in Figure 3.

It can be seen that the graphical representation places the results after a parabolic curve, without significant changes depending on the ester type or concentration. Also, it is noted an accentuated decrease in the ratio $\tau / P_{dyn}$ with the increase of hydrodynamic flow regime and the increase of ester concentration.

By analogy with the circular motion of the fluid in stirring processes [2-4,14], the ratio $\tau / P_{dyn}$ is correlated with $Ta_{Re}$ number by a relatioship of type:

$$\tau / P_{dyn} = C \cdot Ta_{\mathrm{Re}}^{m} \tag{5a}$$

or, in the linear logarithmic form:

$$\ln(\tau / P_{dyn}) = \ln C + m \cdot \ln(Ta_{\mathrm{Re}}) \tag{5b}$$

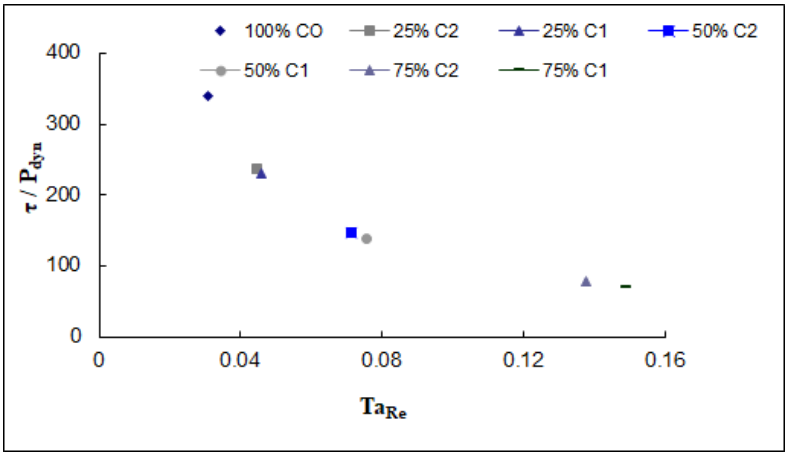


**Figure 3.** Ratio $\tau / P_{din}$ *vs.* $Ta_{\mathrm{Re}}$ for the mixtures adipic ester/castor oil at 40°C

The particular forms of relation (5b), determined for the mixtures C1/CO, at 40°C, are shown in Table 6a, and for the samples with 25 wt.% adipic esters, at different temperature values, are shown in Table 6b.

**Table 6a.** Particular forms of eq. (5b) for the mixtures C1/CO at 40°C

| Ester content, wt.% | **Eq.** $\ln(\tau/P_{din}) = \ln C + m \cdot \ln(Ta_{\mathrm{Re}})$ | C |
|---|---|---|
| 0 | $\ln(\tau/P_{din}) = 2.3515 - 1.0008 \cdot \ln(Ta_{\mathrm{Re}})$ | 10.5 |
| 25 | $\ln(\tau/P_{din}) = 2.3530 - 1.0004 \cdot \ln(Ta_{\mathrm{Re}})$ | 10.517 |
| 50 | $\ln(\tau/P_{din}) = 2.3536 - 1.0002 \cdot \ln(Ta_{\mathrm{Re}})$ | 10.523 |
| 75 | $\ln(\tau/P_{din}) = 2.3539 - \ln(Ta_{\mathrm{Re}})$ | 10.526 |

**Table 6b.** Particular forms of eq. (5b) for the mixtures adipic ester/CO 25/75 wt.%

| Temperature, °C | **Eq.** $\ln(\tau/P_{din}) = \ln C + m \cdot \ln(Ta_{\mathrm{Re}})$ | C |
|---|---|---|
| **C1** | | |
| 25.5 | $\ln(\tau/P_{din}) = 2.5173 - 0.9643 \cdot \ln(Ta_{\mathrm{Re}})$ | 12.395 |
| 40 | $\ln(\tau/P_{din}) = 2.3530 - 1.0004 \cdot \ln(Ta_{\mathrm{Re}})$ | 10.517 |
| 70 | $\ln(\tau/P_{din}) = 2.3443 - 1.0035 \cdot \ln(Ta_{\mathrm{Re}})$ | 10.426 |
| **C2** | | |
| 25.5 | $\ln(\tau/P_{din}) = 2.3540 - \ln(Ta_{\mathrm{Re}})$ | 10.527 |
| 40 | $\ln(\tau/P_{din}) = 2.3530 - 1.006 \cdot \ln(Ta_{\mathrm{Re}})$ | 10.517 |
| 70 | $\ln(\tau/P_{din}) = 2.3538 - 1.0005 \cdot \ln(Ta_{\mathrm{Re}})$ | 10.525 |

The values of parameter $C$ in relation (5a) can be considered as an equilibrium value of Taylor-Reynolds number ($Ta^{*}_{\mathrm{Re}}$), taking into account the condition of equality between shear stress and dynamic pressure ($\tau/P_{dyn} = 1$ or $\ln(\tau/P_{dyn}) = 0$). For all the analyzed samples, the equilibrium values are less than the critical value ($Ta_{\mathrm{Re},cr} = 60$) specific to laminar flow of the fluids in ring-shaped spaces [13,15].

Under these conditions, assuming that the shear stress $\tau$ is equivalent to the friction pressure drop, it can be accept that the ratio of the two parameters is equal to the friction coefficient $\lambda$ corresponding to laminar

flow regime ($\lambda = 64 \cdot \mathrm{Re}^{-1}$). On the other hand, from the equations presented in Tables 6a and 6b, it can be noticed that the values of $m$ are very close to -1, similar to the exponent of Reynolds number in the friction coefficient expression, and that the values of $C$ slightly increase with increasing the ester concentration.

## CONCLUSIONS

It was studied the rheological behavior of the mixtures of castor oil with two types of adipic esters, monitoring the influence of the temperature, as well as that of the ester type and concentration. Also, the behavior of these mixtures at the flow through ring-shaped spaces was analyzed.

For each analyzed sample it was obtained a linear dependence between shear stress $\tau$ and shear rate $\dot{\gamma}$, without yield point $\tau_0$, which shows that castor oil and its mixtures with adipic esters presents Newtonian behavior, regardless of the temperature and type and concentration of the ester, respectively. The addition of adipic esters in castor oil leads to viscosity decreasing, the decrease being proportional to the increase in ester concentration.

From the Arrhenius type equations it is noted that the values of the viscous flow activation energy increase with the increase of the ester concentration in the mixture, but, under the same conditions, the values of the pre-exponential coefficient decrease. At the same concentration of the ester, the values of the two parameters ($E_a$, $A$) are very close, not being influenced by the modify in the number of carbon atoms of the aliphatic alcohol used in the esterification.

For the analyzed mixtures, the dependence between the rheological parameters and the Taylor-Reynolds number, was established. From the graphical representations of this dependence it can be concluded that, through the ring-shaped space (delimited by the two coaxial cylinders) of the Rheotest-2 viscometer, the flow of the mixtures of castor oil with adipic esters takes place in the laminar regime.

## EXPERIMENTAL SECTION

*General procedure for ester preparation*

The preparation of the adipic esters was performed according to our previously reported procedure [5-7] by reacting the adipic acid with 2-(*p*-

Nonylphenoxy)ethanol in conjunction with an aliphatic alcohol of 10 or 13 carbon atoms, by a two steps process, using *p*-toluenesulphonic acid as catalyst. The formed water was extracted azeotropically by means of toluene. These two esters are illustrated in the following general structure $R_1OOC-(CH_2)_4-COOR_2$, where: $R_1$ = isodecyl or isotridecyl; $R_2$ = $-CH_2-CH_2-O-C_6H_4-R_3$; $R_3$ = *p*-nonyl.

The castor oil was supplied by Fluka. The samples preparation was realized at room temperature (25°C), under intense stirring.

The physico-chemical properties were determined by using standardized techniques: the pycnometer method for density determination and the Abbe refractometer for refractive indices.

The rheological measurements were carried out under thermostatic conditions, at different temperatures ranging from 25.5ºC to 70ºC, using a Rheotest-2 rotational viscometer with the system vat-drum $S/S_1$. The device allows the measurement of the torsion moment appeared thanks to the ring-shaped substance layer placed between a fixed cylinder and a rotating one with known revolution. The torsion moment is correlated with the shear stress. The revolution and the ring-shaped layer thickness determine the shear rate. Shear rate values were changed in the range $3 \div 729\ s^{-1}$.

## REFERENCES


1. A.Z.Syahir, N.W.M. Zulkifli, H.H. Masjuki, M.A. Kalam *et.al., Journal of Cleaner Production,* **2017**, *168*, 997.
2. S. Boran, A. Tămaș, *Studia UBB Chemia,* **2013**, *LVIII, 3,* 21
3. S. Boran, A. Tămaș, *Journal of the Serbian Chemical Society,* **2014**, *79(2),* 241.
4. Z. Gropșian, A. Tămaș, R. Minea, N. Borș, *Bulletin of Romanian Chemical Engineering Society,* **2014**, *1(1),* 91.
5. L. Mirci, S. Boran, *Materiale Plastice,* **2007**, *44(4),* 383.
6. L. Mirci, S. Boran, P. Luca, V. Boiangiu, 15th International Colloquium Tribology- Technische Akademie Esslingen, Ostfildern, Germania, **17-19 Jan. 2006**, Synopses Synthetic Oils, 236.
7. L. Mirci, S. Boran, RO 122.453, **2009.**
8. L. Xia, D. Cao, H. Zhang, Y. Guo, *Construction and Building Materials,* **2016**, *112,* 949.
9. G. Totaro, L. Cruciani *et.al., European Polymer Journal,* **2014**, *56*, 174.
10. R.M.A. Saboya, J.A. Cecilia, C. Garcia-Sancho, A.V. Sales *et.al., Industrial Crops and Products,* **2017***, 104*, 52.

11. M. Ozcanli, M. Atakan Akar, A. Calik, H. Serin, *International Journal of Hydrogen Energy,* **2017**, *42, 23366.*
12. S. Boran, A. Tămaș, *Materiale Plastice,* **2016**, *53(3),* 505.
13. N. Borș, "Contributions to the study of the influence of some chemical substances on improving flow", PhD Thesis, Ed. Politehnica, Timișoara, **2010**, 80.
14. A. Tămaș, N. Borș, R. Minea, *Petroleum-Gas University of Ploiești Bulletin, Technical Series,* **2008**, *LX*, 105.
15. D.E. McMillan, J. Strigberger, N.G. Utterback, *Biorheology,* **1987**, *24(4),* 401.

STUDIA UBB CHEMIA, LXIV, 1, 2019 (p. 103-112)
(RECOMMENDED CITATION)
DOI:10.24193/subbchem.2019.1.08

# EXCESS AND DEVIATIONS PROPERTIES FOR THE BINARY SOLVENT MIXTURES OF TETRAHYDROFURFURYL ALCOHOL WITH SOME AROMATIC HYDROCARBONS AT 298.15K

**DHAFIR TAMWEEN AJEEL AL-HEETIMI[a]*, ZAINAB ABBAS AL-DULAIMY[a], ASAL AHMED AL-JAWARY[a], OMAR SABEEH AL-KHAZRAJY[a]**

**ABSTRACT.** In this work, excess properties (e.g. excess molar volume ($V^E$), excess viscosity ($\eta^E$), excess Gibbs free energy of activation of viscos flow ($\Delta G^{*E}$) and molar refraction changes ($\Delta n_D$) of binary solvent mixtures of tetrahydrofurfuryl alcohol (THFA) with aromatic hydrocarbons (benzene, toluene and p-xylene) have been calculated. This was achieved by determining the physical properties including density ρ, viscosity η and refraction index $n_D$ of liquid mixtures at 298.15K. Results of the excess parameters and deviation functions for the binary solvent mixtures at 298.15 K have been discussed by molecular interactions that occur in these mixtures. Generally, parameters showed negative values and have been found to fit well to Redlich-Kister equation which has been used to obtain the coefficients and evaluate the standard error.

***Keywords:*** *Binary systems, Tetrahydrofurfuryl alcohol, Deviations and excess properties, Density, Viscosity.*

## INTRODUCTIONS

Interest in studying the theoretical and experimental properties of solvents mixtures has been significantly increased in the last two decades. The thermodynamic and transport information (e.g. fluids flow, heat and mass transfer) of mixtures systems are important in many chemical industries,

[a] *University of Baghdad, College of Education for pure science Ibn-Al-Haitham, Department of Chemistry, Baghdad, Iraq.*
** Corresponding Author: E-mail: dhafir1973@gmail.com; E-mail: dhafir.t.a@ihcoedu.uobaghdad.edu.iq*

solution theories and biological processes [1-4]. Moreover, for profound understanding the interaction properties between component molecules of liquid mixture, in terms of nature, strength of interaction and behavior of solution, the experimental excess properties are very important [5-8].

Tetrahydrofurfuryl alcohol (THFA), benzene, toluene and p-xylene are widely used in chemical industries. These solvents have been used in fuel, perfumes, cosmetics, lubricants, paints, dyes, printing ink, drugs, gums, resins, etc. [9,10]. The excess properties for these organic solvents are useful in investigating the molecular motion and packing, and interaction in their mixtures [11].

In this study, physical properties such as density, viscosity and refractive index were determined over a range of binary systems ((THFA+ Benzene), (THFA +Toluene) and (THFA+P-Xylene)) concentrations at 298.15K. Excess molar properties including $V^E$ $\eta^E$, $\Delta G^{*E}$ and refractive index deviation were derived. Up to our knowledge, those binary solvent mixtures have not been studied for $V^E$, $\eta^E$, $\Delta G^{*E}$, and $\Delta n_D$ at any temperature.

## RESULTS AND DISCUSSION

In this work the retrieved data from experimentally obtained density (ρ) for binary systems (THFA + benzene, THFA + toluene and THFA + p-xylene) at 298.15 K were used to calculate $V^E$ for binary solvent mixtures using following equation (1) [12]:

$$V^E = \frac{X_1M_1 + X_2M_2}{\rho_{12}} - \frac{X_1M_1}{\rho_1} - \frac{X_2M_2}{\rho_2} \quad (1)$$

where $X_1$ and $X_2$ are the mole fractions, $M_1$ and $M_2$ are the molar masses and $\rho_1$, $\rho_2$ are densities of solvents 1 and 2; while $\rho_{12}$ is the density of the mixture. Values of $V^E$ and ρ of the binary solvent systems at a range of mole fractions of THFA with benzene, toluene and p-xylene are presented in Table 1. Excess viscosities were obtained using equation (2) [13]:

$$\eta^E = \eta_{12} - (X_1\eta_1 + X_2\eta_2) \quad (2)$$

where $\eta_1$ and $\eta_2$ are viscosities of solvents 1 and 2, respectively, $\eta_{12}$ is the viscosity of mixture. The results are listed in Table 1.

Equation 3 was used to calculate ($\Delta G^{*E}$) [14]:

$$\Delta G^{*E} = RT[\ln(\eta_{12}V_{12}) - (X_1\ln\eta_1V_1) - (X_2\ln\eta_2V_2)] \quad (3)$$

where R is gases universal constant and T is the absolute temperature (K). $V_1$, $V_2$ are the molar volumes of solvents 1 and 2; while $V_{12}$ is the molar volume for binary system. Table 1 shows the values of $\Delta G^{*E}$ determined from equation 3. $V_{12}$ has been obtained from the below equation:

$$V_{12} = (X_1M_1 + X_2M_2)/\rho_{12} \quad (4)$$

Molar refraction ($n_D$) was calculated using the Lorentz-Lorenz equations (5,6, and 7) [15]

$$n_D = \left(\frac{n_{12}^2-1}{n_{12}^2+2}\right)\frac{X1M1+X2M2}{\rho_{12}} \quad (5)$$

$$n_{D1} = \left(\frac{n_1^2-1}{n_1^2+2}\right)\frac{X1M1}{\rho_1} \quad (6)$$

$$n_{D2} = \left(\frac{n_2^2-1}{n_2^2+2}\right)\frac{X2M2}{\rho_2} \quad (7)$$

where $n_{12}$ is the refractive index of the mixture; whereas $n_1$ and $n_2$ are the refractive index of solvent 1 and 2, respectively. The deviation from a molar fraction average of the molar refraction was computed according to the equation (8) [16,17]:

$$\Delta n_D = n_D - X_1 n_{D1} - X_2 n_{D2} \quad (8)$$

where $\Delta n_D$ represents the deviation value from molar fraction. Table 1 lists experimental $n_D$ and $\Delta \mathbf{n_D}$ for the binary solvent mixtures.

For binary solvent mixtures, the excess function was determined using Redlich-Kister model equation (9) [18]:

$$X^E = X_i X_j \sum_{K=0}^{n} A_K (X_i - X_j)^k \quad (9)$$

where $X^E$ may represent $V^E$, $\eta^E$, $\Delta G^{*E}$ or $\Delta n_D$. $X_i$ and $X_j$ are the mole fractions of the components i and j, respectively. n is the degree of polynomial expansion and $A_k$ denotes the polynomial coefficients.The equation (10) was used to calculate standard deviation (σ) for the excess parameters [19]:

$$\sigma = \left[\sum \left(X_{exp}^E - X_{calc}^E\right)^2/(M-n)\right]^{1/2} \quad (10)$$

where *M* is the number of data points and *n* is the number of estimated parameters. The values of these coefficients and the standard deviation are given in Table 2.

For all the studied systems, the negative values of $V^E$, $\eta^E$, $\Delta G^{*E}$, $\Delta n_D$ follow the order: Benzene > Toluene > p-xylene. Fig.1 shows the deviations in molar volume for all the systems (THFA+ benzene), (THFA+ toluene) and (THFA+ p-xylene). The obtained negative values of $V^E$ can be attributed to the interactions of dipolar-induced forces between the benzene ring of the aromatic hydrocarbons and hydroxyl group (OH) or oxygen of the THFA, which results the formation of electron donor-acceptor complexes and the breaking of the self-associations existing in pure solvents [20,21].

**Table 1**. Experimentally obtained and calculated values of density, viscosity and refractive index, $V^{E,}$ $\eta^{E}$, $\Delta G^{*E}$, $n_D$ and $\Delta n_D$ for binary solvent mixtures of THFA+benzene, THFA+ toluene and THFA+ p-xylene at 298.15K.

| **$X_1$ THFA + $X_2$ benzene at 298.15K** | | | | | | | |
|---|---|---|---|---|---|---|---|
| **$X_1$** | ρ(g.cm$^{-3}$) | $V^E$ cm$^3$mol$^{-1}$ | Ƞ | Ƞ$^E$ mpa.s | $\Delta G^{*E}$ (J.mol$^{-1}$) | $n_D$ | $\Delta n_D$ |
| 0.0000 | 0.87372 | 0.00000 | 0.59951 | 0.00000 | 0.0000 | 1.4975 | 0.0000 |
| 0.0867 | 0.89294 | -0.11763 | 0.65845 | -0.08836 | -218.2600 | 1.4882 | -0.2377 |
| 0.2012 | 0.91623 | -0.16936 | 0.81019 | -0.12150 | -299.6432 | 1.4754 | -0.5832 |
| 0.3078 | 0.93673 | -0.19441 | 0.99374 | -0.14121 | -348.0611 | 1.4664 | -0.7895 |
| 0.3622 | 0.94663 | -0.18579 | 1.10746 | -0.14713 | -362.5572 | 1.4636 | -0.8175 |
| 0.5033 | 0.97132 | -0.16189 | 1.48353 | -0.15119 | -372.4340 | 1.4581 | -0.8077 |
| 0.5528 | 0.97965 | -0.15214 | 1.65007 | -0.14877 | -366.4779 | 1.4571 | -0.7589 |
| 0.6664 | 0.99804 | -0.11675 | 2.13172 | -0.13130 | -323.4082 | 1.4552 | -0.6238 |
| 0.8307 | 1.02332 | -0.06816 | 3.09948 | -0.10213 | -251.8803 | 1.4545 | -0.3136 |
| 0.9082 | 1.03474 | -0.04150 | 3.77085 | -0.06886 | -169.9206 | 1.4536 | -0.1879 |
| 1.0000 | 1.04761 | 0.00000 | 4.89883 | 0.00000 | 0.0000 | 1.4532 | 0.0000 |

| **$X_1$ THFA + $X_2$ toluene at 298.15K** | | | | | | | |
|---|---|---|---|---|---|---|---|
| **$X_1$** | ρ(g.cm$^{-3}$) | $V^E$ cm$^3$mol$^{-1}$ | Ƞ | Ƞ$^E$ mpa.s | $\Delta G^{*E}$ (J.mol$^{-1}$) | $n_D$ | $\Delta n_D$ |
| 0.0000 | 0.86224 | 0.00000 | 0.55464 | 0.00000 | 0.0000 | 1.4950 | 0.0000 |
| 0.0801 | 0.87733 | -0.17517 | 0.55817 | -0.16815 | -416.0727 | 1.4855 | -0.3714 |
| 0.2024 | 0.89945 | -0.27578 | 0.67662 | -0.24213 | -598.5265 | 1.4750 | -0.7081 |
| 0.3004 | 0.91712 | -0.30678 | 0.82295 | -0.25982 | -641.8989 | 1.4670 | -0.9415 |
| 0.3968 | 0.93436 | -0.28668 | 1.01161 | -0.26343 | -650.4906 | 1.4624 | -0.9856 |
| 0.5022 | 0.95335 | -0.24312 | 1.27016 | -0.26543 | -655.2431 | 1.4581 | -0.9821 |
| 0.5867 | 0.96872 | -0.19668 | 1.55083 | -0.24986 | -616.8046 | 1.4562 | -0.8887 |
| 0.7005 | 0.98983 | -0.13909 | 2.08992 | -0.19942 | -492.1386 | 1.4553 | -0.6653 |
| 0.7915 | 1.00704 | -0.09509 | 2.64994 | -0.16026 | -395.4876 | 1.4547 | -0.4714 |
| 0.8996 | 1.02791 | -0.04847 | 3.57807 | -0.09546 | -235.6671 | 1.4539 | -0.2334 |
| 1.0000 | 1.04761 | 0.00000 | 4.89883 | 0.00000 | 0.0000 | 1.4532 | 0.0000 |

| $X_1$ THFA + $X_2$ p-xylene at 298.15K | | | | | | | |
|---|---|---|---|---|---|---|---|
| $X_1$ | ρ(g.cm$^{-3}$) | $V^E$ cm$^3$mol$^{-1}$ | Ƞ | $Ƞ^E$ mpa.s | $\Delta G^{*E}$ (J.mol$^{-1}$) | $n_D$ | $\Delta n_D$ |
| 0.0000 | 0.85676 | 0.00000 | 0.61225 | 0.00000 | 0.0000 | 1.4945 | 0.0000 |
| 0.1074 | 0.87474 | -0.20439 | 0.66272 | -0.14414 | -350.8699 | 1.4859 | -0.5063 |
| 0.2045 | 0.89176 | -0.38483 | 0.73091 | -0.24813 | -604.0360 | 1.4773 | -0.9615 |
| 0.2921 | 0.90681 | -0.42023 | 0.84477 | -0.28553 | -693.5423 | 1.4710 | -1.2382 |
| 0.3968 | 0.92537 | -0.43209 | 1.02825 | -0.30671 | -743.5405 | 1.4669 | -1.3145 |
| 0.5168 | 0.94742 | -0.40192 | 1.29614 | -0.32474 | -787.1356 | 1.4629 | -1.2905 |
| 0.6108 | 0.96535 | -0.35118 | 1.59703 | -0.31146 | -754.8408 | 1.4602 | -1.1920 |
| 0.7255 | 0.98808 | -0.25996 | 2.08926 | -0.28134 | -682.6599 | 1.4585 | -0.9179 |
| 0.7811 | 0.99944 | -0.20241 | 2.43108 | -0.24543 | -595.6440 | 1.4577 | -0.7568 |
| 0.8856 | 1.02173 | -0.10211 | 3.30304 | -0.15625 | -379.6321 | 1.4548 | -0.4554 |
| 1.0000 | 1.04761 | 0.00000 | 4.89883 | 0.00000 | 0.0000 | 1.4532 | 0.0000 |

The results of deviations in viscosity ($Ƞ^E$) for mixtures (THFA+ benzene), (THFA+ toluene) and (THFA+ p-xylene) are illustrated in Fig.2. Interaction between components molecules believed to be due dispersion or weak dipole-dipole forces [22]. Moreover, THFA contains molecules with high polarity while aromatic hydrocarbon are non-polar molecules having $\pi$ -electrons on the ring. THFA molecules would induce a small dipole moment in the aromatic hydrocarbon molecule when mixed. A formation of a weak dipole-induced dipole interaction between the component molecules is also expected. In addition, donor acceptor interaction between $\pi$-electrons of benzene ring and oxygen of O-H group of THFA results in negative values of $Ƞ^E$ [11].

The plots of $\Delta G^{*E}$ versus mole fractions ($X_1$) at 298.15K for all the three binary systems (THFA + benzene, THFA + toluene and THFA + p-xylene) are presented in Fig.3. Values of $\Delta G^{*E}$ were found to be negative for all the systems under study. The experimentally obtained negative $\Delta G^{*E}$ and $Ƞ^E$ values for all binary solvents mixtures show weak interactions between unlike molecules and indicate that flow is easier for the binary solvent mixtures when compared with that of pure solvents [23,24].

The deviations in $\Delta n_D$ (molar refraction) was found to be negative for all binary systems over the composition range at investigated temperature (Fig.4). Generally, the negative values of $\Delta n_D$ suggest weak interactions between the component molecules in the system [15]. For all binary solvent

mixtures, the interactions of self-association are stronger than the specific interaction of unlike molecules, and the average interaction strength in mixture is weaker than that in the pure solvents.

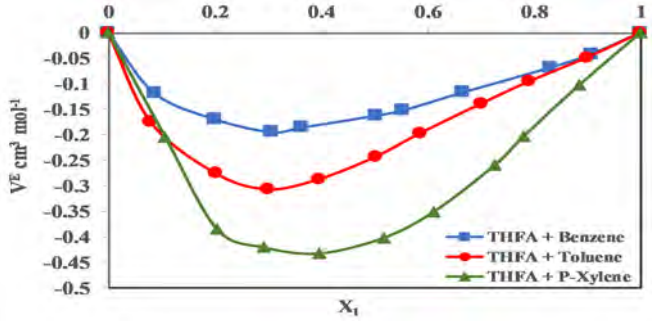


**Figure 1.** $V^E$ versus $X_1$ for (■) $X_1$ THFA +$X_2$ benzene, (●) $X_1$ THFA + $X_2$ toluene and (▲) $X_1$ THFA + p-xylene at 298.15K**.**

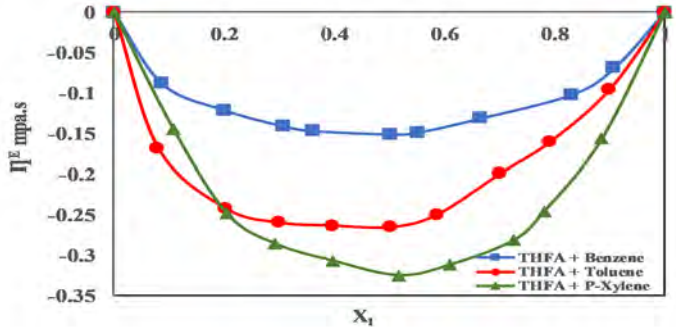


**Figure 2.** $\eta^E$ versus $X_1$ for (■) $X_1$ THFA+ $X_2$ benzene, (●) $X_1$ THFA+ $X_2$toluene and (▲) $X_1$ THFA + $X_2$ p-xylene at 298.15K.

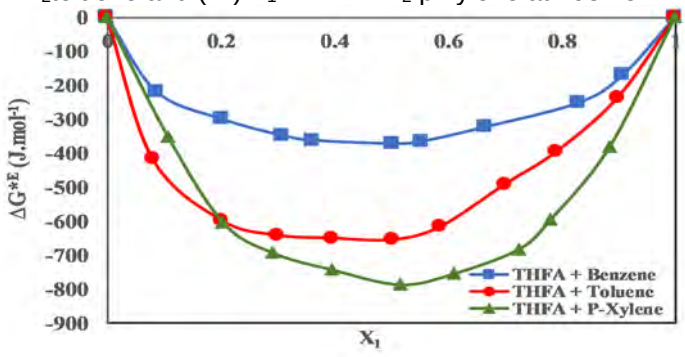


**Figure 3.** $\Delta G^{*E}$ versus $X_1$ for (■) $X_1$ THFA + $X_2$ benzene,(●) $X_1$ THFA+ $X_2$ toluene and (▲) $X_1$ THFA +$X_2$ p-xylene at 298.15K.

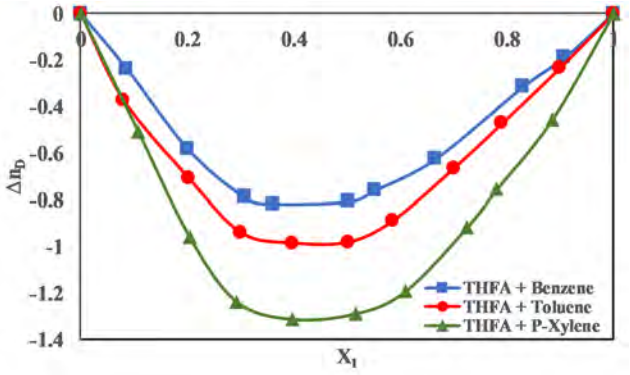


**Figure 4.** Excess refractive index versus $X_1$ for (■) $X_1$ THFA + $X_2$ benzene, (●) $X_1$ THFA+$X_2$ toluene and (▲) $X_1$ THFA + $X_2$ p-xylene at 298.15K.

**Table 2**. Polynomial coefficients ($A_k$) and standard deviations (σ) for binary solvent mixtures at 298.15K.

| Function | System | $A_0$ | $A_1$ | $A_2$ | σ |
|---|---|---|---|---|---|
| VE ($cm^3.mol^{-1}$) | THFA + Benzene | -0.64840 | 0.50722 | -0.41527 | 0.00005 |
| VE ($cm^3.mol^{-1}$) | THFA + Toluene | -0.96620 | 0.99681 | -0.58565 | 0.02326 |
| VE ($cm^3.mol^{-1}$) | THFA + P-Xylene | -1.65665 | 0.87340 | -0.07943 | 0.02937 |
| Function | System | $A_0$ | $A_1$ | $A_2$ | σ |
| $\eta^E$ (mPa.s) | THFA + Benzene | -0.58614 | 0.07922 | -0.45357 | 0.02414 |
| $\eta^E$ (mPa.s) | THFA + Toluene | -1.02289 | 0.43810 | -0.70071 | 0.03616 |
| $\eta^E$ (mPa.s) | THFA + P-Xylene | -1.29209 | 0.00408 | -0.47842 | 0.01902 |
| Function | System | $A_0$ | $A_1$ | $A_2$ | σ |
| $\Delta n_D$ ($cm^3.mol^{-1}$) | THFA + Benzene | -3.26617 | 1.03140 | 0.76222 | 0.03357 |
| $\Delta n_D$ ($cm^3.mol^{-1}$) | THFA + Toluene | -3.89318 | 1.43064 | 0.49336 | 0.03873 |
| $\Delta n_D$ ($cm^3.mol^{-1}$) | THFA + P-Xylene | -5.29561 | 1.18722 | 0.44150 | 0.03461 |
| Function | System | $A_0$ | $A_1$ | $A_2$ | σ |
| $\Delta G^{*E}$ ($J.mol^{-1}$) | THFA + Benzene | -1443.65 | 196.1852 | -1124.19 | 1.20126 |
| $\Delta G^{*E}$ ($J.mol^{-1}$) | THFA + Toluene | -2524.99 | 1086.265 | -1737.40 | 1.80019 |
| $\Delta G^{*E}$ ($J.mol^{-1}$) | THFA + P-Xylene | -3131.71 | 15.89403 | -1185.48 | 0.94697 |

## EXPERIMENTAL SECTION

### Chemicals

All solvents in this study (THFA, benzene, toluene and p-xylene) were purchased from Sigma-Aldrich and with purity of ≥99%, therefore, no further purifications were needed. Density ***ρ***, viscosity Ƞ and refractive index $n_D$ for solvents have been checked and examined against those listed in the literature (Table 3).

### Measurements

The densities (ρ) were calculated (an average of three replicates) with accuracy of (±0.00001 g.cm$^{-3}$) using a digital density meter (Anton paar, Model DMA 60/602). A controlled temperature suspended-level Ubbelohde viscometer was used for the measurement of viscosity (η) under atmospheric pressure at 298.15± 0.01K.

The determinations of refractive indices for pure solvents and their binary solvent mixtures were performed using a digital Abbe refractometer (model: BOE 32400). For refractometer calibration, double distilled water used at 298.15.

**Table 3**. Experimental and literature physical properties [density (ρ), viscosity (Ƞ) and refractive index ($n_D$)] of pure solvents at 298.15K.

| Compound | T/ K | ρ (g.cm$^{-3}$) | | Ƞ mpa.s | | $n_D$ | |
|---|---|---|---|---|---|---|---|
| | | Exp. | Lit.[ref] | Exp. | Lit.[ref] | Exp. | Lit.[ref] |
| THFA | 298.15 | 1.04761 | 1.04761[25] | 4.89883 | 4.89883 [25] | 1.4532 | 1.45322[25] |
| Benzene | 298.15 | 0.87372 | 0.87357 [26]<br>0.87361[27]<br>0.87360 [28]<br>0.87342[29] | 0.59951 | 0.6038[26]<br>0.604 [28] | 1.4975 | 1.4980[27]<br>1.4971[29] |
| Toluene | 298.15 | 0.86224 | 0.86301[26]<br>0.86236[27]<br>0.86220 [28]<br>0.86226[29] | 0.55464 | 0.5540 [26]<br>0.556 [28] | 1.4950 | 1.4942[27]<br>1.4931[29] |
| p-xylene | 298.15 | 0.85676 | 0.85670 [26]<br>0.85682 [27]<br>0.85662 [28]<br>0.85670[29] | 0.61225 | 0.6078[26]<br>0.611 [28] | 1.4945 | 1.4933[27]<br>1.4926[29] |

Exp.: experimental, Lit.: literature, [ref]: reference

## CONCLUSIONS

The values of ρ, Ƞ, and $n_D$ were calculated in binary solvent mixtures THFA with benzene, toluene and p-xylene over a range of mole fractions. Various excess properties like $V^E$, $Ƞ^E$, $\Delta G^{*E,}$ $\Delta n_D$ were calculated from experimentally obtained thermodynamic values. For the binary solvent mixtures studied, benzene showed the most negative values of ($V^E$, $Ƞ^E$, $\Delta G^{*E,}$ $\Delta n_D$ ) while *p*-xylene showed the least.

The experimental values of $V^E$, $Ƞ^E$, $\Delta G^{*E,}$ $\Delta n_D$ were fitted well to Redlich-Kister equation. For all binary solvent mixtures, the interactions of self-association are stronger than the specific interaction of unlike molecules, while, the average interaction strength in mixture is weaker than that in the pure solvents.

## ACKNOWLEDGMENTS

The authors wish to thank the College of Education for pure Science Ibn Al-Haitham for providing the chemicals.

## REFERENCES

1. B. García, R. Alcalde, J.M. Leal, J.S. Matos, *Journal of the Chemical Society, Faraday Transactions*, **1996**, 92(18), 3347.
2. Y. Maham, C.N. Liew, A. E. Mather, *Journal of solution chemistry*, **2002**, *31(9),* 743.
3. R. M. Pires, H.F. Costa, A.G.M. Ferreira, I.M.A. Fonseca, *Journal of Chemical & Engineering Data*, **2007**,*52*, 1240.
4. M.S. Lakshmi, R.R. Raju, C. Rambabu, GV. R. Rao and K. Narendra, *Research and Reviews: Journal of Chemistry*, **2013**, *2(1)*,12.
5. P. Anila, K.R. Reddy, G.S. Rao, P.V.S. Sairam, D. Ramachandran,C. Rambabu, *Thermochimica Acta*, **2015**, *620*, 1.
6. M.N. Sovilj, *Journal of Chemical & Engineering Data*, **1995**, *40(5)*, 1058.
7. F. Giro, M.F. Goncalves, A.G.M. Ferreira, I.M.A. Fonseca, *Fluid phase equilibria*, **2003**, *204*, 217.
8. Z.A. AL-Dulaimy, D.T. AL-Heetimi, H.S. Khalaf, A.M. Abbas, *Oriental Journal of Chemistry,* **2018**, *34(4)*, 2074.
9. H. Yilmaz, *Turkish Journal of Physics*, **2002**, *26(3)*, 243.

10. A. Boruń, M. Żurada, A. Bald, *Journal of thermal analysis and calorimetry*, **2010**, *100(2)*, 707.
11. S. Sharma, K. Thakkar, P. Patel, M. Makavana, *Advances in Physical Chemistry*, **2013**, *2013*, 1.
12. K.R. Reddy, D.B.K. Kumar, G.S. Rao, P. Anila, C. Rambabu, *Thermochimica Acta*, **2014**, *590*, 116.
13. M. Yasmin, M. Gupta, *Journal of solution chemistry*, **2011**,40(8),1458.
14. A.S. Al-Jimaz, J.A. Al-Kandary, A.H.M. Abdul-Latif, *Fluid Phase Equilib.*,**2004**, *218(2)*, 247.
15. P. Brocos, Á. Piñeiro, R. Bravo, A. Amigo, *Physical Chemistry Chemical Physics*, **2003**, *5(3)*, 550.
16. T.M. Aminabhavi, H.T. Phayde, R.S. Khinnavar, B. Gopalakrishna, K.C. Hansen, *Journal of Chemical & Engineering Data*, **1994**, *39(2)*, 251.
17. T.M. Aminabhavi, B. Gopalakrishna, *Journal of Chemical & Engineering Data*, **1995**, *40(2)*, 462.
18. O. Redlich, A.T. Kister, *Industrial & Engineering Chemistry* ,**1948**, *40(2)*, 345.
19. Z.P. Visak, A.G. Ferreira, I.M. Fonseca, *Journal of Chemical & Engineering Data*, **2000**, *45(5)*, 926.
20. S.P. Šerbanović, M.L. Kijevčanin, I.R. Radović, B.D. Djordjević, *Fluid Phase Equilibria*, **2006**, *239(1)*, 69.
21. I.R. Radović, M.L. Kijevčanin, E.M. Djordjević, B.D. Djordjević, S.P. Šerbanović, *Fluid Phase Equilibria*, **2008**, *263(2)*, 205.
22. P. Jain, M. Singh, *J. Chem. Eng. Data*, **2004**, *49(5)*, 1214.
23. S. Sharma and M. Makavana, *Fluid Phase Equilibria*, **2014**, *375*, 219.
24. Dikio, E.D., *Oriental Journal of Chemistry*, **2014**, *30(3)*, 953.
25. S.A. Salman, S.A. Al-Khfaji, K.I. Hussain, Z.A. Al-Dulaimy, A.M. Abbas, D.T.A. Al-Heetimi, *RASĀYAN Journal of Chemistry*, **2018**,*11(2)*, 589.
26. C. Yang, P. Ma and Q. Zhou, *Journal of Chemical & Engineering Data*, **2004**, *49(4)*, 881.
27. A.K. Nain, P. Chandra, J.D. Pandey, S. Gopal, *Journal of Chemical & Engineering Data*, **2008**, *53(11)*, 2654.
28. J.A. Al-Kandary, A.S. Al-Jimaz, A.H.M. Abdul-Latif, *Journal of Chemical & Engineering Data*, **2006**, *51(6)*, 2074.
29. J.G. Baragi, and M.I. Aralaguppi, *The Journal of Chemical Thermodynamics*, **2006**, *38(12)*, 1717.

STUDIA UBB CHEMIA, LXIV, 1, 2019 (p. 113-123)
(RECOMMENDED CITATION)
DOI:10.24193/subbchem.2019.1.09

# INFLUENT TEMPERATURE EFFECTS ON THE ACTIVATED SLUDGE PROCESS AT A MUNICIPAL WASTEATER TREATMENT PLANT

**MARIUS-ADRIAN BREHAR[a], MELINDA VÁRHELYI[a,*], VASILE-MIRCEA CRISTEA[a], DANIEL CRÎSTIU[a], ȘERBAN-PAUL AGACHI[a]**

**ABSTRACT.** The influent temperature has an important effect on the activated sludge process at the municipal Wastewater Treatment Plants (WWTPs). This research is associated to a case study of a Romanian municipal WWTP with Anaerobic-Anoxic-Aerobic ($A^2O$) layout. Based on mathematical modelling it was studied the influent wastewater temperature effect on the effluent components concentration and on the concentration of pollutants and biomass concentrations at the outlet of biodegradation basins aerobic zone. Three influent temperature profiles were considered and implemented in the simulator. They reveal the representative 22 days period of the months: February (coldest water season), May (intermediate season) and July (warmest season). The simulations were performed both in steady and dynamic state. It was observed that higher influent temperatures intensify the nitrification and denitrification processes. As a result, the concentration of the nitrogen compounds in the effluent and at the end of the bioreactors decreases with the increase of the temperature. The carbon rich organic components feature a minor increase in the effluent. The study reveals that short time daily influent temperature changes do not have significant effect on the effluent components concentration, but the long-term ones affect the WWTP performance.

***Keywords:*** *wastewater treatment, mathematical modelling, Activated Sludge Model No. 1, Benchmark Simulation Model No. 1, influent temperature effects*

[a] *Babeş-Bolyai University, Faculty of Chemistry and Chemical Engineering, 11 Arany Janos str., RO-400028, Cluj-Napoca, Romania*
**Corresponding author e-mail: mvarhelyi@chem.ubbcluj.ro*

## INTRODUCTION

Wastewater Treatment Plants (WWTPs) reproduce in an intensified way the biodegradation processes that naturally occur in rivers, lakes and other natural water systems [1]. The most versatile and effective of all wastewater treatment processes and the most commonly used system for the treatment of municipal wastewater is the activated sludge process. Nitrification and denitrification are the two major parts of the activated sludge process together with the carbon and phosphorus transformations [2]. Microorganisms are used to degrade and to remove the pollutants from the sewage network originating wastewater.

Research in the field of wastewater treatment has largely gained importance during the past years. Usually, limited reliable online measurements for process monitoring and process control at full-scale WWTPs are available and, as a result, complex mathematical models have been constantly developed. The Activated Sludge Models (ASMs) describe the carbon, nitrogen and phosphorus removal, whereas the Benchmark Simulation Models (BSMs) also add the sedimentation process model. Mathematical models are used for the study of the complex activated sludge process, for the evaluation of different influential factors' effects on plant performance and for the implementation of advanced control algorithms [3,4]. A calibrated WWTP simulator has become a very valuable tool for analyzing the internal processes taking place at the WWTPs and finding solutions to process control or to operating problems [5,6].

Temperature has a significant influence on the growth of autotrophic microorganisms and plays an important role in the nitrification process. The development of the heterotrophic biomass is also dependent on the temperature of wastewater [7]. Influent wastewater temperature depends on a series of factors such as: ambient temperature, architecture of the sewer system and the weather events (e.g. rain, storm, snow). In the context of climate change, significant temperature changes can be expected influencing accordingly the influent wastewater temperature. Advanced control algorithms, such as model predictive control, may be an efficient solution for the efficient management of WWTPs, but the effect of temperature needs to be investigated as it is an important predictable disturbance. Noteworthy, potential heat recovery can be achieved from the sewage water but this requires an assessment of influent temperature effect on the operation of the WWTP [8].

This paper presents the investigation of the influent temperature effects on the concentration of pollutants in the WWTP effluent and at the outlet of the biodegradation tanks. Based on steady and dynamic state

mathematical modelling and simulation results, the analysis is performed by considering different influent temperature profiles measured at the WWTP inlet, covering both short-time and long-time temperature changes.

## MODEL DESCRIPTION AND CALIBRATION

The dynamic municipal WWTP simulator used in the present study is describing an $A^2O$ (Anaerobic-Anoxic-Oxic) plant layout, presented in Figure 1. The WWTP simulator is based on the Activated Sludge Model No. 1 (ASM1) presented by Henze *et al* and the COST/IWA Benchmark Simulation Model No. 1 (BSM1) [9]. The model includes a primary settler, five bioreactors and a secondary clarifier. The primary settler is based on the Otterpohl and Freund model and describes the partial removal of particulate pollutants from the raw wastewater. The five bioreactors are connected in series. The first bioreactor is an anaerobic bioreactor. It receives the wastewater leaving the primary settler and the return activated sludge recycle stream (external recirculation). The second bioreactor is an anoxic one and has the main role in the denitrification process. It processes the wastewater collected from the anaerobic part of the biodegradation basins and the nitrate recirculation stream (internal recirculation). The last three bioreactors are aerated bioreactors where the nitrification process takes place. According to ASM1, the biodegradation processes consider two types of microorganisms: heterotrophs and autotrophs [10]. Basically, 8 main biochemical processes and the behavior of 13 different compounds (state variables) are described by a set of non-linear mass conservation and constitutive differential equations. The secondary settler is based on the settler model of Takács *et al*, which considers the settling velocity being described as a double-exponential function [11].

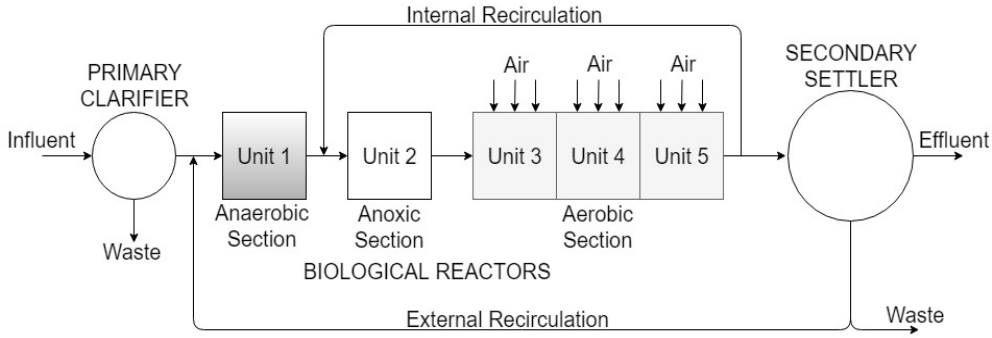


**Figure 1.** The $A^2O$ configuration of the investigated municipal WWTP

The calibration of the WWTP simulator was accomplished using data from the online Supervisory Control and Data Acquisition (SCADA) system and laboratory measured influent and effluent data. The flow rates of the recycle streams and the air entering the aerobic biodegradation tanks, associated to the plant configuration, dimensions and characteristics of equipment collected from the studied municipal WWTP were included in the calibrated simulator. The model was calibrated with the dynamic and average data collected during the month May 2016, taking into consideration the first 22 days of this month. A set of influent variables, combined with a few of process and settler parameters, were determined using steady state Pareto multiobjective optimization. The WWTP model calibrated in steady state was also evaluated in dynamic state with measured data at every 10 minutes, showing a good fit between the simulated and measured effluent data. The calibration was accomplished successfully and the calibrated dynamic WWTP was used in the present research.

## RESULTS AND DISCUSSION

The effects of the influent wastewater temperature on the biomass composition and the effluent quality indicators were investigated with the calibrated simulator. In the warm season the cellular activity of microorganisms is intensified. It is also known from the WWTP process work that in the cold season the aeration processes are intensified, as the dissolved oxygen concentration in the bioreactor decreases when temperature increases. These main effects are demonstrated by practice operation data. Analysis and interpretations of the influent temperature effects have been made based on both steady state and dynamic WWTP behavior.

### Influent Temperature Effects – Steady State

The model was calibrated with the influent temperature of 15.83°C, i.e. the average influent temperature of the WWTP measured data during the intermediate season (May month). After calibration, five new steady state simulations were run, in which the mentioned average temperature was replaced with the following new influent temperature values: 10°C, 13°C, 16°C, 19°C and 22°C. Both the influent temperature and influent concentrations were considered constant, until steady state was obtained. The results of the steady state simulations are presented in Table 1, for the wastewater leaving the aerated section and for the secondary setter effluent.

**Table 1.** The influent temperature effects in steady state

| Variable | Notation | Temperature | | | | |
|---|---|---|---|---|---|---|
| | | 10°C | 13°C | 16°C | 19°C | 22°C |
| Aerated section – Unit 5 | | | | | | |
| Readily biodegradable substrate [g COD/m$^3$] | $S_S$ | 1.02 | 1.03 | 1.06 | 1.08 | 1.11 |
| Slowly biodegradable substrate [g COD/m$^3$] | $X_S$ | 46.55 | 47.23 | 48.46 | 49.74 | 51.00 |
| Heterotrophic biomass [g COD/m$^3$] | $X_{BH}$ | 2080.11 | 2081.81 | 2082.59 | 2083.11 | 2083.50 |
| Autotrophic biomass [g COD/m$^3$] | $X_{BA}$ | 114.46 | 119.23 | 120.64 | 121.29 | 121.76 |
| Dissolved oxygen [g $O_2$/m$^3$] | $S_O$ | 4.19 | 4.45 | 4.56 | 4.53 | 4.44 |
| Nitrate and nitrite nitrogen [g N/m$^3$] | $S_{NO}$ | 4.28 | 3.99 | 3.43 | 2.91 | 2.44 |
| Free and saline ammonia [g N/m$^3$] | $S_{NH}$ | 1.36 | 0.39 | 0.17 | 0.09 | 0.06 |
| Soluble biodegradable organic nitrogen [g N/m$^3$] | $S_{ND}$ | 0.96 | 0.85 | 0.75 | 0.67 | 0.59 |
| Particulate biodegradable organic nitrogen [g N/m$^3$] | $X_{ND}$ | 3.45 | 3.49 | 3.58 | 3.67 | 3.76 |
| Total suspended solids [g SS/m$^3$] | TSS | 4604 | 4611 | 4613 | 4615 | 4616 |
| Effluent | | | | | | |
| Chemical oxygen demand [g COD/m$^3$] | COD | 21.10 | 21.13 | 21.16 | 21.19 | 21.22 |
| Total suspended solids [g SS/m$^3$] | TSS | 12.21 | 12.22 | 12.23 | 12.23 | 12.24 |
| Free and saline ammonia [g N/m$^3$] | $S_{NH}$ | 1.36 | 0.39 | 0.17 | 0.09 | 0.06 |
| Nitrate and nitrite nitrogen [g N/m$^3$] | $S_{NO}$ | 4.28 | 3.99 | 3.43 | 2.91 | 2.44 |
| Organic nitrogen [g N/m$^3$] | $N_{org}$ | 2.05 | 1.94 | 1.85 | 1.76 | 1.69 |
| Total nitrogen [g N/m$^3$] | $N_{total}$ | 7.70 | 6.33 | 5.44 | 4.76 | 4.19 |
| Total Kjeldahl nitrogen [g N/m$^3$] | TKN | 3.42 | 2.34 | 2.01 | 1.86 | 1.75 |
| Return activated sludge | | | | | | |
| Total suspended solids [g SS/m$^3$] | TSS | 12702 | 12720 | 12727 | 12732 | 12736 |

Simulation results show that when temperature increases the concentrations of heterotrophic ($X_{BH}$) and autotrophic biomass ($X_{BA}$) become higher in the biodegradation tanks. This is a consequence of the maximum specific growth rate of the heterotrophic ($\mu_H$) and the autotrophic biomass ($\mu_A$)

that are modelled by temperature dependent relationships. Due to the increase of the biomass concentration in the system the concentration of products derived from the death of microorganisms are also increased. For this reason, the concentrations of the slowly biodegradable substrate ($X_S$), inert particulate substrate ($X_P$) and particulate biodegradable organic nitrogen ($X_{ND}$) increase at higher temperatures. The temperature rise favors also the anoxic and aerobic hydrolysis of $X_S$ into readily biodegradable substrate ($S_S$). Consequently, the readily biodegradable substrate ($S_S$) increases with the influent temperature increase. It may be also noticed that concentration of total suspended solids (TSS) in the bioreactors and in the return activated sludge increase with the influent temperature rise. The concentration of total suspended solids is increasing since the majority of the particulate components from the activated sludge process are increasing when the influent temperature gets higher. The dissolved oxygen concentration ($S_O$) is influenced by the value of the dissolved oxygen saturation value that is decreasing when the temperature increases. On the other hand, dissolved oxygen concentration is also influenced by the mass transfer coefficient $K_La$, as the latter increases when the temperature is higher. As a consequence, the dissolved oxygen concentration is affected by these two opposing effects of the influent temperature.

The autotrophic biomass has an important role in the nitrification process. According to the steady state simulations the autotrophic biomass is increased by 6.4% at the temperature of 22°C compared to the value at 10°C influent temperature. At increased temperature, higher amount of free and saline ammonia ($S_{NH}$) are transformed into nitrites and nitrates ($S_{NO}$). As a result, the $S_{NH}$ concentration at the outlet of the aerated zone of the bioreactors is decreasing. Likewise, the nitrification process, the denitrification is also intensified at higher temperature. This causes the increase of the eliminated nitrogen gas and results in the decrease of the $S_{NO}$ in the bioreactors. The increase of influent temperature favors the ammonification process of transforming the soluble biodegradable organic nitrogen ($S_{ND}$) into $S_{NH}$. Therefore, the $S_{ND}$ concentration decreases at higher temperature values. The ammonification process is dependent on the ammonification rate ($k_a$) and this is revealed by the developed model.

The study of the effluent stream reveals that when influent temperature increases from 10°C to 22°C the concentrations of COD and TSS are slightly increased by less than 1%. All of nitrogen compounds are decreased, as total nitrogen concentration ($S_{total}$) decreases roughly by 46%, and total Kjeldahl nitrogen (TKN) by almost 49%. The highest influence can be noticed at the ammonia, which decreases by nearly 96%. As a general assessment, it may be stated that in the terms of nitrogen removal the wastewater treatment plant can be operated more efficiently at the higher influent temperatures of the warmer seasons.

### Influent Temperature Effects – Dynamic State

The effects of the influent wastewater temperature were investigated in dynamic state as well. Three influent temperature profiles consisting in 22 days of the different considered seasons (cold, intermediate and warm) were analyzed, according to the WWTP temperature measurements. Figure 2 presents the influent temperature profiles of this 22 days-period for the months of February, May and July.

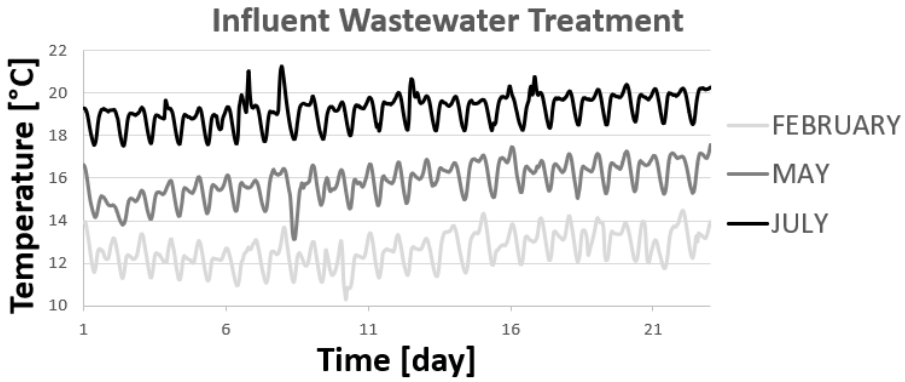


**Figure 2.** Time variation of the influent's temperature depending on the season (months February, May and July)

The dynamic state simulations considered variable influent temperature values, while the other influent components were considered constant. The dynamic simulations, showing the influent temperature effects on the effluent wastewater concentrations, are presented in Figure 3 for the last 18 days of the considered periods of time.

It may be observed that dyanmic results are complying with the steady state results. The concentration of COD, soluble COD and total suspended solids increase with the influent temperature increase. In the warm season the concentration of nitrogen compounds are lower due to the intensified nitrification and denitrification processes. This is a consequence of the already concluded main trend, according to which at higher temperature the growth of heterotrophs and autotrophs is intensified. It can be noticed that the variation of ammonia effluent concentration is lower at high temperatures. Due to this, in warm seasons the higher temperature may act in a favourabe way to the task of maintaining the ammonium concentration below the regulation limit.

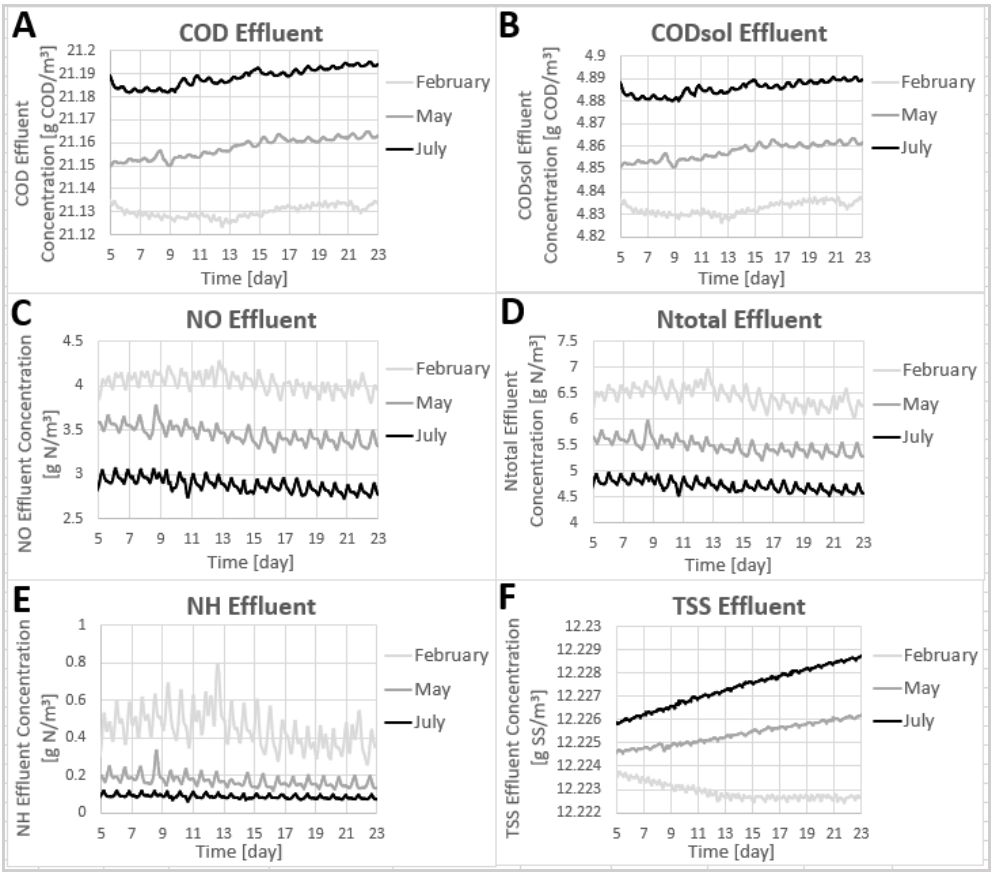


**Figure 3.** The influent temperature dynamic effects on the effluent concentrations, as response to the three influent temperature changing profiles: A. Total COD, B. Soluble COD, C. Nitrates and nitrites, D. Total nitrogen, E. Ammonia, F. Total suspended solids

It might be also concluded that disturbances featuring relatively long-lasting influent temperature decrease (e.g. persistent rain or frost) may negatively affect the performance of the wastewater treatment, requesting for predictive counteracting actions that may be offered by feedforward or advanced control algorithms.

Figure 4 shows the dynamic state effect of the influent temperature on the wastewater components in the last aerated bioreactor.

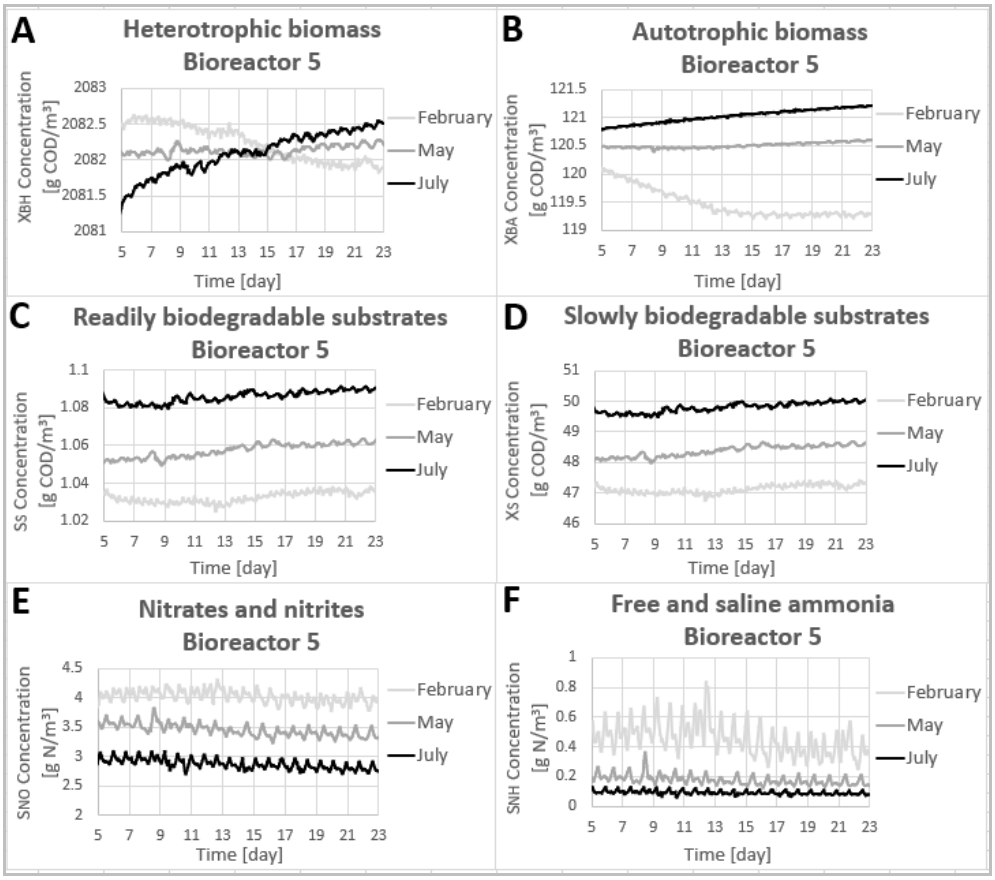


**Figure 4.** The influent temperature effects on the concentrations in the last aerated bioreactor, as response to the three influent temperature changing profiles: A. Heterotrophic biomass, B. Autotrophic biomass C. Readily biodegradable substrate, D. Slowly biodegradation biomass, E. Nitrates and nitrites, F. Ammonia

It can be noted that wastewater composition changes at the outlet of the biodegradation basins are in agreement with the steday state results, i.e. high influent temperature leads to the increase of $X_{BA}$, $S_S$, $X_S$ and to the decrease of $S_{NO}$, $S_{NH}$. It was also observed that in the case of heterotrophic biomass concentration, short-term and long-term influent temperature efects are changing with time. This behaviour may be attributed to the fact that $X_{BH}$ concentration is influenced by the two counteracting dynamic effects on the dissolved oxygen concentration, having associated different time constants.

## CONCLUSIONS

The study of the influent wastewater temperature effects on wastewater quality was performed both in steady and dynamic state. Based on a calibrated WWTP simulator three different temperature profiles corresponding to the cold, intermediate and warm seasons were considered. It was shown that the increase of the influent temperature leads to the slowly increase of the COD and TSS concentrations in the effluent, respectively to the decrease of the nitrogen components in the effluent and activated sludge system. Investigating the nitrogen removal and specifically the ammonia oxidation to nitrates, the higher temperatures are the most favorable for plant operation with desired performance. It was observed that short-time variations in the influent temperature do not have a strong effect on the effluent concentrations, but the long-time, persistent ones may have important consequences. These effects were quantitatively assessed.

The perspectives of using this research results are showing promising applications. Based on the calibrated simulator that includes the temperature impact, the operation of the WWTP may be improved by the revealed predictions of the influent temperature effects. They are necessary for the application of feedforward or model predictive control system implementation and may directly integrate the weather forecast as estimated disturbance. Additionally, assessment of the influent temperature effects on the WWTP performance may be used to the design of the heat exchanger network aimed to recover heat from the sewage system originating wastewater.

## EXPERIMENTAL SECTION

MATLAB software and the Simulink graphical programming extension were used in the present research. The developed simulator is based on the Benchmark Simulation Model provided by COST Action 682 and the IWA Working Group on Assessment of Control Strategies for Wastewater Treatment Plants. The equations of the bioreactors model and the primary and secondary clarifier equations are written in C programming language. To reduce simulation time and preserve computing resources, the codes have been compiled and incorporated into the Simulink environment by S-Function blocks. Simulink ODE15s numerical solving algorithm were used to solve the set of differential and algebraic equations of the model.

## REFERENCES


1. C. Martin, P.A. Vanrolleghem, *Environmental Modelling & Software*, **2014**, *60*, 188.
2. M.H. Gerardi, “Nitrification and Denitrification in the Activated Sludge Process”, A. John Wiley & Sons Inc. Publication, New York, **2002**.
3. G.S. Ostace, V.M. Cristea, P.Ș. Agachi, *Environmental Engineering and Management Journal*, **2012**, *11*, 147.
4. M. Várhelyi, M. Brehar, V.M. Cristea, ”Control strategies for wastewater treatment plants aimed to improve nutrient removal and to reduce aeration costs”, paper presented at the *2018 IEEE International Conference on Automation, Quality and Testing, Robotics, AQTR 2018 – THETA 21st Edition, Proceedings*, **2018**, 1-6.
5. A. Nair, V.M. Cristea, P.Ș. Agachi, M. Brehar, *Water and Environmental Journal*, **2018**, *32*, 164.
6. X. Wang, H. Ratnaweera, J.A. Holm, V. Olsbu, *Journal of Environmental Management*, **2017**, *193*, 1.
7. S. Balku, *Celal Bayar University Journal of Science*, **2018**, *14*, 77.
8. O. Wanner, V. Panagiotidis, P. Clavadetscher, H. Siegrist, *Water Research*, **2005**, *39*, 4725.
9. J.B. Copp (ed.), “The COST Simulation Benchmark: Description and Simulator Manual”, Office for Official Publications of the European Communities, European Commission. Directorate-General for Research COST Action 624, Luxembourg, **2002**.
10. M. Henze, W. Gujer, T. Mino, M.C.M. van Loosdrecht, "Activated Sludge Models: ASM1, ASM2, ASM2d and ASM3", Scientific and Technical Report, IWA Publishing, London, **2000**.
11. I. Takács, G.G. Patry, D. Nolasco, *Water Research*, **1991**, *25*, 1263.

STUDIA UBB CHEMIA, LXIV, 1, 2019 (p. 125-133)
(RECOMMENDED CITATION)
DOI:10.24193/subbchem.2019.1.10

# STUDY OF THE HYDROGEN PEROXIDE BASED WHITENING GEL ON THE CORROSION OF DENTAL METALLIC ALLOYS

**IOANA CARMEN FORT[a], GRAZIELLA L. TURDEAN[a,*], REKA BARABAS[b], DANIELA POPA[c], ANA ISPAS[c], MARIANA CONSTANTINIUC[c]**

**ABSTRACT.** The corrosion effect of the bleaching gel based on hydrogen peroxide on two types of dental metallic alloys, frequently used as restorative, prosthetic and implants materials was investigated by electrochemical impedance spectroscopy. The anti-corrosive behavior of Co-Cr and Cr-Ni alloys was found very different for the same experimental conditions. The best results were obtained with Co-Cr alloy, recommending the use of this material in dental treatments.

***Keywords:*** *dental alloys, hydrogen peroxide, electrochemical impedance spectroscopy*

## INTRODUCTION

Nowadays, the pharmaceutical industry must answer to an increased demand of products that must guarantee the obtaining of the "perfect brilliant white smile", which is not only a social-media and advertising expectation, but also a shifting of the paradigm of practicing dentistry. Consequently, dental bleaching and fluoride treatment agents become popular for esthetic or cosmetic whitening of stained or discolored teeth, but also for prevention of plaque and caries formation [1].

[a] *"Babeş-Bolyai" University, Faculty of Chemistry and Chemical Engineering, Department of Chemical Engineering, Cluj-Napoca, Romania*
[b] *"Babeş-Bolyai" University, Faculty of Chemistry and Chemical Engineering, Department of Chemistry and Chemical Engineering in Hungarian Language, Cluj-Napoca, Romania*
[c] *"Iuliu Hatieganu" University of Medicine and Pharmacy, Faculty of Dental Medicine, Department of Prosthetic and Dental Materials, Cluj-Napoca, Romania*
** Corresponding author: gturdean@chem.ubbcluj.ro*

Thousands of years ago, tooth cleaning and polishing formulations were based on sea-shells, egg shells and bones ground, as active cleaning components. The first esthetic treatment using bleaching agents was reported at the end of 19$^{th}$ century [2, 3]. In our time, whitening process consists in discoloring dentition by exposing it to various oxidizing materials, such as: hydrogen peroxide ($H_2O_2$) [4-9] or $H_2O_2$ releasing agents (*i.e*., carbamide peroxide (CP) [2, 9-12], and sodium perborate) over a period of time, in order to obtain a lighter color of teeth. CP is a very unstable compound and in contact with tissues and saliva will immediately degrade into about one-third $H_2O_2$ and two-thirds urea, being in fact a source of $H_2O_2$ [6, 13]. It is well-known that $H_2O_2$ acts as a strong oxidizing agent leading to the formation of free radicals, reactive oxygen molecules, and anions [5, 13].

The whitening procedure could be applied *in-office* (using power bleaching formula containing high concentration of $H_2O_2$, about 25% - 35%, for professional use by dentists), [3, 7, 13, 14], *at-home* (using materials furnished by dentists and used by patients at home for bleaching during night) [3, 13], *over-the-counter* (OTC) bleaching (using products available directly to consumers from drugstores for home use, constituting a low cost alternative to traditional bleaching agents, with little clinical evidence on the safety and effectiveness of the whitening results) [3, 13, 14]. Taking into account the advantages and disadvantages of different commercial products, the main challenge for dentists is not only to determine the effectiveness of various tooth-whitening products, but also to keeping patients' safety [14].

In practical life, bleaching agents may come into contact with restorative materials, particularly when using mouth guard bleaching or home kits [4] causing undesirable changes, such as softening and degradation by wear and corrosion of the teeth and/or restorative materials [10, 13] prosthetic and implant systems [15]. In this context, extensively research were performed in order to evaluate the surface properties and/or surface alterations of different esthetic restorative materials by different methods, such as: surface roughness measurements [2, 4, 11]; surface topography evaluation by scanning electron microscopy (SEM) [2, 8, 11] or by atomic force microscopy (AFM) [7]; profilometric analysis [12]; determination of the alterations in atomic weight by energy dispersive X-ray spectroscopy (EDS) [2, 10] or by X-ray photoelectron spectroscopy (XPS) [9]; metal ions release from dental alloys by inductively coupled plasma-mass spectrometry (ICP-MS) [4]; crystallinity index analysis by Raman spectroscopy [5, 7]; color measurements by spectrophotometry [5, 7]. The corrosion parameters obtained by using electrochemical techniques of investigation of dental metallic alloys in contact with whitening agents are related to the biocompatibility and long-life of different restorative, prosthetic and/or implant systems [4].

Hydroxyapatite is a main inorganic component of bones and teeths, with very excellent biocompatibility. The presence in the studied matrix is due to its properties as promoter of the osteosynthesis in case of small damages of the enamel of tooth [12b].

Until now, for the best of our knowledge, the corrosive effect of these agents (containing $H_2O_2$) on dental metallic materials has not been well documented. The aim of this work was to present the preliminary data obtained by investigating the corrosive effect of a $H_2O_2$ based whitening gel product on two types of metallic alloys extensively employed in dentistry (*i.e.*, Co-Cr and Co-Ni), by using electrochemical impedance spectroscopy.

## RESULTS AND DISCUSSION

In Figure 1 is presented the electrode surface before and after deposition of the whitening gel used in bleaching treatment of teeth obtained with an optical microscope. The exposure of the metallic interface with whitening gel containing aggressive $H_2O_2$ lead to affect the integrity of the thin protective oxide passive layer formed at the metallic surface in contact with the air.

**Figure 1.** Magnified images (x 400) of Co-Cr and Co-Cr/Gel-Nafion surfaces.

In order to obtain information of the corrosion resistance of the dental alloys (i.e., Cr-Ni, Co-Cr) electrochemical impedance spectroscopy (EIS) measurements were performed on different type of artificial saliva - electrode interfaces after the stabilization of OCP during 1 hour. EIS data were plotted as Nyquist diagrams. The experimental data were modeled using two standard equivalent circuit model (*i.e.*, $R_s(QR_{ct})$ and $R_s(QR_{ct})(Q_1R_1)$).

The correspondence of the elements of the electric circuit is the following: $R_s$ stands for uncompensated solution resistance, Q called constant phase element stands for the double electrical layer capacity and $R_{ct}$ stands for charge transfer resistance, $Q_1$ and $R_1$ correspond to constant phase element and resistance of a passive compounds formed at the metallic interface.

The Q value is calculated using the formula $Q = (C_{dl} R_{ct})^{1/n}/R_{ct}$, where: $C_{dl}$ is the capacitance of the double layer and *n* a roughness factor (*i.e.*, n = 1 is the case of a perfectly smooth surface of an ideal capacitor and n = 0 is the case of an ideal resistance) [16].

The value of $R_{ct}$ could be considered as a quantitative parameter, which provides information about the degree of corrosion of the surface or in other words, about the degree of protection of the passive thin oxide film formed on the alloy-electrolyte interface.

The Nyquist diagrams presented in Figure 2 show a semicircle which can be explained by the presence of a surface passive layer, and quantified by a corrosion resistance of this layer. Thus, the $R_{ct}$ values decrease in the order: 55.97 kΩ cm$^2$ (at Cr-Ni) > 17 kΩ cm$^2$ (at Cr-Ni/Gel) ≈ 7.2 kΩ cm$^2$ (at Cr-Ni/Gel-Nafion) and 2.93 kΩ cm$^2$ (at Cr-Ni/HAP/Gel-Nafion). As expected, the presence of the aggressive $H_2O_2$ compound in the whitening gel lead to the decrease of the $R_{ct}$ values because of the destruction of the passive metallic oxide film. Even in the presence of HAP, which is less conductive and may constitute an electrons transfer barrier, the elimination of the corrosion processes occurring at metallic interface doesn't take place.

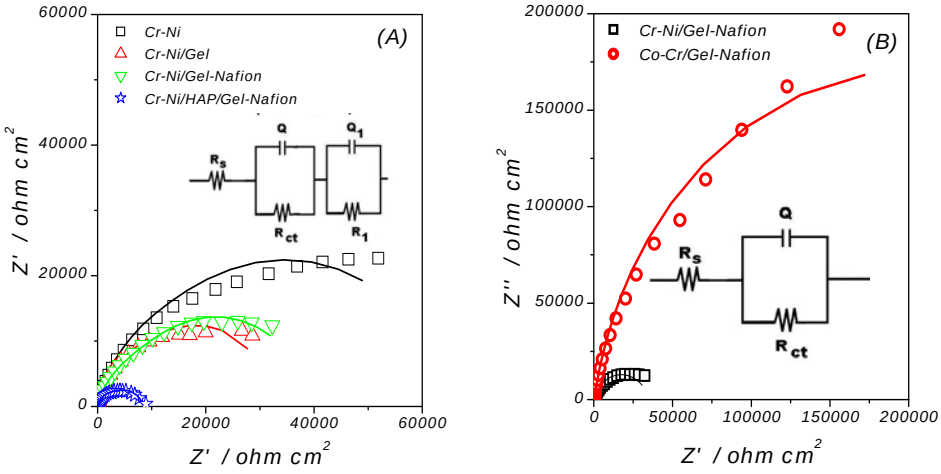


**Figure 2.** Nyquist diagram of different Cr-Ni modified electrode (see inset) (**A**) and Alloy/Gel-Nafion electrode (**B**) in artificial saliva solution of pH 7 recorded at OCP after 1 h of stabilisation. Experimental conditions: frequencies, 10 kHz - 10 mHz; amplitude, 0.1 V; room temperature. The line corresponds to the fitting curve of the experimental data using the $R_s(QR_{ct})(Q_1R_1)$ (A) and the simplified Randles circuit model $R_s(QR_{ct})$ (B) (see insets).

Comparing the two different metallic specimens (*i.e.*, Cr-Ni and Co-Cr) it can be observed in Figure 3, that the behavior of Co-Cr alloy is quite different than of the Cr-Ni alloy. Using the Randles equivalent circuit, the obtained $R_{ct}$ values are 404.5 kΩ cm$^2$ in the case of Co-Cr/Gel-Nafion and 35 kΩ cm$^2$ in the case of Cr-Ni/Gel-Nafion electrode. The difference of magnitude order between time in the two cases could be explained by the well know best anticorrosive behavior of Co-Cr alloy due to a more adherent oxide layer on its surface [17].

Usually the duration of a whitening treatment session is between 30 min to1 hour. For the worst case of electrode's composition (*i.e.* Alloy/ HAP/Gel-Nafion), the influence of time on the $R_{ct}$ value was studied. As seen in Figure 4, for both dental metallic alloy specimens, the increase of contact time with the whitening gel lead to an increase of the $R_{ct}$ values and to the appearance of a slow diffusion process. The parameters resulted by fitting the experimental curve with the $R_s(Q\ R_{ct})$ equivalent circuits are summarized in Table 1.

The analysis of the fitted date gives rise to the observations that in the case of Cr-Ni/HAP/Gel-Nafion electrode an increase of 11 times of the $R_{ct}$ value occurs during 1 hour of contact between whitening gel and Cr-Ni alloy. In the case of Co-Cr/HAP/Gel-Nafion electrode, the same parameter increases only 3 times and remains quasi-constant after few minutes of contact.

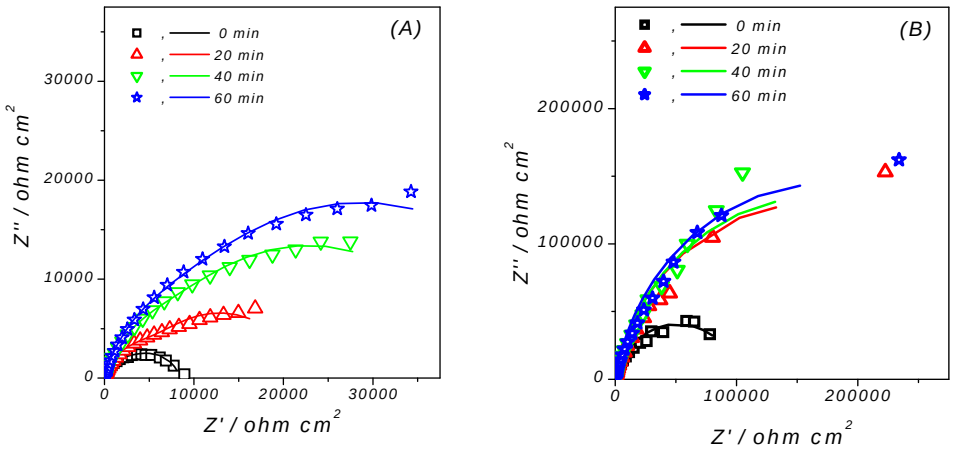


**Figure 3**. Nyquist diagram of Cr-Ni/HAP/Gel-Nafion (**A**) and Co-Cr/HAP/Gel-Nafion (**B**) electrode at different time (see inset) of exposure to artificial saliva solution of pH 7 recorded at OCP, after 1 h of stabilisation. Experimental conditions: see Fig 2.

**Table 1.** Fitted EIS parameters of Co-Cr/HAP/Gel-Nafion and Cr-Ni/HAP/Gel-Nafion electrode using $R_s(QR_{ct})$ and $R_s(QR_{ct})(Q_1R_1)$ equivalent circuit models. Experimental conditions: see Fig. 2.

| | Co-Cr/HAP/Gel-Nafion | | | | Cr-Ni/HAP/Gel-Nafion | | | |
|---|---|---|---|---|---|---|---|---|
| Time/ (min) | 0 | 20 | 40 | 60 | 0 | 20 | 40 | 60 |
| $R_s$ ($\Omega$ cm$^2$) | 33.51 ± 2.13 | 32.87 ± 3.05 | 34.52 ± 2.11 | 36.55 ± 3.82 | 40.32 ± 1.3 | 39.72 ± 0.8 | 44.51 ± 0.83 | 43.99 ± 0.81 |
| Q (S s$^n$/cm$^2$) | 4.75 $10^{-5}$ ± 1.85 | 4.28 $10^{-5}$ ± 2.46 | 4.29 $10^{-5}$ ± 1.59 | 3.86 $10^{-5}$ ± 2.94 | 8.19 $10^{-5}$ ± 1.4 | 38.82 $10^{-5}$ ± 2.9 | 18.86 $10^{-5}$ ± 4.9 | 22.9 $10^{-5}$ ± 3.76 |
| n | 0.855 | 0.877 | 0.869 | 0.886 | 0.870 | 0.819 | 0.839 | 0.829 |
| $R_{ct}$ (k$\Omega$ cm$^2$) | 102.8 ± 4.33 | 325.8 ± 12.29 | 331.2 ± 7.53 | 345.6 ± 12.78 | 2.93 ± 4.42 | 16.29 ± 1.5 | 42.59 ± 2.22 | 32.68 ± 1.7 |
| $Q_1$ (S s$^n$/cm$^2$) | - | - | - | - | 26.9 $10^{-5}$ ± 4.4 | 10.61 $10^{-5}$ ± 9.08 | 12.59 $10^{-5}$ ± 3.6 | 12.08 $10^{-5}$ ± 2.17 |
| n | - | - | - | - | 0.814 | 0.837 | 0.843 | 0.843 |
| $R_1$ (k$\Omega$ cm$^2$) | - | - | - | - | 5.46 ± 2.6 | 5.53 ± 2.3 | 9.49 ±6.7 | 8.06 ± 4.4 |
| chi$^2$ | 4.96 $10^{-3}$ | 1.71 $10^{-3}$ | 5.06 $10^{-3}$ | 1.73 $10^{-3}$ | 1.45 $10^{-3}$ | 0.74 $10^{-3}$ | 0.79 $10^{-3}$ | 0.71 $10^{-3}$ |

± relative standard error (RSD), expressed in percent (%).

However, the highest values of $R_{ct}$ in the case of Co-Cr/HAP/Gel-Nafion electrode indicate good anti-corrosive behavior and an important surface topography alteration [11] in the case of Cr-Ni/HAP/Gel-Nafion electrode. The instability of the gel film on the surface of Cr-Ni/HAP/Gel-Nafion electrode may be also a reason of this behavior, the initiating of a slow diffusion process being more visible than in the case of Co-Cr/HAP/Gel-Nafion electrode(see Fig 4A-B), in the studied range of frequencies. The Chi-square distribution test ($\chi^2$) having value between $10^{-2}$ - $10^{-3}$ indicates good agreement between the experimental data and the used equivalent circuit [18, 19].

## CONCLUSIONS

Knowing that the bleaching agents may cause structural changes on restorative, prosthetic and implant metallic materials leading to compromise their physical properties and to a premature failure of the treatment, a study of corrosion process of two dental metallic alloys (Cr-Ni and Co-Cr) when in contact with a $H_2O_2$ based whitening gel were realised.

The electrochemical impedance spectroscopy data reveal that the presence of Gel and even of HAP on the metallic surface lead to a decrease of the corrosion resistance probably due to the destruction of the protective passive metallic oxide film by the aggressive oxidant agent.

In the case of Alloy/Gel-Nafion and Alloy/HAP/Gel-Nafion electrode, the Co-Cr alloy show a better anticorrosive resistance comparing with the Cr-Ni alloy, recommending the first material for its use in restorative, prosthetic and implant treatments.

## EXPERIMENTAL SECTION

*Reagents*

Two specimens of dental metallic alloys were purchased by MESA di Sala Giacomo & C S.n.c. Their content was for Ni-Cr: Ni 63%, Cr 25%, Mo 10%, Si 1.5%, others Mn, Al, Zr, Ce, La, and for Co-Cr: Co 65%, Cr 29%, Mo 5%, C 0.4%, Si 0.35%, Mn 0.25%.

Because it is quite impossible to obtain an artificial saliva solution which replicates the really complex matrix of natural saliva, a receipt proposed by Mondelli [20] was prepared by using appropriate quantities of the following salts: NaCl (0.5 g/L), KCl (0.5 g/L), $CaCl_2*2H_2O$ (0.795 g/L), $NaH_2PO_4*H_2O$ (0.78 g/L), urea (1 g/L), $(NH_4)_2SO_4$ (0.3 g/L), $NaHCO_3$ (0.1 g/L) supplied from Sigma Aldrich and “Reactivul” Bucuresti.

White dental Beauty NOVON® enhanced formula gel for professional use (Gel), containing 6% was obtained from Optident Ltd.

Nafion® perfluorinated resin solution (5 wt. % in lower aliphatic alcohols and water) from Sigma Aldrich was diluted to a concentration of 3 % in ethanol.

All solutions were prepared in distilled water. The chemicals of analytical purity were used as received without any purification.

*Electrochemical Methods*

Electrochemical impedance spectroscopy measurements were performed using an AutoLab potentiostat (PGSTAT302N EcoChemie, Utrecht, Netherlands) controlled by FRA 2.1 software. The conventional electrochemical cell contains a working electrode of modified dental metallic Ni-Cr and Co-Cr alloys, an Ag/AgCl, $KCl_{sat}$ reference electrode and a platinum wire auxiliary electrode.

For corrosion tests, prior to measurements, the electrodes were stabilized 1 hour under open circuit conditions for recording the open circuit potential (OCP). Impedance spectra on the modified dental Ni-Cr and Co-Cr alloys electrodes were recorded at the OCP value, by using an AC signal with amplitude of ±10 mV and a frequency interval from 10 kHz to 0.01 Hz. Using an equivalent electric circuit, the experimental impedance data were fitted using ZSimpWin 3.21 software. The values of circuit components were subsequently correlated with the processes occurring in the electrochemical cell.

The pH of the electrolyte solutions was adjusted using a glass combined electrode (HI 11310) connected to a pH-meter (type MV 870, Pracitronic, Germany).

*Preparation of alloys modified electrodes*

The dental Ni-Cr and Co-Cr metallic alloys as cylinders samples, were cut into small pieces to a reduced size of 3 mm diameter and introduced into a Teflon tube, allowing just a controlled surface of 0.0765 $cm^2$ to be exposed to the artificial saliva solution. Before modification or testing, the metallic alloys electrodes were mechanically cleaned with silicon carbide papers of 500, 800, 1000 grids and then well-rinsed with distilled water and dried. A quantity of whitening gel was drop on the clean electrode surface and dried in air for obtaining the Alloy/Gel interface. For immobilizing the gel on the metallic electrode interface, 3 μL of Nafion 3% was deposited on Alloy/Gel interface and evaporating the solvent by drying in air, obtaining the Alloy/Gel-Nafion electrode. The metallic surface was covered by dropping 5 μL suspension of hydroxyapatite (3 mg HAP in 1 ml distillated water) and then dropping the same volumes of Gel and Nafion, in order to obtain the Alloy/HAP/Gel-Nafion modified electrode. Between each step of covering the evaporation of solvent was expected.

## REFERENCES

1. Y. Oshida, C.B. Sellers, K. Mirza, F. Farzin-Nia, *Materials Science and Engineering C*, **2005**, *25*, 343.
2. S.B. Turker, T. Biskin, *The Journal of Prosthetic Dentistry*, **2003**, *89(5)*, 466.
3. Y. Li, *Food and Chemical Toxicology,* **1996**, *34*, 887.
4. S.K. Al-Salehi, P.V. Hatton, A. Johnson, A.G. Cox, C. McLeod, *Journal of Oral Rehabilitation*, **2008**, *35*; 276.
5. H. Eimar, R. Siciliano, M.-N. Abdallah, S.A. Nader, W.M. Amin, P.-P. Martinez, A. Celemin, M. Cerruti, F. Tamimi, *Journal of Dentistry*, **2012**, *40S*, e25.
6. A. Joiner, G. Thakker, *Journal of Dentistry*, **2004**, *32*, 19.
7. L. Sun, S. Liang, Y. Sa, Z. Wang, X. Ma, T. Jiang, Y. Wang, *Journal of Dentistry*, **2011**, *39*, 686.
8. A.M.A. Pizani, B. Tholt, S. Paciornik, K.R.H.C. Dias, P.P.A.C. de Albuquerque, C.S. Queiroz, *Brazilian Journal of Oral Science*, **2015**, *14(2)*, 154.
9. E. Tamam, A.K. Aydin, *Clinical Oral Investigations*, **2011**, *15*, 375.
10. P.A. Oskoee, M.A. Kahnamoui, S.S. Oskoee, F. Zadfattah, F. Pournaghi-Azar, *European Journal of Dentistry*, **2010**, *4*, 23.

11. C.A. Mohsen, *Journal of Prosthodontics*, **2010**, *19*, 33.
12. F.A.L. Farawati, S.-M. Hsu, E. O'Neill, D. Neal, A. Clark, J. Esquivel-Upshaw, *The Journal of Prosthetic Dentistry*, **2018**, article in press. (b) Y. Oshida, Hydroxyapatite. Synthesis and applications, Momentum Press, New York, 2015, p. 10-15.
13. H. Yu, C.-Y. Zhang, S.-L. Cheng, H. Cheng, *Journal of Dental Sciences*, **2015**, *10*, 345.
14. B.A. Matis, M.A. Cochran, G. Eckert, *Operative Dentistry,* **2009**, *34-2*, 230.
15. G.M.P. Juanito, C.S. Morsch, C.A. Benfatti, M.C. Fredel, R.S. Magini, J.C.M. Souza, *Dentistry*, **2015**, *5* 273.
16. G.L. Turdean, C.I. Fort, V. Simon, *Electrochimica Acta*, **2015**,*182*, 707.
17. R. Galo, R.F. Ribeiro, R.C.S. Rodrigues, L.A. Rocha, M.G.C. de Mattos, *Brazilian Dental Journal*, **2012**, *23*, 141.
18. R.W.-W. Hsu, C.-C. Yang, C.-A. Huang, Y.-S. Chen, Materials *Chemistry* and *Physics*, **2005**, *93*, 531.
19. V.S. Saji, H.-C. Choe, *Transactions of Nonferrous Metals Society of China*, **2009**, *19*, 785.
20. G.M. O. de Queiroz, L.F. Silva, J.T. Lima Ferreira, J.A. da Cunha P. Gomes, L. Sathler, *Brazilian Oral Research*, **2007**, *21*, 209.

STUDIA UBB CHEMIA, LXIV, 1, 2019 (p. 135-146)
(RECOMMENDED CITATION)
DOI:10.24193/subbchem.2019.1.11

# HIGH-DOSE STATIN PRIOR TO PRIMARY PERCUTANEOUS CORONARY INTERVENTION REDUCES OXIDATIVE STRESS BURDEN IN PATIENTS WITH ACUTE ST-ELEVATION MYOCARDIAL INFARCTION

**DAN-ALEXANDRU TĂTARU[a,b], DAN-MIRCEA OLINIC[a,b]*, MARIA OLINIC[a,b], ANDRADA-ELENA URDA-CÎMPEAN[a], REMUS ORĂSAN[a], CĂLIN HOMORODEAN[a,b]**

**ABSTRACT.** The current study analysed the effect of high-dose statin loading prior to primary percutaneous coronary intervention on oxidative stress markers, in patients with acute ST-elevation myocardial infarction (STEMI). Besides the lipid lowering effect, statins have antioxidant properties that might reduce myocardial ischemia-reperfusion injury. From a total of 37 patients, 18 patients received high-dose statin before coronarography and were included in the statin group, while 19 statin naive patients were included in the control group. Peripheral venous blood samples were obtained before coronary reperfusion, at 1 hour and 24 hours after that. The following markers of oxidative stress were determined from the serum: malondialdehyde (MDA), reduced glutathione to oxidized glutathione ratio (GSH/GSSG) and total antioxidant capacity (TAC). Values are shown as medians and interquartile ranges. MDA concentration and TAC had non-significant differences between the two groups, at all time frames. Before angioplasty, GSH/GSSG ratio was comparable between the two groups: 3.59 (2.13-5.37) in the statin group vs 2.69 (2.15-5.02) in the control group, p=0.49. At 1 hour after reperfusion, values were still similar: 2.26 (1.32-4.28) in the statin group vs 2.33 (1.88-2.50) in the control group, p=0.55. After 24 hours, there was a significant increase of GSH/GSSG ratio in the statin group 2.41 (1.58-3.28) vs 1.56 (1.12-2.03) in the control group, p=0.01. This finding suggest that, in STEMI patients, high-dose statin loading before primary percutaneous coronary intervention significantly reduces oxidative stress burden, early after administration.

***Keywords:*** *oxidative stress, acute myocardial infarction, statin, glutathione, percutaneous coronary intervention*

[a] *Iuliu Haţieganu University, Faculty of General Medicine, 8 Victor Babeş street, RO-400012, Cluj-Napoca, Romania*
[b] *Cluj County Emergency Hospital, Interventional Cardiology Department, 3-5 Clinicilor street, RO-400006, Cluj-Napoca, Romania*
** Corresponding author: dolinic@yahoo.com*

## INTRODUCTION

Cardiovascular diseases are the leading cause of mortality and morbidity worldwide [1]. Acute ST-elevation myocardial infarction (STEMI) is associated with total coronary occlusion and subsequent myocardial necrosis. The principal objective of therapy is rapid restoration of coronary blood flow to save as much heart muscle as possible. According to current evidence-based guidelines, primary percutaneous coronary intervention (pPCI) is the best method of vessel opening [2,3]. However, a sudden restoration of blood supply, to a previously ischemic myocardium, can lead to myocardial reperfusion injury [4] and increased oxidative stress [5-7] that can paradoxically reduce the beneficial effect of angioplasty.

Statins are lipid-lowering drugs that inhibit cholesterol biosynthesis via down-regulation of 3-hydroxy-3-methyl-glutaryl-CoA (HMG-CoA) reductase. Large secondary prevention trials showed that statins lower the rate of myocardial infarction, ischemic stroke and cardiovascular death [8]. The favourable effect on cardiovascular events depends mostly on the cholesterol-lowering function and plaque stabilization [9], but statins have important pleiotropic effects, like increased nitric oxide production, reduced oxidative stress generation and down-regulation of proinflammatory biomarkers [9]. Overall, statins can have an antioxidant effect, early after administration [10].

The ratio of reduced glutathione (GSH) to oxidized glutathione (GSSG) is an indicator of cellular health, with GSH constituting up to 98% of total glutathione under normal conditions. In various models of oxidative stress, this ratio has been demonstrated to decrease to values of 1:1, meaning that the lower the ratio, the more intense the oxidative process is [11]. In experimental models, measuring GSH/GSSG ratio is an excellent way to assess potential therapeutics efficacy in maintaining cellular redox potential [12].

Reactive oxygen species degrade polyunsaturated lipids, forming malondialdehyde (MDA). This stable end-product aldehyde is used as a biomarker to measure the level of oxidative stress in an organism [13-15].

Total antioxidant capacity (TAC) is a measurement used to assess the antioxidant status of biological samples and can evaluate the antioxidant response against the free radicals produced in a given disease [16-18].

Among patients with STEMI, the current guidelines recommend routine administration of high-dose statin [2,3]. However, the ideal timing of statin initiation, in the acute setting, is not stated. Recent data showed that, in STEMI patients, high-dose statin administration before pPCI significantly reduced 30-day major adverse cardiac events (MACE) [9]. The mechanisms leading to the benefit remain uncertain.

The aim of the current study was to determine the influence of high-dose statin loading prior to pPCI on oxidative stress markers (MDA, GSH/GSSG ratio and TAC), in STEMI patients. The variation of oxidative stress markers was statistically evaluated using the Mann-Whitney U test for non-normally distributed variables.

## RESULTS AND DISCUSSION

Thirty-seven patients were included in the study, 18 patients in the statin group and 19 patients in the control group. The baseline demographic and clinical characteristics are presented in Table 1. The measured variables of the two groups are shown in Table 2.

**Table 1.** Baseline characteristics of the study groups (SD = standard deviation, TSR = time from symptom-onset to reperfusion, BMI = body-mass index)

| **STATIN PRELOAD** | **YES** | **NO** |
|---|---|---|
| **Patients, no (%)** | **18 (48.6)** | **19 (51.4)** |
| **Presentation** | | |
| Age (years), mean ± SD | 66 ± 9.5 | 60 ± 12 |
| Sex (male), no (%) | 10 (55.5) | 14 (73.6) |
| TSR (hours), mean ± SD | 7.3 ± 4 | 5.4 ± 3 |
| **Risk factors** | | |
| Hypertension (yes), no (%) | 13 (72.2) | 13 (68.4) |
| Dyslipidemia (yes), no (%) | 13 (72.2) | 11 (57.8) |
| Smokers (yes), no (%) | 6 (33.3) | 8 (42.1) |
| Diabetes (yes), no (%) | 5 (27.8) | 2 (10.5) |
| BMI (kg/m2), mean ± SD | 28.9 ± 4.8 | 29.2 ± 3.9 |
| **Type of statin** | | |
| Atorvastatin 80 mg, no (%) | 13 (72.2) | |
| Atorvastatin 40 mg, no (%) | 2 (10.5) | |
| Simvastatin 40 mg, no (%) | 2 (10.5) | |
| Rosuvastatin 20 mg, no (%) | 1 (6.8) | |

**Table 2**. Variables of the study groups according to the presence of statin (MDA = malondialdehyde (nmol/ml), GSH/GSSG = reduced glutathione / oxidised glutathione ratio, TAC = total anitioxidant capacity (inhibition %), $P_0$ = before reperfusion, $P_1$ = 1 hour after reperfusion, $P_{24}$ = 24 hours after reperfusion)

| | MDA | | | GSH/GSSG | | | TAC | | |
|---|---|---|---|---|---|---|---|---|---|
| **With statin** | **$P_0$** | **$P_1$** | **$P_{24}$** | **$P_0$** | **$P_1$** | **$P_{24}$** | **$P_0$** | **$P_1$** | **$P_{24}$** |
| **1** | 2.82 | 3.11 | 2.49 | 5.44 | 1.73 | 2.38 | 24.33 | 24.20 | 24.07 |
| **2** | 2.03 | 1.65 | 0.76 | 8.35 | 4.25 | 3.98 | 38.48 | 41.28 | 42.25 |
| **3** | 2.91 | 2.61 | 2.08 | 4.41 | 0.95 | 1.59 | 36.40 | 33.44 | 32.21 |
| **4** | 2.01 | 1.84 | 1.66 | 6.56 | 5.34 | 2.56 | 32.38 | 33.95 | 37.61 |
| **5** | 4.71 | 3.87 | 4.23 | 3.10 | 1.21 | 1.43 | 27.06 | 26.32 | 28.41 |
| **6** | 2.69 | 2.49 | 2.20 | 4.55 | 0.90 | 1.82 | 27.03 | 26.82 | 21.26 |
| **7** | 2.95 | 2.58 | 1.31 | 2.94 | 1.52 | 2.43 | 36.14 | 41.62 | 37.45 |
| **8** | 4.06 | 2.57 | 2.03 | 1.98 | 1.99 | 2.02 | 29.57 | 34.13 | 31.53 |
| **9** | 2.69 | 2.40 | 1.37 | 5.35 | 4.35 | 3.25 | 39.81 | 37.85 | 37.42 |
| **10** | 4.01 | 3.43 | 3.97 | 3.36 | 2.65 | 1.98 | 32.46 | 37.02 | 36.56 |
| **11** | 3.28 | 3.06 | 2.70 | 2.18 | 1.98 | 5.66 | 32.97 | 31.57 | 31.10 |
| **12** | 2.80 | 2.08 | 1.93 | 1.48 | 3.99 | 3.26 | 34.3 | 33.45 | 30.52 |
| **13** | 3.30 | 3.27 | 3.03 | 1.46 | 1.15 | 1.31 | 39.88 | 30.18 | 29.32 |
| **14** | 1.59 | 1.64 | 2.22 | 8.38 | 4.88 | 4.95 | 37.63 | 40.25 | 39.71 |
| **15** | 2.19 | 1.17 | 0.75 | 3.81 | 4.06 | 3.05 | 26.19 | 27.85 | 28.98 |
| **16** | 3.16 | 2.28 | 1.32 | 1.25 | 1.35 | 1.05 | 28.38 | 28.02 | 25.72 |
| **17** | 3.44 | 2.44 | 2.81 | 2.97 | 8.10 | 3.34 | 27.91 | 20.05 | 22.40 |
| **18** | 4.16 | 3.19 | 2.33 | 4.25 | 2.53 | 1.53 | 36.45 | 31.54 | 41.67 |
| **Without statin** | | | | | | | | | |
| **1** | 2.46 | 1.88 | 1.69 | 1.35 | 1.54 | 1.12 | 36.07 | 37.61 | 33.41 |
| **2** | 3.56 | 3.35 | 1.66 | 5.63 | 2.35 | 3.25 | 25.44 | 25.24 | 20.39 |
| **3** | 4.13 | 3.02 | 2.66 | 9.60 | 2.44 | 2.62 | 37.22 | 36.03 | 33.11 |
| **4** | 1.94 | 2.09 | 1.66 | 7.96 | 2.33 | 1.56 | 37.61 | 26.03 | 26.66 |
| **5** | 4.02 | 3.01 | 3.77 | 5.02 | 2.98 | 0.79 | 29.09 | 32.90 | 35.61 |
| **6** | 3.48 | 3.20 | 1.54 | 2.31 | 1.88 | 1.79 | 39.13 | 37.49 | 41.74 |
| **7** | 4.71 | 3.57 | 2.43 | 1.35 | 1.05 | 0.53 | 33.35 | 29.01 | 32.25 |
| **8** | 1.96 | 1.92 | 1.21 | 2.63 | 2.02 | 1.25 | 32.88 | 31.48 | 32.64 |
| **9** | 3.96 | 3.66 | 2.43 | 3.57 | 3.02 | 3.12 | 32.21 | 36.13 | 41.38 |
| **10** | 4.53 | 3.80 | 3.34 | 2.25 | 2.38 | 1.36 | 29.64 | 31.05 | 31.63 |
| **11** | 1.96 | 1.72 | 1.06 | 1.65 | 1.36 | 1.98 | 32.38 | 31.45 | 36.39 |
| **12** | 2.86 | 2.71 | 1.62 | 2.15 | 1.88 | 1.02 | 35.65 | 37.72 | 35.70 |
| **13** | 3.02 | 3.67 | 3.94 | 2.69 | 1.04 | 1.15 | 41.86 | 49.15 | 58.22 |
| **14** | 3.45 | 4.35 | 2.83 | 3.58 | 2.53 | 2.65 | 28.84 | 18.48 | 12.80 |
| **15** | 3.30 | 2.17 | 0.53 | 6.35 | 2.34 | 1.25 | 31.26 | 31.68 | 41.93 |
| **16** | 2.86 | 2.46 | 2.22 | 2.32 | 2.62 | 1.96 | 24.15 | 22.09 | 21.81 |
| **17** | 4.98 | 3.86 | 3.15 | 3.25 | 2.04 | 1.96 | 25.96 | 25.50 | 27.68 |
| **18** | 1.28 | 1.71 | 1.09 | 3.25 | 2.50 | 2.03 | 32.64 | 31.08 | 37.64 |
| **19** | 1.48 | 1.29 | 1.52 | 1.65 | 2.02 | 1.02 | 37.06 | 37.38 | 43.41 |

GSH/GSSG ratio before pPCI ($P_0$) was comparable between the two groups: 3.59 (2.13-5.37) in the statin group vs 2.69 (2.15-5.02) in the control group, p=0.49. At 1 hour after pPCI ($P_1$), no significant differences were noted: 2.26 (1.32-4.28) in the statin group vs 2.33 (1.88-2.50) in the control group, p=0.55. After 24 hours ($P_{24}$), there was a significant increase in GSH/GSSG ratio in statin loaded patients: 2.41 (1.58-3.28) in the statin group vs 1.56 (1.12-2.03) in the control group, p=0.01 (Figure 1).

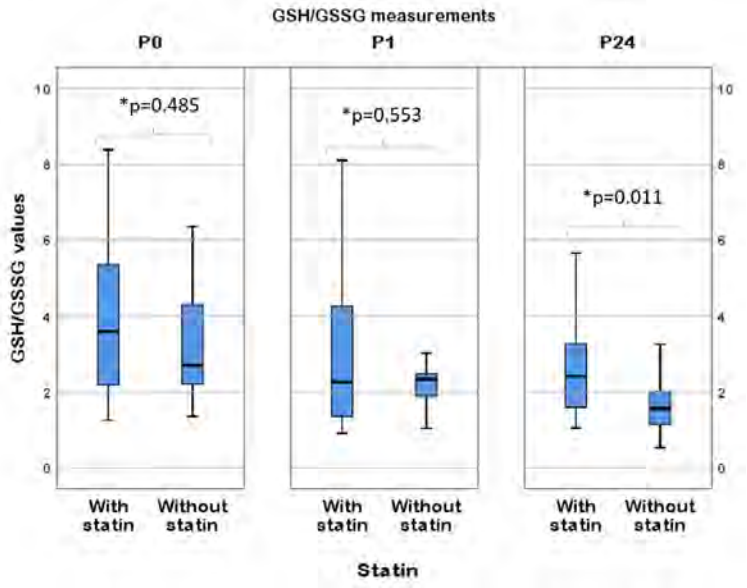


**Figure 1.** Comparison of GSH/GSSG values for $P_0$, $P_1$ and $P_{24}$ measurements according to the presence of statin (* Mann-Whitney U Test; bars = range, box = first quartile to third quartile, horizontal black line = median)

At $P_0$, the median MDA levels were 2.93 (2.57-3.58) nmol/ml for the statin group and 3.3 (1.96-4.02) nmol/ml in the control group, p=0.68. There were no differences between the two groups at 1 hour ($P_1$): 2.53 (2.02-3.12) nmol/ml in the statin group vs 3.01 (1.92-3.66) nmol/ml in the control group, p=0.34. Also at $P_{24}$, MDA levels were similar: 2.14 (1.36-2.73) nmol/ml in the statin group vs 1.69 (1.52-2.83) nmol/ml in the control group, p=0.84 (Figure 2).

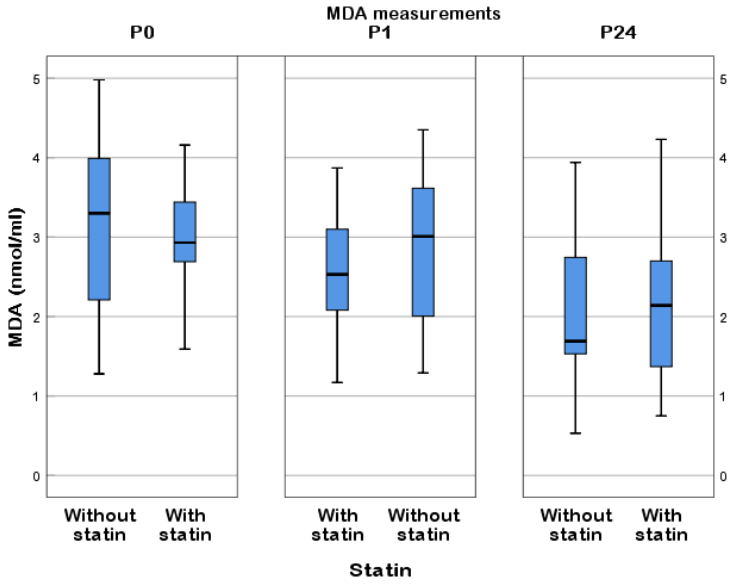


**Figure 2.** Comparison of MDA values for $P_0$, $P_1$ and $P_{24}$ measurements according to the presence of statin (bars = range, box = first quartile to third quartile, horizontal black line = median)

TAC levels were not significantly influenced by statin loading. Baseline levels ($P_0$) were similar: 32.72 (27.69-36.75) inhibition % in the statin group vs 32.64 (29.09-37.06) inhibition % in the control group, p=0.94). Furthermore, after pPCI no significant changes were noted: $P_1$, 32.51 (27.59-37.21) inhibition % in the statin group vs 31.48 (26.03-37.38) inhibition % in the control group, p=0.73; $P_{24}$, 31.32 (27.74-37.49) inhibition % in the statin group vs 33.41 (27.68-41.38) inhibition % in the control group, p=0.44 (Figure 3).

In the settings of acute myocardial infarction, previous papers showed that after vessel opening there is an increase in oxidative stress burden from the first minutes and lasting several days [5,14,19]. These studies showed that some oxidative stress parameters, such as MDA are improved quickly after reperfusion [5,14,19], but TAC [14] and GSH/GSSG ratio [5] decreased after reperfusion, suggesting myocardial reperfusion injury.

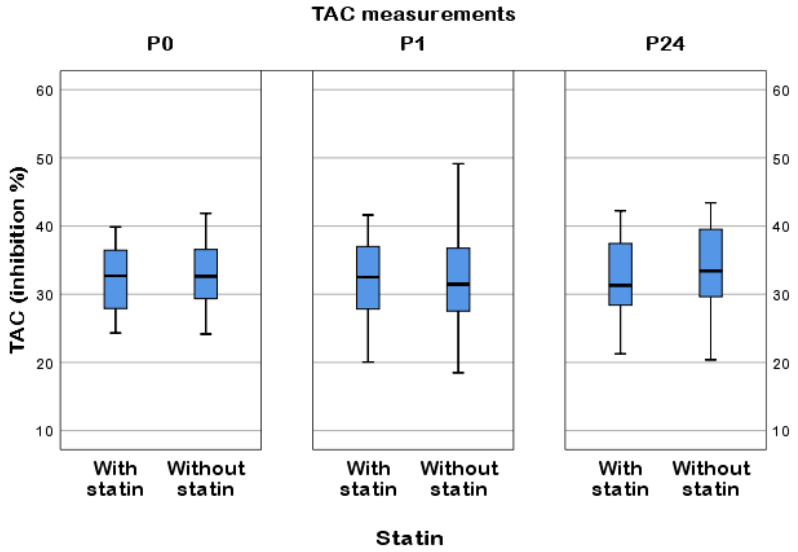


**Figure 3.** Comparison of TAC values for $P_0$, $P_1$ and $P_{24}$ measurements according to the presence of statin (bars = range, box = first quartile to third quartile, horizontal black line = median).

The main finding of the present study showed that, in STEMI patients, high-dose statin loading before pPCI significantly reduced oxidative stress burden by improving GSH/GSSG ratio at 24 hours after successful reperfusion. An improved GSH/GSSG ratio can explain the benefit of statin loading prior to pPCI, by protecting against myocardial reperfusion injury.

Considering that the reduction in oxidative stress occurred early, the mechanism behind this potential effect is probably not the low-density lipoprotein cholesterol reduction. Two major trials [9,20] also support the hypothesis that the possible benefit of statin therapy could extend beyond a lipid-lowering effect.

The CANTOS trial [20] showed that anti-inflammatory intervention reduces MACE in patients with coronary artery disease. Considering that pPCI may result in both local and embolic complications, enhancement of inflammatory activity and atherosclerotic plaque instability [21], these additional effects of statins have the potential to reduce the risk of clinical events.

As mentioned above, a subgroup analysis of the SECURE-PCI trial [9], showed that STEMI patients undergoing pPCI that had a loading dose of 80 mg atorvastatin before angiography had a significant reduction in MACE at 30 days: hazard ratio, 0.54; 95% confidence interval, 0.35-0.84; p=0.01.

MDA results as a product of polyunsaturated fatty acid degradation [13]. MDA levels may be linked to the lipid lowering property of statins, so it is not likely that MDA can decrease in a few hours after statin administration. Two papers, that included patients at high-risk of cardiovascular disease, showed a significant reduction in MDA levels after 4 to 12 weeks of statin treatment [22,23]. In contrast, a recent paper with a similar study population, failed to show a significant reduction in MDA levels in patients treated with atorvastatin or simvastatin [24]. In the positive studies, lipid peroxidation was evaluated by the thiobarbituric acid (TBA) fluorescence method, which has potential limitations with respect to sensibility and specificity. The negative study, used the high-performance liquid chromatography (HPLC) method, which is more specific [25-28].

The potential of statin therapy to increase TAC was demonstrated in patients with established coronary artery disease [29], after a 3-month period of treatment. There are different methods for determining TAC. The scavenging of 1,1-diphenyl-2-picrylhydrazyl (DPPH) was not sensible enough for the acute settings [5], but the quenching of the (2,2'-azino-bis(3-ethylbenzthiazoline-6-sulphonic acid)) radical cation by antioxidants was performed in another pPCI based study, with promising results [14].

So far, in patients with STEMI, early administration of statins before pPCI is not recommended in evidence-based guidelines, but increasing evidence of benefit may guide medical decision making, in these critical scenarios.

## CONCLUSIONS

In STEMI patients, high-dose statin loading before pPCI significantly reduced reperfusion induced oxidative stress, as reflected by the increase in GSH/GSSG ratio at 24 hours after angioplasty.

Statin loading did not influence MDA and TAC levels.

## EXPERIMENTAL SECTION

The study was in accordance with the Declaration of Helsinki [30]. Written consent was obtained from each patient before the procedure. Patients diagnosed with acute STEMI and admitted to Cluj County Emergency Hospital, Interventional Cardiology Department, were enrolled between April 2017 and December 2017. Inclusion criteria were as follows: electrocardiographic evidence of ST elevation of ≥ 1 mV in two or more standard limb leads or

≥ 2 mV in two or more precordial leads; typical chest pain lasting more than 20 minutes; time of presentation under 12 hours since symptom onset. All patients received drug eluting stents and pPCI was confined to the infarct-related artery. Only patients with successful reperfusion were included in the study. All patients were pretreated with antithrombotic medication according to current recommendations [2,3,31]. All demographic, clinical, paraclinical and intraprocedural data were stored in the Departments' structured database for future comparing [32,33].

Patients which received high-dose statin in the Emergency Room, before transferring to the Catheterization Laboratory, were included in the statin group. Patients that did not receive statin before pPCI and were not on chronic statin therapy (statin naive) were included in the control group. All patients subsequently received statin therapy 24 hours after pPCI. High-dose statin treatment was defined as follows: atorvastatin 40 mg or 80 mg, rosuvastatin 20 mg or 40 mg and simvastatin 40 mg or 80 mg.

Peripheral venous blood samples were obtained from each patient immediately before pPCI ($P_0$) and then after 1 hour ($P_1$) and 24 hours ($P_{24}$). Samples were drawn into plastic tubes with ethylenediaminetetraacetic acid (EDTA). Blood was centrifuged within 1 hour at 1500 rpm for 15 minutes and the collected plasma was stored at –30° C until analysis (within 1 month).

All the reagents were supplied by Sigma (Deisenhofen, Germany), were of analytical grade and were used without further purification.

MDA was determined using the method of Conti [34]. Through this process, the resulting MDA reacts with TBA to form a fluorescent adduct. First, 50 µl of plasma was boiled with 1 ml of 10 mM 2-TBA and 1 ml of 75 mM $K_2HPO_4$, pH=3. After quencing, the product was extracted with n-butanol. The fluorescence of the extract was measured at an emission wavelength of 534 nm using a spectrofluorometer (Lambda 35, Perkin Elmer, USA) with a synchronous fluorescence technique at a difference of 14 nm between the excitation and emission wavelength ($\Delta\lambda$). MDA concentration was determined based on a calibration curve consisting of common MDA concentrations using the same measurement technique. MDA levels are expressed in nmol/ml.

GSH was determined as described by Hu [35]. First, 500 µl of plasma are mixed with 500 µl of cold 10% trichloroacetic acid (TCA). After 10 minutes in ice, the mixture is centrifuged at 3000 rpm for 15 minutes, and then, 200 µl of the supernatant is mixed with 1.7 ml of phosphate buffer and 0.1 ml of o-phthalaldehyde. After 15 minutes, the fluorescence at 350 nm excitation and 420 nm emission is read against a blank (Lambda 35, Perkin Elmer, USA).

GSSG was calculated using Vats' method [36]. Initially, 250 µl of the plasma sample was incubated with 0.1 ml of 40 nM N-ethylmaleimide for 30 minutes, followed by addition of 0.65 ml of 0.1 M NaOH. Thereafter, the same procedure was followed for fluorescence development as used in

GSH measurement, except in place of the buffer, 0.1 M NaOH was used. The amounts of GSH and GSSG were calculated from standard curves and are expressed in µmol/ml.

TAC was determined according to Janaszewska [37].The reduction assay was performed by adding 20 µl of plasma to 400 µl of 0.1 mM methanol solution of DPPH and phosphate buffer, pH=7.4. After a 30-minute incubation at ambient temperature, absorbance of the samples at 520 nm was measured (Lambda 35, Perkin Elmer, USA) and compared with that of a reference sample containing only DPPH solution and phosphate buffer. TAC was measured in inhibition % as [(control extinction - serum extinction) / control extinction] x 100.

The statistical analysis was conducted using SPSS software v25 (IBM, USA). The Shapiro-Wilk test was used to assess for a normal distribution. Quantitative data without normal distribution was described using box-plots, median and Q1-Q3, where Q1-Q3 (inter quartile range) stands for the range between 25th percentile (Q1) and 75th percentile (Q3). Normally distributed data was presented as mean ± standard deviation. The Mann-Whitney U test was applied for non-normally distributed variables to check if there was a significant difference between the two independent samples. A p-value equal to or lower than 0.05 was considered statistically significant.

## ACKNOWLEDGMENTS

We thank our colleagues from The Oxidative Stress Laboratory, part of the Physiology Department, “Iuliu Haţieganu” University, Cluj-Napoca, who provided insight and expertise that greatly assisted the research.

## REFERENCES

1. D. Olinic, M. Spinu, M. Olinic, C. Homorodean, D. Tataru, A. Liew, G. Schernthaner, A. Stanek, G. Fowkes, M. Catalano, *International Angiology,* **2018**, *37*, 327.
2. B. Ibanez and the ESC Taskforce, *European Heart Journal*, **2017**, *00*, 1.
3. P.T. O’Gara and the American Heart Association Task Force on Practice Guidelines, J*ournal of American College of Cardiology*, **2013**, *61*, e78.
4. D. Yellon, D. Hausenloy, *New England Journal of Medicine*, **2007**, 357, 1121.
5. D. Tataru, D. Olinic, A. Urda, M. Olinic, R. Orasan, *Studia UBB Chemia*, **2018**, *3*, 117.

6. M. Spînu, D. Olinic, M. Olinic, C. Homorodean, *Romanian Journal of Morphology and Embryology*, **2018**, *59*, 469.
7. C. Homorodean, M. Ober, M. Olinic, R. Homorodean, A. Hassoune, D. Tătaru, M. Spînu, D. Olinic, *Medical Ultrasonography,* **2016**, *18*, 475.
8. Violi, R. Carnevale, D. Pastori, P. Pignatelli, *Trends in Cardiovascular Medicine*, **2014**, *24*, 142.
9. O. Berwanger and the SECURE-PCI Study Group, *JAMA,* **2018**, *319*, 1331.
10. C. Wang, P. Liu, J. Liao, *Trends in Molecular Medicine,* **2008**, *14*, 37.
11. Y. Chai, S. Ashraf, K. Rokutan, R. Johnston, J. Thomas, *Archives of Biochemistry and Biophysics*, **1994**, *310*, 273.
12. B. Owen, D.A. Butterfield, *Methods in Molecular Biology*, **2010**, *648*, 269.
13. D.M. Mitrea, S. Clichici, A. Filip, D. Olteanu, I. Baldea, R. Moldovan, N. Decea, O.A. Hoteiuc, *Studia UBB Chemia,* **2017**, *62*, 89.
14. E. Sedláková, O. Rácz, E. Lovásová, R. Beňačka, M. Kurpas, A. Chmelárová, J. Sedlák, M. Studenčan, *Central European Journal of Medicine,* **2009**, *4*, 26.
15. Coneac, M.S. Orasan, M. Crisan, C. Mare, N. Decea, C.M. Mihu, A. Muresan, V. Lazar, M. Filip, *Studia UBB Chemia*, **2016**, 2, 177.
16. Moldovan, L. David, S.C. Man, *Studia UBB Chemia*, **2017**, *2*, 311.
17. Simon, D. Simedru, L. Dordai, E. Luca, V. Fuss, A. Becze, *Studia UBB Chemia*, **2016**, *61*, 505.
18. S.B. Kedare, R.P. Singh, *Journal of Food Science and Technology*, **2011**, *48*, 412.
19. K. Olsson, J. Harnek, A. Ohlin A, N. Pavlidis, B. Thorvinger, H. Ohlin, *Scandinavian Cardiovascular Journal*, **2002**, *36*, 237.
20. P.M. Ridker and the CANTOS Trial Group, *New England Journal of Medicine*, **2017**, *12*, 1119.
21. A.J. Lansky, G.W. Stone, *Circulation: Cardiovascular Interventions*, **2010**, *3*, 602.
22. G.J. Moon, S.J. Kim, Y. Cho, S. Ryoo, O. Bang, *Journal of Clinical Neurology*, **2014**, *10*, 140.
23. M. Yilmaz, Y. Baykal, M. Kilic, A. Sonmez, F. Bulucu, A. Aydin, A. Sayal, I. Kocar, *Biological Trace Element Research,* **2004**, *2*, 119.
24. P.G. Scheffer, R.K. Schindhelm, V.M. van Verschuer, M. Groenemeijer, S. Simsek, Y. Smulders, P. Nanayakka, *The Netherlands Journal of Medicine,* **2013**, *7*, 359.
25. I. Khalaf, L. Vlase, B. Ivanescu, D. Lazar, A. Corciova, *Studia UBB Chemia*, **2012**, *2*, 113.
26. D. Benedec, I.E. Popica, I. Oniga, D. Hanganu, M. Duma, R. Silaghi-Dumitrescu, C. Bischin, I. Vlase, *Studia UBB Chemia*, **2015**, *4*, 257.
27. A. Dragus, M.S. Beldean-Galea, *Studia UBB Chemia*, **2015**, *2*, 117.
28. A. Ceconi, A. Cargoni, E. Pasini, E. Condorelli, S. Curello, R. Ferrari, *American Journal of Physiology - Heart and Circulatory Physiology*, **1991**, *260*, H1057.
29. H. Buyukhatipoglu, Y. Suzun, A. Yildiz, U. Guntekin, M. Bas, M. Polat, R. Demirbag, A. Taksin, H. Celik, N. Aksoy, *Clinical and Investigative Medicine*, **2010**, *5*, E313.

30. World Medical Association, *Journal of the American Medical Association*, **2013**, *310*, 2191.
31. D. Olinic, D. Tataru, C. Homorodean, M. Spinu, M. Olinic, *Vasa,* **2018**, *47*, 99.
32. D. Olinic, S. Nedevschi, C. Feier, Z. Gal, N. Olinic, *Computers in Cardiology*, **1999**, 443.
33. C. Homorodean, M. Olinic, D.M. Olinic, *Medical Ultrasonography*, **2012**, *14*, 29.
34. M. Conti, P.C. Morand, P. Levillain, A. Lemonnier, *Clinical Chemistry*, **1991**, *37*, 1273.
35. M.L. Hu, *Methods in Enzymology*, **1994**, *233*, 380.
36. P. Vats, V.K. Singh, S.S. Sing, *Aviation, Space and Environmental Medicine*, **2008**, *79*, 1106.
37. A. Janaszewska, G. Bartosz, *Scandinavian Journal of Clinical and Laboratory Investigation,* **2002**, *62*, 231.

STUDIA UBB CHEMIA, LXIV, 1, 2019 (p. 147-159)
(RECOMMENDED CITATION)
DOI:10.24193/subbchem.2019.1.12

# A COMPARISON BETWEEN INSULIN RESISTANCE SCORES PARAMETERS IN IDENTIFYING PATIENTS WITH METABOLIC SYNDROME

**ANGELA COZMA[a,†], ADRIANA FODOR[b,†], OLGA HILDA ORĂȘAN[a,*], RAMONA SUHAROSCHI[c], CRINA MUREȘAN[c], ROMANA VULTURAR[d], DOREL SAMPELEAN[a], VASILE NEGREAN[a], DANA POP[e], ADELA SITAR-TĂUT[a]**

**ABSTRACT** As a consequence of the epidemic of obesity, prediction of metabolic syndrome (MetS) is relevant because of its subsequent association with type 2 diabetes and cardiovascular disease. Also, MetS is considered a state of insulin resistance (IR). This study aimed to evaluate the capacity of different indirect IR scores to identify patients with MetS, compared to standard criteria of MetS diagnosis. To the best of our knowledge, the cut-off values of these indexes, as indicators of MetS, in the Romanian population, have not been established. We used a non-parametric extension of the induced ROC regression methodology to determine the cut-off values of HOMA-IR, QUICKI, McAuley indexes, taking into account the MetS components instead of using 90th percentile criteria. Although HOMA is more commonly used in practice (probably due to its easy use), McAuley Score seems to have a better specificity in identifying patients with MetS. This is different between men and women; if in women, McAuley index has the highest sensitivity, in men, HOMA and QUICKI indexes have the highest sensitivity and specificity.

***Keywords:*** *insulin, glycemia, HOMA, QUICKI, McAuley, metabolic syndrome*

[a] *University of Medicine and Pharmacy "Iuliu Hatieganu", 4th Internal Medicine Department Cluj-Napoca, Romania*
[b] *University of Medicine and Pharmacy "Iuliu Hatieganu" Clinical Center of Diabetes,Nutrition and Metabolic Disease, Cluj-Napoca, Romania*
[c] *University of Agricultural Sciences and Veterinary Medicine of Cluj-Napoca, Faculty of Food Science &Technology*
[d] *University of Medicine and Pharmacy "Iuliu Hatieganu", Department of Cell Biology, Cluj-Napoca, Romania*
[e] *University of Medicine and Pharmacy "Iuliu Hatieganu", Department of Cardiology, Cluj-Napoca, Romania*
*†authors with equal contribution*
**Corresponding author: E-mail: olgaorasan@yahoo.com*

## INTRODUCTION

Metabolic Syndrome (MetS) is associated with increased cardiovascular risk, being a common cause of atherosclerotic vascular disease. Also, MetS is considered a state of insulin resistance (IR).

Insulin resistance causes increased atherogenesis and atherosclerotic plaque instability by inducing proinflammatory activity in vascular and immune cells [1,2]. Insulin resistance enhances the risk of developing type 2 diabetes mellitus and is an independent risk factor for major cardiovascular events in patients with preexisting arterial disease [3,4]. Apart from influencing clinical disease development and mortality [5], IR is now recognized to play an important role in preclinical (silent) CAD. According to recent studies, IR is associated with asymptomatic myocardial perfusion defects in normotensive adults with preclinical diabetes [6] and is linked to angiographically documented silent CAD in patients with type 2 diabetes[7,8].

The quantification of IR can be achieved by evaluating peripheral insulin sensitivity in vivo with methods such as the hyperinsulinemic-euglycemic clamp technique or the intravenous glucose tolerance test. They are complicated, time-consuming and expensive methods, unsuitable for clinical studies. Simpler indirect methods have been promoted for quantification of IR. Moreover, several components of MetS (dysglycemia, abdominal obesity, dyslipidemia) are pathophysiologically related to IR.

This study aimed to evaluate the capacity of different indirect IR scores to identify patients with MetS, compared to standard criteria of MetS diagnosis [9]. The homeostatic model assessment of IR (HOMA-IR) is a mathematical model that predicts insulin sensitivity, measured by fasting blood glucose and basal insulin. It is strongly correlated with the hyperinsulinemic-euglycemic clamp (r=0.88), the gold standard for assessing insulin resistance (IR) [10]. It is also correlated positively with the components of MetS such as central obesity, lipid abnormalities and hypertension. However, there is great variability in the threshold HOMA-IR levels to define IR. Most studies have determined the cut-off values based on the percentile criteria (80th or 90th) of values in the general population.

Quantitative insulin sensitivity check index (QUICKI) can be determined from a fasting blood sample and correlates with glucose clamp measures of insulin sensitivity (r=0.78) [11]. QUICKI is similar to HOMA, except that QUICKI transforms the data by taking both the logarithm and the reciprocal of the glucose-insulin product, thus slightly skewing the distribution of fasting insulin values. Moreover, the two methods correlate well.

McAuley index is a score based on a weighted combination of insulin and triglycerides, corrected for weight, determined from a fasting blood sample [12].It is used for predicting IR in normoglycemic individuals.

IR probability score (IR-PS) is based on insulin, C-peptide, creatinine, TG/HDL-C, and BMI. It has been recently used to assess IR in apparently healthy individuals [13].

The use of these indexes in clinical practice is limited because of the absence of reference values for normal and impaired insulin sensitivity. HOMA-IR and QUIKI are suitable for clinical use, while McAuley index is suitable for epidemiological studies.

To the best of our knowledge, the cut-off values of these indexes, as indicators of MetS, in the Romanian population, have not been established. We used a non-parametric extension of the induced ROC regression methodology [14] to determine the cut-off values of HOMA-IR, QUICKI, McAuley indexes, taking into account the MetS components instead of using 90th percentile criteria. The purpose of this study was to evaluate the capacity of different IR scores to identify patients with MetS, compared to standard criteria of MetS diagnosis.

## RESULTS AND DISCUSSION

The general characteristics of the studied group, including 84 subjects of which 21 men and 63 women with a mean age of 56.89±11.05 years, are shown in Table 1. Mean values for systolic and diastolic blood pressure, BMI, waist circumference, plasma leptin, total cholesterol, triglycerides, HDL cholesterol, fasting glucose, HbA1c and indirect insulin resistance indexes (HOMA, QUICKI, McAuley) are included in these data. Statistically significant differences between the patients with and without MetS were found for age, obesity, abdominal circumference, BMI, hypertension, diabetes, systolic blood pressure, diastolic blood pressure, triglycerides, insulin, HOMA, QUICKI, McAuley indexes.

Patients with MS presented higher insulin resistance (estimated through HOMA index 1.59 vs. 1.04, p=0.0001 and McAuley Score 2.37±0.43 vs. 1.89 ±0.36, p=0.0001) and lower insulin sensitivity (0.35±0.026 vs. 0.37±0.026, p=0.0001).

HOMA was significantly correlated with BMI (correlation coeff =0.372, p<0.001), SBP (correlation coeff =0.250, p=0.022), abdominal circumference (correlation coeff =0.464, p<0.001), glycemia (correlation coeff =0.592, p<0.001), the presence of diabetes (correlation coeff =0.403, p<0.001), serum TG (correlation coeff =0.432, p<0.001), the presence of MS (correlation coeff =0.443, p<0.001), and was inversely correlated with the HDL-cholesterol value (correlation coeff =-0.287, p=0.008)

Performing multivariate regression analysis for HOMA we have found that diabetes was the only independent predictors for HOMA (coefficient of determination = 3.393, p<0.001) (Table 2).

**Table 1.** – Characteristics of the studied group

| | | Total | Without MetS | MetS | p |
|---|---|---|---|---|---|
| **Number** | No (%) | 84 (100) | 29 (34.5) | 55 (65.5) | 0.0064 |
| **Age** | Mean±SD | 56.89±11.05 | 53.10 ±10.69 | 58.89±10.80 | 0.021 |
| **Sex** | No (%) | | | | |
| **F** | | 63 (75) | 27 (93.10) | 36 (65.45) | 0.0118 |
| **M** | | 21 (25) | 2 (6.9) | 19 (34.54) | |
| **Smoking** | No (%) | | | | |
| **Yes** | | 21 (25) | 11 (37.9) | 10 (18.18) | 0.08 |
| **No** | | 63 (75) | 18 (62.1) | 45 (81.81) | |
| **Obesity** | No (%) | | | | |
| **Yes** | | 32 (38.1) | 6 (20.7) | 26 (47.3) | 0.0316 |
| **No** | | 52 (61.9) | 23 (79.3) | 29 (52.7) | |
| **AC** | Mean±SD | 96.57±12.42 | 89.55±11.60 | 100.27±11.27 | 0.0001 |
| **BMI** | Mean±SD | 28.81±4.22 | 26.89±4.42 | 29.82±3.78 | 0.0021 |
| **HTN** | No (%) | | | | |
| **Yes** | | 54 (64.3) | 13 (44.8) | 41 (74.6) | 0.0138 |
| **No** | | 30 (35.7) | 16 (55.2) | 14 (25.4) | |
| **Diabetes** | No (%) | | | | |
| **Yes** | | 13 (15.5) | 0 (0) | 13 (23.6) | 0.0114 |
| **No** | | 71 (84.5) | 29 (100) | 42 (76.4) | |
| **CVD** | No (%) | | | | |
| **Yes** | | 20 (23.8) | 7 (24.1) | 13 (23.6) | NS |
| **No** | | 64 (76.2) | 22 (75.8) | 42 (76.4) | |
| **Glycemia** | Mean±SD | 97.35±16.76 | 86.75±8.30 | 102.94±17.43 | < 0.0001 |
| **Total cholesterol** | Mean±SD | 218.09±43.58 | 221.41±35.86 | 216.34±47.36 | Ns |
| **LDL cholesterol** | Mean±SD | 139.82±37.05 | 148.13±30.30 | 135.43±39.71 | Ns |
| **HDL cholesterol** | Mean±SD | 47.15±8.5 | 51.68±6.93 | 44.76±8.32 | 0.0002 |
| **TG** | Mean±SD | 155.52±78.01 | 108.17±38.30 | 180.49±82.19 | < 0.0001 |
| **SBP** | Mean±SD | 136.42±19.67 | 127.58±16.4 | 141.09±19.78 | 0.0023 |
| **DBP** | Mean±SD | 84.82±10.33 | 80.34±8.85 | 87.18±10.35 | 0.0034 |
| **Insulin*** | Mean±SD (median) | 7.58±5.18 (5.7) | 6.22±4.05 (4.8) | 8.29±5.59 (6.5) | 0.0014 |
| **HOMA index *** | Mean±SD (median) | 1.86±1.47 (1.36) | 1.34±0.91 (1.04) | 2.14±1.63 (1.59) | 0.0001 |
| **HOMA BETA*** | Mean±SD (median) | 88.61±56.36 (73.24) | 98.59±60.73 (78.10) | 83.52±53.86 (69.18) | NS |
| **QUICKI index** | Mean±SD | 0.35±0.02 | 0.37±0.026 | 0.35±0.026 | 0.0001 |
| **Glycemia/insulin** | Mean±SD | 15.88±6.02 | 16.87±5.43 | 15.36±6.30 | NS |
| **McAuley index** | Mean±SD | 2.06±0.45 | 2.37±0.43 | 1.89±0.36 | 0.0001 |

*Not meeting the normality condition; for normal distribution data Student test was used; for not-normally distributed data Mann-Whitney test was used, for categorical data - $\chi 2$ test was used; AC – abdominal circumference, BMI- body mass index, HTN – hypertension, CVD-cardiovascular disease, TG – triglycerides, SBP - systolic blood pressure, DBP - diastolic blood pressure

**Table 2.** – Multivariate regression analysis for HOMA – model summary and coefficients

| Model Summary | | | | | |
|---|---|---|---|---|---|
| Model | R | R Square | Adjusted R Square | Std. Error of the Estimate | a. Predictors: (Constant), SBP |
| 1 | .072[a] | .005 | -.007 | 1.47549 | b. Predictors: (Constant), SBP, AC |
| 2 | .227[b] | .052 | .028 | 1.44949 | c. Predictors: (Constant), SBP, AC, **DM_NO** |
| 3 | .467[c] | .218 | .188 | 1.32472 | d. Predictors: (Constant), SBP, AC, **DM_NO,** TG |
| 4 | .503[d] | .253 | .215 | 1.30242 | e. Predictors: (Constant), SBP, AC, **DM_NO**, TG, HDL |
| 5 | .505[e] | .255 | .207 | 1.30924 | f. Predictors: (Constant), SBP, AC, **DM_NO**, TG, HDL, **MS_NO** |
| 6 | .506[f] | .256 | .198 | 1.31701 | g. Dependent Variable: HOMA index |

| Coefficients[a] | | | | | | |
|---|---|---|---|---|---|---|
| Model | | Unstandardized Coefficients | | Standardized Coefficients | t | Sig. |
| | | B | Std. Error | Beta | | |
| 1 | (Constant) | 1.135 | 1.135 | | 1.000 | .320 |
| | **SBP** | .005 | .008 | .072 | .654 | .515 |
| 2 | (Constant) | -.552 | 1.400 | | -.394 | .694 |
| | **SBP** | -.002 | .009 | -.029 | -.246 | .806 |
| | **AC** | .028 | .014 | .238 | 1.992 | .050 |
| **3** | **(Constant)** | .628 | 1.311 | | .479 | .633 |
| | **SBP** | -.006 | .008 | -.082 | -.744 | .459 |
| | **AC** | .019 | .013 | .159 | 1.429 | .157 |
| | **DM_NO** | 1.708 | .415 | .423 | 4.120 | .000 |
| 4 | (Constant) | .462 | 1.292 | | .358 | .722 |
| | **SBP** | -.006 | .008 | -.077 | -.711 | .479 |
| | **AC** | .014 | .013 | .120 | 1.080 | .283 |
| | **DM_NO** | 1.483 | .424 | .367 | 3.497 | .001 |
| | TG | .004 | .002 | .202 | 1.940 | .056 |
| 5 | (Constant) | .938 | 1.716 | | .547 | .586 |
| | **SBP** | -.005 | .008 | -.073 | -.669 | .506 |
| | **AC** | .013 | .013 | .111 | .978 | .331 |
| | **DM_NO** | 1.497 | .427 | .370 | 3.502 | .001 |
| | TG | .004 | .002 | .187 | 1.675 | .098 |
| | HDL | -.008 | .018 | -.045 | -.424 | .672 |
| 6 | (Constant) | .967 | 1.730 | | .559 | .578 |
| | **SBP** | -.006 | .008 | -.080 | -.711 | .479 |
| | **AC** | .012 | .014 | .104 | .897 | .373 |
| | **DM_NO** | 1.477 | .435 | .366 | 3.393 | .001 |
| | TG | .003 | .002 | .178 | 1.531 | .130 |
| | HDL | -.006 | .019 | -.037 | -.326 | .745 |
| | **MS_NO** | .110 | .385 | .036 | .287 | .775 |

SBP – systolic blood pressure, AC – abdominal circumference, DM_NO- presence/absence of diabetes, MS_ No - presence/absence of metabolic syndrome, TG – triglycerides, HDL- HDL-cholesterol

**Table 3.** – Multivariate regression analysis for QUICKI index – model summary and coefficients

| Model Summary | | | | | |
|---|---|---|---|---|---|
| Model | R | R Square | Adjusted R Square | Std. Error of the Estimate | |
| 1 | .323[a] | .104 | .093 | .02740 | a. Predictors: (Constant), BMI |
| 2 | .417[b] | .174 | .153 | .02648 | b. Predictors: (Constant), BMI, **AC** |
| 3 | .536[c] | .288 | .261 | .02474 | c. Predictors: (Constant), BMI, **AC**, **DM_NO** |
| 4 | .595[d] | .354 | .322 | .02370 | d. Predictors: (Constant), BMI, **AC**, **DM_NO**, TG |
| 5 | .602[e] | .362 | .321 | .02371 | e. Predictors: (Constant), BMI, **AC**, **DM_NO**, TG, HDL |
| 6 | .609[f] | .371 | .322 | .02370 | f. Predictors: (Constant), BMI, **AC**, **DM_NO**, TG, HDL, **MS_NO**<br>g. Dependent Variable: QUICKI index |

| **Coefficients [a]** | | | | | | |
|---|---|---|---|---|---|---|
| Model | | Unstandardized Coefficients | | Standardized Coefficients | t | Sig. |
| | | B | Std. Error | Beta | | |
| 1 | (Constant) | .422 | .021 | | 20.388 | .000 |
| | BMI | -.002 | .001 | -.323 | -3.087 | .003 |
| 2 | (Constant) | .452 | .023 | | 19.685 | .000 |
| | BMI | .000 | .001 | .034 | .198 | .844 |
| | **AC** | -.001 | .000 | -.443 | -2.608 | .011 |
| 3 | (Constant) | .438 | .022 | | 20.104 | .000 |
| | BMI | -7.553E-005 | .001 | -.011 | -.070 | .945 |
| | **AC** | -.001 | .000 | -.323 | -1.990 | .050 |
| | **DM_NO** | -.028 | .008 | -.349 | -3.583 | .001 |
| 4 | (Constant) | .442 | .021 | | 21.119 | .000 |
| | BMI | -8.645E-005 | .001 | -.013 | -.083 | .934 |
| | **AC** | -.001 | .000 | -.271 | -1.734 | .087 |
| | **DM_NO** | -.022 | .008 | -.274 | -2.819 | .006 |
| | TG | .000 | .000 | -.277 | -2.853 | .006 |
| 5 | (Constant) | .421 | .030 | | 14.131 | .000 |
| | BMI | -6.935E-005 | .001 | -.010 | -.067 | .947 |
| | **AC** | -.001 | .000 | -.258 | -1.642 | .105 |
| | **DM_NO** | -.022 | .008 | -.282 | -2.892 | .005 |
| | TG | -8.977E-005 | .000 | -.243 | -2.361 | .021 |
| | HDL | .000 | .000 | .095 | .964 | .338 |
| 6 | (Constant) | .421 | .030 | | 14.142 | .000 |
| | BMI | -5.263E-005 | .001 | -.008 | -.051 | .960 |
| | **AC** | -.001 | .000 | -.230 | -1.440 | .154 |
| | **DM_NO** | -.021 | .008 | -.264 | -2.664 | .009 |
| | TG | -7.924E-005 | .000 | -.215 | -2.014 | .047 |
| | HDL | .000 | .000 | .068 | .668 | .506 |
| | **MS_NO** | -.007 | .007 | -.116 | -1.033 | .305 |

BMI- body mass index, AC – abdominal circumference, DM_NO- presence/absence of diabetes, MS_ No- presence/absence of metabolic syndrome, TG – triglycerides, HDL- HDL-cholesterol

**Table 4.** – Multivariate regression analysis for McAuley index – model summary and coefficients

| Model Summary | | | | | |
|---|---|---|---|---|---|
| Model | R | R Square | Adjusted R Square | Std. Error of the Estimate | a. Predictors: (Constant), BMI |
| 1 | .461[a] | .212 | .203 | .40513 | b. Predictors: (Constant), BMI, **AC** |
| 2 | .501[b] | .251 | .233 | .39743 | c. Predictors: (Constant), BMI, **AC**, **DM_NO** |
| 3 | .572[c] | .327 | .302 | .37915 | d. Predictors: (Constant), BMI, **AC, DM_NO**, HDL |
| 4 | .616[d] | .379 | .347 | .36649 | e. Predictors: (Constant), BMI, **AC**, **DM_NO**, HDL, **MS_NO** |
| 5 | .651[e] | .424 | .387 | .35515 | f Dependent Variable: McAULEY score |

| Coefficients[a] | | | | | | |
|---|---|---|---|---|---|---|
| Model | | Unstandardized Coefficients | | Standardized Coefficients | t | Sig. |
| | | B | Std. Error | Beta | | |
| 1 | (Constant) | 3.486 | .306 | | 11.381 | .000 |
| | BMI | -.049 | .011 | -.461 | -4.699 | .000 |
| 2 | (Constant) | 3.831 | .344 | | 11.127 | .000 |
| | BMI | -.021 | .017 | -.194 | -1.199 | .234 |
| | **AC** | -.012 | .006 | -.332 | -2.052 | .043 |
| 3 | (Constant) | 3.653 | .334 | | 10.946 | .000 |
| | BMI | -.025 | .017 | -.230 | -1.488 | .141 |
| | **AC** | -.009 | .006 | -.234 | -1.483 | .142 |
| | **DM_NO** | -.355 | .118 | -.284 | -3.000 | .004 |
| 4 | (Constant) | 2.876 | .442 | | 6.507 | .000 |
| | BMI | -.024 | .016 | -.225 | -1.501 | .137 |
| | **AC** | -.007 | .006 | -.186 | -1.210 | .230 |
| | **DM_NO** | -.352 | .114 | -.282 | -3.080 | .003 |
| | HDL | .013 | .005 | .234 | 2.573 | .012 |
| 5 | (Constant) | 2.962 | .430 | | 6.893 | .000 |
| | BMI | -.024 | .016 | -.220 | -1.518 | .133 |
| | **AC** | -.004 | .006 | -.116 | -.763 | .448 |
| | **DM_NO** | -.281 | .114 | -.225 | -2.456 | .016 |
| | HDL | .008 | .005 | .155 | 1.650 | .103 |
| | **MS_NO** | -.243 | .098 | -.256 | -2.475 | .015 |

AC – abdominal circumference, DM_NO- presence/absence of diabetes, MS_ NO - presence/absence of metabolic syndrome, TG – triglycerides, HDL- HDL-cholesterol

QUICKI was significantly negatively correlated with BMI (correlation coeff = -0.323, p=0.003), abdominal circumference (correlation coeff =-0.416, p<0.001), the presence of diabetes (correlation coeff = -0.429, p<0.001), glycemia (correlation coeff =-0.530, p<0.001), the TG value (correlation coeff =-0.433,

p=0.001), the presence of MS (correlation coeff =-0.417, p<0.001), and was directly correlated with HDL-cholesterol (correlation coeff =0.262, p=0.016) For QUICKI, the independent predictors factors were found to be – diabetes (coefficient of determination = -2.664, p=0.009) and triglycerides (coefficient of determination =-2.014, p=0.047) (Table 3).

McAuley index was inversely correlated with BMI (correlation coeff = -0.461, p<0.001), abdominal circumference (correlation coeff =-0.488, p<0.001), glycemia (correlation coeff =-0.392, p<0.001), the presence of DM (correlation coeff =-0.375, p<0.001), the serum TG value (correlation coeff =-0.775, p<0.001), the presence of MS (correlation coeff =-0.507 p<0.001), and was directly correlated with HDL (correlation coeff =0.337, p=0.002). For McAuley index, the independent predictors factors were found to be – diabetes (coefficient of determination = -2.225, p=0.016) and metabolic syndrome (coefficient of determination = -2.475, p=0.015) (Table 4).

The determined areas under the ROC curve were as follows: 0.769 for HOMA, 0.769 for QUICKI index, 0.818 for McAuley Score. Diagnostic cut-off levels with optimum sensitivity and specificity were found to be 1.07 for *HOMA* (sensitivity 87.27%, specificity 62.07%), 2.14 for *McAuley* Score (sensitivity 81.82%, specificity 75.86%), 0.37 for *QUICKI* index (sensitivity 87.27%, specificity 62.07%) (Table 5).

**Table 5.** Areas under the ROC for HOMA, QUICKI, McAULEY indexes

| **AUROC (95%CI)** | | **HOMA** | **QUICKI** | **McAuley** | **P*** | **P**** | **P***** |
|---|---|---|---|---|---|---|---|
| | Global | 0.769 (0.664-0.854) | 0.769 (0.664-.854) | 0.818 (0.718-0.893) | NS | NS | NS |
| | Women | 0.736 (0.610- 0.839) | 0.736 (0.609 -0.839) | 0.837 (0.723 - 0.918) | NS | 0.034 | 0.04 |
| | Men | 0.947 (0.754 -0.992) | 0.947 (0.754 -0.992) | 0.737 (0.502 -0.901) | NS | NS | NS |

P* - between HOMA and QUICKI; P** - between HOMA and McAuley;P*** - between QUICKI and McAuley

Subsequently, we calculated the cut-off values for the 3 IR indexes: HOMA, QUICKI and McAuley, globally (Figure 1), in women (Figure 2). Overall, the highest specificity was found for McAuley index (75.86%). By analyzing separately in women the cut-off values of the IR indexes, their

sensitivity and specificity, respectively, it was found that in women, McAuley index had the highest sensitivity (97.2%). It was not possible to performe a detailed analyses for men, because the number of males without MS was very small.

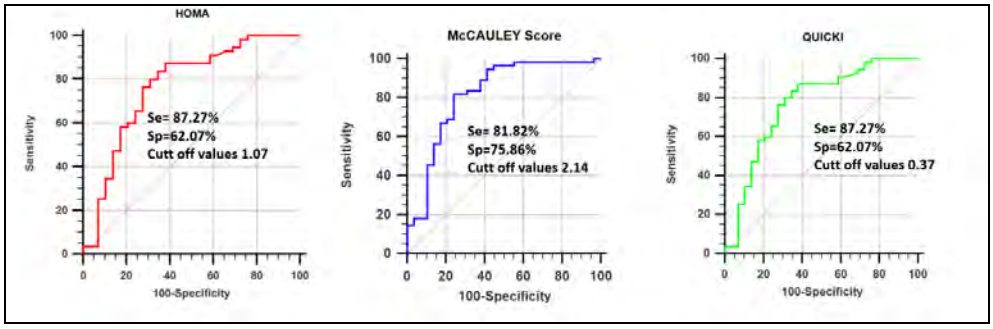


**Figure 1.** – AUROCs, Se, Sp and cut-off values - globally

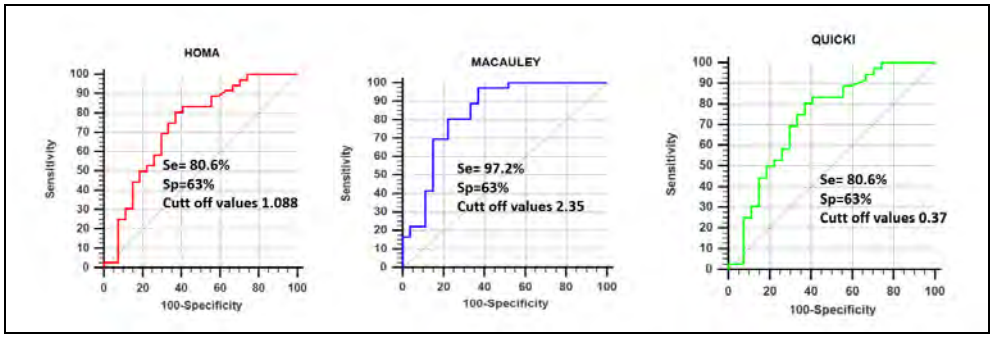


**Figure 2.** – AUROCs, Se, Sp and cut-off values in women

Although other authors [15] consider that the insulin resistance diagnosis is established at a HOMA index value >2.7 [16], in our study, the cut-off value for the diagnosis of MS was 1.07.

Cut-off values differ depending on the definition of MS; thus, Gayoso-Diz et al. [14] showed that using the IDF definition, like in our study, the ROC value was 0.69, and using the ATPIII definition, the ROC value was 0.72.

These results are similar to the study conducted by Esteghamati, who found an AUC of 0.65 (0.63, 0.67) for IDF and 0.68 (0.66, 0.70) for ATPIII [17]. In the current study, the ROC value was 1.07 for the HOMA index.

HOMA-IR is a reliable surrogate method to estimate IR in an epidemiological or clinical setting. However, its threshold levels vary widely; the cut-off values of HOMA-IR are usually defined by population-based percentile criteria. Moreover, these cut-off values are different depending on ethnicity, clinical methods of estimation, and metabolic conditions of the studied populations [18,19].

In the Spanish population, the threshold value of HOMA-IR decreases from 3.46 using 90th percentile criteria [20] to 2.05 taking into account the MetS components. Our HOMA-IR cut-off levels are relatively low compared to those reported in a study on healthy Italian patients [21], with a value of 2.77, and in a Spanish non-diabetic population [22], with a value of 3.8.

Gayoso-Diz et al. [14] concluded that the effect of age and gender on the ability of HOMA-IR to identify subjects with a cardiometabolic risk phenotype should be taken into account when estimating its values in different populations.

Shalaurova [23] showed in a study that the IR score was strongly correlated with triglycerides ($r = 0.74$) and fasting insulin levels ($r = 0.51$), and was inversely correlated with HDL-C ($r = -0.67$), like in the current study, where the best correlation with TG was found for McAuley index.

Tosi et al. [24] reported that the insulin resistance indexes HOMA and QUICKI had a sensitivity of 50.9 and 57.7, respectively, in identifying insulin resistance, significantly lower compared to the current study, while their specificity was 88.3, and 86.2, respectively, AUC for HOMA and QUICKI being 0.798. In our study, the specificity of these indexes in identifying patients with MS was lower, and AUC was higher. The authors of this study concluded that these IR indexes were very well correlated with the hyperinsulinemic-euglycemic clamp, which is the gold standard in IR diagnosis. McAuley index has the highest sensitivity, in women. An important element in the current study is the fact that independent predictors for the insulin resistance indexes are different: for HOMA: diabetes, for QUICKI: diabetes and triglycerides and for McAuley: diabetes and metabolic syndrome.

## CONCLUSIONS

The measurement of IR remains a challenge. The current gold standard test is the hyperinsulinemic-euglycemic clamp technique, in which a constant rate of insulin infusion is balanced with concomitant variable glucose infusion to maintain euglycemia; it is an invasive time- and labor-intensive approach - not suitable for epidemiological and diagnostic studies. Although HOMA is more commonly used in practice (probably due to its easy use), McAuley Score seems to have a better specificity in identifying patients with MetS. In women, McAuley index has the highest sensitivity.

## EXPERIMENTAL SECTION

The study was carried out at the 4th Department of Internal Medicine, Cluj-Napoca; The rights of the patients regarding the confidentiality of personal information were respected in agreement to Helsinki declaration of Ethical Principles for Medical Research Involving Human Subjects.

84 consecutive participants completed a questionnaire regarding their personal and family medical history. All were subjected to a complete physical exam.

For each patient, weight, height and abdominal circumference (midway between the inferior margin of the last rib and the iliac crest in horizontal plane while in upright position) were measured. The body mass index (BMI) was calculated (weight (kg)/[height (m)]2); subjects with a BMI ≥ 30 kg/m2 were considered obese.

Blood samples were collected after an overnight fast of >8 h. Plasma glucose levels were measured using a hexokinase enzymatic reference method. Fasting insulin levels were measured using a radioimmunoassay method or ELISA. Fasting lipids were analyzed, and for the present study, serum levels of cholesterol ≥5.172 mmol/L and triglycerides ≥1.7 mmol/L were considered abnormal.

The diagnosis of MetS was made based on International Diabetes Federation criteria, including the presence of abdominal obesity (waist circumference ≥94 cm for men and ≥80 cm for women) plus at least two of the following criteria: 1) fasting glucose ≥100 mg/dL; 2) systolic blood pressure ≥130 mmHg or diastolic blood pressure ≥85 mmHg or treatment of previously diagnosed hypertension; 3) HDL-cholesterol <40 mg/dL for men and <50 mg/dL for women or treatment with high-dose omega-3 therapy; 4) triglycerides ≥150 mg/dL or drug treatment with fenofibrate.

Insulin resistance was assessed by:

- HOMA-IR = insulin (µU/mL) * glycemia (mg/dl) / 405;
- QUICKI =1 / [log (insulin (µU/mL)) + log (glycemia)];
- McAuley = exp [3.29-0.25 * log (insulin) - 0.22 * log (BMI) – 0.28 * log (triglyceride)];

The blood insulin level can be expresed in international units, such as µIU/mL or in molar concentration, a typical blood level between meals is 8–11 µIU/mL (57–79 pmol/L). Statistical analysis – *the* data were analyzed using SPSS 16.0 for Windows and MedCalc 10.3.0.0 software programs. Descriptive statistics was performed. Data's normality was assessed using Kolmogorov-Smirnov test. Numerical data were compared using Student or Mann-Whitney test; for categorical variable $\chi 2$ test was used. Univariate and

multivariate analysis was performed. Cut-off values, optimum sensitivity, specificity and area under the receiver operating characteristic (ROC) curve were evaluated. $p < 0.05$ was considered significantly statistic.

## ACKNOWLEDGMENTS

Authors greatly acknowledge the financial support offered by GRANT ID 2246.

## REFERENCES

1. Bertoni A.G., Wong N.D., Shea S., Ma S., Liu K, Preethi S., Jacobs D.R., Wu C., Saad M.F., Szkio M., *Diabetes Care*, **2007**, *30,* 2951–2956.
2. Montecucco F., Steffens S., Mach F., *Mediators of Inflammation,* **2008**, 767623.
3. Tenenbaum A., Adler Y., Boyko V., *American Heart Journal*, **2007**; *153*, 559.
4. Verhagen S.N., Wassink A.M., van der Graaf Y., Gorter P.M., Visseren F.L., *Cardiovascular Diabetology*, **2011**; *10*, 100.
5. Zuliani G., Morieri M.L., Volpato S, *Atherosclerosis*, **2014**; *235*, 538.
6. Nasr G., Sliem H., *The International Journal of Cardiovascular Imaging* **2011**; *27*, 335.
7. Gazzaruso C., Solerte S.B., De Amici E., *The American Journal of Cardiology*, **2006**; 97: 236–239.
8. Tataru D.A., Olinic D.M., Urda A., Olinic M., Orasan R., *Studia UBB Chemia*, **2018**, *62*, 127.
9. Alberti, K.G., P. Zimmet and J. Shaw, Diabetic Medicine, 2006, 23(5) 469.
10. Matthews, D.R., J.P. Hosker, A.S. Rudenski, B.A. Naylor, D.F. Treacher and R.C. Turner, *Diabetologia,* **1985***, 28(7)* 412.
11. Katz, A., S.S. Nambi, K. Mather, A.D. Baron, D.A. Follmann, G. Sullivan and M. J. Quon, *The Journal of Clinical Endocrinology and Metabolism*, **2000,** *85(7)* 2402.
12. McAuley K.A., Williams S.M., Mann J.I., Walker R.J., Lewis-Barned N.J., Temple L.A., Duncan A.W., *Diabetes Care,* **2001**, *24(3),* 460.
13. Abbasi, F., D. Shiffman, C.H. Tong, J.J. Devlin and M.J. McPhaul, *Journal of the Endocrine Society*, **2018**, *2(9)*,1050.
14. Gayoso-Diz, P., A. Otero-Gonzalez, M.X. Rodriguez-Alvarez, F. Gude, F. Garcia, A. De Francisco and A.G. Quintel, *BMC Endocrine Disorders,* **2013**, 13, 47.
15. Carvalho C., *Nutrition,* **2018**, https,//doi.org/10.1016/j.nut.2018.07.014.
16. Geloneze B., Vasques A.C., Stabe C.F., Pareja J.C., Rosado L.E., Queiroz E.C., *Arquivos Brasileiros de Endocrinologia & Metabologia*, **2009**, *53*, 281-7.

17. Esteghamati A., Ashraf H., Khalilzadeh O., Zandieh A., Nakhjavani M., Rashidi A., Haghazali M., Asgari F., *Nutrition & Metabolism*, **2010**, *7,* 26.
18. Antuna-Puente B., Disse E., Rabasa-Lhoret R., Laville M., Capeau J., Bastard, *Diabetes & Metabolism*, **2011**, *37*, 179.
19. Saplontai-Pop A., Moldovan M., Oprean R. Orasan. O., Saplontai S., Ionescu C., *Studia UBB Chemia*, **2014**, *59(4)*, 39.
20. Gayoso-Diz P., Otero-González A., Rodriguez-Alvarez M.X., Gude F., Cadarso-Suarez C., García F., De Francisco A, *Diabetes Research and Clinical Practice,* **2011**, *94*, 146.
21. Miccoli R., Biamchi C., Odoguardi, *Nutrition, Metabolism and Cardiovascular Diseases, NMCD*, **2005**, *15*, 250.
22. Ascaso J.F., Romero P., Real J.T., Priego A., Valdecabres C., Carmena R. *Medicina Clinica (Barc),* **2001**, *117*, 530.
23. Shalaurova I., Connelly M.A., Garvey T.W., and Otvos D.J., *Metabolic syndrome and related disorders,* **2014**, *(12) 8*, 422.
24. Tosi F., Bonora E., Paolo Moghetti P, *Human Reproduction,* **2017**, *32(12)*, 2515.

STUDIA UBB CHEMIA, LXIV, 1, 2019 (p. 161-172)
(RECOMMENDED CITATION)
DOI:10.24193/subbchem.2019.1.13

# RADIOPACITY ANALYSIS OF SOME CHAIRSIDE COMPUTER-AIDED DESIGN-COMPUTER-AIDED MANUFACTURING MILLING MATERIALS

**ADRIAN MIHAI VARVARA[a], CRISTINA GASPARIK[a], BOGDAN CULIC[a]*, COSMINA IOANA BONDOR[b], ELENA BIANCA VARVARA[a], GABRIEL FURTOS[c], MARIOARA MOLDOVAN[c], DIANA DUDEA[a]**

**ABSTRACT.** In this study, the radiopacity of chairside Computer-Aided Design-Computer-Aided Manufacturing (CAD-CAM) milling materials was evaluated in comparison with dental structures. 105 specimens of 7 different thicknesses from 5 different types of chairside CAD-CAM milling materials: feldspar ceramic, hybrid ceramic, lithium disilicate glass-ceramic, zirconia-reinforced lithium silicate ceramic and a resin nano-ceramic were used for this in vitro study. Digital radiographs were obtained using an aluminum step wedge, a specimen of a tooth slice and 3 specimens from each material. Radiodensity was determined for each material using dedicated software. Lava Ultimate and Vita Suprinity were found as having higher radiopacity, whilst Vita Mark II and Vita Enamic were lower in radiopacity in comparison with dental structures. The radiodensity of Emax CAD was between enamel and dentine. Radiopacity of each CAD-CAM milling material was different and both material's type and thickness significantly affected the radiopacity.

***Key words:*** *CAD-CAM, chairside, milling materials, radiopacity*

[a] *"Iuliu Haţieganu" University of Medicine and Pharmacy, Department of Prosthetic Dentistry and Dental Materials, Faculty of Dental Medicine, Cluj Napoca, Romania*

[b] *"Iuliu Haţieganu" University of Medicine and Pharmacy Department of Informatics and Biostatistics, Faculty of Medicine, Cluj Napoca, Romania*

[c] *"Babes-Bolyai" University, "Raluca Ripan" Institute of Research in Chemistry, Cluj Napoca, Romania*

**Corresponding author: E-mail: bculic@umfcluj.ro*

## INTRODUCTION

In the last three decades, exciting new developments in dental materials and computer science have led to the success of contemporary dental computer-aided design / computer-aided manufacturing (CAD-CAM) technology. The user friendly and easy manufacturing of very precise esthetic restorations, in a short period of time, made CAD-CAM technology an optimal option for prosthetic treatment in a large range of indications. Nowadays, several highly sophisticated chairside and laboratory CAD-CAM systems have been introduced and are continuously improving [1, 2, 3].

Milling materials designed for CAD-CAM techniques are also in evolution. If initially only glass ceramic was used, over time, new materials, based on different constituents were developed: zirconia in 2002, reinforced ceramics in 2005, composite resins in 2007 and hybrid ceramics in 2012. Each new material aims improved properties such as good mechanical, surface and optical characteristics, optimal quality of adhesion to adjacent structures and ease of usage [4].

One of the most important clinical characteristics of dental materials is radiopacity, which allows to identify the restoration under radiologic examination, to assess its relation with the adjacent dental structures and to diagnose the possible pathology of the respective tooth.

In most clinical cases, for a complete diagnosis, a complementary x-ray examination is necessary. It was suggested that less than 15% of inadequate restorations are detected clinically, while the rest are diagnosed only radiographically [5]; moreover, in 80-90% of the cases, secondary caries are located at the proximal gingival margin, where radiography is often the only way for their detection [6]. Therefore, all restorative materials should have intrinsic characteristics, to allow their detection and delimitation against enamel, dentin or cement. Therefore, radiopacity of restorative dental materials is of paramount importance because it helps the clinician to detect secondary caries, restorations' integrity and contours, missing interproximal contacts, marginal defects, voids, interfacial gaps, cement overhangs or misplaced fragments in case of trauma [7, 8, 9, 10, 11, 12]. However, excessive radiopacity would mask the dental structures and consequently may reduce the ability to diagnose recurrent caries [13, 14].

As in conventionally processed materials, radiopacity of restorative dental materials used in CAD-CAM technology is influenced by the structure and type of filler particles (heavy metals such as aluminum, barium, strontium, or zirconium [8]. Excessive incorporation of radiopaque fillers in the restorative dental materials results in reduced translucency, but affects also mechanical properties, increases thermal expansion and causes hydrolysis of silane bonding agents [8, 15, 16].

According to the International Organization for Standardization (ISO), the radiopacity of dental materials is expressed as an optical density value or in terms of equivalent aluminium (Al) thickness (in millimeters) by using a reference calibration curve under controlled radiographic conditions [17, 18]. Accordingly, restorative dental materials should have their radiopacity equal to or greater than that of Al [19], considering that there are studies which showed that the radiopacity of dentin was approximately equivalent to that of Al samples of the same thickness, whilst enamel had approximately twice the value of Al at the same thickness [20, 21].

It was stated that the radiopacity of dental materials has to be equal or higher than the radiopacity of dentin [14, 22] or enamel [23]. Radiopacity of conventional and resin modified glass-ionomers [21, 24], conventional and flowable resin composites [21], dental ceramics [20, 25] has been studied; however, most literature address materials processed by conventional techniques [25]. There is little research focused on the radiopacity of CAD-CAM processed materials: Dicor MGC and Vita Blocks [26] or zirconia ceramics [25, 27, 28]. To the best of our knowledge there is no study of the radiopacity of newer materials such as hybrid ceramics or zirconia-reinforced lithium silicate ceramic. The purpose of this study was to evaluate the radiopacity of five frequently used chairside CAD-CAM milling materials at different thicknesses and to compare it with the radiopacity of hard dental structures.

The first null hypothesis was that radioopacity was not influenced by the type of material and the second null hypothesis was that the thickness of the slices can’t influence the radiodensity.

## RESULTS AND DISCUSSIONS

An in vitro study was conducted using 105 specimens of five different chairside CAD-CAM milling materials: feldspar ceramic (Vita Mark II -Vita), hybrid ceramic (Vita Enamic - Vita), lithium disilicate glass-ceramic (e.max CAD - Ivoclar), zirconia-reinforced lithium silicate ceramic (Vita Suprinity - Vita) and a resin nano ceramic (Lava Ultimate - 3M ESPE) (Table 1). For each material, specimens were cut and prepared at 7 different thicknesses. The three samples with the same thickness of each material, the tooth slice with the corresponding thickness and the aluminum step wedges were placed on an intraoral sensor and radiographed using a dental X-ray machine.

**Table 1.** CAD-CAM milling materials' characteristics

| | Brand | Manufacturer | Structure | Composition |
|---|---|---|---|---|
| 1 | Vita Mark II | Vita Zahnfabrik, Bad Säckingen, Germany | feldspar ceramic | $SiO_2$: 56-64%<br>$Al_2O_3$: 20-23%<br>$Na_2O$: 6-9%<br>$K_2O$: 6-8%<br>CaO: 0,3-0,6%<br>$TiO_2$: 0,0-0,1% |
| 2 | Vita Enamic | Vita Zahnfabrik, Bad Säckingen, Germany | hybrid ceramic | Ceramic part (86 wt% / 75 vol%):<br>$SiO_2$: 58-63%<br>$Al_2O_3$: 20-23%<br>$Na_2O$: 9-11%<br>$K_2O$: 4-6%<br>$B_2O_3$: 0,5-2%<br>$ZrO_2$ <1%<br>CaO >1%<br>Polymer part (14 wt% / 25 vol%):UDMA (urethane dimethacrylate), TEGDMA (triethylene glycol dimethacrylate) |
| 3 | E.max CAD | Ivoclar Vivadent Schaan, Liechtenstein | lithium disilicate glass-ceramic | $SiO_2$: 57-80%<br>$Li_2O$: 11-19%<br>$K_2O$: 0-13%<br>$P_2O_5$: 0-11%<br>$ZrO_2$: 0-8%<br>ZnO: 0-8%<br>$Al_2O_3$: 0-5%<br>MgO: 0-5%<br>Colouring oxides: 0-8% |
| 4 | Vita Suprinity | Vita Zahnfabrik, Bad Säckingen, Germany | zirconia-reinforced lithium silicate ceramic | $ZrO_2$: 8 – 12%<br>$SiO_2$: 56 – 64%<br>$Li_2O$:15 – 21%<br>$La_2O_3$: 0.1%<br>Pigments <10%<br>Various > 10% |
| 5 | Lava Ultimate | 3M ESPE, Seefeld, Germany | resin nano ceramic | Nanoceramic part (80 wt%):<br>Silica particles<br>Zirconia particles<br>Resin matrix (20 wt%): |

Both, material's type and thickness significantly affected the radiopacity (Figure 1 and Figure 2). The thickness of the material was significantly positively correlated with radioopacity ($r$ ranged between 0.93 and 1, $p$<0.001) for all restorative materials, but also for enamel and dentin. The radiopacity of all samples (chairside CAD-CAM milling materials and tooth structures) increased with the thickness (Figure 1).

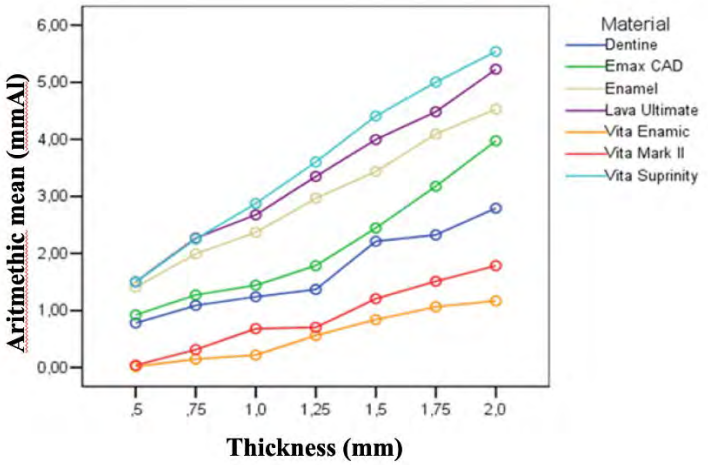


**Figure 1.** Radiopacity mean value of studied materials as well as of natural teeth structures versus sample thickness

The ascending sequence of the radiopacity for the evaluated materials' samples was Vita Enamic, Vita Mark II, dentine, Emax CAD, enamel, Lava Ultimate and Vita Suprinity. The mean radiopacity of chairside CAD-CAM milling materials ranged between 0.57±0.44 mm Al (Vita Enamic) and 3.60±1.41 mmAl (Vita Suprinity). The mean values for the radiopacity of dental structures were 2.97±1.07 mmAl for the enamel and 1.69±0.71 mmAl for the dentine (Figure 2).

Vita Enamic had statistically significant lower radiopacity values than dentine, enamel and all the others CAD-CAM materials ($p$≤0.007) except Vita Mark II ($p$=0,945). Lava Ultimate and Vita Suprinity had statistically significant higher radiopacity values than dentine and all the other CAD-CAM materials ($p$≤0.002, $p$≤0.001) but not significantly different than the enamel ($p$=0.870, $p$=0.398). The mean radiopacity values for EmaxCAD was statistically significant different from Vita Mark II, Vita Suprinity, Lava Ultimate and Vita Enamic ($p$≤0.002), but not from hard dental tissues ($p$=0.110 for enamel and $p$=0.750 for dentine). The mean radiopacity values for Vita Mark II were statistically significant different from

emax CAD, enamel, Lava Ultimate and Vita Suprinity ($p \leq 0.001$), but nor for dentine ($p=0.138$) and Vita Enamic ($p=0.945$). The mean radiopacity values for enamel were statistically significant different from Vita Enamic, Vita Mark II and dentine ($p \leq 0.001$) (Figure 2).

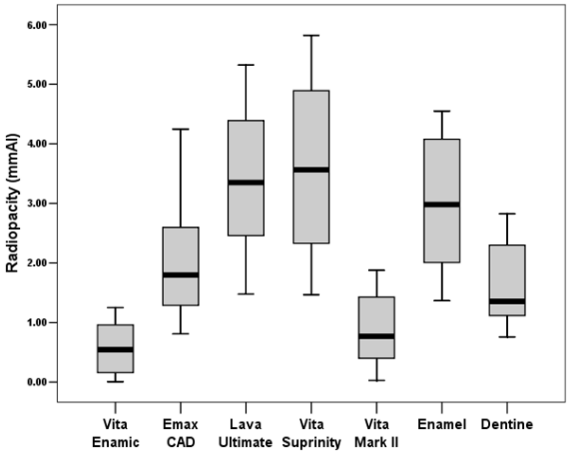


**Figure 2**. Radiopacity values (p<0.001) (Median, 25th-75th Percentile, Minimum - Maximum)

The analysis of thickness influence on radiopacity for the chairside CAD-CAM milling materials is revealed in Table 2. The radiopacity of CAD - CAM milling materials ranged from 0.02±0.01mmAl (Vita Enamic at 0.5mm) to 5.54±0.26mmAl – (Vita Suprinity at 2 mm).

Multivariate analysis revealed that at all evaluated materials, including dentin and enamel, size and material type had a combined effect on the radiopacity (p<0,001). We found that if the thickness increases, the difference between radiopacity of the materials increases (Figure 3).

However, for Vita Enamic and Vita Mark II (effect size 0.32), Vita Mark II and Dentine (effect size 0.8), Dentine and Emax CAD (effect size 0.46), Emax CAD and Enamel (effect size 0.82), and for Enamel, Lava Ultimate and Vita Suprinity (effect size 0.39 respectively 0.24) no significant difference was found between radiopacities ($p>0.05$). The post hoc power analyses conducted showed that the achieved power for the difference between the radioopacities in our tested materials where p was not significant was between 0.07 for an effect size of 0.24 and 0.60 for an effect size of 0.82, where p was significant was between 0.85 for an effect size of 1.12 and 0.95 for an effect size of 1.28.

**Table 2**. Radioopacity of tested materials, for the considered thicknesses (Means ± standard deviations).

| | **Radiopacity (mmAl)** | | | | | | |
|---|---|---|---|---|---|---|---|
| **Thickness** | **0.5mm** | **0.75mm** | **1mm** | **1.25mm** | **1.5mm** | **1.75mm** | **2mm** |
| Vita Enamic | 0.02±0.01[1] | 0.15±0.07[1] | 0.22±0.10[1] | 0.56±0.06[2] | 0.84±0.11[3] | 1.06±0.11[3,4] | 1.17±0.07[4] |
| Emax CAD | 0.92±0.11[1] | 1.27±0.02[1] | 1.44±0.01[1] | 1.79±0.02[1,2] | 2.45±0.21[2,3] | 3.18±0.75[3,4] | 3.97±0.47[4] |
| Lava Ultimate | 1.50±0.02[1] | 2.27±0.17[2] | 2.68±0.20[3] | 3.35±0.06[4] | 4.00±0.10[5] | 4.49±0.10[6] | 5.23±0.08[7] |
| Vita Suprinity | 1.50±0.03[1] | 2.25±0.08[2] | 2.88±0.14[3] | 3.60±0.10[4] | 4.41±0.07[5] | 5.00±0.15[6] | 5.54±0.26[7] |
| Vita Mark II | 0.04±0.01[1] | 0.31±0.07[1] | 0.68±0.08[2] | 0.70±0.18[2] | 1.21±0.15[3] | 1.51±0.14[3,4] | 1.79±0.11[4] |
| Enamel | 1.41±0.04[1] | 1.99±0.02[2] | 2.37±0.01[3] | 2.97±0.03[4] | 3.44±0.02[5] | 4.09±0.02[6] | 4.53±0.02[7] |
| Dentine | 0.78±0.03[1] | 1.09±0.04[2] | 1.24±0.04[3] | 1.37±0.03[4] | 2.21±0.02[5] | 2.32±0.02[6] | 2.79±0.03[7] |
| Analysis was performed for each material (row in the table) separately. Different superscript (in the same row) indicates statistically significant difference ($p<0.05$) between radiopacities from the same material (same row). | | | | | | | |

Sample size calculations using the minimum above mentioned effect sizes, $\alpha$=0.05, and power of 0.90 showed that the minimum number of observations per group needed to find an effect is 315.

This study evaluated the radiopacity of some of the newest most used chairside CAD-CAM milling materials, using digital radiography and pixel gray-scale measurement (ex: Emax CAD used from 2006, Lava Ultimate from 2012, Vita Enamic and Vita Suprinity from 2013).

Both null hypotheses were rejected, since we found that the radiopacity depends on the material's type and thickness.

The influence of the material type upon the radiodensity may be related to the composition.

Materials with low atomic numbers elements in their composition (such as silicone and alumina) appear radiolucent, whereas materials having elements with high atomic numbers (such as zinc, strontium, zirconia, barium glass or sulfate, lanthanum, and ytterbium) appear radiopaque [8, 12, 13, 29, 30].

Our study is in accordance with the existing research. Vita Mark II and Vita Enamic have an important percentage of silicon oxide (56-64% respectively 58-63%) and aluminum oxide (20-23%) in their composition, resulting a lower radiopacity of these materials, while Vita Suprinity and Lava Ultimate were the materials that showed the highest radiopacity of all

evaluated materials. The high radiopacity level could be attributed to zirconia added in their composition (ex: Vita Suprinity has 8-12% zirconia in the composition) or lanthanum oxide (0,1% in Vita Suprinity). Even if the tested materials had approximately the same level of silicon oxide (between 56% and 80%), the level of zirconia oxide was different: lower than 1% for Vita Mark II and Vita Enamic, between 0% and 8% for Emax CAD and higher than 8% for Vita Suprinity and Lava Ultimate (Table 1). As a practical consequence, it could be assumed that the radiopaque restoration is evident, the limit between the restorations and the adjacent dental structures (enamel or dentine) is visible and the lack of continuity between the two surfaces is detectable.

However, due to the Mach effect, excessively radiopaque restorations may hinder a clinician's ability to spot marginal defects [31]. The latter phenomenon is a visual illusion which enhances the contrast between two areas of different radiopacities, making the dark border area darker. This effect might be misinterpreted as pathology in certain situations [9].

Emax CAD was the only material that had radiopacity values within values of hard dental tissues, enamel and dentine. The values of radiopacity for Emax CAD were higher than those of dentine and lower than that of enamel, for all seven thicknesses. This may need a particular attention to distinguish the restoration in comparison with the adjacent structures.

However, diagnostic challenges arise in clinical situations when radiographic images present barely discernible radiopacity differences between dental tissues and restorative materials [32, 33]. This is even more challenging when treating patients with multiple pathologies and a high caries risk. Vita Mark II and Vita Enamic had radiopacity values lower that the dentine, in our study. This might involve that the use of radiopaque luting cement is essential to permit detection of possible pathology around CAD-CAM restorations when using these classes of materials.

The samples from the previous studies have greater thicknesses (1mm or 2mm) [20, 25, 26]. In a time when minimally invasive dentistry gains more and more terrain, there is a need for the assessments of smaller thicknesses as well (0.5mm). In our study, the effect of the thickness upon the radiopacity varies differently, according to the material considered. In the case of Vita Suprinity and Lava Ultimate, statistically significant differences between the radiopacity values appear among all thickness of the samples. The same outcome is noticed for the dental structures (enamel and dentine).

On the other hand, Vita Mark II, Emax CAD and Vita Enamic have no statistically significant differences between the radiopacity values at low thicknesses (1mm±0.25); instead differences between the radiopacity values were significant only from this dimension upwards. It is very often that the restorations have lower thicknesses.

Moreover, previous studies focused on 1, 2 or maximum 3 types of thicknesses [12, 20, 28]. Our results offer data regarding the radiopacity of an extended range of thicknesses and materials that cover a wide area of the treatment indications via CAD-CAM restorations.

When choosing the right chairside CAD-CAM milling material for prosthetic restorations, the radiopacity has to be taken into consideration, in correlation with the thickness of the future restoration, in order to prevent difficulties in detection of adjacent pathology.

With increasingly recommendations of minimally invasive restorations that involve chairside CAD-CAM, our results of radiopacity for different materials in seven different thicknesses, have considerable clinical significance. The importance of radiographic characteristics is indispensable in the clinical diagnosis of secondary lesions, restoration integrity control, marginal adaptation or misplaced fragments.

The clinical value of this study is enhanced by the objectivity of the radiographic examinations. All the data from one thickness of the same material were analyzed on the same radiography. The sample size of 3, chosen for this study, is the maximum number of samples that can be radiographed using one examination.

## CONCLUSIONS

In the limitations of this study, it can be concluded that both material's type and thickness significantly affected the radiopacity. The chemical composition of the materials has its role in these radiographic characteristics and the amount of elements with high atomic numbers seems to be an important factor in the radiopacity of the materials.

Additionally, the radiodensity of CAD-CAM milling materials was different from that of the human dentin and enamel and the radiopacity of the tested materials increased as follows: Vita Enamic, Vita Mark II, dentine, Emax CAD, enamel, Lava Ultimate and Vita Suprinity.

Further studies should be conducted for other relevant thicknesses and new materials.

## EXPERIMENTAL SECTION

### Specimen Preparation

For each material, specimens were cut and prepared at 7 different thicknesses (0.5mm, 0.75mm, 1mm, 1.25mm, 1.5mm, 1.75mm, and 2mm) (3 specimens for each thickness) with a precision saw (IsoMet 1000 -

Buehler) using a diamond cutting blade for hard brittle materials and structured ceramics (IsoMet Diamond Wafering Blade, 5in, 15LC - Buehler) at a speed of 100 rotations per minute.

To reach the desired thickness (±0.01mm) the samples were measured with an electronic micrometer and polished using sandpaper (Klingspor) with increasing grits (P240, followed by P400, P800, P1000 and P1200).

In addition, four freshly extracted intact premolars were cut in slices, preparing sections of teeth in the same seven thicknesses (0.5mm, 0.75mm, 1mm, 1.25mm, 1.5mm, 1.75mm, and 2mm. A 1–10 mm thick aluminum step wedge with the purity of 99.52% Al with 0.22% Fe and 0.001% Cu was used as reference for the evaluation of the radiodensity of the materials under controlled radiographic conditions.

**Radiograph images**

The three samples with the same thickness of each material, the tooth slice with the corresponding thickness and the aluminum step wedges were placed on an intraoral sensor and radiographed using a dental X-ray machine (Intraoral X-Ray Soredex, Minray) at 70kV, 7mA, 0.04s with the target sensor at the distance of 30 cm. (Fig. 3)

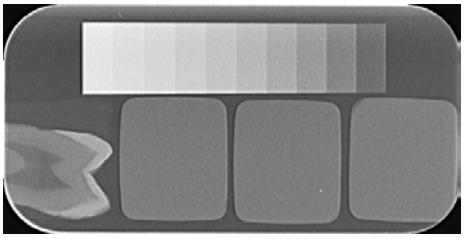

**Figure 3.** Radiography with 3 specimens of chairside CAD-CAM milling material (Lava Ultimate at 1mm thickness), 1 specimen of tooth structures and an aluminum step wedge

The mean gray value of each aluminum step wedge and selected materials were measured by outlining a region of interest using the equal-density area tool of the Image J software. For the 148 x 180 pixels' area in each image type, the mean gray-scale value and standard deviation were calculated. The gray value of each specimen was recorded from the mean of the three readings. In a same procedure the enamel and the dentin slices were also measured in three different regions. The radiopacity values of the samples were expressed in terms of the equivalent thickness of aluminum per 1 mm unit thickness of material.

### Statistical analysis

The processed data varied according to two parameters: slice thickness and type of material. Both univariate and multivariate analysis were performed.

In the univariate analysis the data were compared with the Anova test followed by Tukey HSD post-hoc analysis. Correlation analysis was determined by calculating the *r* Pearson correlation coefficients between radiopacity and slice thickness.

Multivariate analysis was performed by applying Anova two-way test. Each material was tested against enamel and dentine separately. The data were assessed for the influence of the slice thickness. The combined effect of the slice thickness and the difference between the material and the enamel or dentin was also reported.

The statistical significance was considered if $\alpha<0.05$. Statistical analysis was conducted in software package SPSS 25.0. Post hoc power analyses and sample size calculations were conducted using the software package GPower (Gpower v.3.1.9.2., Kiel, Germany), for each studied material.

## ACKNOWLEDGMENTS

This study was supported by the PhD Research Project (PCD 2016) Nr.7690/115 from 15.04.2016 University of Medicine and Pharmacy "Iuliu Haţieganu" Cluj Napoca, Romania.

## REFERENCES

1. P.R. Liu, *Compendium of Continuing Education in Dentistry,* **2005**, *26*, 507.
2. B. Culic, C. Gasparik, M. Varvara, C. Culic, C. Dragos, L. Silaghi-Dumitrescu, D. Dudea, *Studia UBB Chemia*, 2017, *62(1)*, 61.
3. T. Miyazaki, Y. Hotta, J. Kunii, S. Kuriyama, Y. Tamaki, *Dental Materials Journal*, **2009**, *28*, 44.
4. L.H.D. Silva, E. Lima, RBP. Miranda, S.S. Favero, U. Lohbauer, P.F. Cesar, *Brazilian Oral Research*, **2017**, *31*, 58.
5. J.H. Poorterman, I.H. Aartman, H. Kalsbeek, *Community Dentistry and Oral Epidemiology,* **1999**, *27*, 331.
6. I. Mjör, *Quintessence International,* **1998**, *29*, 313.
7. L.M.P. Salzedas, M.J.Q. Louzada, AB. Oliveira Filho, *Journal of Applied Oral Science*, **2006**, *14*, 147.

8. A.T. Hara, MC. Serra, F. Haiter-Neto, AL. Jr. Rodrigues, *American Journal of Dentistry,* **2001**, *14*, 383.
9. I. Espelid, A.B. Tveit, R.L. Erickson, S.C. Keck, E.A. Glasspoole*, Dental Materials,* **1991**, *7,* 114.
10. S. Nandini, *Journal of Conservative Dentistry,* **2010**, *13*, 184.
11. K.S. Oikarinen, T.M. Nieminen, H. Mäkäräinen, J. Pyhtinen, *International Journal of Oral and Maxillofacial Surgery,* **1993**, *22*, 119.
12. S. Saridag, D. Helvacioglu-Yigit, G. Alniacik, M. Özcan, *Dental Materials Journal,* **2015**, *34*,13.
13. J. Sabbagh, J. Vreven, G. Leloup, *Operative Dentistry,* **2004**, *29*, 677.
14. M.D. Turgut, N. Attar N., A. Onen, *Operative Dentistry,* **2003***, 28*, 508.
15. A. Amirouche-Korichi, M. Mouzali, DC Watts, *Dental Materials,* **2009**, *25*, 1411.
16. M. Taira, H, Toyooka, H. Miyawaki, M. Yamaki, *Dental Materials,* **1993**, *9*, 167.
17. International Standards Organization, "Test method for determining radio-opacity of materials", ISO 13116:2014,1st ed, **2014**.
18. International Standards Organization, "Polymer-based restorative materials", ISO 4049:2009, 4th ed, **2009**.
19. D.C. Watts, J.F. McCabe*. Journal of Dentistry,* **1999**, *27*, 73.
20. S. Hosney, M. Kandil, O. El-Mowafy, *International Journal of Prosthodontics*, **2016**, *29*, 271.
21. T. Hitij, A. Fidler, *Clinical Oral Investigations,* **2013**,*17*, 1167.
22. O.M. El-Mowafy, C. Benmergui, *Operative Dentistry,* **1994**, *19*, 11.
23. G. Pekkan, S. Saridag, N.C. Beriat, *Avicenna Journal of Dental Research,* **2011**, *35*, 2.
24. R.B. Fonseca, C.A. Branco, PV Soares, L. Correr-Sobrinho, F. Haiter-Neto, AJ. Fernandes-Neto, *et al*., *Clinical Oral Investigations,* **2006**, *10*, 114.
25. G. Pekkan, K. Pekkan, M.G. Hatipoglu, S.H. Tuna, *Journal of Prosthetic Dentistry,* **2011**, *106*, 109.
26. O.M. El-Mowafy, J.W. Brown, D. McComb, *Journal of Dentistry.,* **1991**, 19, 366.
27. F. Martinez-Rus, A.M. Garcia, A.H. de Aza, G. Pradies, *International Journal of Prosthodontics*. **2011**, *24*,144.
28. G. Pekkan, S. Saridag, K. Pekkan, D.Y. Helvacioglu, *Dental Materials Journal*., **2016**, *35*, 257.
29. Z. Ergücü, LS. Türkün, E. Önem, P. Güner, *Operative Dentistry*, **2010**, *35*, 436.
30. K.D. Jandt, AMO. Al-Jasser, K. Al-Ateeq, RW. Vowles, GC. Allen, *Dental Materials* **2002**,*18*, 429.
31. H.M. Berry Jr., *The Journal of the American Dental Association,* **1983**, *106*, 622.
32. H.B. Akerboom, C.M. Kreulen W.E van Amerongen, A. Mol, *Journal of Prosthetic Dentistry* **1993**, *70*, 351.
33. A.D. Cruz, R.G. Esteves, IAVP Poiate, P.P. Portero, S.M. Almeida, *Operative Dentistry* **2014**, *39*, 90.

STUDIA UBB CHEMIA, LXIV, 1, 2019 (p. 173-184)
(RECOMMENDED CITATION)
DOI:10.24193/subbchem.2019.1.14

# CHEMICAL STABILIZATION OF FATS RICH IN LONG CHAIN POLYUNSATURATED FATTY ACIDS BY ANTIOXIDANTS ADDITION

**FLAVIA POP[a,*], DANIEL NĂSUI[a], ZORICA VOȘGAN[a], CRISTINA MIHALI[a], CLAUDIA BUTEAN[a]**

**ABSTRACT.** The research was conducted in order to evaluate the effect of natural (*β*-carotene and ascorbic acid) antioxidants on the oxidative stability of alimentary chicken fat in order to improve its safety and extend the shelf life. Peroxide value was significantly influenced by the storage time ($p < 0.001$) in chicken fat and 0.01% additivated fat. In control was found the highest level of peroxide value followed by 0.01% and 0.05% additivated fat. Regardless of the type of fat, the highest peroxide index level was found at 180 days of storage. Saturated fatty acids content increased, but monounsaturated and polyunsaturated fatty acids content decreased during refrigerated storage. Storage time showed to be most correlated with monounsaturated fatty acids for control ($r = 0.93$), followed by 0.01% additivated fat ($r = 0.87$) and 0.05% additivated fat ($r = 0.76$). The development of rancidity in chicken fat was significantly ($p < 0.01$) reduced by the addition of *β*-carotene and ascorbic acid in concentration of 0.05%.

***Keywords:*** *chemical stabilization, β-caroten, ascorbic acid, peroxide index, fatty acid profile*

## INTRODUCTION

Storage of food products rich in polyunsaturated fatty acids even in refrigerated and frozen conditions affects in time the organoleptic, physicochemical and nutritional properties following oxidative or lipolytic

[a] *Technical University of Cluj-Napoca, North University Center of Baia Mare, Chemistry and Biology Department, 76A Victoriei Str., 430122, Baia Mare, Romania*
**Corresponding author e-mail: flavia_maries@yahoo.co*

rancidity and may result in reduction of their shelf life. Lipid oxidation products affect food quality due to changes in color, flavor, texture and nutritional value [1]. A high oxidative stability of lipids is very important for human health and for economic reasons. Antioxidants can be used to inhibit or retard the effects of oxidative rancidity. Synthetic antioxidants are the most used, but their safety has been questioned due to potential toxicological concerns. The natural antioxidants have gained increased interest because of the belief that natural food ingredients are better and safter than synthetic ones [2, 3].

*β*-Carotene is an organic, red-orange pigment abundant in plants and fruits. It is a member of the carotenes, which are terpenoids (isoprenoids), synthesized biochemically from eight isoprene units and having 40 carbons (Fig. 1). Among the carotenes, *β*-carotene is distinguished by having beta-rings at both ends of the molecule. When used as a food coloring, it has the E number E160a. In nature, *β*-carotene is a precursor to vitamin A via the action of beta-carotene 15,15'-monooxygenase [4, 5].

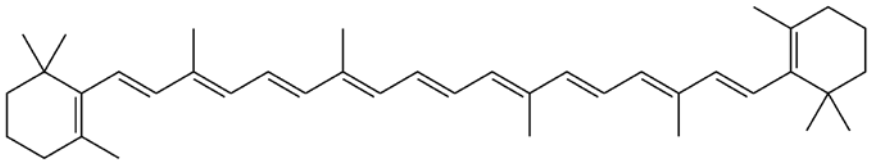

**Figure 1.** *The chemical structure of β-carotene[4]*

Ascorbic acid (AA), commonly known as vitamin C, plays an important role in the human body, although its function at the cellular level is not yet clear. It is necessary for the synthesis of collagen, a protein that has many connective functions in the body [6]. Ascorbic acid is the enolic form of one *α*-ketolactone. Ascorbic acid solution is easily oxidized to the diketo form referred to as dehydroascorbic acid, which can easily be converted into oxalic acid, diketogulonic acid or threonic acid. It contains several structural elements that contribute to its chemical behavior: the structure of lactones, two enolic hydroxyl groups and a primary and secondary alcohol group. Enediol structure motivates the antioxidant properties, as can easily oxidized enediols to diketones [7-10].

Ascorbic acid is considered an antioxidant because it can supply an electron to a species with an unpaired electron to stabilize the radical (Fig. 2). Because radicals normally poach electrons from surrounding molecules to pair with their lone electron, they normally cause a chain reaction where

their victim goes on to pull electrons from another neighboring molecule (oxidation), and so on and so forth. However, because the ascorbyl radical is stable, it is less likely to poach an electron from another molecule in its environment, preventing the chain reaction from occurring [11, 12].

The objective of the study consisted in analysis the effect of natural (*β*-carotene and ascorbic acid) antioxidants at two concentrations (0.01 and 0.05%) on the oxidative stability of alimentary chicken fat in order to improve its safety and extend the shelf life.

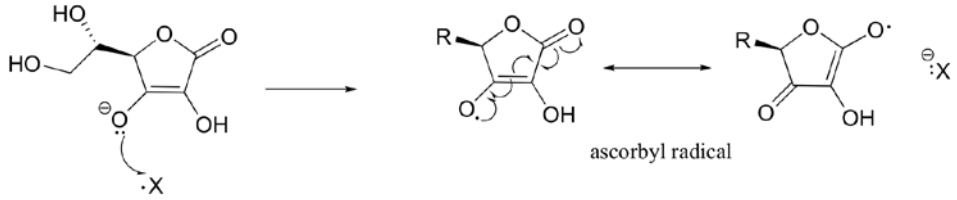


**Figure 2.** *The antioxidant mechanism of ascorbic acid [11]*

## RESULTS AND DISCUSSION

Acid value, peroxide value, refractive index value, iodine value and fatty acids profile were determined in order to asses the effect of antioxidants addition on chicken fat stability in order to improve its shelf life during refrigerated storage.

Acid value represents an analytical parameter which is used to evaluate the hydrolysis extension in fats during storage. An increase in this parameter indicates a higher presence of free fatty acids, a direct consequence of hydrolysis, and it is an important indicator of fat chemical deterioration [13].

The results of chemical analysis for chicken fat and additivated fat are tabulated in Tables 1-3, respectively. In chicken fat (control) was found the highest level of acid value followed by 0.01% ascorbic acid, 0.01% *β*-carotene, 0.05% ascorbic acid and 0.05% *β*-carotene additivated fat. Regardless of the type of fat, the highest acid value was found at 180 days of storage. Acid value increased from 0.18 to 1.24 g oleic acid/100 g in control; to 1.16 g oleic acid/100 g in 0.01% *β*-carotene additivated fat; to 1.21 g oleic acid/100 g in 0.01% ascorbic acid additivated fat; to 1.08 g oleic acid/100 g in 0.05% *β*-carotene additivated fat and to 1.11 g oleic acid/100 g in 0.05% ascorbic acid additivated fat stored at 2-4°C. Acid values exceeded the limit (≤ 1 g oleic acid/ 100 g fat) after 120 days of

storage in chicken fat, 150 days in 0.01% *β*-carotene and 0.01% ascorbic acid additivated fat, and 180 days in 0.05% *β*-carotene and 0.05% ascorbic acid additivated fat.

Pereira et al., reported that the formation of free fatty acids was significantly lower in cod liver oil with natural antioxidant from barley husks than in the control samples [14].

Peroxide value is a measure of primary lipid oxidation, indicating the amount of peroxides formed during oxidation. The products of lipid oxidation such as peroxides, free radicals, malonaldehyde and other cholesterol oxidation products are reported to promote coronary heart disease and atherosclerosis [15].

Peroxide value was significantly influenced by the storage time ($p < 0.001$) in chicken fat and 0.01% additivated fat. In control was found the highest level of peroxide value followed by 0.01% and 0.05% additivated fat. Regardless of the type of fat, the highest peroxide index level was found at 180 days of storage. Peroxide index values increased from 2.18 to 15.28 meq $O_2$/kg in control; to 12.77 meq $O_2$/kg in 0.01% *β*-carotene additivated fat and to 11.16 meq $O_2$/kg in 0.05% *β*-carotene additivated after 180 days of refrigerated storage. Peroxide index values at the end of refrigerated storage were 14.17 meq $O_2$/kg in 0.01% ascorbic acid additivated fat and 11.39 meq $O_2$/kg in 0.05% ascorbic acid additivated fat. Peroxide value exceeded the limit (10 meq $O_2$/kg ) after 90 days of storage in control, 120 days in 0.01% *β*-carotene and 0.01% ascorbic acid additivated fat, and 150 days in 0.05% *β*-carotene and 0.05% ascorbic acid additivated fat.

**Table 1.** Changes in quality parameters of chicken fat during refrigerated storage

| **Storage time** | **Chicken fat (control)** | | | |
|---|---|---|---|---|
| | PV (meq $O_2$/kg fat) | AV (g oleic acid/100 g fat) | RIV (refractometric degrees) | IV (g $I_2$/100 g fat) |
| 1 day | $2.18^{ij}$ | $0.18^{h}$ | $1.4648^{a}$ | $89.7^{a}$ |
| 30 days | $3.57^{hi}$ | $0.35^{g}$ | $1.4637^{a}$ | $88.4^{ab}$ |
| 60 days | $6.83^{g}$ | $0.58^{f}$ | $1.4625^{ab}$ | $86.9^{b}$ |
| 90 days | $9.14^{de}$ | $0.83^{cd}$ | $1.4605^{bc}$ | $84.1^{bc}$ |
| 120 days | $11.41^{c}$ | $0.96^{b}$ | $1.4583^{c}$ | $82.2^{c}$ |
| 150 days | $13.89^{b}$ | $1.18^{ab}$ | $1.4562^{d}$ | $80.1^{d}$ |
| 180 days | $15.28^{a}$ | $1.24^{a}$ | $1.4539^{de}$ | $77.4^{e}$ |
| *p* | *< 0.001**** | *< 0.001**** | *< 0.01*** | *< 0.01*** |

[a)] PV, peroxide value; AV, acid value; RIV, refractive index value; IV, iodine value.
[b)] Values are expressed as mean.
[c)] Different letters in the same column indicate statistically significant differences (Tukey's test $p < 0.05$).
[d)] Significant differences are denoted by asterisks: *$p < 0.05$; **$p < 0.01$; ***$p < 0.001$; $p \geq 0.05$, non-significant.

The results of several research confirm the efficacy of a natural and synthetic antioxidants to slow down the progress of lipid hydrolysis and increase oxidative stability in fatty foods [16-19]. Pereira et al. reported that the natural antioxidant derived from barley husks has a better antioxidant activity in cod liver oil than *t*-butyl-4-hydroxyanisole (BHA) or 2,6-di-*t*-butyl-*p*-hydroxytoluene (BHT) in reducing the production of primary and delaying secondary oxidation products [14].

The effects of natural (*α*-tocopherol) and synthetic (BHA and BHT) antioxidants on the oxidative stability of butter were investigated by Ozturk and Cakmakci [20]. The researchers found that butter samples treated with 50 and 100 ppm of the antioxidants provided significantly lower peroxide index values compared to the control group. The study showed that butter samples with 50 ppm *α*-tocopherol could be stored for more than 180 days at 4°C without spoilage. Zuta et al. studied the effect of 50, 100, 250 and 500 ppm concentrations of *α*-tocopherol on the oxidation of unrefined mackerel oil, and reported that low concentrations of *α*-tocopherol minimized autooxidation of unrefined mackerel oil, while higher concentrations of *α*-tocopherol were less effective as antioxidant [21].

**Table 2.** Changes in quality parameters of *β*-carotene additivated fat during refrigerated storage

| **Storage time** | **0.01% *β*-Carotene additivated fat** | | | | **0.05% *β*-Carotene additivated fat** | | | |
|---|---|---|---|---|---|---|---|---|
| | PV | AV | RIV | IV | PV | AV | RIV | IV |
| 1 day | $2.17^{gh}$ | $0.17^{fg}$ | $1.4647^{a}$ | $89.6^{a}$ | $2.15^{ef}$ | $0.16^{e}$ | $1.4648^{a}$ | $89.5^{a}$ |
| 30 days | $2.83^{ef}$ | $0.28^{e}$ | $1.4639^{a}$ | $88.9^{a}$ | $2.51^{de}$ | $0.21^{d}$ | $1.4641^{a}$ | $89.1^{a}$ |
| 60 days | $5.74^{d}$ | $0.47^{d}$ | $1.4628^{ab}$ | $87.5^{b}$ | $5.03^{cd}$ | $0.39^{cd}$ | $1.4635^{a}$ | $88.4^{ab}$ |
| 90 days | $7.82^{cd}$ | $0.79^{c}$ | $1.4611^{b}$ | $84.9^{bc}$ | $6.82^{c}$ | $0.67^{c}$ | $1.4616^{b}$ | $86.7^{b}$ |
| 120 days | $9.14^{c}$ | $0.91^{b}$ | $1.4589^{bc}$ | $82.9^{c}$ | $8.65^{b}$ | $0.85^{bc}$ | $1.4594^{bc}$ | $83.8^{bc}$ |
| 150 days | $11.31^{b}$ | $1.02^{ab}$ | $1.4571^{cd}$ | $81.1^{cd}$ | $9.36^{ab}$ | $0.92^{ab}$ | $1.4581^{c}$ | $82.1^{c}$ |
| 180 days | $12.77^{a}$ | $1.16^{a}$ | $1.4548^{d}$ | $78.8^{e}$ | $11.16^{a}$ | $1.08^{a}$ | $1.4559^{cd}$ | $80.4^{d}$ |
| *p* | <0.001 | <0.001 | <0.01 | <0.01 | <0.01 | <0.01 | <0.01 | <0.01 |

[a] PV, peroxide value (meq $O_2$/kg); AV, acid value (g oleic acid/100 g); RIV, refractive index value (refractometric degrees); IV, iodine value (g $I_2$/100 g).
[b] Values are expressed as mean.
[c] Different letters in the same column indicate statistically significant differences (Tukey's test $p < 0.05$).
[d] Significant differences are denoted by asterisks: *$p < 0.05$; **$p < 0.01$; ***$p < 0.001$; $p \geq 0.05$, non-significant.

**Table 3.** Changes in quality parameters of ascorbic acid additivated fat during refrigerated storage

| Storage time | 0.01% Ascorbic acid additivated fat | | | | 0.05% Ascorbic acid additivated fat | | | |
|---|---|---|---|---|---|---|---|---|
| | PV | AV | RIV | IV | PV | AV | RIV | IV |
| 1 day | $2.16^{h}$ | $0.16^{f}$ | $1.4647^{a}$ | $89.6^{a}$ | $2.14^{ef}$ | $0.15^{e}$ | $1.4648^{a}$ | $89.4^{a}$ |
| 30 days | $2.77^{g}$ | $0.31^{e}$ | $1.4638^{a}$ | $88.5^{ab}$ | $2.57^{de}$ | $0.23^{d}$ | $1.4643^{a}$ | $89.1^{a}$ |
| 60 days | $5.93^{ef}$ | $0.45^{cd}$ | $1.4631^{ab}$ | $87.7^{b}$ | $5.16^{cd}$ | $0.41^{cd}$ | $1.4633^{a}$ | $88.2^{ab}$ |
| 90 days | $8.11^{d}$ | $0.85^{bc}$ | $1.4609^{b}$ | $85.1^{bc}$ | $7.66^{bc}$ | $0.72^{c}$ | $1.4618^{b}$ | $86.1^{b}$ |
| 120 days | $9.67^{c}$ | $0.94^{b}$ | $1.4587^{bc}$ | $82.5^{cd}$ | $8.51^{b}$ | $0.88^{bc}$ | $1.4591^{bc}$ | $83.7^{bc}$ |
| 150 days | $12.03^{b}$ | $1.09^{ab}$ | $1.4569^{cd}$ | $80.8^{d}$ | $9.88^{ab}$ | $0.96^{ab}$ | $1.4576^{c}$ | $81.9^{c}$ |
| 180 days | $14.17^{a}$ | $1.21^{a}$ | $1.4544^{d}$ | $78.3^{e}$ | $11.39^{a}$ | $1.11^{a}$ | $1.4555^{cd}$ | $79.8^{d}$ |
| *p* | <0.001 | <0.001 | <0.01 | <0.01 | <0.01 | <0.01 | <0.01 | <0.01 |

[a)]PV, peroxide value (meq $O_2$/kg); AV, acid value (g oleic acid/100 g); RIV, refractive index value (refractometric degrees); IV, iodine value (g $I_2$/100 g).
[b)] Values are expressed as mean.
[c)] Different letters in the same column indicate statistically significant differences (Tukey's test $p < 0.05$).
[d)] Significant differences are denoted by asterisks: *$p < 0.05$; **$p < 0.01$; ***$p < 0.001$; $p \geq 0.05$, non-significant.

Refractive index value and iodine value are measures of the degree of unsaturation of fatty acids. Refractive index value declines linearly with iodine value. Refractive index value and iodine value were significantly influenced ($p < 0.01$) by the storage time in all treatments. Positive correlations between refractive index value and iodine value were found in control ($r = 0.83$; $p < 0.01$), 0.01% $\beta$-carotene additivated fat ($r = 0.79$; $p < 0.01$), and 0.01% ascorbic acid additivated fat ($r = 0.85$; $p < 0.01$). Regardless of the type of fat, the lowest iodine index level was found at 180 days of storage. The decrease of refractive index and iodine index levels at storage indicates a reduction of the unsaturation degree of fatty acids, by the split of unsaturated fatty acids double bonds.

Fatty acids represent the main constitutes of the saponifiable fraction of fats, the fatty acids profile at the beginning and at the end of refrigerated storage is reported. The total lipids of the fat samples showed a predominance of monounsaturated fatty acids (MUFA) and polyunsaturated fatty acids (PUFA).

The fatty acids profile of chicken fat was rich in olei (C18:1), vaccenic (C18:$1_i$), eicosenoic (C20:1), linoleic (C18:2), linolenic (C18:3) and arachidonic (C20:4) fatty acids, followed by palmitic (C16:0), stearic (C18:0) and miristic (C17:0) acids (Fig. 3).

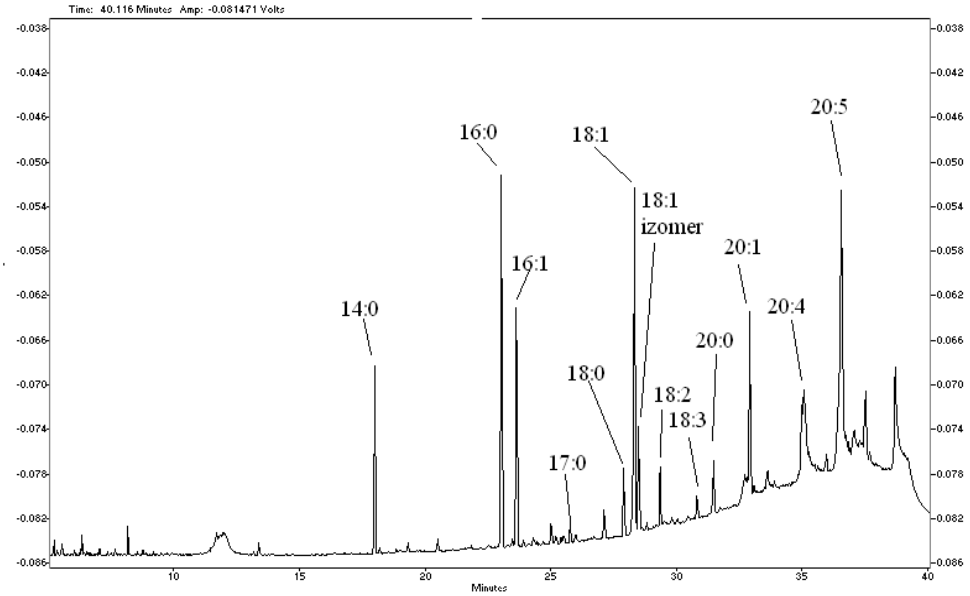


**Figure 3.** Gas chromatogram of fresh chicken fat

Saturated fatty acids (SFA) content increased, but monounsaturated and polyunsaturated fatty acids content decreased during refrigerated storage. Storage time showed to be most correlated with MUFA for control ($r$ = 0.93), followed by 0.01% additivated fat ($r$ = 0.87) and 0.05% additivated fat ($r$ = 0.76).

Storage time inflicted changes in fatty acids profile of chicken fat. Analyzing the fatty acids by their common nature, the most affected fraction was the polyunsaturated fatty acids (PUFA), directly related with their higher number of double bonds, with higher susceptibility to oxidation (Fig. 4, Fig. 5). At 180 days of refrigerated storage, PUFA content decreased around 13% in control and around 9% in 0.05% additivated fat. Taking into account that in chicken fat was found the highest level of peroxide value, the decrease of total PUFA during storage may be due to the oxidation of polyunsaturated fatty acids.

Jankowski et al. determined the effect of diets with a different *n*-6/*n*-3 PUFA ratio (7.31, 4.43 and 0.99) and antioxidants on the fatty acid profile, oxidative status and sensory properties of turkey fat. The researchers showed that fat of turkeys fed with linseed oil enriched with *α*-tocopherol, ascorbic acid and selenium was characterized by higher concentrations of

total PUFA, a significantly lower *n*-6/*n*-3 PUFA ratio, a higher thiobarbituric acid reactive substances content, and after 4 months of deep-freeze storage the *n*-6/*n*-3 PUFA ratio did not deteriorate [22].

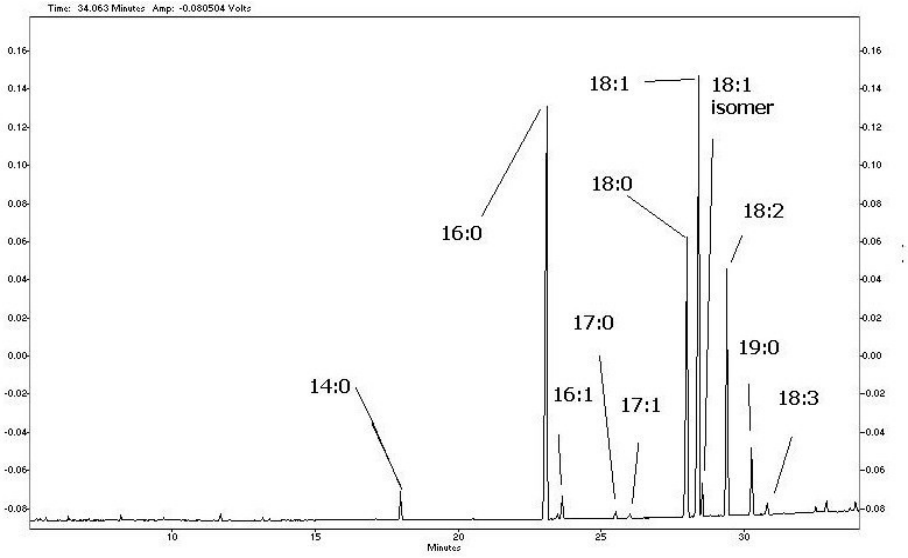


**Figure 4.** Gas chromatogram of chicken fat at 180 days of storage

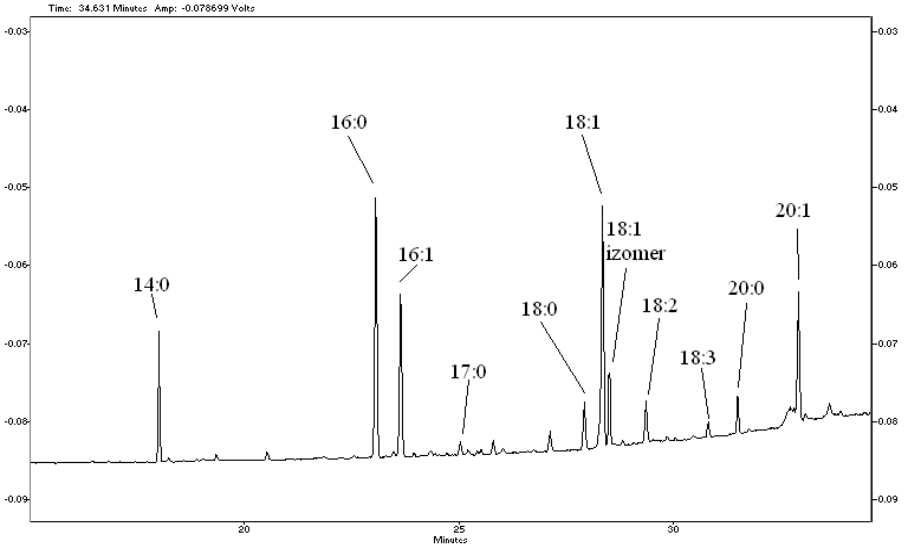


**Figure 5.** Gas chromatogram of 0.05% additivated fat at 180 days of storage

## CONCLUSIONS

Lipid oxidation in chicken fat varied with the duration of storage, type and concentration of antioxidant.

Peroxide value was significantly influenced by the storage time ($p < 0.001$) in chicken fat and 0.01% additivated fat. Chicken fat without antioxidants was more unstable at storage, producing higher amounts of hydroperoxides.

Positive correlations between refractive index value and iodine value were found in control, 0.01% *β*-carotene additivated fat, and 0.01% ascorbic acid additivated fat. Regardless of the type of fat, the lowest iodine index level was found at 180 days of storage.

Storage time inflicted changes in fatty acids profile, the most affected fraction was the polyunsaturated fatty acids, directly related with their higher number of double bonds, with higher susceptibility to oxidation.

The addition of *β*-carotene and ascorbic acid in proportion of 0.01% extended the shelf life of chicken fat stored at 2-4°C by 30 days, and antioxidants addition in proportion of 0.05% extended the shelf life by 60 days. Statistical analysis of the data revealed that the development of rancidity in chicken fat was significantly ($p < 0.01$) reduced by the addition of *β*-carotene and ascorbic acid in concentration of 0.05%.

## EXPERIMENTAL SECTION

### *Samples*

The research was conducted on alimentary chicken fat and after the addition of antioxidants. Raw material was collected immediately after its obtaining from the slaughtered birds and consisted in abdominal fat out off the carcass. An average weight of 500 g of abdominal fat was cut into small pieces, heated at 65-75°C, centrifuged, and filtered. *β*-Carotene and ascorbic acid were dissolved in the melted fat, each of them in two concentrations: 0.01 (0.01 g/100 g of fat) and 0.05% respectively (0.05 g/100 g of fat). The following treatments were investigated: (1) control (without antioxidant), (2) *β*-carotene (0.01%), (3) *β*-carotene (0.05%), (4) ascorbic acid (0.01%), and (5) ascorbic acid (0.05%).

In order to carry out fat analyses during storage for 180 days, more samples of 50 g from each treatment were packed in closed jars, stored under refrigeration (2-4°C), and at 30 days intervals were used for chemical analysis. For evaluation of fat stability and monitoring the deterioration

during storage, methods included peroxide value, acid value, refractive index value, iodine value and fatty acid composition. Three replications were carried out to examine each sample. All chemicals used were of analytical grade and obtained from Merck (Germany); *β*-carotene and ascorbic acid were purchased from Sigma (Sigma Chemicals, Shanghai, China).

### *Physicochemical examination*

Peroxide value was determined using UV-VIS spectrophotometer. Thiocyanate ions ($SCN^-$) react with $Fe^{3+}$ ions to give a red-violet chromogen that can be determined spectrophotometrically, the absorbance of each solution was read at 500 nm. To quantify PV, a calibration curve (absorbance at 500 nm vs. $Fe^{3+}$ expressed in µg) was constructed and peroxide value was expressed as meq $O_2$/kg sample. Iodine value was determined using Hanus method, was calculated as g $I_2$/100 g sample [23].

To determine the refractive index we used the PAL-RI (Tokyo, Japan) with the following technical characteristics: field: 1,3306-1,5284; resolution: 0.0001; accuracy: ± 0.0003; measuring temperature: 5-45$^o$C (resolution 1$^o$C); measuring time: 3s; in accordance with the requirements of EMC Directive 93/68/EEC. Acid value determination consists in neutralizing acidity with sodium hydroxide 0.1 N, using phenolphthaleine, as an indicator. Acidity was expressed as oleic acid grams to 100 grams sample [23].

Fatty acids composition was determined using a Shimadzu GC-17 A gas chromatograph (Tokyo, Japan) coupled with a flame ionization detector. The gas chromatography column is Alltech AT-Wax, (60 m x 0.32 mm x 0.5 µm), stationary phase (polyethylene); helium was used as a carrier gas at a pressure of 147 kPa, temperature of the injector and detector was set to 260°C, and the oven program was the following: 70°C for 2 minutes, then the temperature was raised to 150°C with a gradient of 10°C/minute, a level of 3 minutes, and the temperature was raised to 235°C with a gradient of 4°C/minute. Identification and quantification of FA were performed by comparison with standards. Results were expressed as g/100 g fat [24].

### *Statistical analysis*

All analytical determinations were performed at least in triplicate. Values of different parameters were expressed as the mean ± standard deviation (X ± SD). Tukey's honest significance test was carried out at a 95% confidence level ($p < 0.05$). The Pearson's correlation (α=0.05) with two-tailed probability values was used to estimate the strength of association between chemical parameters.

## ACKNOWLEDGMENT

The results presented in this paper were obtained in the framework of the GNaC 2018 ARUT grant “Increasing the Chemical Stability of Animal Fats Rich in Unsaturated Fatty Acids by Antioxidants Addition”, research Contract no. 3015/2019, with the financial support of the Technical University of Cluj-Napoca.

## REFERENCES

1. C.A. Costa, A.S. Carlos, G.P. Gonzalez, R.P. Reis, *European Journal of Nutrition,* **2012**, *51*, 191.
2. F. Shahidi, in: Natural Antioxidants. Chemistry, Health Effects, and Applications. Ed. AOCS Press, Champaign, Illinois (USA), **1997**, 11.
3. E.N. Frankel, *Food Chemistry*, **1996**, *57*, 51.
4. R.A. Riemersma, *European Journal of Lipid Science and Technology*, **2002**, *104*, 419.
5. B. Sultana, F. Anwar, R. Przybylski, *Food Chemistry,* **2007**, *104*, 997.
6. R. Kim, F. Labella, *Journal of Lipid Research*, **2010**, *28*, 1110.
7. E.N. Frankel, *Progress in Lipid Research*, **1998**, *19*, 24.
8. N.V. Yanishlieva, K. Aitzetmüller, V.G. Raneva, *Fett/Lipid,* **1998**, *10*, 444.
9. O. Roman, B. Heyd, B. Broyart, R. Castillo, M. N. Maillard, *LWT - Food Science and Technology,* **2013**, *52*, 49.
10. B. Roszkowska, M. Tanska, S. Czaplicki, I. Konopka, *European Journal of Lipid Science and Technology,* **2015**, *117*, 673.
11. E. Choe, D.B. Min, *Comprehensive Reviews in Food Science and Food Safety,* **2006**, *5*, 169.
12. S. Azadmard-Damirchi, F. Habibi-Nodeh, J. Hesari, M. Nemati, B.F. Achachloei, *Food Chemistry,* **2014**, *121*, 1211.
13. A. Kamal-Eldin, *European Journal of Lipid Science and Technology*, **2006**, *58*, 1051.
14. D.A. Pereira de Abreu, K.V. Rodriguez, J.M. Cruz Freire, *Food Chemistry*, **2006**, *113*, 1395.
15. K.H. Wagner, F. Wotruba, I. Elmadfa, *European Journal of Lipid Science and Technology*, **2011**,*103*, 746.
16. S. Schmidt, J. Pokorny, *Czech Journal of Food Science*, **2015**, *23*, 93.
17. F. Caponio, A. Pasqualone, T. Gomes, *European Food Research and Technology,* **2014**, *215*, 114.
18. R.M. El-Abassy, P. Donfack, A. Materny, *Food Research International,* **2010**, *43*, 694.

19. N. Rodrigues, R. Malheiro, S. Casal, M.C. Manzanera, *Food and Chemical Toxicology,* **2012**, *50*, 2894.
20. S. Ozturk, S. Cakmakci, *European Journal of Lipid Science and Technology*, **2006**, *108*, 951.
21. P.C. Zuta, B.K. Simpson, X. Zhao, L. Leclerc, *Food Chemistry*, **2007**, *100*, 800.
22. J. Jankowski, Z. Zdunczyk, D. Mikulski, J. Pomianowski, P. Zdunczyk, *European Journal of Lipid Science and Technology*, **2012**, *114*, 1025.
23. F. Pop, L. Mihalescu, *International Journal of Food Properties,* **2017**, *20*, 1085.
24. F. Pop, *Studia Universitatis Babes-Bolyai Chemia*, **2018**, 63, 43.

STUDIA UBB CHEMIA, LXIV, 1, 2019 (p. 185-196)
(RECOMMENDED CITATION)
DOI:10.24193/subbchem.2019.1.15

# A PILOT STUDY FOR THE USE OF COUMARIN-480 TO ENHANCE THE FINGERMARKS

**MUHAMMAD YASEEN[a,*], NOUMAN RASOOL[b], ZAHID FAROOQ[c], SHAHBAZ NAZIR[d], SHUMAILA CHOHAN[e]**

**ABSTRACT.** A new alternative super glue post-treatment method for the enhancement of fingermarks over two different non-porous surfaces including glass slides and high density polyethylene (HDPE) sheets have been investigated. This is the first documented application of 2,3,6,7-tetrahydro-9-methyl-1H,5H-quinolizino(9,1-gh)coumarin or coumarin-480 for the enhancement of cyanoacrylate fumed fingermarks. Coumarin-480 in ethanol was used as cyanoacrylate post-treatment dye. Fingermarks of seven different donors were aged for three different time periods (1 day, 1 week and 4 weeks) over non-fluorescent glass slides and HDPE sheets and developed with cyanoacrylate fumes. Upon staining with coumarin-480, fingermarks of varying qualities were observed under long UV radiations. Rhodamine 6G was used to assess the relative sensitivity of the coumarin-480 for the enhancement cyanoacrylate developed fingermarks. Pseudo-operational trials were conducted on glass bottles and high density polyethylene shopping bags. Coumarin-480 produced superior enhancement on HDPE shopping bags and glass bottles than the rhodamine 6G.

***Keywords:*** *Fingermarks enhancement, Cyanoacrylate post treatment dye, Coumarin-480, Fluorescent dye*

## INTRODUCTION

One of the most valuable physical evidence found at almost every crime scene are latent fingermark [1]. A variety of techniques for the development and enhancement of latent fingermarks are reported in the

[a] *Department of Chemistry, University of Education (Lahore), Faisalabad campus, Pakistan*
[b] *Department of Biochemistry, University of Management and Technology, Lahore, Pakistan*
[c] *Department of Physics, University of Education (Lahore), Faisalabad campus, Pakistan*
[d] *Department of Education, Govt. of Punjab, Pakistan*
[e] *Institute of Chemistry, University of Punjab, Pakistan*
** Corresponding author yaseen747pk@hotmail.com*

literature [2]. Cyanoacrylate or super glue fuming is an extremely efficient and simple method for the development of latent fingermarks. In the late 1970s, investigators in Japan and UK almost simultaneously discovered the abilities of cyanoacrylate to develop the latent fingermarks [3]. This method is based upon the inherent property of alkyl substituted cyanoacrylate esters to get polymerized over the fingerprint residue to produce visible three-dimensional fingermarks [4-6]. The exact chemical process of this technique is still under debate and is not well understood [7-9]. However, it is believed that anionic polymerization of alkyl cyanoacrylate is initiated by a variety of compounds like amino acids, fatty acids, and proteins present in the fingerprint residue. The main limitation of cyanoacrylate fuming is the whitish colour of the developed latent fingermarks which often lack the contrast with the light coloured substrates. To overcome such limitations, several super glue post-treatment methods have been developed [10-13]. These post-treatment methods range from dusting the cyanoacrylate fumed fingermarks with colour or fluorescent powders [14] or staining with a fluorescent dye solution like Ardox [13], basic yellow 40 and rhodamine 6G [15]. These fluorescent techniques provide a better contrast of the developed friction ridge impressions than the non-fluorescence techniques.

Many efforts have been made by the scientific community to explore the alternative fluorescent materials for the detection and enhancement of latent fingermarks [16-17]. Non-substituted coumarin (2-oxo-2*H*-chromene) exhibits very weak or zero fluorescence. However, its substituted derivatives exhibit intense fluorescence and are used in different branches of biology, physics, chemistry, and medicine [18]. For the first time in 1977, Dalrymple and co-workers reported the use of coumarin-6 in conjunction with argon laser to develop the latent fingermarks [19]. Next year, Thornton reported a modified fingerprint powder by mixing coumarin-6 with conventional black fingerprint powder [20]. In 1983, Kobus and co-workers investigated the application of coumarin-540 as super glue post-treatment dye [21]. The staining dye, coumarin-540, was none other than coumarin-6 that had earlier been reported by Dalrymple [19]. High prices and the limited availability of forensic light sources and lasers in the early 1980s stimulated the scientific community to investigate alternative dyes and stains that can be excited by long wave ultra violet radiations [13]. Consequently, in 1992 Ardox was offered as an alternative to Rhodamine 6G that can be excited by using UV light [22]. It works well with laser and UV lamps. Ardox stained fingermarks fluoresce under 365 nm whereas better results could also be obtained under 450-480 nm excitation. Different, one step fluorescent cyanoacrylate products such as PolyCyano UV, Lumicyano and CN-Yellow are now a days commercially available [23-25]. Hahn and Ramotowski has reported that the

effectiveness of Polycyano UV is highly dependent on the surface itself in addition to the use of a modified fuming chamber to deliver the Polycyano UV powder into the glue dish [26].

Because of the availability of low-cost UV light sources than the expensive alternative light sources, there is still a large potential to explore alternative UV excited dyes that can stain the latent fingermarks either in one step or in two steps. However, the use of such dyes in conjunction with UV light requires special personal protective equipment to protect the skin and eyes. We decided to explore the use of coumarin-480 as a super glue post-treatment dye. The first part of this study aims to compare the sensitivity of coumarin-480 with rhodamine 6G for the enhancement of cyanoacrylate developed fingermarks over microscopic glass slides and HDPE sheets. The second part of this study consists of pseudo-operational trials that were conducted on two hundred shopping bags and two hundred glass bottles so as to establish whether the results obtained in the laboratory are reproducible or not.

## RESULTS AND DISCUSSION

The preliminary task for this research work was to study the optical properties of coumarin-480 so as to determine the excitation wavelength and the type of barrier filters. The excitation wavelength was explored by measuring the UV-Visible spectrum in ethanol at room temperature. In ethanol, coumarin-480 exhibited two intense absorptions, one in shortwave UV region at 210 nm and the second in long wave UV region 390 nm in addition to a weak absorption at 258 nm. Upon excitation at 390 nm, $10^{-4}$ M solution of coumarin-480 in ethanol produced a broad emission band between 430-520 nm with emission maxima at 465 nm (Figure 1).

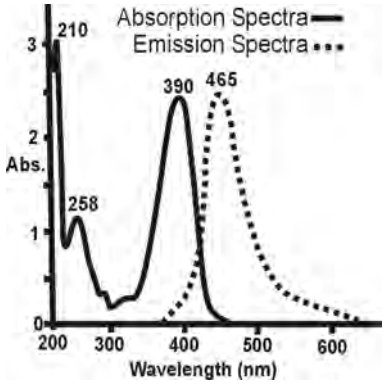


**Figure 1.** UV-Visible and emission spectra of coumarin-480 in ethanol

Seven fingermark donors deposited thirty five split latent fingermarks (five depleted marks from each donor) over seventy microscopic glass slides according to the protocol as described above. Similarly, same fingermarks donors also deposited another set of thirty five split fingermarks (five depleted marks from each donor) over eighty HDPE sheets. After cyanoacrylate development, right half of every depleted fingermark was stained with coumarin-480 and the left half with rhodamine 6G solution. Negative controls (cyanoacrylate fumed fingermarks without any fluorescent stain) were run to check any inherent luminescence under wavelength of 390 nm. Because of an intense absorption band exhibited by coumarin-480 at 390 nm, this wavelength was explored to excite the coumarin-480 stained split fingermarks (right halves only). The images of fluorescent fingermarks were captured by using LP415 UV block filter having cut-on wavelength 415 nm. Images of enhanced fingermarks were saved in tagged image file format (TIFF) without any processing (Figure 2).

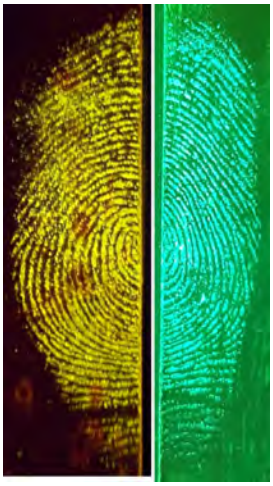

**Figure 2.** A split fingermark enhanced with coumarin-480 (right half) and rhodamine 6G (left half) on a glass slide

Each fingermark was given a comparative score (Table 1) based on the clarity of ridge details, contrast and background interferences [27]. The results of comparison between the performance of coumarin-480 and rhodamine 6G for the enhancement of one day old split fingermarks on microscopic glass slides and HDPE sheets are summarized below (Figure 3).

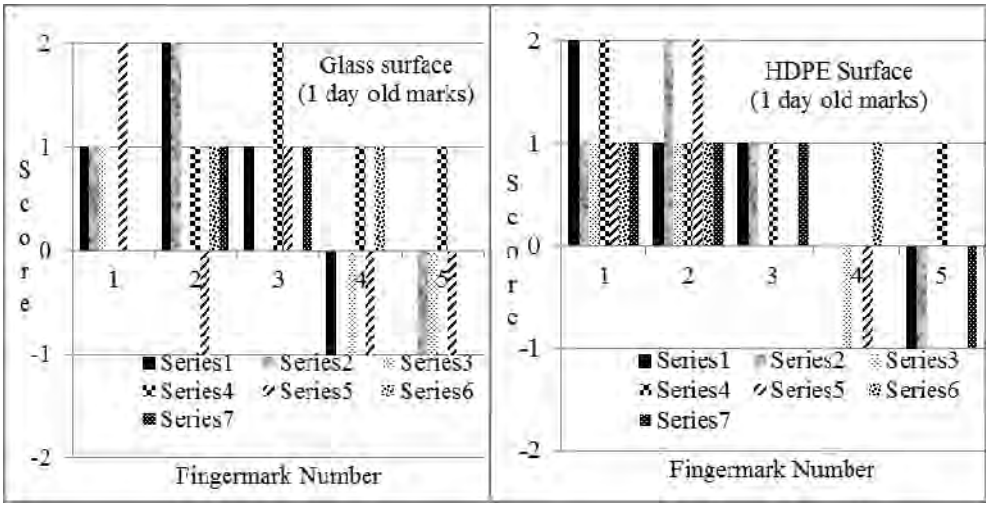


**Figure 3.** UC score of coumarin-480 enhanced one day old fingermarks on glass and HDPE surfaced

Although standard protocols were used to provide the degree of consistency and reproducibility between the fingermarks but because of many factors like emotional stress, the number of sweat pores, health, deposition time and pressure which are beyond the control of fingermark donor, natural variations among the developed fingermarks was observed. After direct comparison by using UC scale [27], coumarin-480 produced superior enhancement among 46% and 57% of one day old cyanoacrylate developed marks on glass and HDPE surfaces respectively than rhodamine 6G. UC score [27] for the enhancement of one and four week old cyanoacrylate developed marks on glass and HDPE surfaces with coumarin-480 are given below (Figure 4 and 5).

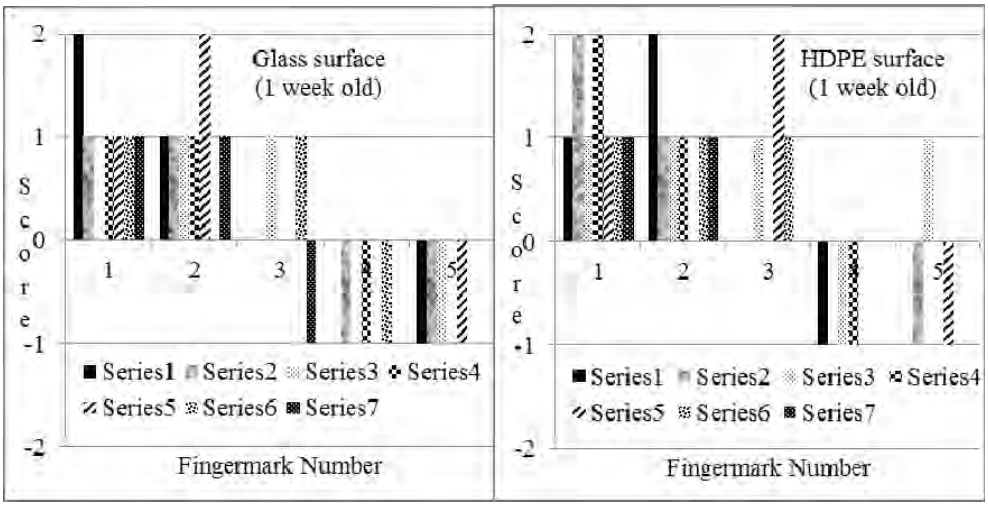


**Figure 4.** UC score of coumarin-480 enhanced one week old fingermarks on glass and HDPE surfaced

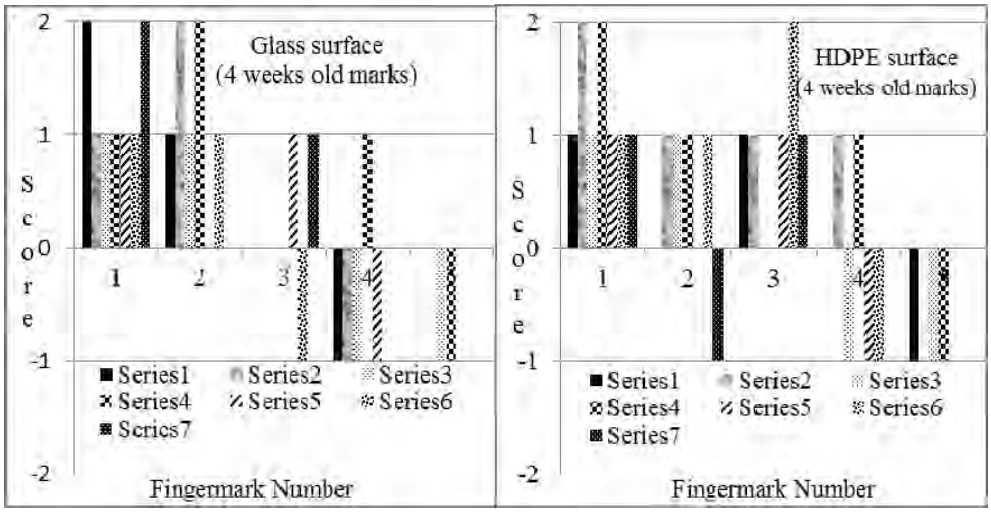


**Figure 4.** UC score of coumarin-480 enhanced four week old fingermarks on glass and HDPE surfaced

Overall, coumarin-480 produced better enhancement than rhodamine 6G among 41% of cyanoacrylate developed fingermarks of three different ages on glass slides and 52% on HDPE surface. Coumarin-480 failed to produce greater enhancement than rhodamine 6G among 20% of the marks on glass surface and 16% of the marks on HDPE surface. On both glass and HDPE surfaces, coumarin-480 was found to be superior super glue post treatment enhancement dye than rhodamine 6G. Furthermore, the enhancement results were entirely dependent upon the amount of deposited cyanoacrylate polymer that is consistent with conventional cyanoacrylate stains.

Polythene shopping bags and glass bottles are often encountered in routine casework. Glass bottles and HDPE shopping bags were decided to be tested for pseudo-operational trials. All collected substrates were treated within two weeks of collection during which these were stored inside the laboratory at 25 °C and relative humidity around 55%. Shopping bags were cut from the middle (vertically from top to bottom) and each piece after cyanoacrylate fuming was treated with a different enhancement technique. Similarly, glass bottles were randomly divided into two batches so that each batch consists of 100 glass bottles. All substrates were treated with cyanoacrylate fumes. Any mark with continuous ridge details and an area greater than 64 $mm^2$ was counted [27-28]. Marks that showed signs of over fuming or overdevelopment were also noted. The total numbers of cyanoacrylate developed fingermarks detected under day light in each batch of shopping bags and glass bottles were counted. One batch of shopping bags and glass bottles was stained with coumarin-480 solution and the counter batched were stained with rhodamine 6G. Figure 5 graphically illustrate the total number of fingermarks detected after cyanoacrylate fuming and subsequent enhancement with coumarin-480 and rhodamine 6G stains.

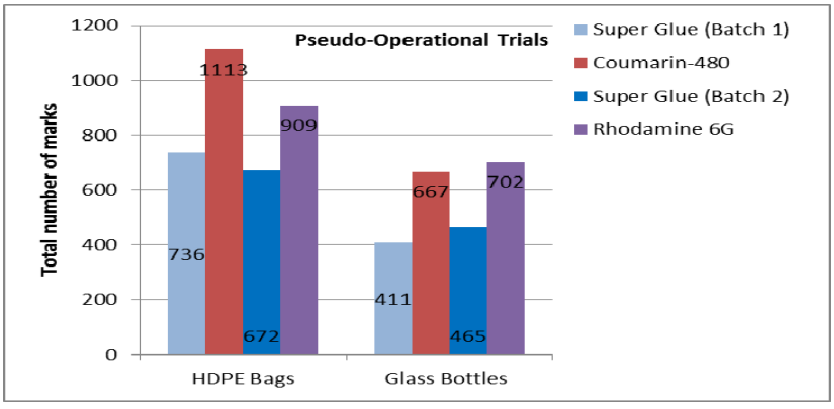


**Figure 5.** Pseudo-operational trials of coumarin-480 on shopping bags

## CONCLUSIONS

This study has revealed the potential of coumarin-480 as a superior super glue post treatment dye than the rhodamine 6G on HDPE and glass surfaces.

## EXPERIMENTAL SECTION

Absorption and emission spectra of coumarin-480 were recorded in ethanol so as to determine its absorption and emission maxima which helped us to select appropriate excitation wavelength and the barrier filter. The UV-visible absorption spectrum of coumarin-480 was measured with Shimadzu UV-2450 spectrophotometer using a quartz cell of path length 1 cm, whereas the emission spectrum was recorded with a commercial fluorimeter (Cary Eclipse from Varian).

Cyanobloom™ purchased from Foster and Freeman, the UK was used as a source of cyanoacrylate fumes. Laser-grade coumarin-480 was obtained from Exciton, USA and was used as received. Cyanoacrylate fuming was performed in CyanoSafe™ filtered cyanoacrylate fuming chamber (Product No. CAS30, Sirchie, USA) having an internal volume of 0.43 $m^3$ by using 2 grams of Cyanobloom™ as a source of cyanoacrylate fumes. Temperature and humidity of the cyanoacrylate chamber were maintained at 120 ℃ and at 80% respectively. After 45 minutes, all samples were removed from the chamber and stored at room temperature for the next 48 hours. Polilight® PL500 (Rofin, Australia Pty. Ltd.) was used as an excitation source.

Rhodamine 6G was purchased from Sirchie, USA and was used as received. Solvent grade methanol, 2-propanol, methyl ethyl ketone and ethanol were purchased from Sigma Aldrich, USA and were used after distillation. The working solution of rhodamine 6G was prepared as used by the Australian Federal Police [29] by dissolving 0.2 g of rhodamine 6G in 200 ml of isopropanol followed by the addition of 300 ml of methyl ethyl ketone to obtain 500 ml of stock solution. The 250 ml of stock solution of rhodamine 6G was diluted with 750 ml of water to obtain 1000 ml of working solution of rhodamine 6G.

For the optimization of coumarin-480, only charged fingermarks were used to ensure that sufficient cyanoacrylate was deposited. This involved donors rubbing fingers on their forehead, and then rubbing their hands together for homogenization prior to depositing fingermarks on the surface. Coumarin-480 was tested in a number of carrier solvents but the formulation that produced the best results was 0.25 g of dye dissolved in

1000 ml of ethanol. The higher concentration caused sufficient background staining and the lower concentrations decreased the contrast of the developed marks. The optimal wavelength for the excitation of coumarin-480 was found to be 390 nm which is its absorption maximum.

In the first part of this pilot study, non-fluorescent plain microscopic glass slides (VWR, USA) and transparent HDPE sheets were used as substrates without any treatment. For pseudo-operational trials, one hundred HDPE shopping bags were collected from the dust bins and the old stationary store room of the campus whereas, two hundred glass empty bottles of different brands were collected from the dust bins and an abandon cafeteria.

In order to check the inter-variability of developed latent fingermarks four males and three females all having ages between 25-40 years were randomly selected from a pool of twenty people. They were asked not to apply any cosmetics on their bodies before coming to work. All fingermark donors deposited their natural fingermarks by pressing the volar pad of one finger at the junction of two microscopic slides and the other finger at the junction of two HDPE sheets for two seconds each. It left one-half fingermark on each substrate and allowed the two halves of the same fingermark to be processed separately by two different techniques. Before deposition of fingermarks on microscope slides and HDPE sheets all donors were directed to gently rub their fingers and palms on another in order to uniformly distribute the secretions.

The concept of depletion series was used to evaluate the enhancement of relatively weak developed cyanoacrylate fingermarks. A series of fingermarks were deposited by each donor by the successive pressing of the same finger against the same surface. By doing so, the quantity of fingermark residue decreases successively from first to the last fingermark. Before this study, seven selected fingermark donors were tested for natural marks by cyanoacrylate fuming followed by enhancement with rhodamine 6G to select the appropriate number of depletion marks over microscopic slides and HDPE sheets. Seven donors were ranked and assigned an alphabet on the basis of developed fingermarks. Alphabet “A” was assigned to an excellent judged natural fingermark donor whereas alphabet “G” was assigned to the worst judged fingermark donor. For each donor, a depletion series till $20^{th}$ mark was obtained by following the same protocol as described earlier. It was observed that for two fingermark donors (the worst donors) no fingermarks were observed after the third and fourth mark. Since the quality of fingermark is dependent on many factors like health of donor, emotional stress, deposition pressure and time etc. So we selected not to go beyond the fifth depletion mark by acknowledging the problems of depletion discussed in another study [30]. Hence, three sets of

fingermarks on microscopic glass slides and three sets of fingermarks on HDPE sheets (five depletion fingermarks from each donor) were prepared so that each set consist of thirty five depleted fingermarks. As recommended by Kent [31] three sets of fingermarks on glass slides and three on HDPE sheets were aged for three different time intervals (one day, one week and four weeks). During the aging period, all fingermarks were stored at room temperature (25 °C, relative humidity 55%) inside the laboratory over a table.

Working solution of coumarin-480 and rhodamine 6G were applied to the right and left halves of each set of cyanoacrylate developed marks respectively by spraying with a squirt bottle. After 10 seconds, the excess of rhodamine 6G and coumarin-480 were removed by washing with distilled water. All substrates after washing were air dried under darkness.

The right halves of each set of coumarin-480 stained fingermarks (35x3x2 marks) were excited under 390 nm light which was accomplished by down tuning the 415 nm filter of Polilight® by selecting the t25 position. The output power of Polilight® PL500 was maintained at P3. Clear splash goggles with UV filtration up to 400 nm, (Item no. 1005-007, UVPS®, Chicago, IL, USA) were used to locate the coumarin-480 stained fluorescent fingermarks. Coumarin-480 enhanced fingermarks were captured by using LP415 UV block filter (Midwest Optical Systems, Inc. USA; Cut-on wavelength 415 nm) mounted in front of a 16-megapixel digital camera (Nikon L25). The left halves of each set of rhodamine 6G stained fingermarks (35x3x2 marks) were excited under 505 nm and were photographed by using OG550 long pass barrier filter in front of a 16-megapixel digital camera (Nikon L25). All photos were captured under darkness within 1 h after the staining and drying. The angle of incident light (light guide) was maintained at approximately 45° and the camera was held at the right angle.

The quality of enhanced fingermark images was visually assessed by one certified competent latent fingerprint examiner on a 15-inch monitor always under the same conditions of optical brightness. Enhanced fingermarks were numerically graded (Table 1) according to the published procedure [32-33]. It permits the pictorial appearance of enhanced latent fingermarks to be converted into a numerical value that can be used to compare the relative effectiveness of two development techniques.

**Table 1.** Fingermark grading system

| Score | Level of Detail |
|---|---|
| +2 | Significant increase in enhancement when compared to rhodamine 6G |
| +1 | Slight increase in enhancement when compared to rhodamine 6G |
| 0 | No enhancement |

## ACKNOWLEDGMENTS

Authors are thankful to all the participants who voluntarily donated their fingermarks.

## REFERENCES

1. C. Champod, C. Lennard, P. Margot, M. Stoilovic, *Fingerprint and other ridge skin impressions*, CRC Press, Boca Raton, USA, **2004**.
2. H.C. Lee, R.E. Gaensslen, *Advances in fingerprint technology*, 2nd ed., CRC Press, Boca Raton, USA, **2001**.
3. B. Yamashita, M. French, *The fingerprint sourcebook,* National Institute of Justice, **2011**.
4. P. Casault, N. Gilbert, B. Daoust, *Candian Society of Forensic Science Journal.,* **2017**, *50*, 1.
5. M. Tahtouh, S.A. Scott, J.R. Kalman, B.J. Reedy, *Forensic Science International,* **2011**, *207*, 223.
6. G. Groeneveld, S. Kuijer, Mde. Puit, *Science & Justice,* **2014**, *54*, 42.
7. P. Czekanski, M. Fasola, J. Allison, *Journal of Forensic Sciences,* **2006**, *51*, 1323.
8. S.P. Wargacki, L.A. Lewis, M.D. Dadmun, *Journal of Forensic Sciences,* **2007**, *52*, 1057.
9. S.P. Wargacki, L.A Lewis, M.D. Dadmun, *Journal of Forensic Sciences,* **2008**, *53*, 1138.
10. B.K. Chesher, J.M. Stone, W.F. Rowe, *Forensic Science International,* **1992**, *57*, 163.
11. D.A. Wilkinson, J.E. Watkin, *Forensic Science International,* **1993**, *60*, 67.
12. M. Takatsu, O. Shimoda, H. Teranishi, *Journal of Forensic Sciences,* **2012**, *57*, 515.
13. M.M. McCarthy, *Journal of Forensic Identification,* **1990**, *40*, 75.
14. L. Liu, Z. Zhang, L. Zhang, Y. Zhai, *Forensic Science International,* **2009**, *183*, 45.
15. W.D. Mazella, C.J. Lennard, *Journal of Forensic Identification,* **1995**, *45*, 5.
16. C. Xu, R. Zhou, W. He, L. Wu, P. Wu, X. Hou, *Analytical Chemistry,* **2014**, *86*, 3279.
17. H.L. Barros, V. Stefani, *Forensic Science International,* **2016**, *263*, 83.
18. B. Valeur, *Molecular Fluorescence: Principles and Aplications,* Wiley-Verlag Chemie GmbH.:Weinheim, Germany, **2001**, 79.
19. B. Dalrymple, J.M. Duff, E.R. Menzel, *Journal of Forensic Sciences,* **1977**, *22*, 106.
20. J. Thornton, *Journal of Forensic Sciences,* **1978**, *23*, 536.

21. H.J. Kobus, R.N. Warrener, M. Stoilovic, *Forensic Science International,* **1983**, *23*, 233.
22. J. F. Fallano, *Journal of Forensic Identification,* **1992**, *42*, 91.
23. S. Chadwick, L. Xiao, P. Maynard, C. Lennard, X. Spindler, C. Roux, *Australian Journal of Foresic Sciences,* **2014,** *46***,** 471.
24. C. Prete, L. Galmichi, F-G. Quenum-Possy-Berry, C. Allain, N. Thiburce, T. Colard, *Forensic Science International,* **2013**, *233*, 104.
25. D.E. Weaver, E.J. Clary, *Journal of Forensic Identification,* **1993**, *43*, 481.
26. W. Hahn, R. Ramotowski, *Journal of Forensic Identification,* **2012**, *62*, 279.
27. V.G. Sears, S.M. Bleay, H.L. Bandey, V.J. Bowman, *Science & Justice,* **2012**, *52*,145.
28. R.P. Downham, S. Mehmet, V.G. Sears, *Journal of Forensic Identification,* **2012**, *62*, 661.
29. M. Stoilovic, C. Lennard, *Fingermark Detection & Enhancement,* 4 ed., National Centre for Forensic Studies, Canberra, **2010**.
30. S. Fieldhouse, *Forensic Science International,* **2011**, *207*, 96.
31. T. Kent, *Journal of Forensic Identification,* **2010**, *60*, 371.
32. C. McLaren, C. Lennard, M. Stoilovic, *Journal of Forensic Identification,* **2010**, *60*, 199.
33. International Fingerprint Research Group (IFRG) Guidelines for the Assessment of Fingermark Detection Techniques, *Journal of Forensic Identification,* **2014**, *64*, 174.

STUDIA UBB CHEMIA, LXIV, 1, 2019 (p. 197-206)
(RECOMMENDED CITATION)
DOI:10.24193/subbchem.2019.1.16

# DETERMINATION OF NITRATE AND NITRITE CONTENT IN *ZONAR* MILK SERUM AND DERIVED DAIRY DRINKS USING ION-PAIR REVERSED-PHASE HIGH PERFORMANCE LIQUID CHROMATOGRAPHY*

**MIUȚA FILIP[a] *, DOINA PRODAN[a], MARIOARA MOLDOVAN[a], MIHAELA VLASSA[a]**

**ABSTRACT.** The presence of nitrite and nitrate in milk and dairy products may cause serious health problem for consumers. Thus, a simple and accurate ion-pair reversed-phase high performance liquid chromatographic (IP-RP-HPLC) method has been developed and validated for determination of nitrite and nitrate in some dairy drinks based on *Zonar* Milk Serum.

The separation was achieved on a Synergy Hydro-RP polar endcapped C18, 80Å, 4μm (250 × 4.6 mm) column using isocratic elution with 0.01M *n*-octylamine and methanol, 90:10 (v/v) at pH=7; with flow rate of 1 mL·min$^{-1}$ and detection at 214 nm and 25°C. A linear response ($R^2$ ≥ 0.9994) was observed in the range between 3.125 and 75 μg mL$^{-1}$ for the nitrite and nitrate standard solutions. The limits of detection (LOD) and quantification (LOQ) were found as 0.25 μg mL$^{-1}$ and 0.8 μg mL$^{-1}$ for nitrite and 0.4 μg mL$^{-1}$ and 1.2 μg mL$^{-1}$ for nitrate, respectively.

The method was validated according to ICH guidelines with respect to selectivity, linearity, detection and quantitation limits, accuracy, precision. The good analytical performance verified for this method indicates that it is suitable the monitoring of nitrite and nitrate in dairy drinks based on *Zonar* Milk Serum.

***Keywords:*** *Nitrite, Nitrate, IP-RP-HPLC, validation, Zonar Milk Serum dairy drinks*

---

[a] **This paper was presented at the „1st SChR Symposium of Separation Science Section "Separation Sciences in the RChS Centenary" Organized by the Separation Science Section of SChR, October 26th, 2018, Cluj-Napoca, Romania"*

*„Babeș-Bolyai" University, „Raluca Ripan" Institute for Researh in Chemistry, 30 Fântânele Street, 400294 Cluj-Napoca, Romania.*

** Corresponding author: filip_miuta@yahoo.com; filip.miuta@ubbcluj.ro*

## INTRODUCTION

Nitrite and nitrate are naturally compounds occurring in foods, especially plant foods and vegetables, and are also used as additives in industrially processed foods. Major sources of exogenous nitrate exposure are vegetables and drinking water, whereas processed meat and animal food products are major nitrite-containing foods [1].

Nitrites and nitrates are considered harmful food additives. Maximum levels of nitrates (E 251 - E 252) have been defined in Annex II to Regulation (EC) No 1333/2008 on food additives and they were previously evaluated by the EU Scientific Committee for Food, the Joint FAO/WHO Expert Committee on Food Additives, and the European Food Safety Authority. The current acceptable daily intakes for sodium and potassium nitrate (expressed as nitrite ion) are both at 0 - 3.7 $mg \cdot kg^{-1}$ body weight per day [2].

The increasing of nitrite and nitrate level in food products as cheese, meat, and fish, commonly used as curing and preservatives, has cause serious hazards to animal and human. The presence of nitrates and nitrites in food is associated with an increased risk of gastrointestinal cancer and methemoglobinemia at infants [3].

The widespread use of fertilizers, domestic, agricultural, and industrial wastes have increased the chances of nitrite and nitrate into manufactured dairy products [4].

Traditionally, milk whey has been viewed as a by-product of dairy industry with little value for the consumers. However, in last decades, there is a growing interest focused on the nutritional properties of whey proteins and whey-derived products and its role upon human health. Therefore, the detection of nitrate and nitrite in milk is of great importance to the consumer's health [5].

The nitrate may naturally be present in milk and the level of it depends on the quality of feeding materials (i.e. water, feeds) of cows. Part of the nitrates from the ration of ruminants are converted into assimilable products in the rumen, and some will be found in the blood, organs and muscles that will be eliminated in the urine and even milk.

A study for determination of nitrate and nitrite in 100 samples of milk and milk powder in Taiwan, show that the average nitrate concentration of colostrum fortified milk, it ranged from 14.1 to 136 ppm, while in ordinary milk ranged between 57.9 and 157.6 ppm. For the whey fortified milk the average nitrate concentration ranged from 42.6 to 242.8 ppm [11].

Another study shows that the level of nitrate and nitrite content in both raw milk samples or samples collected during cold and warm months were 52.87 ± 26.9 and 70.48 ± 29.8 mg·L-1 respectively. These may be attributed to both external sources such as contamination by nitrate fertilizers, forage and agricultural drinking water [14].

Osvat at al., determined the nitrate content in mixed milk, pasteurized milk, sheep's milk and reconstituted milk powder from Romanian areas, of Iasi, Cluj-Napoca and Timisoara. They found that at the four categories of milk investigated, the maximum nitrate level for all categories was below 10 $mg \cdot L^{-1}$ [15].

Several analytical methods for the determination of nitrite and nitrate in different matrices have been reported [19]. These methods include ion chromatography (IC) [4, 10, 11], high performance liquid chromatography (HPLC) [6-8, 12, 13], differential pulse voltammetry [8], capillary electrophoresis [9] or others analytical method [19].

During the past decade, IC and HPLC methods have been developed for analysis of nitrite and nitrate, due to by their accurate and precise determinations of the compounds [4, 10, 12, 13].

Because milk is one of the most important sources for infant and babies and adults it is necessary to control the level of nitrite and nitrate in milk and dairy products, for their excess not to cause it serious health problems for consumers [4].

In this study, a simple and rapid IP-RP-HPLC method with UV detection was optimized and validated for quantification of nitrite and nitrate in five samples of dairy drinks based on *Zonar* Milk Serum.

## RESULTS AND DISCUSSION

### Developing and validation of method

The use of HPLC for the quantification and separation of the nitrite and nitrate in different matrices is one of the most commonly used techniques in the laboratory.

Thus, the ion-pair chromatographic method developed by the Najdenkoska [12] was improved, optimized and validated by us, in order to identify and quantify the nitrite and nitrate in dairy drinks based on *Zonar* Milk Serum. By using a Synergy Hydro-RP polar endcapped C18 column shows increased hydrophobic retention and polar retention compared to other C18 phases.

Also, in this method is takes place a mobile phase modification that allows the reversed-phase column (typically C-18) to separate ionic analytes which would typically not be retained otherwise.

Nitrates and nitrites are ionized compounds. Modification of the mobile phase occurs through the addition of the ion-pair reagent, *n*-octylamine, as a component [6]. As using ion-pair reagent which increase retention time and improve separation of analytes, the isocratic elution mode was adopted.

The validation of this analytical method was evaluated by the parameters: selectivity, linearity, limit of detection (LOD), limit of quantification (LOQ), accuracy and precision [16].

*Selectivity* was tested by comparing the chromatogram of a standard solution of sodium nitrite and sodium nitrate, with those of *Zonar* Milk Serum dairy drinks (Figure 1).

Our result showed that there is no interference at the retention time of nitrite and nitrate in blank and spiked *Zonar* Milk Serum samples. The retention time of nitrite and nitrate presented chromatograms were at 8.16 and 9.2 min, respectively.

*Linearity* was assessed based on a plot of the analyte peak area against analyte concentration.

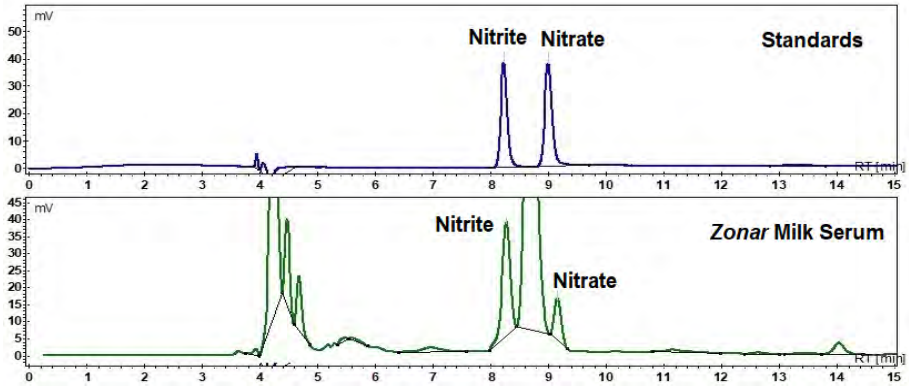


**Figure 1.** HPLC chromatograms of the standard mixture and *Zonar* Milk Serum sample.

The results proved to be linear and acceptable, as the correlation coefficients ($R^2$) were greater than 0.9994 for the two analytes (Table 1). Calibration range was between 3.125 - 75 µg·mL$^{-1}$ which is significant for our determinations.

**Table 1.** Linear regression data, LOD and LOQ of the dairy beverages.

| Parameters / compound | Nitrite ($NO_2^-$) | Nitrate ($NO_3^-$) |
|---|---|---|
| [a] RT [min] | 8.16 | 9.02 |
| [b] Calibration curve | Y=1.6294X+0.73367 | Y=1.71245X+0.68354 |
| [c] Regression coefficient $R^2$ | 0.9994 | 0.9997 |
| Linear range (µg mL$^{-1}$) | 3.125 - 75 | 3.125 - 75 |
| [d] LOD (µg mL$^{-1}$) | 0.25 | 0.4 |
| [d] LOQ (µg mL$^{-1}$) | 0.8 | 1.2 |

[a] RT, the retention time; [b] Y, the peak area; X, the concentration of reference compound (µg·mL$^{-1}$); [c] $R^2$ regression coefficient of calibration curve (n=6, six points); [d] LOD, the limit of detection (S/N = 3); [d] LOQ, the limit of quantification (S/N = 10);

The LOD values was 0.25 μg $mL^{-1}$ for nitrite and 0.4 μg $mL^{-1}$ for nitrate, respectively, and the LOQ values was 0.8 μg $mL^{-1}$ for nitrite and 1.2 μg $mL^{-1}$ for nitrate, respectively. This low values indicate a good sensitivity of the proposed method. In all samples the concentrations of both nitrate and nitrite were higher than the method LOD levels.

The intra-day and inter-day *precision* were expressed as percentage of relative standard deviation (% RSD).

The precision data are shown in Table 2 and the results show the % RSD is lower than 4.85 % for nitrite and 5.13 % for nitrate, respectively. In addition, there were no significant differences between the results of the test, indicating that the precision of the proposed method was satisfactory.

**Table 2.** Intra- and inter-day precision of nitrite and nitrate

| Comp. | Conc. (μg·$mL^{-1}$) | Intra-Day Precision (n = 6) | | Inter-Day Precision (n = 9) | |
|---|---|---|---|---|---|
| | | Measured conc. Mean [a] ± SD [b], (μg·$mL^{-1}$ | RSD [c] (%) | Measured conc. Mean [a] ± SD [b], (μg·$mL^{-1}$ | RSD [c] (%) |
| Nitrite ($NO_2^-$) | 50 | | | 50.34 ± 2.44 | 4.85 |
| | 12.5 | 12.35±0.41 | 3.36 | 12.35±0.35 | 2.86 |
| | 3.123 | | | 3.023±0.045 | 1.50 |
| Nitrate ($NO_3^-$) | 50 | | | 50.34 ± 2.58 | 5.13 |
| | 12.5 | 12.27± 0.59 | 4.81 | 11.98± 3.39 | 3.30 |
| | 3.125 | | | 3.128± 0.05 | 1.62 |

[a] Mean = Average of *n* determination; [b] SD = Standard deviation; [c] RSD = Relative standard deviation; comp. = compound; conc. = concentration.

In Table 3 are presented the recovery degree values of nitrite and nitrate in studied sample at three different concentration levels of 3.125 μg·$mL^{-1}$ (low level), 12.5 μg·$mL^{-1}$ (intermediate level) and 50 μg·$mL^{-1}$ (high level), of standard mixtures added to the *Zonar* Milk Serum sample. The recoveries are calculated as an average of the triplicate analyses.

**Table 3.** Recovery degree values of nitrite and nitrate in samples

| Compound | Recovery at low level (%) | | Recovery at intermediate level (%) | | Recovery at high level (%) | |
|---|---|---|---|---|---|---|
| | Mean [a] ± SD [b] | RSD [c] | Mean [a] ± SD [b] | RSD [c] | Mean [a] ± SD [b] | RSD [c] |
| Nitrite ($NO_2^-$) | 98.67 ± 1.27 | 1.29 | 100.98 ± 2.73 | 2.70 | 104 ± 4.45 | 4.37 |
| Nitrate ($NO_3^-$) | 97.88 ± 1.85 | 1.89 | 101.40 ± 3.29 | 3.25 | 100.68 ± 5.12 | 5.09 |

[a]Mean = Average of n determination; [b]SD = Standard deviation; [c]RSD = Relative standard deviation.

Mean recovery values for nitrite and nitrate concentration in the spiked samples at different levels were found to be between 98.88 - 104 % for nitrite and 97.88 - 101.4 % for nitrate. The RSD% values for recovery varied between 1.29 - 4.37 % for nitrite and 1.89 - 5.09 % for nitrate, respectively (Table 3). These parameters were evaluated as acceptable for validated HPLC method.

### Application of IP-RP-HPLC method for quantification of nitrites and nitrates in dairy drinks based on *Zonar* Milk Serum

The analytical method were applied for analysis of in five samples of dairy drinks based on *Zonar* Milk Serum.

The results obtained are shown in Figure 2. The samples noted with -1 and -2 represented *Zonar* dairy drinks obtained from different milk batches.

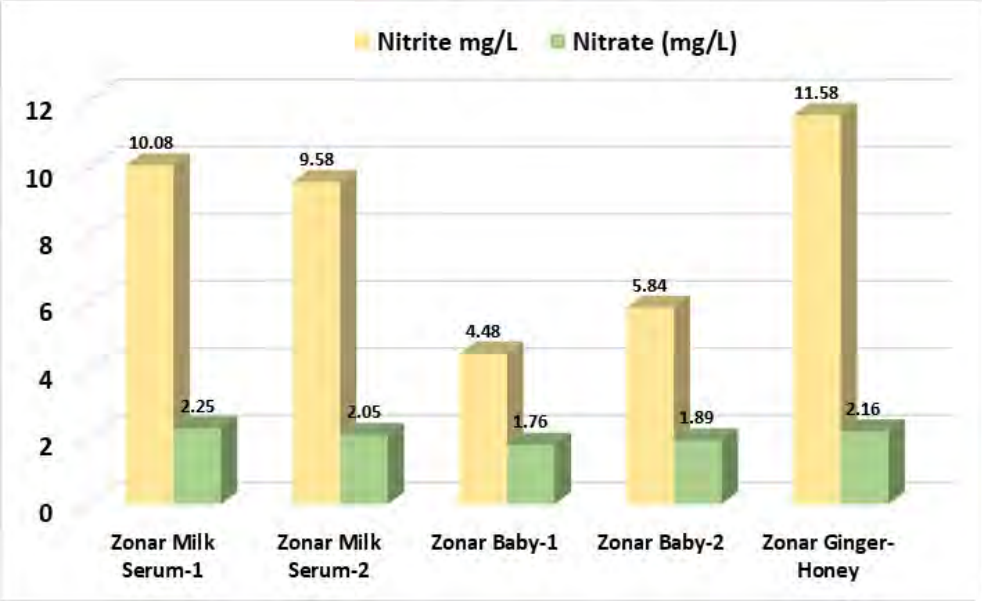


**Figure 2.** Nitrite and nitrate content in dairy drinks *based* on *Zonar* Milk Serum.

Thus, it can be observe that the amounts of nitrite and nitrate in dairy drinks based on *Zonar* Milk Serum were found in ranges of 4.48 - 11.58 $mg \cdot L^{-1}$ and 1.76 - 2.25 $mg \cdot L^{-1}$, respectively.

In *Zonar* Baby-1 and -2 samples, the dairy drinks for babies, we found the smallest amounts of nitrite (4.48 and 5.84 $mg \cdot L^{-1}$) and nitrate (1.76 and 1.89 $mg \cdot L^{-1}$) and much smaller then milk samples [11, 15]. All samples studied contain nitrites and nitrates below the permissible limit of 200 $mg \cdot L^{-1}$ by EU regulation in baby food (milk) [2].

These results obtained are comparable with literature data. The average nitrate concentrations of whey fortified milk ranged from 42.6 to 242.8 ppm and for ordinary milk ranged from 57.9 to 157.6 ppm in Taiwan [11]. The quantity of nitrate in whey samples determined by sequential injection using an in-line cadmium-reducing column were find between 0.91 and 4.76 $mg \cdot L^{-1}$ [18]. In others dairy products, mean nitrite and nitrate content ranged 0.14-0.45 mg 100 $g^{-1}$ and 1.26-5.75 mg 100 $g^{-1}$ [1]. An investigation on levels of nitrate in 95 fresh milk samples, in Romania, carried out during the years 2007 - 2010, show that the mean level of nitrate was 2.66, 2.39, 3.08, and 2.67 $mg \cdot L^{-1}$ respectively. The level of nitrate in 40 pasteurized milk samples was 2.48 and 2.75 $mg \cdot L^{-1}$ in 2009 and 2010, respectively [15].

## CONCLUSIONS

A simple and efficient IP-RP-HPLC method was successfully optimized and validated for quantification of nitrite and nitrate in some dairy drinks based on *Zonar* Milk Serum.

The developed RP-HPLC method was selective providing satisfactory accuracy with low limits of detection. It has ensured a precise quantification of nitrite and nitrate in five samples of dairy drinks based on *Zonar* Milk Serum. In *Zonar* Baby samples were obtained the smallest amounts of nitrite and nitrate.

The results of our study indicate that nitrate and nitrate levels in all samples were less then maximum limits accepted by EU regulation in baby food (milk).

Therefore, investigation of nitrite and nitrate contents in different foods would be of great importance for both safety and nutrition intake recommendation.

## EXPERIMENTAL SECTION

### Chemicals and reagents

All reagents were of analytical grade. Sodium nitrite and sodium nitrate and *n*-octylamine were purchased from Sigma-Aldrich (USA, Germany).

Analytical grade water was obtained from Milli-Q Ultrapure water purification system (Millipore, USA). The methanol of HPLC grade and phosphoric acid were purchased from Merck (Darmstadt, Germany).

**Instrumentation and chromatographic conditions**

The analyses were performed using an High Performance Liquid Chromatograph Jasco 980 (Japan) equipped with Intelligent HPLC pump (Model PU-980), low pressure gradient unit (Model LG-980-02), in-line degasser (Model DG-980-50), intelligent Column Thermostat (CO-2060), UV-Vis detector (Model UV-970/975), manual injection through a Rheodyne valve of 20 μL loop (Hamilton Rheodyne Syringe, 50 μL). Data collection and analyses were performed using ChromPass software. The separation was achieved on a Synergy Hydro-RP polar endcapped C18, 80Å 4μm (250 × 4.6 mm) column using isocratic elution. The mobile phase was composed of the mixture of 0.01M *n*-octylamine and methanol in a 90:10 (v/v) ratio, at pH=7 with phosphoric acid. All solutions were degassed and filtered through a 0.45 μm pore filter membrane (Nordic Chemicals, Romania). Using these chromatographic conditions, the retention times of nitrite and nitrate could be confirmed by the standards injection.

**HPLC sample preparation**

A volume of 2 mL of studied sample was diluted with 4 mL Millipore water and filtered through a 0.45 μm syringe filter and injected in the HPLC system.

For this study we use five dairy drinks based on Zonar Milk Serum: *Zonar* Milk Serum - n, is dairy drinks based on *Zonar* Milk Serum obtained from different milk batches, n=2; *Zonar* Baby - n is a dairy drinks based on *Zonar* Milk Serum for baby children, from different batches, n=2; *Zonar* Ginger-Honey is a dairy drinks based on *Zonar* Milk Serum with ginger extract and honey.

**Preparation of the standard solution**

Standard stock solutions (1 $mg \cdot mL^{-1}$) for each standard were prepared by dissolving the solid compound in Millipore water. The solutions were kept in the refrigerator at 4°C and were stable for three weeks. Working standard solutions were prepared as needed by appropriate dilution of the concentrated stock solutions in water.

**Method validation**

In the validation of the analytical method used to quantify the nitrite and nitrate in dairy drinks based on *Zonar* Milk Serum, the following parameters were determined: selectivity, linearity, limit of detection (LOD), limit of quantification (LOQ), accuracy and precision [16].

*Selectivity* was tested by comparing the chromatogram of a standard solution of sodium nitrite and sodium nitrate compounds, with those of studied samples.

*Linearity* was assessed based on a plot of the analyte peak area against analyte concentration. Calibration range was between 3.125 - 75 $\mu g \cdot mL^{-1}$ from each standard.

*LOD* and *LOQ* parameters were calculated as the concentration corresponding to three and ten times respectively, of the background noise of the blank (signal-to-noise ratio, S/N).

The *intra-day precision* was obtained from the data of the 6 replicate analysis of 12.5 $\mu g \cdot mL^{-1}$ standard concentration; *Inter-day precision* (three replicate for three consecutive days) determinations were performed on the three different concentrations of standard solutions; The precision was expressed as percentage of relative standard deviation (% RSD).

*Accuracy* of the method was study the recovery degree. Three different concentration levels of 3.125 $\mu g \cdot mL^{-1}$ (low level), 12.5 $\mu g \cdot mL^{-1}$ (intermediate level) and 50 $\mu g \cdot mL^{-1}$ (high level) of standard mixtures were added to the Zonar Milk Serum sample. Spiked samples were prepared in triplicate. The recovery was calculated as follows equation:

$$Recovery\ \% = \frac{Detected\ amount - Original\ amount}{Spiked\ amount} \cdot 100$$

## ACKNOWLEDGMENTS

This work was financially supported by the Romanian Programme for Research, Development and Innovation PNCDI III, Cod: PN-III-P2-2.1-BG-2016-0335, Contract no 28BG/2016, http://www.usamvcluj.ro/profi-zonar/.

The authors thank to S.C. EmbryOm Capital investment S.R.L., Satu-Mare, Romania for providing the dairy drinks samples.

## REFERENCES

1. Z. Bahadoran, P. Mirmiran, S. Jeddi, F. Azizi, A. Ghasemi, F. Hadaegh, *Journal of Food Composition and Analysis*, **2016**, *51*, 93.
2. European Commission. (2011). Commission Regulation (EC) No. 1333/2008 of the European Parliament and of the Council by establishing a Union list of food additives, Re-evaluation of sodium nitrate (E 251) and potassium nitrate (E 252) as food additives, *EFSA Journal* **2017**, *15*(6), 4787.

3. C.S. Bruning-Fann, J.B. Kaneene, *Veterinary and human toxicology*, **1993**, *35*, 521.
4. S. Chamandust, M.R. Mehrasebi, K. Kamali, R. Solgi, J. Taran, F. Nazari, M-J. Hosseini, *International Journal of Food Properties*, **2016**, *19*, 1983.
5. Ty B. Wagoner, E.A. Foegeding, *Food Hydrocolloids*, **2017**, *63*, 130-138.
6. I.M.P.L.V.O. Ferreira, S. Silva, *Talanta*, **2008**, *74*, 1598.
7. T. Tamme, M. Reinik, M. Roasto, K. Juhkam, T. Tenno, A. Kiis, *Food Additives and Contaminants*, **2006**, *23* (04), 355.
8. M. Ćurčić Jovanović, M. Djukić, I. Vasiljević, M. Ninković, M Jovanović, *Journal of Serbian Chemical Society*, **2007**, *72* (4), 347.
9. D.F. Betta, L. Vitali, R. Fett, A.C. Costa, *Talanta*, **2014**, *22*, 23.
10. I. Shah, A. Petroczi, R.A. James, D.P. Naughton, *Analytical & Bioanalytical Techniques*, **2013**, *S12*, 003. doi:10.4172/2155-9872.S12-003.
11. T.S. Yeh, S.F. Liao, C.Y. Kuo, W.I. Hwang, *Journal of Food and Drug Analysis*, **2013**, *21* (1), 73.
12. A. Najdenkoska, *Journal of Agricultural, Food and Environmental Sciences*, **2016**, *67*, 33.
13. S.S. Chou, J.C. Chung, D.F. Hwang, *Journal of Food and Drug Analysis*, **2003**, *11*(3), 233.
14. T.H. Mohamed, *Assiut Journal of Agricultural Sciences*, **2010**, *42* (2), 106.
15. M. Osvat, V. Bara, *Analele Universității din Oradea Fascicula Ecotoxicologie, Zootehnie si Tehnologii de Industrie Alimentară*, **2010**, *9*(9), 1.
16. ICH harmonised tripartite guideline. Validation of analytical procedures: Text and methodology Q2 (R1). **2005**. http://www.ich.org/fileadmin/Public_Web_Site/ICH_Products/Guidelines/Quality/Q2_R1/ Step4/Q2_R1_Guideline.pdf, pp. 1-17.
17. M.N. Moshoeshoe, V. Obuseng, S. Afr. J. Chem., **2018**, *71*, 79.
18. M.J. Reis Lima, S.M.V. Fernandes, A.O.S.S. Rangel, *International Dairy Journal* **2006**, *16*, 1442.
19. Q-H. Wang, L-J. Yu, Y. Liu, L. Lin, R. Lu, J. Zhu, L. He, Z-L. Lu, *Talanta,* **2017**, *165,* 709.

STUDIA UBB CHEMIA, LXIV, 1, 2019 (p. 207-218)
(RECOMMENDED CITATION)
DOI:10.24193/subbchem.2019.1.17

# INNOVATIVE CHEMICAL COATING PROTOCOL FOR TITANIUM ALLOY IMPLANTS

**GABRIEL ARMENCEA[a], CRISTIAN BERCE[b], MILICA TODEA[c], ADRIANA VULPOI[c], DAN LEORDEAN[d], SIMION BRAN[e]*, CRISTIAN DINU[a]*, MADALINA LAZAR[e], ONDINE LUCACIU[f], LIANA CRISAN[a], IOAN BARBUR[e], BOGDAN CRISAN[e], FLORIN ONISOR[a], SERGIU VACARAS[a], GRIGORE BACIUT[a], MIHAELA BACIUT[e]**

**ABSTRACT.** This paper aims to investigate the "*in vivo*" behavior (over an extended period of time - six months) of hydroxyapatite and $SiO_2$-$TiO_2$ coating of $Ti_6Al_7Nb$ alloy implants manufactured by selective laser melting. Innovative chemical implant coating by immersion technique was studied and the results were analyzed by optical and scanning electron microscopy (SEM). The results showed better osseointegration process for the coated implants and a much stabler biological behavior on the surface of the chemical treated implants.

***Keywords****: chemical coating, $Ti_6Al_7Nb$, surface treatment, bioactivity, SLM, laser processing*

[a] *Department of Oral and Maxillo-Facial Surgery, "Iuliu – Hatieganu" University of Medicine and Pharmacy, Cluj-Napoca, Romania*
[b] *Laboratory Animal Facility - Centre for Experimental Medicine, "Iuliu Hatieganu" University of Medicine and Pharmacy, Cluj-Napoca, Romania*
[c] *Faculty of Physics & Institute of Interdisciplinary Research in Bio-Nano-Sciences, Babes Bolyai University, Cluj-Napoca, Romania*
[d] *Department of Manufacturing Engineering, Technical University, Cluj-Napoca, Romania*
[e] *Department of Implantology and Maxillofacial Surgery, "Iuliu Hatieganu" University of Medicine and Pharmacy, Cluj-Napoca, Romania*
[f] *Department of Oral Rehabilitation, "Iuliu Hatieganu" University of Medicine and Pharmacy, Cluj-Napoca, Romania*
** Corresponding authors e-mail: dinu_christian@yahoo.com; dr_brans@yahoo.com*

## INTRODUCTION

Osseointegration improvement of titanium and titanium-based alloys is one of the most challenging tasks in modern medicine. The bioinert behaviour grants titanium the first treatment of choice when bone reconstruction is wanted, having clinical application in dentistry, orthopedics and neurosurgery [1]. The drawback of commercial pure titanium, mainly the mechanical properties, seemed to be resolved in the early 2000`s by introducing alloys such as $Ti_6Al_4V$ or $Ti_6Al_7Nb$ with improved physical properties [2]. New technologies such as SLS (Selective Laser Sintering) or SLM (Selective Laser Melting) opened the path of creating virtually any type of custom made implant with complex shape and design [3]. This led to the search for new methods of increasing the osseointegration and improving the biocompatibility of the alloys by changing the composition and the morphology of the implant surface. Different types of coatings, such as HA (hydroxyapatite), calcium phosphate or $SiO_2$ with different coating techniques (immersion-coating, high-temperature sintering, high-pressure sintering, laser cladding process) have been tested with encouraging result [4]. The current paper presents a new coating protocol of HA and $SiO_2$-$TiO_2$ solutions: immersion followed by thermal treatment for $Ti_6Al_7Nb$ implants made by SLM.

One of the most frequently encountered complications in the use of Ti implants is lack or poor osseointegration, due to fibrotic tissue formation at the implant-bone contact area [5]. The use of new surface treatment protocols may be one of the solutions to this problem and also the use of alloys that can promote osteoblast-cell growth [6].

Previous studies have analysed the osteogenic properties of Ti coatings “in vitro” and “in vivo” for periods up to 18 weeks, few of them having taken into consideration the three-dimensional characteristics of the implants [7]. Our “in vivo” study extends over a period of 24 months proving a good stability of the osseointegration in time, as well as a faster and better biological behavior for the coating protocol used.

## RESULTS AND DISCUSSION

Macroscopy examination of the specimens consisting in implant and surrounding bone showed no signs of inflammation or implant displacement at 1 or 6 months, moreover the implants with $SiO_2$-$TiO_2$ coating showed bone overgrowing the neck of the implant. Optical miscroscopy showed good osseointegration of all implants, no connective tissue at 1 and 6 months post insertion, and percentages of mineralized bone vs. osteoid (unmineralized bone) surrounding the implants were calculated with the method described by Gheban D., Armencea G. et al. [8,9,10] as presented in table 1.

**Table 1**. Percentages of mineralized bone vs. osteoid

| | 1 month | | 6 months | |
|---|---|---|---|---|
| | **Osteoid** | **Mineralised bone** | **Osteoid** | **Mineralised bone** |
| $Ti_6Al_7Nb$ | 6.37% | 93.63% | 4.56% | 95.44% |
| $Ti_6Al_7Nb$ - $SiO_2$-$TiO_2$ | 1.44% | 98.56% | 2.57% | 97.43% |
| $Ti_6Al_7Nb$ - HA | 0.82% | 99.28% | 2.70% | 97.30% |

Further investigation of the contact suface between the implant and the bony structure was done at 6 month by SEM. Perfect attachment of the bone to the implant site was noticed for both of the surface coatings (figure 1) and lacunar areas were present in the bone surrounding the uncoated implant (figure 2).

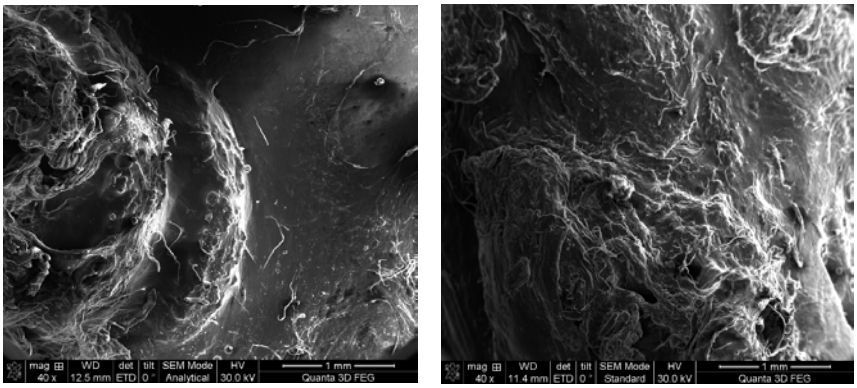

**Figure 1.** SEM at 40X magnification for the bone-implant area $Ti_6Al_7Nb$ - $SiO_2$-$TiO_2$ (left) and $Ti_6Al_7Nb$ – HA (right).

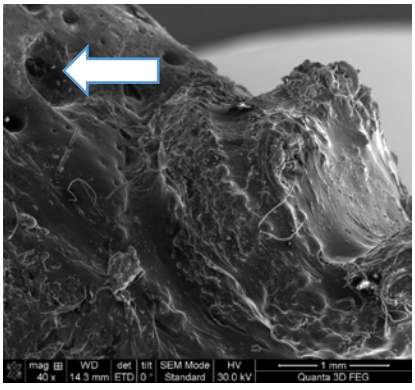

**Figure 2.** SEM at 40X magnification for the bone-implant area $Ti_6Al_7Nb$. Lacunar areas in the bone surrounding the implant (white arrow).

Greater magnification of the lacunar areas around the implant (300X) revealed round shape particles into the bone foramens that can be alloy particles detached from the implant body (figure 3), in the absence of the coating material.

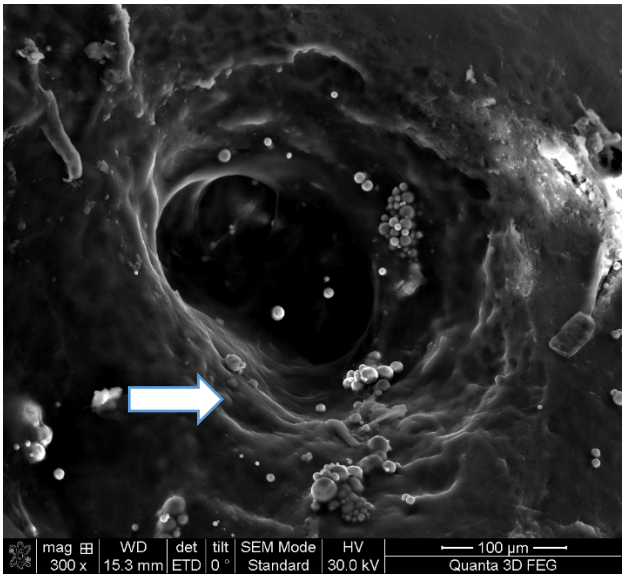


**Figure 3.** SEM 300X magnification of the bone foramen next to the $Ti_6Al_7Nb$ implant showing round particles (white arrow) migrated into the lacunae

Implant osseointegration is considered to be perfect when there is no gap between the implant and the surrounding tissue, when no connective or granulative tissue exists at the implant surface [11]. None of the above were seen in our study. Better, faster and stabler osseointegration are difficult tasks to be achieved for the Ti alloys. The quality of the osseointegration (the amount of mineralized new bone formed) on the external aspect of the implant depends on the type of alloy used, on the surface morphology and coatings of the implant [12]. It is clinically proven that Ti and its alloys have a better biological behaviour than other alloplastic materials [13]. These characteristics are due to the bioinert behaviour of Ti, it alone never promoting positive effects on the recipient sites but, most notable, preventing negative biological effects from happening [14]. Osseointegration enhacement, which is an ongoing process until 6 months after insertion, can be achieved by surface treatments. Over time several types of materials such as HA, bioreactive glass, $SiO_2$, $SiO_2$-$TiO_2$, $SiO_2$-HA and different types of coating or

cladding have been tried (laser cladding, dip coating-sintering technique, immersion-coating technique, HIP - hot isostatic pressing - technique, sputter) with promising results [15].

The best “in vitro” results were obtained by immersion-coating techniques, other methods having serious limitation to be considered for “in vivo” studies because of adverse effects caused by high-temperature sintering cycle on the mechanical properties of the metallic substrate materials and loss of the alloy wrought structure [16]. Combination of HA and $SiO_2$ proved to be ineffective in promoting cell adhesion [17]. Other authors recommend a sputter coating to be method of choice for forming a dense, adherent coating of HA onto a metal substrate [15, 16].

We have chosen to test the immersion technique for HA and $SiO_2$-$TiO_2$ coating of $Ti_6Al_7Nb$ under specific controlled physico-chemical environment that leads to even surface distribution of the coating material. We considered the “in vivo” test for $Ti_6Al_7Nb$ alloy because it represents a better choice for the commercial $Ti_6Al_4V$ that proved to be cytotoxic and causing neurological problems under certain conditions [18, 19]. We studied the behavior of the implants in time, due to the dynamic mineralization and demineralization that the bone structure around the implant has, monitoring the healing process from implant insertion up to six months [20]. Other studies of similar implants proved that demineralization processes can be encountered even at 6 months after implant insertion [9], so extensive follow-up is mandatory.

Macroscopically all the implants in this study proved to be stable at 1 and 6 months, the best result having the group with $SiO_2$-$TiO_2$ coating, that showed bone overgrowth at 6 months even at the neck of the implant, so the implant bone embedding was extensive.

Optical microscopy and calculation of mineralized bone at the implant surface presented similar results for the coated implants, with higher amount of mineralization vs. the uncoated control group; result similar with other studies [20, 9]. This shows the better biological behavior of the coated implants, without any significant changes from 1 to 6 months (98.56% to 97.43% for the $SiO_2$-$TiO_2$ coating and 99.28% to 97.30% for $Ti_6Al_7Nb$ – HA coating). However, the top mineralization surrounding the implant is present at the HA coating group at 1 month, and at 6 months both coatings have reached a stable degree of bone mineralization of about 97%, explicable by the physiological bone remodeling [21]. Even without coating, the alloy has a good percentage of mineralization, due to the fact that Nb oxides are similar to Ti oxides being stable in time, corrosion-free and thus a better chemical and biological stability than pure Ti or $Ti_6Al_4V$. The difference in mineralization surrounding the implant can be explained

by the difference in surface morphology, coated implants having a more homogenous surface than the uncoated ones [22]. $SiO_2$-$TiO_2$ coating has the potential of electric barrier able to reduce the corrosion process, thus creating best premises for osseointegration [10,23]. Several studies have demonstrated good cell adhesion on HA or $SiO_2$-$TiO_2$ laser cladded or immersed coatings, changes in surface chemistry and surface morphology that improves bioactivity and biocompatibility of titanium endosseous implants [4]. However, the majority of these studies were done “in vitro”, and had no quantification method for the newly formed bone at the interface of the implant. Our “in vivo’ study supports by numerical percentage quantification similar studies, showing the best bone apposition on coated implants, the immersion chemical protocol for coating being one of the most facile and stable.

In our immersion chemical coating protocol, the treatment can be easily distributed on the implant surface more homogenously than other options like cladding, spraying or sputtering the substance. This even distribution of an uniform HA or $SiO_2$-$TiO_2$ solution most likely is the main factor for obtaining mineralization results close to 100% on the implant surface.

SEM was another investigation done to check the microscopic behavior of the bone–implant site; the examination was performed 6 months from implantation, time when theoretically the bond implant-bone is most stable. In the uncoated group lacunae were observed in large numbers in the bone structure next to the implant, and for the coated implants no lacunae were seen. These hollow structures can be Howship lacunae – erosions caused by osteoclasts` enzymes, caused by an intense remodeling of the bone structure next to the uncoated implants [24]. Osteoclasts remodel the bone structure, so at 6 months there still is an ongoing remodeling process at the surface of uncoated implants, on the other hand the coated implants look more stable in terms of bone remodeling. The coating procedure with HA and $SiO_2$-$TiO_2$ proved to inhibit the natural osteoclast activity, seen in the control group or in physiological bone remodeling [25]. The surface structure of coated implants suffers changes of greater corrosion resistance and also in apatite formation due to the occurrence of passive oxide layer [26]. Future studies should be done to investigate the osteoblasts and osteocytes adhesion on coating materials such as HA or $TiO_2$, as well as the possibility to create osteoclastic inhibition [27, 28].

In the bone lacunae of the control group round particles were observed with 300X SEM magnification. These particles could be alloy parts that can migrate in the surrounding bone during implant insertion. No signs of particle detachment were seen for the coated groups, meaning that the coating material has a stabilizing role for the $Ti_6Al_7Nb$ alloy or at least creates a better surface environment more suitable for osseointegration.

## CONCLUSIONS

The immersion technique for HA and $SiO_2$-$TiO_2$ coatings proves to be an efficient, simple and reliable process to enhance osseointegration and to biologically stabilize the surface of Ti alloy implants. This procedure offers an important alternative to the currently challenging problem of osseointegration improvement.

Future “in vivo” studies should be conducted in order to analyze the cellular behavior at the surface of these alloys.

## EXPERIMENTAL SECTION

In order to study the biological behavior of the surface treatment, 30 screw type implants were manufactured by SLM (figure 4), divided into 3 groups: coating free (control group), HA and $SiO_2$-$TiO_2$ coating groups. The devices were inserted into the femur of New Zealand White Rabbits, and samples containing the implants and the surrounding bone were harvested one and six months post insertion. The samples were studied by optical and scanning electron microscopy (SEM).

### *Implant design*

The implants were manufactured from $Ti_6Al_7Nb$ alloy powder (ATI Allvac, Monroe NC, USA) by selective laser melting technology (Realizer SLM 250 machine, Realizer GmbH, Borchen, Germany) with a controlled porosity of 24–25%, as determined through Archimede’s method ISO 2738–99 (figure 4).

Earlier published results, proved that the density and porosity of samples manufactured by SLM method using a laser power of 50 W are 3.43 g $cm^{-3}$, 25% total porosity and 25% open porosity, while by increasing the applied laser power above 50 W, the density of the SLM manufactured samples increases and the porosity decreases. Moreover, the samples obtained with low laser power of 50 W display mainly irregular interconnected pores with a minimum diameter of 70–100 μ and a maximum diameter of 200–400 μ [29].

Screw-type shape led to perfect primary stability of the implants (mandatory condition to promote osseointegration). The devices had 10 mm length and 3.3 mm diameter. The implants were divided into three categories: control group - $Ti_6Al_7Nb$ with no surface treatment; $Ti_6Al_7Nb$ with HA and $Ti_6Al_7Nb$ with $SiO_2$-$TiO_2$ coating.

**Figure 4.** Final shape of $Ti_6Al_7Nb$ implants after SLM, before the coating process

Physical properties of the alloy are: melting temperature 2,800 - 3,000°F (1,538 - 1,649°C); density 0.163 lbs/cu. in.; 4.52 gm /cc. Chemical and mechanical properties are showed in table 2 [30].

**Table 2.** Chemical and mechanical properties of $Ti_6Al_7Nb$ [30].

| **Chemical Composition** | | | | | | | | | |
|---|---|---|---|---|---|---|---|---|---|
| | **Al** | **Nb** | **Ta** | **Fe** | **O** | **C** | **N** | **H** | **Tl** |
| % w/w min. | 5.5 | 6.5 | - | - | - | - | - | - | Bal. |
| % w/w max. | 6.5 | 7.5 | 0.50 | 0.25 | 0.20 | 0.08 | 0.05 | 0.009 | Bal. |

| **Mechanical Property Data** | | | | | | |
|---|---|---|---|---|---|---|
| | **Product Form and Condition** | **Thickness, inches** | **UTS, min ksi (MPa)** | **YS 0.2%, min ksi (MPa)** | **% El, min.** | **% RA, min.** |
| ASTM F 1295 | Bar, Rod, and Wire Annealed and Cold Finished | Up to 4.00 in. diameter or thickness | 130.5 (900) | 116 (800) | 10 | 25 |
| ISO 5832-11 | Bar Annealed and Cold Finished | Up to 100 mm diameter or thikness | (900) | (800) | 10 | 25 |

Specification minimum values

***Chemical coating protocol***

The surface coating was done as follows:

The hydroxyapatite solution was prepared and included two types of calcium phosphate precipitates: A (pH=4.5) and B (pH=10). The precipitates were obtained by wet chemical precipitation from $Ca(NO_3)_2.4H_20$ and $(NH_4)_2HPO_4$ (Sigma Aldrich, St. Louis, Missouri, USA).

Calcium phosphate was synthesized based on a wet chemical precipitation method at room temperature using calcium nitrate tetrahydrate ($Ca(N0_3)_2 \cdot 4H_20$) and diammonium hydrogen phosphate ($(NH_4)_2HPO_4$). All chemicals were reagent grade (Sigma Aldrich, St. Louis, Missouri, USA) and used without further purification. Diammonium hydrogen phosphate hydrolyzed sol was added dropwise to the constantly stirred aqueous calcium nitrate solution at the molar ratio of Ca to P equal to 1.67. The mixed sol solution was then continuously stirred for about 50 minutes to obtain a white consistent sol with pH=4.5. The precipitate was taken at an aging time period of one week at room temperature. After infiltration and a suitable heat treatment, calcium phosphate turns into apatite type material.

The $SiO_2$-$TiO_2$ solution was prepared by sol-gel method from titanium isopropoxide (TIP), with the formula $Ti(OCH(CH_3)_2)_4$, and tetraethylorthosilicate (TEOS), with the formula $Si(OC_2H_5)_4$. The first stage of $SiO_2$-$TiO_2$ solution preparation included the hydrolysis of $Ti(OCH(CH_3)_2)_4$ in order to form a uniform solution. Ethanol and nitric acid were used to dilute the titanium isopropoxide to form a transparent colloid. The obtained molar ratio of $Ti(OCH(CH_3)_2)_4$:$C_2H_5OH$:$H_2O$:HCl was 1:15:10:0.89. The second stage included TEOS hydrolysis with a molar ratio of $Si(OC_2H_5)_4$:$C_2H_5OH$:$H_2O$:HCl = 1:7:6:25:0.28. The $SiO_2$-$TiO_2$ solution was obtained by adding the $TiO_2$ solution to $SiO_2$ solution. The final solution was left at room temperature for 30 minutes to obtain a proper homogenization.

The coating procedure was performed by immersion of the screws either into hydroxyapatite (HA) or $SiO_2$-$TiO_2$ solutions and kept in vacuum (100 mbar) for 15 minutes. After immersion the implants were placed for 30 minutes in an 100°C oven. A thermal treatment was conducted at 600°C for 30 minutes in the case of hydroxyapatite implants (figure 6 a) and at 400°C for 60 minutes for the $SiO_2$-$TiO_2$ implants (figure 6 b). The implants were sterilized using dry heat at 180°C for 2 hours.

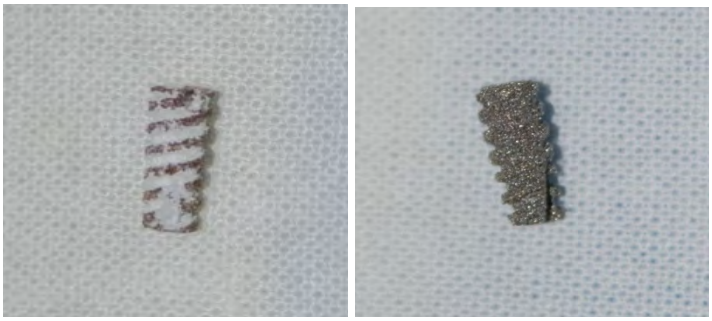

**Figure 6.** a) $Ti_6Al_7Nb$ implant coated with HA; b) $Ti_6Al_7Nb$ implant coated with $SiO_2$-$TiO_2$

***Experimental design***

Ten male rabbits of the New Zealand White Rabbits (Oryctolagus cuniculus) breed were used. The vivarium conditions were according to the EU Directive 63/2010. Ethics Committee approval was obtained (No. 407/03.12.2014). The control and coated implants were inserted into the femur of the specimens by low speed drilling and continuous cooling method with a torque among 25 to 30 Ncm, having perfect initial stability. Half of the specimens were sacrificed at one month and half at 6 months. The samples were prepared for optical microscopy evaluation and quantification of the quality and quantity of the bone surrounding the implants with the method described by Gheban D., Gamal M. et al., Armencea G. et al. [8, 9,31]. Scanning electron microscopy of the bone surrounding the implant was done.

## ACKNOWLEDGMENTS

This paper was published under the frame of European Social Fund, Human Resources Development Operational Programme 2007–2013, project no. POSDRU/159/1.5/S/138776.

## REFERENCES

1. A. Insua, A. Monje, H.L. Wang, R.J. Miron, *J Biomed Mater Res A,* **2017**, *105* (*7)*, 2075.
2. L. Bolzoni, E.M. Ruiz-Navas, E. Neubauer, E. Gordo, *J Mech Behav Biomed Mater*, **2012**, *9*, 91.

3. S. Ponader, C. von Wilmowsky, M. Widenmayer, R. Lutz, P. Heinl, C. Körner, R. F. Singer, E. Nkenke, F. W. Neukam, K.A. Schlegel, *J Biomed Mater Res A*, **2010**, *92*, 56.
4. Y. Yang, K. Serpersu, W. He, S. Paital, N.B. Dahotre, *Materials Science and Engineering*, **2011**, *31,* 1643.
5. K. Kordbacheh, J. Finkelstein, P.N. Papapanou, *Clin Oral Implants Res*, **2019**, *15*, 145.
6. E. Pippenger, M. Rottmar, B.S. Kopf, S. Stübinger, T.F.H. Dalla, S. Berner, K.M. Weber, *Clin Oral Implants Res*, **2019**, *30*, 99.
7. A.B. Novaes, S. L. de Souza, R. R. de Barros, K. K. Pereira, G. Lezzi, A. Piattelli, *Braz Dent J*, **2010**, *21*, 471.B.
8. D. Gheban, *J Rom Patologie*, **2005**, *8,* 193.
9. G. Armencea, C. Berce, H. Rotaru, S. Bran, D. Leordean, C. Coada, M. Todea, C.A. Jula, D. Gheban, G. Baciut, M. Baciut, R.S. Campian, *Clujul Med*., **2015**, *88*, 408.
10. G. Armencea, C. Berce, H. Rotaru, S. Bran, S. Vesa, D. Leordean, C.A. Jula, D. Gheban, M. Lazar, G. Baciut, M. Baciut, R.S. Campian, *Optoelectronics and Advanced Materials-Rapid Communications*, **2015**, *9*, 865-871.
11. M. Ramazanoglu, Y. Oshida, I. Turkyilmaz, *Implant Dentistry-A Rapidly Evolving Practice*, **2011**, *31*, 134.
12. K. Søballe, *Acta Orthop Scand Suppl*, **1993**, *255*, 1-58.
13. Eisenbarth, D. Velten, M. Müller, R. Thull, J. Breme, *Biomaterials*, **2004,** *25,* 5705.
14. C. Castellani, R.A. Lindtner, P. Hausbrandt, E. Tschegg, S.E. Stanzl-Tschegg, G. Zanoni, S. Beck, A.M. Weinberg, *Acta Biomater*., **2011**, *7*, 432.
15. Y. Yang, S. Paital, N.B. Dahotre, *J of Materials Science. Materials in Medicine*, **2010**, *21*, 2511.
16. W.R. Lacefield, N.Y. Ann, *Acad Sci*, **1988**, *523,* 72.
17. T. Moskalewicz, A. Babkiewicz, B. Dubiel, M. Kot, A. Radziszewska, A. Łukaszczyk, *Archives of Metallurgy and Materials*, **2016***, 61*, 52.
18. V. Sansone, D. Pagani, M. Melato, *Clin Cases Miner Bone Metab*, **2013**, *10*, 34.
19. C.C. Gomes, L.M. Moreira, V.J. Santos, A.S. Ramos, J.P. Lyon, C.P. Soares, F.V. Santos, *Genet Mol Biol*, **2011**, *34*, 116.
20. T.L. Alzubaydi, S.S. Alameer, T. Ismaeel, A.Y. Alhijazi, M. Geetha, *J Mater Sci Mater Med*, **2009**, *20*, 35.
21. B. Shuai, L.Shen, Y. Yang, C. Ma, R. Zhu, X. Xu, *PLoS One*, **2015**, *10*, 110.
22. R. Family, M. Solati-Hashjin, N. S. Namjoy, A. Nemati, *Caspian J Intern Med*, **2012**, *3*, 460-466.
23. M. Hussein, A. Mohammed, N. Al-Aqeeli, *Materials*, **2015**, *8*, 2749.
24. S.L. Teitelbaum, *Science*, **2000**, *289*, 1504.
25. M.G. Mullender, R. Huiskes, H. Weinans, *Journal of Biomechanics*, **1994**, *27*, 1389.
26. M. Todea, A. Vulpoi, C. Popa, P. Berce, S. Simon, *Journal of Materials Science & Technology*, **2019**, *35*, 418.

27. R. Barabas, M. Rigo, M.E. Bodogh, C. Moisa, O. Cadar, *Studia UBB Chemia*, **2018**, *LXIII*, 137.
28. O. Cadar, R. Balint, G. Tomoaia, D. Florea, I. Petean, A. Mocanu, O. Horovitz, M.T. Cotisel, *Studia UBB Chemia*, **2017**, *LXII*, *4*, Tom II, 269.
29. T. Marcu, M. Todea, L. Maines, D. Leordean, P. Berce, C. Popa, *Powder Metall*., **2012**, *55*, 309.
30. ATI Titanium 6Al-7Nb Alloy, *Technical Data Sheet*, *http://www.atimetals.com/allvac/pages/PDF/ tech/TI-023%20Ti-6Al-7Nb%20.pdf*
31. M.D. Gamal, M. Mohamed, M.E. Hussiein, M.E. Beltagi, *J. Gastroenterology and Hepatology*, **2004**, *19*, 78.

STUDIA UBB CHEMIA, LXIV, 1, 2019 (p. 219-231)
(RECOMMENDED CITATION)
DOI:10.24193/subbchem.2019.1.18

# DEVELOPMENT OF A RAPID CAPILLARY ZONE ELECTROPHORESIS METHOD TO QUANTIFY LEVOFLOXACIN AND MELOXICAM FROM TRANSDERMAL THERAPEUTIC SYSTEMS

**AURA RUSU[a], PAULA ANTONOAEA[a], ADRIANA CIURBA[a,*], MAGDALENA BÎRSAN[b], GABRIEL HANCU[a], NICOLETA TODORAN[a]**

**ABSTRACT.** Capillary zone electrophoresis (CZE) could be a useful technique for the quantification of active substances from transdermal therapeutic systems (TTSs). TTSs are pharmaceutical forms in development that may release one or more active substances with some significant advantages as increased compliance to treatment, avoidance of first hepatic passage and low manufacturing costs. A simple, reliable, efficient, and low-cost CZE method was developed and validated for the simultaneous determination of levofloxacin (fluoroquinolone) and meloxicam (non-steroidal anti-inflammatory) from TTSs. The selected experimental parameters were 50 mM borax (pH 9.3) as background electrolyte, +25 kV applied voltage, 50 mbar/5 seconds hydrodynamic injection and 40°C temperature, using an uncoated fused-silica capillary with (51 cm total length/43 cm effective length, 50 µm i.d.). CZE experiments were performed in less than four minutes with a resolution of 7.79 at a wavelength of 335 nm. Validation of the method presented good linearity data, precision (RDS% < 1 for migration times and RDS% < 2 for peaks area) and sensitivity (LOD 3.43 and 16.05 $\mu g \cdot mL^{-1}$, LOQ 10.38 and 54.55 $\mu g \cdot mL^{-1}$ for levofloxacin and meloxicam, respectively). Recovery of the active substances ranged between 85.14% and 96.38%. Our developed CZE method proved its applicability for analysis of the two substances from TTSs.

***Keywords:*** *levofloxacin, meloxicam, capillary zone electrophoresis, transdermal therapeutic systems*

[a] *University of Medicine, Pharmacy, Sciences and Technology of Târgu Mureş, Faculty of Pharmacy, 38 Gheorghe Marinescu str., RO-540139, Târgu Mureş, Romania*
[b] *"Grigore T. Popa", University of Medicine and Pharmacy of Iaşi, Faculty of Pharmacy, 16 Universitatii str., RO-700115, Iaşi, Romania,*
** Corresponding author adriana.ciurba@umftgm.ro*

## INTRODUCTION

Capillary electrophoresis (CE) is an analytical method increasingly used in the analysis of pharmaceutical products due to several advantages related to its simplicity, rapid method development and the low-costs of operation. Besides, this method may also be appropriate for the analysis of the complex samples, where analytes can be separated due to their different electrophoretic behaviour [1]. Capillary Zone Electrophoresis (CZE) is the simplest CE technique in which the analytes are separated using a simple buffer, without any additives, the separation taking place due to the differences between the own electrophoretic mobilities of the analytes. Our primary objective was the development, optimization and validation of a simple CZE method for the quantification of two active substances from new experimental transdermal therapeutic systems (TTSs).

TTSs are generally referred to as "patches". These are innovative pharmaceutical forms that may include one or more pharmaceutically active substances. Although there are many challenges in the TTS design (e.g. permeability and skin irritation) the advantages of using these devices are unquestionable as the administration of these pharmaceutical forms can improve the patient's adherence and compliance to treatment by reducing the frequency of dosing (a TTS per day up to a TTS per week) in the conditions where the first hepatic passage is avoided (thus requiring lower doses), which makes it possible to reduce both treatment and manufacturing costs [2,3]. The two selected active substances in this study are levofloxacin (LVF) and meloxicam (MLX) (Figure 1).

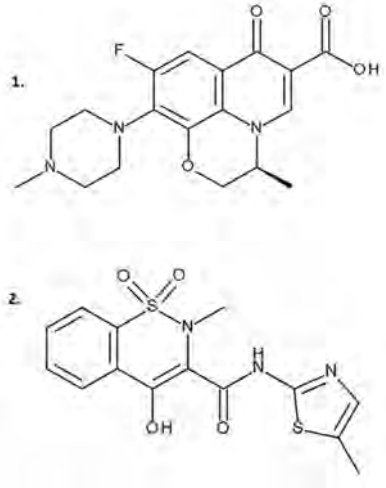


**Figure 1.** Chemical structures of LVF **(1)** and MEL **(2)**.

LVF ((*S)*-9-fluoro-2,3-dihydro-3-methyl-10-(4-methylpiperazin-1-yl)-7-oxo-7H-pyrido[1,2,3-de]-1,4-benzoxazine-6-carboxylic acid), is a third-generation fluoroquinolone, the levorotatory isomer of ofloxacin. The antibacterial spectrum of LVF includes Gram-positive bacteria, Gram-negative bacteria and atypical bacteria. LVF is indicated in the treatment of a variety of bacterial infections and is administered both internally and externally [4,5]. Several studies and patents for topical pharmaceutical products with LVF are already published in the literature [6-9].

MLX (4-hydroxy-2-methyl-N-(5-methylthiazol-2-yl)-2H-1,2-benzothiazine-3-carboxamide 1,1-dioxide) is an effective non-steroidal anti-inflammatory drug (NSAID) which is used in the treatment of rheumatoid arthritis, osteoarthritis, and ankylosing spondylitis. In the last decade, several studies have been published regarding preparation and testing TTSs containing MLX with encouraging results in skin permeability [10-13].

Co-administration of a fluoroquinolone with an NSAID in a TTS may be beneficial in both local and systemic treatment. However, few previous studies have followed this possible association. At the administration of MLX, a significant decrease of plasma antioxidant activity occurs and also when LVF is co-administered with MLX in rabbits; the body weight of the rabbits was not influenced [14]. Other similar studies present the effects on oxidative balance in blood and the immunolocalisation of ABCG-2 transporter protein in rabbit retina [15,16]. Another research shows that co-administration of MLX with ofloxacin in goats does not require any adjustment in dosage regimens, but in another study addressed on cross-bred calves, it is recommended the change of LVF dosage when is co-administered with MLX [17,18].

The aim of our study was the development of a new CZE method applicable for the simultaneous quantification of two active substances (LVF and MLX) from three different experimental TTS formula.

## RESULTS AND DISCUSSION

Several previously published CE methods analysed both LVF and MLX. The used background electrolyte (BGE) solutions are summarized in Table 1.

**Table 1.** The BGE composition used in different CE methods for the analysis of LVF and MLX *(Ref. – References).*

| **LVF** | | **MLX** | |
|---|---|---|---|
| ***BGE composition*** | ***Ref.*** | ***BGE composition*** | ***Ref.*** |
| 25 mM borax (pH 9.2) | [19] | 100 mM borax buffer (pH 8.5) | [22] |
| 60 mM hydroxylpropyl-beta-cyclodextrin in 50 mM phosphate buffer (pH 2.30) | [20] | 10 mM Tris buffer with 60 mM sodium octane-sulfonate and 20% acetonitrile (pH 11) | [23] |
| 20 mM phosphate buffered (pH 8.0) | [21] | 18 mM sodium phosphate buffer (pH 5.90) | [24] |

The p$K_a$ values for LVF and MLX are very similar (as HA - protonated form a weak acid). Also, the results of previous research regarding the separation of a large number of antibacterial quinolones have been taken into consideration, research in which the selected BGE was 25 mM borax [25]. By correlating the information presented in Table 1 with the physical properties of the two active substances comprised in Table 2 it was considered that an appropriate BGE for our separation method might be a solution containing 25 mM borax at pH 9.3.

**Table 2.** Physical properties of LVF and MLX *(MW – molecular weight, HA – a protonated form a weak acid, $BH^+$ -a protonated form of a weak base, DMF – dimethylformamide).*

| **Compound** | **MW ($g \cdot mol^{-1}$)** | **Solubility** | **p$K_a$** | **Log*P*** | **Ref.** |
|---|---|---|---|---|---|
| **LVF** | 361.37 | freely soluble in glacial acetic acid, chloroform, sparingly soluble in water | (HA) 5.59 ($BH^+$) 7.94 | 1.268 | [26,27] |
| **MLX** | 351.4 | insoluble in water, soluble in DMF, very slightly in methanol; $1.736\ M \cdot 10^{-3}$ (in 0.2 M phosphate buffer pH 7.4 at 37 °C) | (HA) 4.5 ($BH^+$) 3.05 | 2.71 | [28-31] |

LVF shows maximum absorption in UV at 300 nm and an additional maximum absorption of 327 nm [32,33]. MLX shows maximum absorption in UV light at 360 nm [34,35]. Thereby, the appropriate wavelength for the determination of both substances was set at 335 nm. To optimise the CZE method, the influence of BGE concentration, pH, applied voltage, injection pressure, injection time, and system temperature on the separation were analysed systematically using a “one factor at a time” optimization approach. The maximum current flow was set to 150 µA, to avoid instability of the electrophoretic system [36].

Figure 2 shows the influence of BGE concentration, pH of the BGE, voltage, and temperature on the migration times in the optimisation process.

The pH of the BGE was adjusted by addition of NaOH 1M and boric acid 1M. Thus, the best separation conditions were selected to provide adequate migration time and good peak symmetry, resolution, and selectivity (Figure 3).

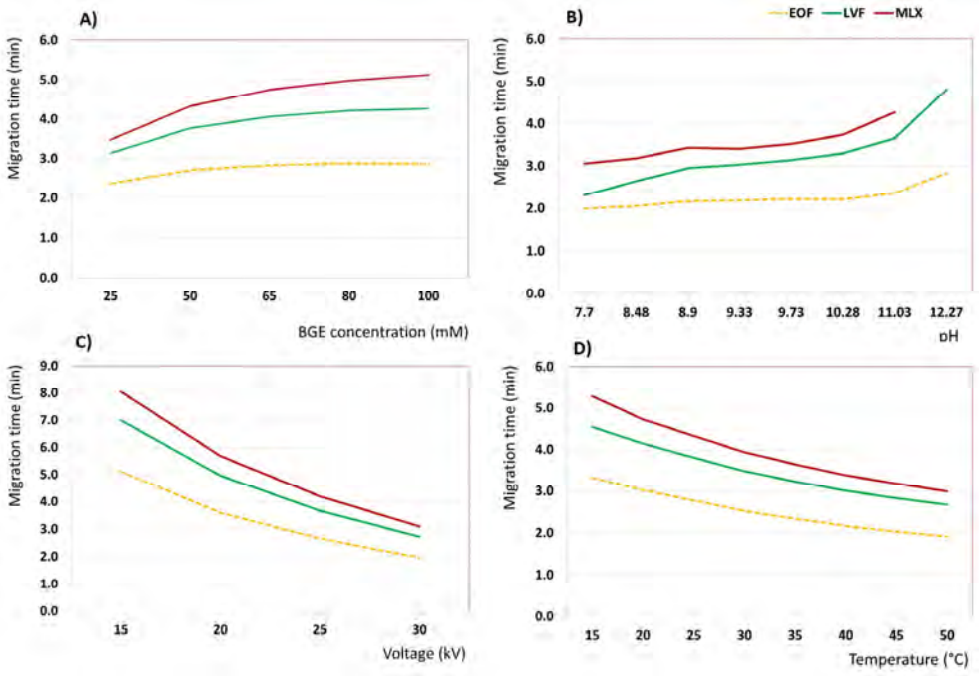


**Figure 2.** The influence of **A)** BGE concentration, **B)** pH of the BGE, **C)** voltage and **D)** temperature on the migration times in the optimisation process of the CZE method.

The best separation using the optimised analytical conditions of LVF and MLX by CZE is represented in Figure 4 and the parameters of the CZE experiment in Table 3.

**Method validation.** The method was verified regarding validation parameters according to ICH Q2(R1) Guideline [37]. The specificity of the method was proved using the UV spectra and the migration times of the analytes Thereby, the LVF and MLX could be identified simultaneously from a mixture without any interference. The migration order was established as being: LVF followed by MLX. As in the preliminary experiments, the EOF migration time values were constantly similar; we considered that it was not necessary to use an internal standard. Linearity and detectability (limit of detection – LOD, limit of quantification – LOQ) of the method were also determined. Thus, an excellent linear signal-concentration relationship for the two compounds was demonstrated (Table 4).

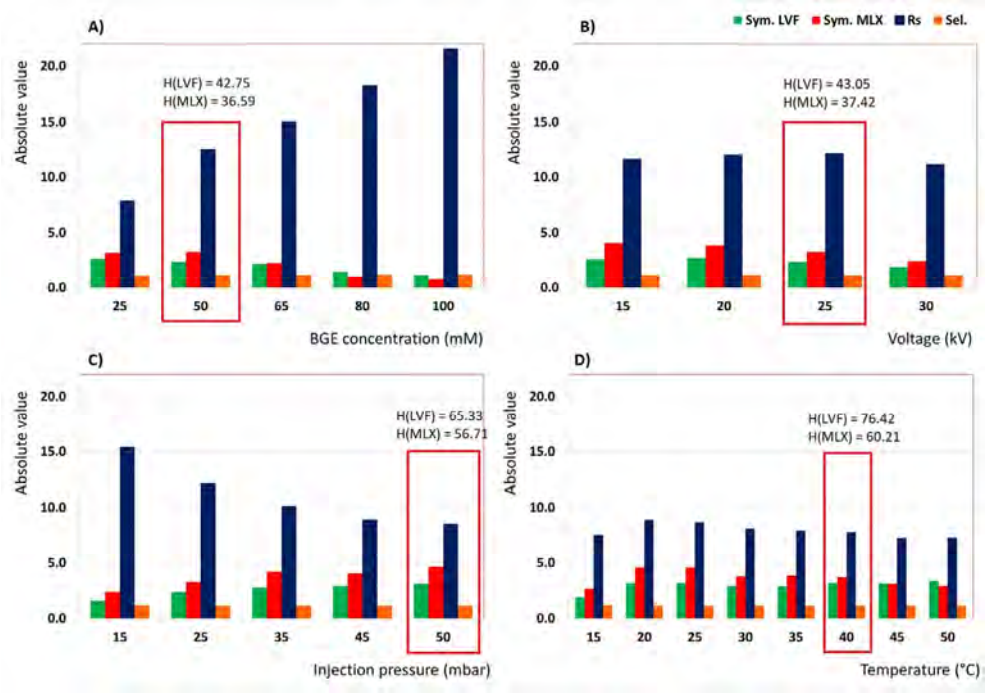


**Figure 3.** Variation of symmetry, resolution and selectivity of analytes signals in terms of **A)** BGE concentration, **B)** voltage, **C)** injection pressure and **D)** temperature *(Sym. – symmetry, Rs – resolution, Sel. – selectivity, H – height of peak)*.

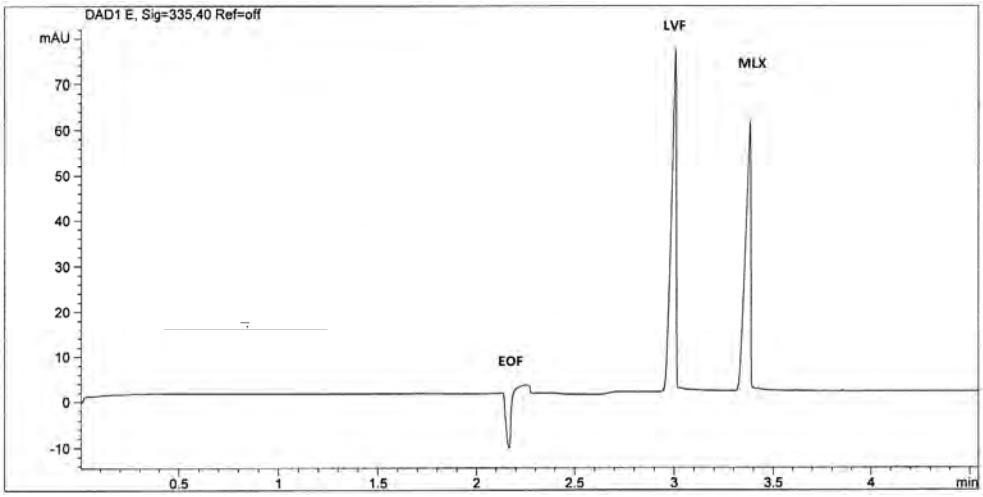


**Figure 4.** The electropherogram of LVF and MLX separation (BGE 50 mM borax, +25 kV applied voltage, 50 mbar/5 seconds hydrodynamic injection, 40°C temperature).

**Table 3.** Electrophoretic parameters of LVF and MLX separation using the optimized analytical conditions (EOF migration time 2.17, concentration 0.5 mg · mL-1) *(MT – migration time, A – area, H – height, Sym. – symmetry, P – plates, Res. – resolution, Sel. – selectivity).*

| **Compounds** | **MT** (min) | **A** (mAU*s) | **H** (mAU) | **Sym.** | **P** | **Res.** | **Sel.** |
|---|---|---|---|---|---|---|---|
| **LVF** | 3.00 | 128622 | 76.30 | 3.19 | 67497 | - | - |
| **MLX** | 3.38 | 112586 | 57.99 | 3.71 | 73023 | 7.79 | 1.13 |

LOD and LOQ were calculated based on the standard deviation of the response (Sy.x) and the slope (S). Excellent correlation coefficients and low detection limits for LVF and MLX were obtained. The LOD and LOQ for LVF are comparable with those previously published in the literature [19], while for MLX are slightly higher than other in published materials [23]. The concentration range of the method is between 6.25 $\mu g \cdot mL^{-1}$ – 1000 $\mu g \cdot mL^{-1}$. Also, the robustness of the CZE method is supported by the variation of internal (system temperature, applied voltage, injection parameters) and external (BGE composition, concentration, pH) parameters in the optimisation part of the research.

**Table 4.** Linearity and detection limits of the separation CZE method.

| Linearity parameters and detection limits | LVF | MLX |
|---|---|---|
| Regression equation | y = 267.44x + 0.1345 | y = 238.48x - 0.8388 |
| Correlation coefficient | 0.9990 | 0.9983 |
| Y intercept | 0.1345 | -0.8388 |
| Slope of the regression line (S) | 267.44 | 238.48 |
| Standard deviation of residuals from the line (Sy.x) | 0.2777 | 1.3010 |
| LOD (μg·mL$^{-1}$), calculated LOD = $\frac{3.3\ Sy.x}{S}$ | 3.43 | 16.05 |
| LOQ (μg·mL$^{-1}$), calculated LOQ = $\frac{10\ Sy.x}{S}$ | 10.38 | 54.55 |

**Table 5.** The obtained RDS% values for intra-day and inter-day precision *(Conc. – concentration, RSD – residual standard deviation).*

| Compound | Conc. (μg·mL$^{-1}$) | Intra-day precision (RSD%) n = 6 | | | Inter-day precision (RSD%) n= 18, days 3 | | |
|---|---|---|---|---|---|---|---|
| | | $MT_{EOF}$ | MT | A | $MT_{EOF}$ | MT | A |
| **LVF** | **500** | 0.228 | 0.167 | 1.456 | 0.849 | 0.824 | 1.396 |
| | **300** | 0.765 | 0.807 | 1.366 | 0.738 | 0.629 | 1.969 |
| | **100** | 0.218 | 0.273 | 1.514 | 0.378 | 0.398 | 1.740 |
| **MLX** | **500** | 0.228 | 0.219 | 1.401 | 0.849 | 0.623 | 1.353 |
| | **300** | 0.765 | 0.699 | 1.977 | 0.738 | 0.562 | 1.982 |
| | **100** | 0.218 | 0.299 | 0.423 | 0.378 | 0.465 | 1.963 |

The precision of the method was evaluated regarding repeatability and intermediate precision (Table 5). The obtained RDS% values are comparable with previously published data and support a good precision (intra-day and inter-day) of the method [19,23,24].

**Application of the CZE method for the quantification of LVF and MLX from TTSs.** Three experimental TTSs containing LVF and MLX (Table 6) were evaluated using the optimized CZE method. Dissolving the TTSs in the appropriate solvent represented a significant challenge taking into consideration both active substances and excipients. Ethylcellulose (EC) is insoluble in water but is freely soluble in chloroform. If EC contains

not less than 46.5% of ethoxy groups, this is freely soluble in ethanol (96°) and methanol. Hydroxypropyl methylcellulose (HPMC) is soluble in cold water, practically insoluble in chloroform, ethanol (96°) but soluble in a mixture of ethanol and dichloromethane, methanol and dichloromethane, water and ethanol (96°) [38]. The TTS samples mentioned in Table 6 were introduced in 25 mL volumetric flasks and dissolved in a mixture of organic solvents, with or without distilled water. Based on known solubility's of LVF, MLX, and polymers, several combinations of solvents were tested to obtain an appropriate solution for injection in the CE system.

**Table 6.** Composition of three experimental TTSs *(HPMC E5 - hydroxypropylmethylcellulose type E5, HPMC 15000 - hydroxypropylmethylcellulose type 15000, EC 10 - ethylcellulose type 10)*.

| Components (m/m %) | TTS 1 | TTS 2 | TTS 3 |
|---|---|---|---|
| LVF | 0.5 | 0.5 | 0.5 |
| MLX | 0.5 | 0.5 | 0.5 |
| HPMC E5 | 3 | - | - |
| HPMC 15000 | - | 2 | 1 |
| EC 10 | - | - | 1 |
| Ethanol (96% v/v) | 30 | 30 | 30 |
| Propylene glycol | 10 | 10 | 10 |
| Polysorbate 20 | 1 | 1 | |
| Distilled water | up to 100 | up to 100 | up to 100 |

The solvent systems used were as follows: for TTS 1 - 2 ml DMF, 9 ml ethanol, and distilled water up to 100 ml; for TTS 2 - 2 ml DMF, 2 ml chloroform, and ethanol : dichloromethane (1:1) up to 100 ml; and for TTS 3 - 2 ml DMF, 5 ml chloroform, 5 ml methanol, and ethanol : dichloromethane (1:1) up to 100 ml. After 20 minutes stirring on the ultrasonic vibration, the mixtures were filtrated through 90 mm Whatman® qualitative filter paper and diluted adequately with methanol (theoretical concentration of the active substances in samples is 0.1 mg $mL^{-1}$). Although HPMC is soluble in a mixture of water and ethanol (96% v/v) the samples of TTS 2 and TTS 3 did not dissolve. The bulky precipitates were filtered, and the obtained solutions were additionally diluted with methanol. The collected quantitative results were unsatisfactory probably due to the retention of active substances in the precipitate. The obtained recovery results for LVF were satisfactory for all three experimental TTSs; however, MLX recovery values were lower (Table 7). According to some authors, recovery testing tends to be less critical, as long as the values of detection limits, precision and accuracy are acceptable [39].

**Table 7.** The composition of three experimental TTSs.

| TTSs | Active substance | Theoretical concentration ($mg \cdot mL^{-1}$) | Found concentration ($mg \cdot mL^{-1}$) | Recovery (%) ± SD |
|---|---|---|---|---|
| 1 | LVF | 0.1 | 0.096 | 96.38 ± 4.37 |
| | MLX | 0.1 | 0.091 | 91.23 ± 7.76 |
| 2 | LVF | 0.1 | 0.091 | 91.31 ± 5.05 |
| | MLX | 0.1 | 0.088 | 90.03 ± 9.45 |
| 3 | LVF | 0.1 | 0.090 | 90.10 ± 5.23 |
| | MLX | 0.1 | 0.085 | 85.14 ± 4.63 |

## CONCLUSIONS

The developed CZE method proved to be appropriate to quantify the LVF and MLX simultaneously from TTSs. A BGE containing 50 mM borax (pH 9.3) was used and the following optimised experimental conditions were applied: +25 kV applied voltage, 50 mbar/5 seconds hydrodynamic injection, 40°C temperature, detection at a wavelength of 335 nm. The method validation parameters have been verified and also the recovery of the active substances. The main advantages of this new method consist in its simplicity, rapidity (under four minutes), and low volumes consumption of solvents and analytes with consequently low costs of operation. Thus, we consider that our newly developed CZE method may be an alternative to classical HPLC in quantitative determinations of TTSs.

## EXPERIMENTAL SECTION

**Apparatus and chemicals.** The CZE experiments were performed on an Agilent 1600 CE (with diode-array detector). The software used to process the data was Chemstation 7.01 (Agilent). An uncoated fused-silica capillary (Agilent) with 51 cm total length (43 cm effective length) and 50 µm internal diameter was used in the experiments. The pH of the samples was measured with a Hanna Instruments HI2215 pH-meter.

Active substances and polymers were supplied as follows: LVF and EC 10 (EC 10 mPa·s) from Sigma Aldrich Co. (Germany), MLX from Techno Drugs & Intermediates Ltd. (India), HPMC 15000 (Metolose 90SH - 15000 mPa·s) from Shin-Etsu Chemical Co., Ltd. (Tokyo, Japan), and HPMC E5 (Methocel E5 - 5 mPa·s) from Dow Chemical Co. (Midland, USA). All chemicals and solvents were of analytical reagent grade, and ultrapure water was obtained using a Millipore Direct-QS water distiller.

The stock solutions were prepared daily using methanol for LVF and a mixture of methanol – DMF in ratio 9:1 for MLX, at a concentration of 1 mg $mL^{-1}$. The solutions were kept at +4°C in the refrigerator and diluted with methanol to obtain the appropriate concentrations.

**Capillary preconditioning and conditioning.** To ensure optimal run-to-run analytical conditions, reproducible migration times and a constant EOF, the capillary was conditioned by flushing with 1M NaOH (20 min), ultra-pure water (5 min), and BGE (20 min) at the beginning of each day. Between experiments, the capillary was preconditioned by flushing with BGE (2 min).

**Preparation of TTSs.** The samples of TTSs were obtained in the form of the thin matrices (polymeric films) by casting and solvent evaporation technique, according to a previously published method [40].

## ACKNOWLEDGEMENTS

Funding supported this research through the Internal Research Grant from the University of Medicine and Pharmacy of Târgu Mureş (contract no. 275/6/11.01.2017).

## REFERENCES

1. S. Orlandini, R. Gotti, S. Furlanetto, *Journal of Pharmaceutical and Biomedical Analysis*, **2014**, *87*, 290.
2. K.S. Paudel, M. Milewski, C.L. Swadley, N.K. Brogden, P. Ghosh, A.L. Stinchcomb, *Therapeutic Delivery,* **2010**, *1*, 109.
3. K. Kathe, H. Kathpalia, *Asian Journal of Pharmaceutical Sciences*, **2017**, *12*, 487.
4. A.M. Noreddin, W.F. Elkhatib, K.M. Cunnion, G.G. Zhanel, *Drug, Healthcare and Patient Safety,* **2011**, *3*, 59.
5. G.M. Keating, *Drugs,* **2009**, *69*, 1267.
6. P. Gao, X. Wang, S. Huang, Y. Wang, J. Guan, Y. Li, Z. Tao, *Journal of Biomedical Engineering,* **2014**, *31*, 806.
7. C. Wang, H. Fu, L. Chen, L. Zhang, R. Liu, Q. Liang, *Patent No. CN107224425-A,* **2017**.
8. Nazar M.F., Saleem M.A., Bajwa S.N., Yameen B., Ashfaq M., Zafar M.N., M. Zubair, *The Journal of Physical Chemistry B,* **2017**, *121*, 437.
9. J.R. Ray, *Patent No. US2018147212-A1,* **2018**.

10. M. Ochi, K. Kimura, A. Kanda, T. Kawachi, A. Matsuda, K. Yuminoki, Hashimoto N. *AAPS PharmSciTech*, **2016**, *17*, 932.
11. J. Chen, Y. Gao, *Drug Delivery*, **2016**, *23*, 3146.
12. W. Wei, X. Li, A. Liu, D. Jing, L. Li, *Patent No. CN106551918-A*, **2017**.
13. Y. Sun, X. Xu, M. Yao, *Patent No. CN106924223-A,* **2017**.
14. A.M. Khan, S. Rampal, *Veterinary World,* **2013**, *6*, 950.
15. A.M. Khan, S. Rampal, N.K. Sood, Human & Experimental Toxicology. **2017**, *36*, 42.
16. A.M. Khan, S. Rampal, N.K. Sood, *Environmental Science and Pollution Research*, **2018**, *25*, 8853.
17. V.K. Dumka, H. Singh, A.K. Srivastava, *Environmental Toxicology and Pharmacology*, **2008**, *26*, 56.
18. R.S. Yadav, S.K. Garg, A. Rahal, *Veterinarski Arhiv*, **2014**, *84*, 625.
19. H. Sun, Y. Zuo, *Current analytical chemistry,* **2013**, *9*, 157.
20. Y.-H. Tsai, M.-J. Bair, C.-C. Hu, *Journal of the Chinese Chemical Society*, **2007**, *54*, 991.
21. Y.M. Liu, J.T. Cao, W. Tian, Y.L. Zheng, *Electrophoresis,* **2008**, *29*, 3207.
22. E. Nemutlu, S. Kir, *Journal of Pharmaceutical and Biomedical Analysis*, **2003**, *31*, 393.
23. Y.H. Hsieh, S.J. Lin, S.H. Chen, *Journal of Separation Science*. **2006**, *29*, 1009.
24. S.E. Vignaduzzo, L. Vera-Candioti, P.M. Castellano, H.C. Goicoechea, T.S. Kaufman, *Chromatographia*, **2011**, *74*, 609.
25. A. Rusu, G. Hancu, G. Völgyi, G. Tóth, B. Noszál, A. Gyéresi, *Journal of Chromatographic Science*, **2014**, *52*, 919.
26. I. Ahmad, R. Bano, M.A. Sheraz, S. Ahmed, T. Mirza, S.A. Ansari, Acta Pharmaceutica, **2013**, *63*, 223.
27. *Tuberculosis*, **2008**, *88*, 119.
28. C.E., "European Pharmacopoeia" 9th edition, Council of Europe, Strasbourg, **2016,** chapter Capillary electrophoresis.
29. M. El-Badry, *Scientia Pharmaceutica*, **2011**, *79*, 375.
30. J.M. Beale, J.H. Block, "Wilson and Gisvold's Textbook of Organic Medicinal and Pharmaceutical Chemistry". 12th edition, Lippincott Williams&Wilkins, Philadelphia, **2011**, chapter Appendix.
31. Romani LFA, Yoshida MI, Gomes ECL, Machado RR, Rodrigues FF, Coelho MM, M.A. Oliveira, M.B. Freitas-Marques, R.A.S. San Gil, W.N. Mussel. *Journal of Pharmaceutical Analysis*, **2018**, *8*, 103.
32. A. Rusu, S. Imre, E. Mircia, G. Hancu, *Acta Medica Marisiensis*, **2015**, *61*, 328.
33. "The Japanese Pharmacopoeia" English Version, 17th edition (the electronic version), The Ministry of Health, Labour and Welfare Ministerial, **2016**, Ultraviolet visible reference spectra [Cited 2018 Oct 19] Available from *http://jpdb.nihs.go.jp/jp17e/*
34. E.M. Hassan, *Journal of Pharmaceutical and Biomedical Analysis*, **2002**, *27*, 771.

35. “The United States Pharmacopeial Convention Revision Bulletin”, Official March 1, **2012**, Meloxicam [Cited 2018 Oct 19] Available from *https://www.uspnf.com/official-text/accelerated-revision-process/accelerated-revision-history/meloxicam*
36. S. Ahuja, M.I. Jimidar, “Capillary Electrophoresis Methods for Pharmaceutical Analysis”, Academic Press Elsevier, Inc., Amsterdam, **2008**, chapter 4.
37. European Medicines Agency, CPMP/ICH/381/95, ICH Q2 (R1) Validation of analytical procedures: text and methodology. **1995**, [Cited 2018 Oct 19] Available from *http://www.ema.europa.eu/ema/index.jsp?curl=pages/regulation/general/general_content_000768.jsp&mid=WC0b01ac0580028e8d*
38. R.C. Rowe, P.J. Sheskey, M.E. Quinn, “Handbook of pharmaceutical excipients. American Pharmacists Association.” 6th edition, Pharmaceutical Press, American Pharmacists Association, London, Chicago, Washington, **2009**.
39. G. Tiwari, R. Tiwari, Pharmaceutical Methods, **2010**, *1*, 25.
40. P. Antonoaea, A.G. Cârje, A. Ciurba, N. Todoran, A.R. Vlad, D.L. Muntean, *Acta Medica Marisiensis*, **2017**, *63*, 178.